DOE/CE/40936--T5-Vol. 3

Black Liquor Combustion
Validated Recovery Boiler Modeling
Final Year Report

Volume 3
(Appendicies II, sections 2-3 & III)

by

T.M. Grace, W.J. Frederick, M. Salcudean, and R.A. Wessel

August 1998

A Summary Report
of the Project

Work Performed Under Contract DE-FG07-90CE40936

Prepared for

The U.S. Department of Energy
Office of Industrial Technologies
Washington, D.C.

Prepared by

The Institute of Paper Science and Technology
Atlanta, GA

Oregon State University
Corvallis, OR

University of British Columbia
Vancouver, BC, Canada

Babcock & Wilcox Company
Alliance, OH

DISCLAIMER

Table of Contents
Volume 3

APPENDIX II cont'd

APPENDIX III
University of Toronto Report

FORMATION AND DESTRUCTION OF NITROGEN OXIDES IN RECOVERY BOILERS

By:

Kristiina Iisa,

Rungsun Pianpucktr.

Nopadol Rompho,

Vichien Tangpanyapinit.

Qun Jing,

Jennie Conn

TABLE OF CONTENTS

LIST OF FIGURES

LIST OF TABLES

Introduction

The following sub-studies of nitrogen reactions were made here:

- N release and NO formation during black liquor pyrolysis and combustion
- NO formation from combustion air during black liquor combustion
- NH_3 oxidation and destruction by fume compounds
- NO reduction by black liquor char and fume.

A model for N release and NO formation and destruction is formulated based on these studies, the results from the previous DOE project (report DOE/CE/40936-T3), and research by other investigators.

N Release and NO Formation During Combustion and Pyrolysis of Black Liquor

Experimental

All the experiments of black liquor combustion and pyrolysis were made in a laminar entrained-flow reactor. In it, solid particles of the material to be studied are entrained into a primary gas flow and fed to the top of a mullite tube reactor. The particles and the primary gas are heated rapidly by radiation from the hot reactor walls and convection from a preheated secondary gas. The secondary gas flow is typically two hundred times the primary gas flow rate, and particle heating rates of up to 10000 °C/s can be obtained. The gases and particles exit the reactor via a water-cooled collector in which they are rapidly cooled down by the addition of a quench gas. The flow of the quench gas is equal to or greater than that of the secondary gas. The residence time in the reactor can be adjusted by changing the position of the collector and/or changing the gas flow rates. A computational fluid dynamics model developed by Flaxman and Hallett (1987) was used for determining the residence time in the reactor.

The temperatures studied were 400-1100 °C, and the residence times 0.3-2 s. The gases fed to the reactor were nitrogen and oxygen, which were mixed to obtain O_2 contents of 0, 4 and 21%. Additional experiments in which the nitrogen was replaced by a mixture of helium and argon were made when determining the effect of the nitrogen in the combustion air. The outlet NO concentrations were measured by a chemiluminescence NO-NOx analyzer, and the nitrogen retained in the char was measured by a modified Kjehldahl nitrogen method at the Soil Science Department at Oregon State University.

A southern pine black liquor was dried to make dry black liquor solids, which were ground and sieved to the particle size of 90-125 um. The elemental composition of the black liquor is given in Table 1. The nitrogen contents of the black liquor solids varied somewhat from batch to batch, and were 0.07 % in the low temperature (400-600°C) pyrolysis studies, 0.09 % in the combustion and high temperature (700-1100 °C) pyrolysis studies, and 0.06 % in the determination of NO formation from combustion air.

Table 1. Composition of the black liquor solids used in the pyrolysis and combustion experiments.

Element	Wt %
Carbon	35.70
Hydrogen	3.05
Sodium	22.65
Sulfur	2.85
Potassium	0.62
Chloride	0.67
Nitrogen	0.06-0.09*
Oxygen**	34.37-34.40

* depending on batch of drying

** obtained by difference

N Release and NO Formation During Pyrolysis

The nitrogen release and NO formation during pyrolysis were studied earlier in the laminar entrained-flow reactor, and the results are given in DOE report DOE/CE/40936-T3, Carangal (1994) and Iisa et al. (1995). Other studies of nitrogen release during black liquor pyrolysis include Aho et al. (1994a) and (1994b). A considerable fraction of the nitrogen is released during pyrolysis, mainly as N_2 and NH_3. The laminar entrained-flow reactor experiments showed that some NO was formed during black liquor pyrolysis as well. There was a maximum in the NO content of the pyrolysis gases as a function of residence time: the NO content first increased, and then decreased. The highest amount of NO corresponded to 20 % of the nitrogen in the black liquor being converted to NO and was detected at 900°C at 0.5 s. The NO reduction was rapid, and at the same temperature the NO content had reduced to less than 4 % by 1.6 s. The total nitrogen release was 35-65 % in 0.3-1.6 s.

In this project, N release during low temperature pyrolysis was measured. Pyrolysis can be divided into two stages: devolatilization and extended pyrolysis. Devolatilization refers to the initial rapid loss of volatile material from the fuel, and extended pyrolysis to the effect of continued heating on the residue after devolatilization. The rapid devolatilization is over by the shortest residence times at the temperatures 700-1100 °C in the LEFR. In order to study the kinetics during the rapid devolatilization stage, low temperature (400-600 °C) pyrolysis experiments were made, and the N release during these experiments was studied as well.

Additional experiments of black liquor pyrolysis were made in the study of black liquor combustion at 700-1100 °C. Their main purpose was to serve as a reference point for the combustion studies. The results of the high temperature pyrolysis experiments are presented here; those of the low temperature pyrolysis in conjunction with the other pyrolysis data. A model for N release during pyrolysis based on the low and high temperature data is developed.

The low temperature pyrolysis measurements are included in detail in the thesis by Phimolmas (1997), the high temperature pyrolysis and combustion data in the thesis by Pianpucktr (1995), and the model for N release during pyrolysis in the thesis by Rompho (1997).

High Temperature (700-1100 °C) Pyrolysis

Figure 1 shows the char yields as a function of residence time in the experiments made at 700-1100 °C. At 900-1100 °C the rapid devolatilization was over by the shortest residence time 0.3 s but at 700 °C the devolatilization continued until 0.6 s. At the end of the rapid devolatilization or at the shortest residence time, the char yields varied from 65 to 50%.

The char nitrogen contents (by weight) versus residence time are shown in Figure 2 for all the temperatures studied. The nitrogen content remained constant at 900 and 1100°C but decreased with time at 700 °C. This indicates that, at 700°C, nitrogen is released from the black liquor faster than total mass. Because the amount of nitrogen in the char was very low and only one sample for each point was analyzed, there may be considerable error in the analysis. Carangal (1994) who used the same laboratory for nitrogen measurement found that the deviation in the analysis was ±0.01 wt.% nitrogen.

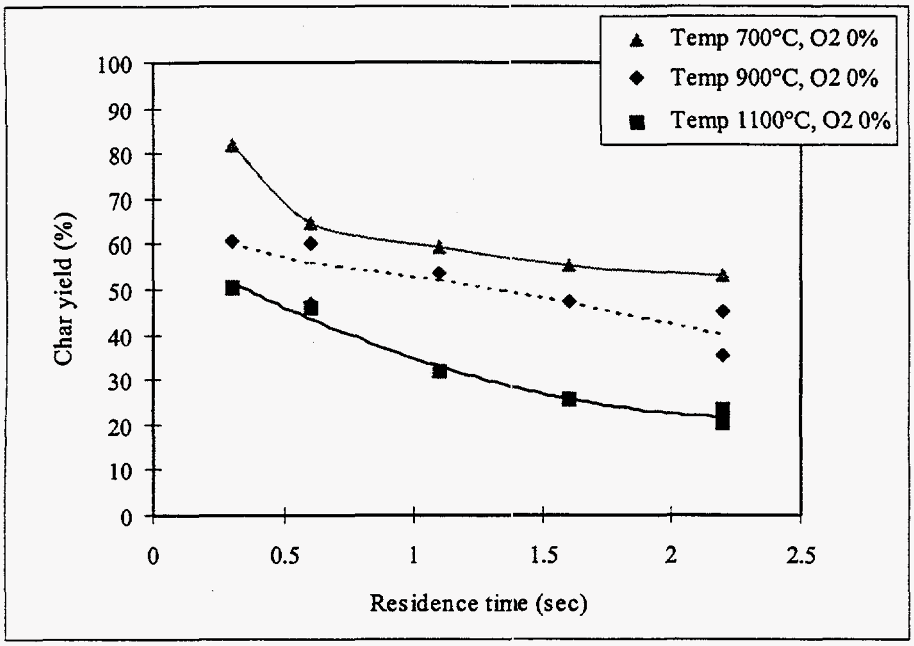

Figure 1. Char Yield as a Function of Residence Time During Black Liquor Pyrolysis at 700-1100 °C.

The measurement of the nitrogen content of black liquor and black liquor char is difficult due partly to the low N content. Forssen et al. (1995a) had compared three methods for N measurement: Kjehldahl, high temperature and low temperature combustion. The correlation between the low temperature and either of the two other methods was poor. There was a linear relationship between the Kjehldahl analysis and the high temperature combustion measurements. However, the high temperature combustion method gave values that were on average 68 % of those by the Kjehldahl method. The high temperature combustion method is based on the assumption that all N is converted to NO. The conversion may not have been complete, which would explain the lower values by that method. Considering these results, the Kjehldahl method, albeit not perfect, is currently the best method for measuring N contents in black liquors.

Figure 3 shows nitrogen release as a percentage of nitrogen originally present in the black liquor solids as a function of residence time. At 0.3 seconds, fractions of nitrogen released were 22% of fuel nitrogen at 700°C, 46% of fuel nitrogen at 900°C, and 58% of fuel nitrogen at 1100°C. The fraction of nitrogen released increased as residence time increased.. At 700°C, the amount of nitrogen released increased rapidly to 50% of fuel nitrogen at 1.1 seconds, then increased more gradually and reached 55% of fuel nitrogen at 2.2 seconds.

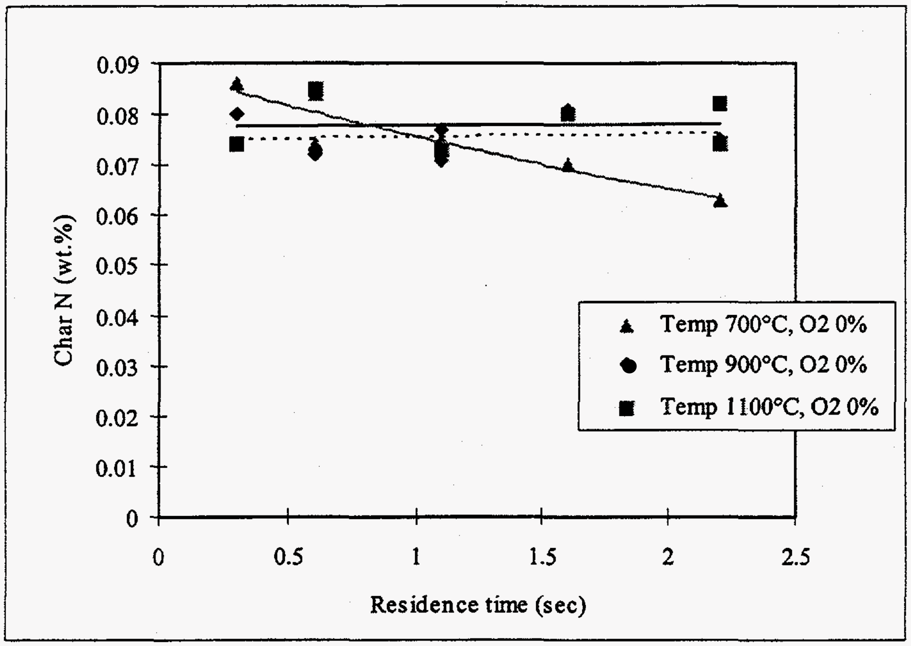

Figure 2. Char Nitrogen Content by Weight as a Function of Residence Time During Black Liquor Pyrolysis.

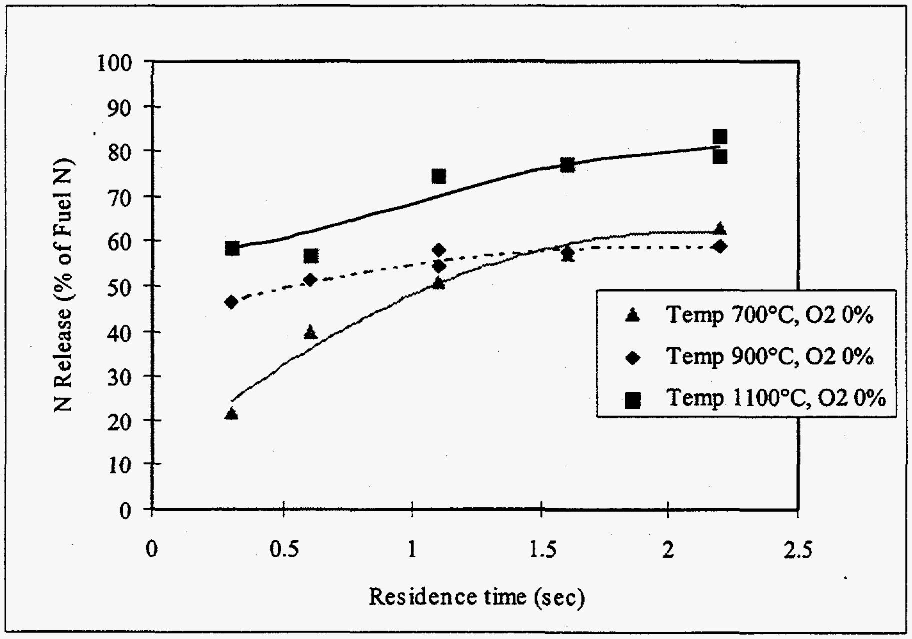

Figure 3. Nitrogen Release as a Function of Residence Time During Black Liquor Pyrolysis.

At 900 and 1100°C, the amount of nitrogen released increased gradually during the residence time range studied, 0.3-2.2 seconds. The lowest char yield in this study was 20% at 1100°C and 2.2 seconds; i.e. 80% of black liquor solids were released into the gas phase. The amount of nitrogen release was also 80%. The nitrogen release increased with rising temperature as well, except at 700 and 900°C, when it was about the same at residence times 1.6-2.2 seconds. The results agree with the experiments of Carangal (1994).

From the data, it can be concluded that the nitrogen release was 20-60% of black liquor nitrogen at 700°C, 45-70% of black liquor nitrogen at 900°C, and 60-80% of black liquor nitrogen at 1100°C. Carangal (1994) found that the nitrogen release was 40-60% of black liquor nitrogen at 0.85 seconds and temperatures of 700-1100°. This agrees with our experiments that the nitrogen release was 40-70% of fuel nitrogen in black liquor at 0.6-1.1 seconds and 700-1100°C.

Forssén et al. (1995a) reported considerably higher nitrogen release for liquors with nitrogen contents of 0.06-0.09 wt.%. They found that at 600-900°C the fraction of nitrogen remaining in the char was constant at an average of 20-30% of fuel nitrogen (which corresponds to 70-80% of black liquor nitrogen released). They used a single droplet reactor in which the droplet is kept at the Almost all of the nitrogen in black liquor was released at 1100°C. The main reason for the higher fractions of nitrogen released during pyrolysis in Forssén's experiments is believed to be the longer residence time in their apparatus. In the experiments of Forssén et al. the pyrolysis time was much longer than in our experiments (hundreds of seconds versus a couple of seconds). Thus, more of the volatile nitrogen in the black liquor might be released in their experiments. In our experiments, the nitrogen release continued at 2.2 seconds. In recovery boilers, char combustion typically begins in a couple of seconds. Consequently the values from the laminar entrained-flow reactor are going to be used as a basis for the model of nitrogen release during pyrolysis.

Figure 4 shows the conversion of nitrogen originally present in black liquor solids to NO during black liquor pyrolysis as a function of residence time at temperatures 700, 900, and 1100°C. The results indicate that NO formation is dependent on residence time and the temperature. At 700 and 900°C, the NO level initially increased with increasing residence time, and then decreased as residence time further increased. The maximum in the amount of NO formed was at a residence time between 1.1 and 2.2 seconds at 700°C, and at 900°C the maximum was between 0.3 and 1.1 seconds. The highest NO conversion was roughly 12% of the nitrogen originally present in the black liquor solids at both 700 and 900°C.

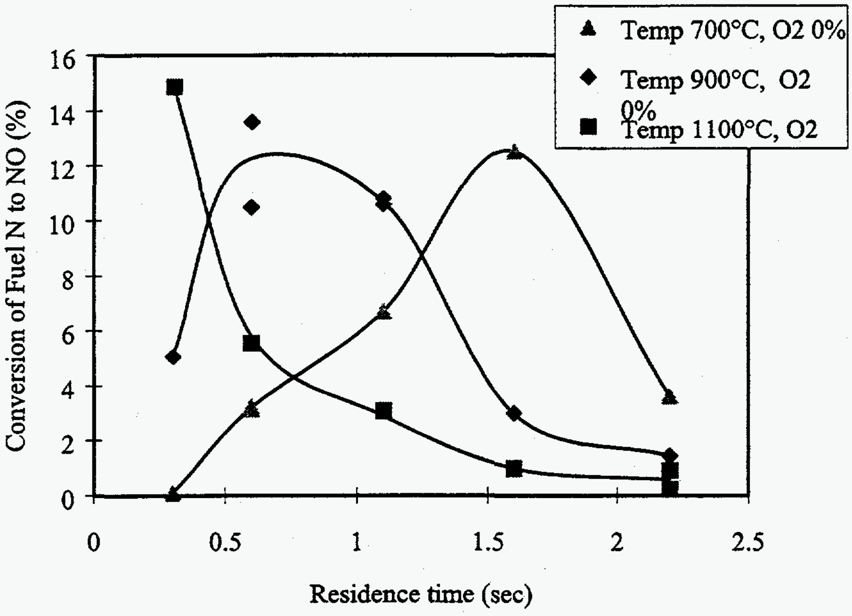

Figure 4. NO Formation as a Function of Residence Time During Black Liquor Pyrolysis

At 1100°C, the NO level decreased with increasing residence time and, in the residence time range studied (0.3-2.2 seconds), no maximum in the amount of NO formed can be observed. Since there is no NO formed at 0 second residence time, there must be a maximum in the amount of NO formed at a residence time below or near 0.3 seconds. The highest amount of fuel nitrogen in black liquor that was converted to NO was 15% at the shortest residence time studied, 0.3 seconds. The NO level decreases at long residence times because NO destruction takes place and the rate of NO destruction is higher than the rate of NO formation. At 1100°C, the destruction of NO probably already dominates at the shortest residence time studied. The NO destruction may be due to homogeneous reactions of NO with other gas species and/or heterogeneous reactions of NO with fume or char to form molecular nitrogen. Based on rates of NO reduction by black liquor char and fume, Iisa et al. (1995) concluded that the dominating NO destruction mechanism is the reduction of NO by char.

In the similar pyrolysis experiments of Carangal (1994), the maximum NO level at 900°C was observed at 0.5 seconds. At 700°C, the highest NO formation measured was at 1.7 seconds, which was the longest residence time in her experiments. The NO level only slightly increased from 1.4 to 1.7 seconds, which may imply that there was a maximum in the amount of NO formed near 1.7 seconds. The highest amount of NO formed was approximately 16% of fuel nitrogen at 700°C and 19% of fuel nitrogen at 900°C in Carangal experiments. This indicates that the results from both of the black liquor pyrolysis experiments agree well. The slight difference in the amount of NO formed may have been due to the fact that, in our experiments, only 5 residence times were used. Thus the actual maximum NO level might have been higher at other residence times. The other reason may be differences in the black liquor solids. Although the black liquor was the same, they were dried at different batches and at different times. For instance, the nitrogen content of black liquor solids in our experiments was 0.09% by weight, and 0.11% by weight in Carangal's experiments. The decrease in nitrogen content from 0.11 to 0.09 was probably because more volatile nitrogen was lost. Thus it is reasonable that the NO formed during pyrolysis was lower for the 0.09% nitrogen liquor. Aho et al. (1994a and 1994b) found that the fuel nitrogen released as N_{fix} (NH_3, NO and HCN) is higher for a black liquor that has a higher nitrogen content.

Nitrogen Release Model for Pyrolysis

A model for nitrogen release during pyrolysis was developed based on the low temperature pyrolysis experiments at 400, 500, and 600°C and those at 700, 900, and 1100°C presented in the previous section. The experimental results are combined in Figure 5, which shows the nitrogen release as a function of residence time during black liquor pyrolysis at those six furnace temperatures.

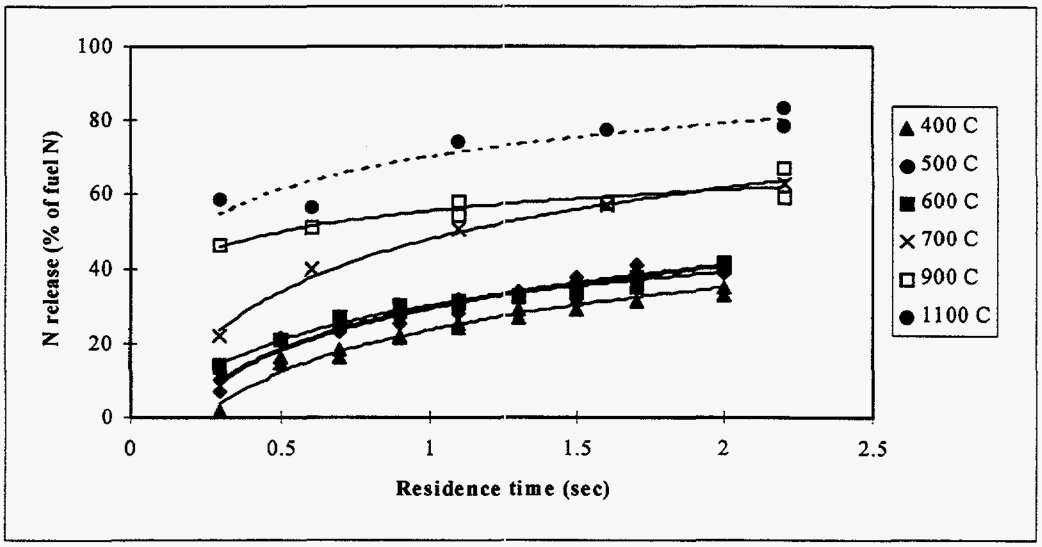

Figure 5. Nitrogen release as a percentage of nitrogen originally present in the black liquor solids as a function of residence time during black liquor pyrolysis.

The nitrogen release increased as residence time increased at all temperatures. At low temperatures (400 - 600°C), nitrogen release increased at about the same rate at all temperatures. At high temperatures (700 - 1100°C), on the other hand, the amount of nitrogen released increased rapidly until 0.3 seconds and after that it increased gradually during 0.3 to 2.2 seconds.

The nitrogen release also increased as temperature increased. Figure 6 shows the nitrogen release as a percentage of nitrogen originally present in the black liquor solids as a function of temperature.

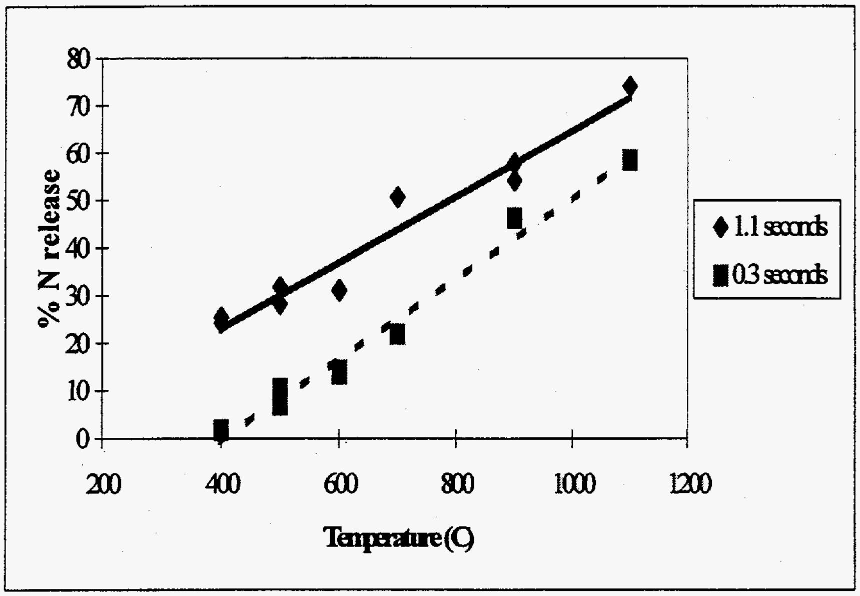

Figure 6. Nitrogen release as a percentage of nitrogen originally present in the black liquor solids as a function of temperature.

A model for nitrogen release during pyrolysis could be developed from these data by separating the pyrolysis stage into two sub-stages. The first stage is the initial stage during which nitrogen is rapidly released from black liquor solids. The amount of nitrogen release during this stage depends on temperature, and increases as temperature is increased. At high temperature, the initial stage was over by 0.3 seconds. At 1100°C, more than 50 % of the nitrogen was released in less than 0.3 seconds. At low temperatures, the effect of the first stage is negligible.

The second stage is in the residence time range during which nitrogen is released gradually compared to the first stage. In the second stage, the nitrogen release depends on temperature and residence time. Here, an attempt was made to correlate all the nitrogen release data in the two studies with a common equation. The percentages of nitrogen release (% of fuel nitrogen originally present in black liquor solids) were fitted with residence time by using a logarithmic relationship of the form

Eq. 1: N release (% of fuel N = A ln(t) + B

where t = residence time (s)
A and B = functions of temperature

A and B were obtained from a fit according to Eq. 1 at each temperature. The values are A presented in Table 2.

Table 2. A and B versus temperature for nitrogen release model for pyrolysis.

Temperature (°C)	A	B	Equation (Aln(t) + B)
1100	13.037	70.491	13.037ln(t) + 70.491
900	8.254	55.594	8.254ln(t) + 55.594
700	20.236	47.821	20.236ln(t) + 47.821
600	13.177	30.028	13.177ln(t) + 30.028
500	16.319	29.451	16.319ln(t) + 29.451
400	16.466	23.577	16.466ln(t) + 23.577

A was estimated to be constant and is given as the average of A at different temperatures that is with 95 % confidence interval

Eq. 2: $A = 14.6 \pm 4.3$

and B was found to be linear as respect to temperature that is

Eq. 3: $B = 0.0687T - 5.24$

Figure 7 shows the relationships between A and B, and temperature.

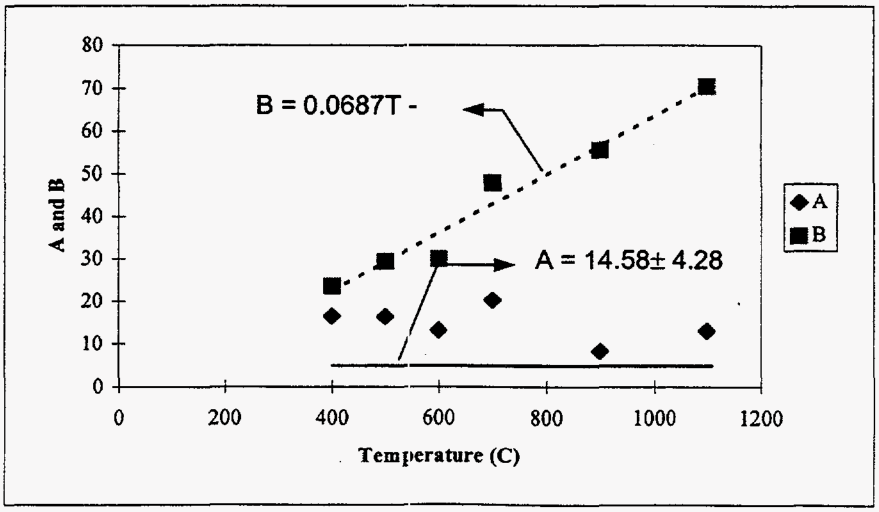

Figure 7. The relationship between A, B and temperature.

Thus, Eq. 1 becomes

Eq. 4: N release (% of fuel N) $= 14.58 \ln(t) + 0.0687T - 5.24$

where t = residence time (seconds)
T = temperature (°C)

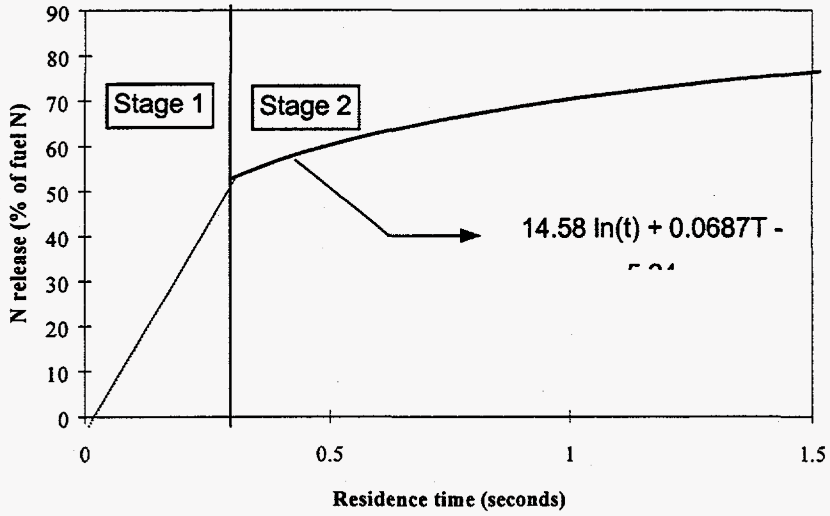

Figure 8. A schematic diagram of the sub-stages during pyrolysis

This equation is valid at residence times 0.3 - 2.0 seconds and temperatures 400-1100°C for pyrolysis experiments. A schematic diagram of the sub-stages during pyrolysis is illustrated in Figure 8.

Figure 9 shows the fit of the model with the data at 400 - 1100°C. The data seem to fit very well at 400, 500, and 1100°C. However, at 600°C, the model predicts higher values than those obtained from the experiments. At 700°C, on the other hand, the model predicts somewhat lower values than those obtained from the experiments for all residence times. At 900°C, the model predicts slightly lower values at short residence times and slightly higher values at long residence time.

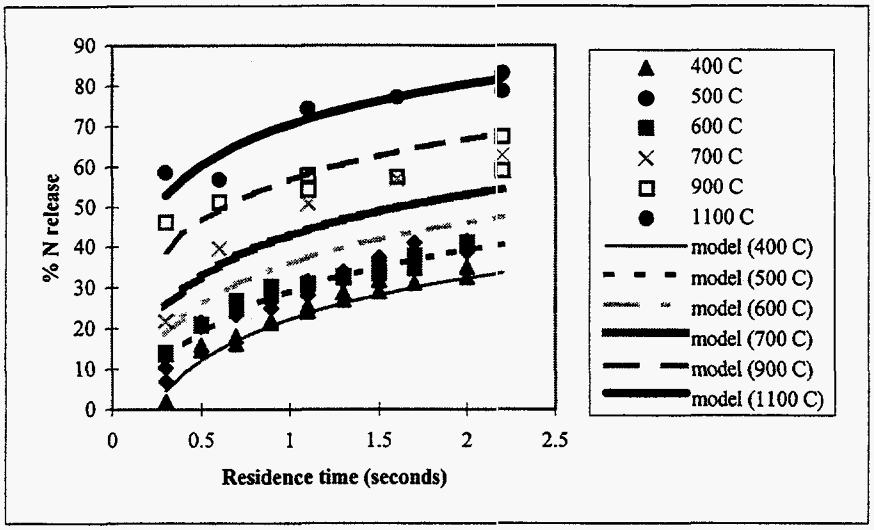

Figure 9. The model versus the values obtained from the experiments at 400 - 1100 °C.

Carangal (1994) had conducted pyrolysis experiments at 0.85 seconds residence time at temperature 500 - 1100°C as well. The fuel nitrogen that was released during pyrolysis in her experiments is shown along with values predicted by our model in Figure 10. The predicted values agree quite well with her data.

A model correlating nitrogen release to carbon release was developed based on the low temperature (400 - 600°C) pyrolysis experiments. The amounts of carbon and nitrogen release were calculated from his data. Figure 11 shows the nitrogen release as a function of carbon release for 400-600°C.

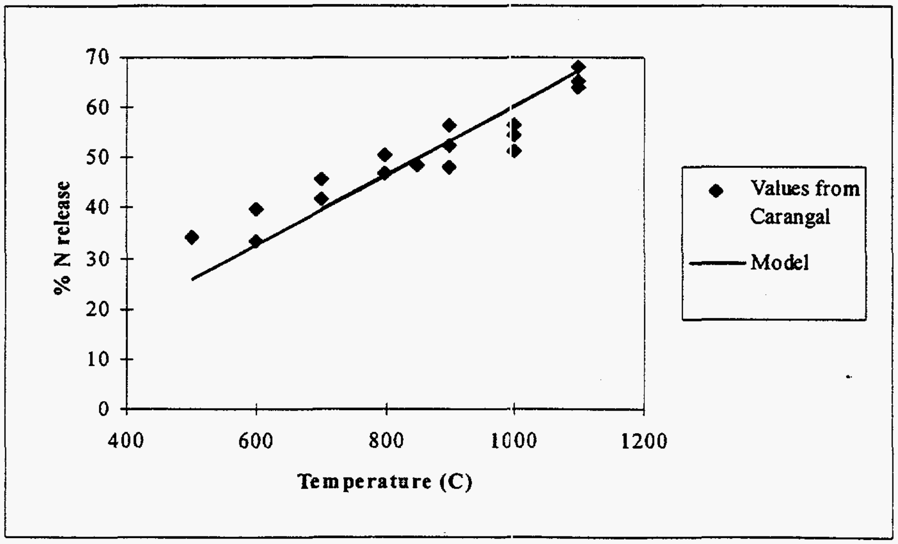

Figure 10. The fuel nitrogen that was released during pyrolysis in the experiments by Carangal (1994) and values predicted by our model at 0.85 seconds

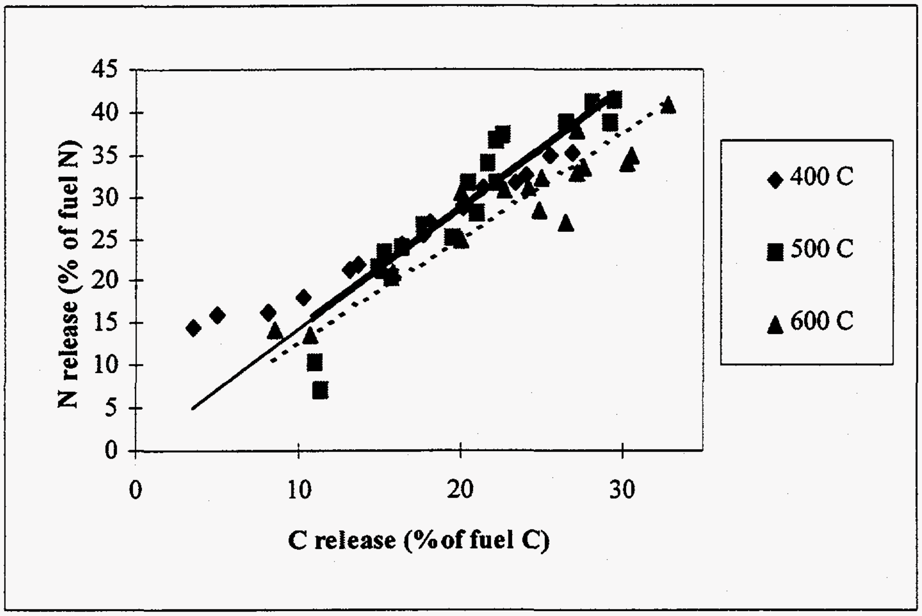

Figure 11. The fractional nitrogen release as a function of fractional carbon release for 400-600°C.

The results indicate that nitrogen was released faster than carbon at all temperatures studied. The rates of nitrogen release with respect to the rate of carbon release were almost the same at the three temperatures studied. The data were fitted by linear correlations. At 400 and 500°C, nitrogen was released at a rate 1.44 times the rate of carbon release. However, at 600°C, nitrogen release was slightly slower but still 1.25 times the carbon release. This suggests that the rates of nitrogen release with respect to the rate of carbon release decrease as temperature is increased, and that nitrogen may be released slower than carbon at high temperatures.

In the experiments presented here, only NO in the gas phase was measured. Aho et al. (1994a) measured the NH_3 and NO during pyrolysis of single droplets at different furnace temperatures. The total amounts of N release and NH_3 and N_{fix} measured in the gas phase are shown in Figure 12. At 500-600 °C, approximately 50 % of the N release was NH_3. At higher temperatures the fraction was less than 50 %. This may, however, be due to increased NH_3 reduction and oxidation at the higher temperatures. These reactions will be taken into account in other parts of the model. Therefore, the N release during pyrolysis is modeled so that 50 % is released as NH_3, and the rest as N_2 as long as there is hydrogen left in the char, i.e. until completion of devolatilization. After completion of devolatilization, that is during extended pyrolysis, all of the nitrogen is released as N_2.

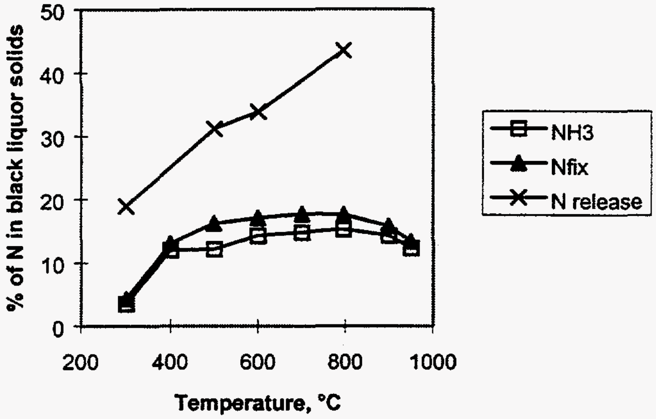

Figure 12. Release of nitrogen, and formation of NH_3 and N_{fix} (= NH_3 + NO) during pyrolysis of black liquor in a single droplet reactor. Data based on Aho et al. (1994).

N Release and NO Formation During Black Liquor Combustion

The combustion experiments are reported in detail in the thesis by Pianpucktr (1995). Black liquor combustion experiments were made at temperatures 700-1100°C, and O_2 concentrations of 4 and 21 %. Figure 13, Figure 14, and Figure 15 show the char yields at constant temperatures during both pyrolysis and combustion.

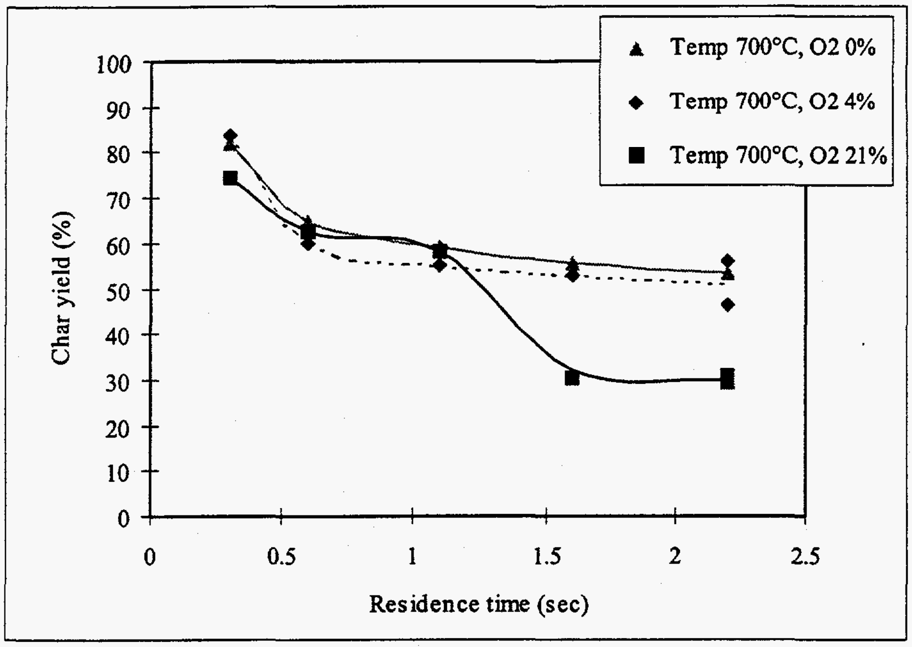

Figure 13. Char Yield as a Function of Residence Time During Pyrolysis and Combustion of Black Liquor at Reactor Temperature 700°C.

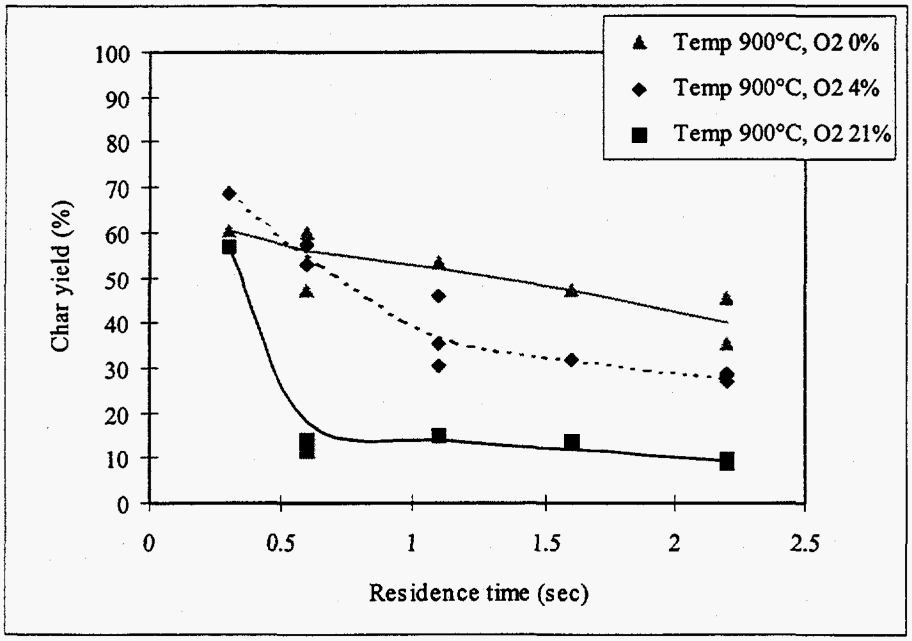

Figure 14. Char Yield as a Function of Residence Time During Pyrolysis and Combustion of Black Liquor at Reactor Temperature 900°C.

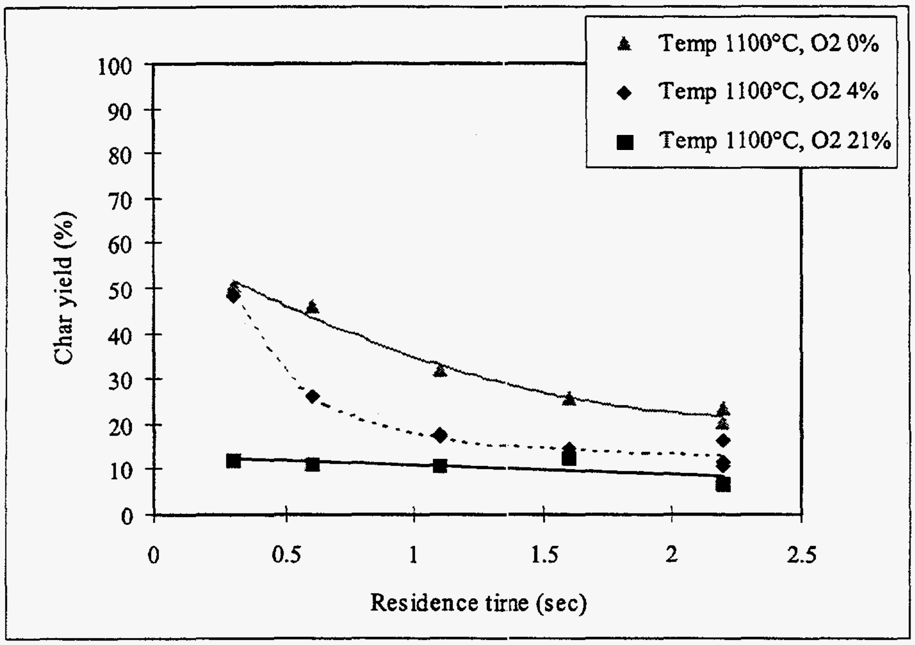

Figure 15. Char Yield as a Function of Residence Time During Pyrolysis and Combustion of Black Liquor at Reactor Temperature 1100°C.

At 700°C, the char yields with 4% O_2 were the same as during pyrolysis at all residence times, and with 21 % O_2 they were the same at 0.3-1.1 s. This suggests that only pyrolysis took place at 700°C, except at 1.6 and 2.2 seconds in 21% oxygen when combustion begun. No distinction between char burning and volatile combustion is made here, and we refer to both as combustion.

Based on the char yield, at 900°C, the ignition occurred between 0.6 and 1.1 s in 4 % O_2 and between 0.3 and 0.6 s in 21 % O_2. At 1100°C, the ignition occurred between 0.3 and 0.6 s in 4 % O_2 and before the first measurement point at 0.3 s in 21 % O_2.

Besides the onset of combustion, information on the completeness of combustion can be obtained from the char yield. The char yield remains approximately constant after complete combustion. At 1100°C the combustion is complete by the first measurement point, 0.3 s, and in 4 % O_2 at approximately 1.5 s. At 900°C, combustion was complete in 0.6 s but in 4 % O_2 combustion appears to continue still at 2.2 s. At 700°C there was combustion only with 21 % O_2. There is very little change in the char yield between 1.6 and 2.2 s, which suggests that the combustion is complete. However, there may have been only volatiles combustion at this condition, and no char or very slow char oxidation.

Table 3 summarizes the procession of combustion at different conditions. This information is important for the interpretation of N release and NO formation results.

Table 3. Ignition and completion of combustion at different conditions. t_{ign} = time at ignition, t_{end} = time at completion of combustion, char $yield_{end}$ = char yield at completion of combustion.

Temperature, °C	O_2, %	t_{ign}, s	$time_{end}$, s	Char $yield_{end}$, %
700	4	-	-	-
700	21	1.1-1.6	1.1-1.6	33
900	4	0.6-1.1	> 2.2 s	
900	21	0.3-0.6	0.3-0.6	14
1100	4	0.3-0.6	1.1-1.6	14
1100	21	<0.3	<0.3	11

N Release

Figure 16 and Figure 17 show the nitrogen remaining as a percentage of the char weight versus residence time in 4 and 21% oxygen. There is considerable scatter in the N content measurements, which makes the interpretation of the results more difficult. In particular at 900° with 21 % O_2 there seems to be erroneous points at 0.6-1.1 s. At 1100°C with 4 % O_2 the nitrogen content decreased sharply when combustion took place (0.3-1.1 s). The data at 1100°C, however, suggests that there was a gradual decrease in the nitrogen content even after combustion was complete (0.3-2.2 s).

Figure 18 and Figure 19 show the cumulative nitrogen release versus residence time in 4 and 21% oxygen. In 4% oxygen, at 700°C no combustion took place. There is rapid N release during the initial devolatilization (until 0.6 s) and more gradual N release during the extended pyrolysis (after 0.6 s). There was combustion at 900°C until the longest residence time 2.2 s with 4 % O_2 and until 0.6 s with 21% O_2, and at 1100°C until 1.1 s with 4 % O_2. When combustion takes place there is relatively rapid nitrogen release. At all conditions with complete combustion there seems to be continued slow nitrogen release.

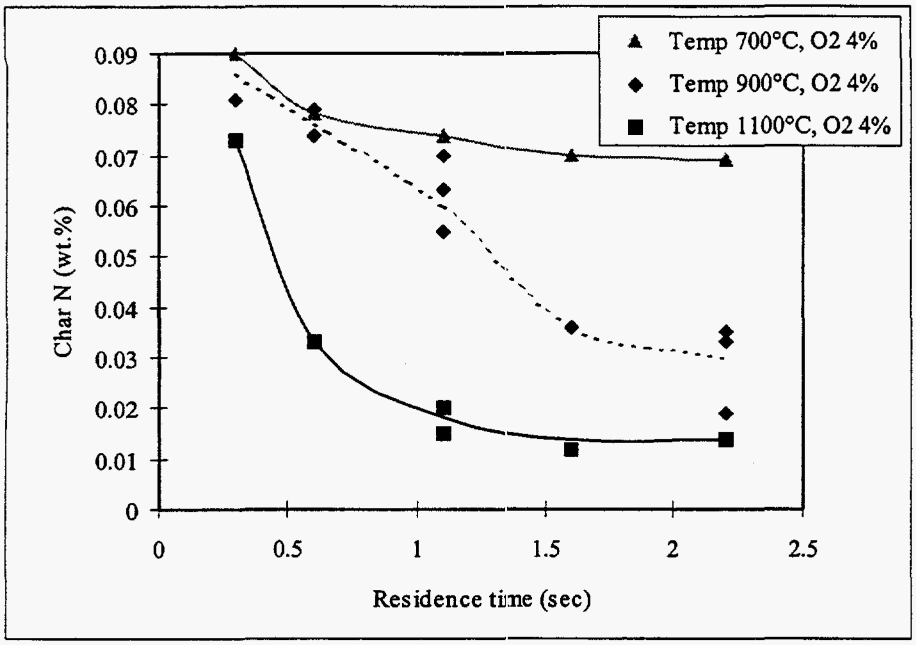

Figure 16. Char Nitrogen Content as a Function of Residence Time During Black Liquor Combustion in 4% Oxygen.

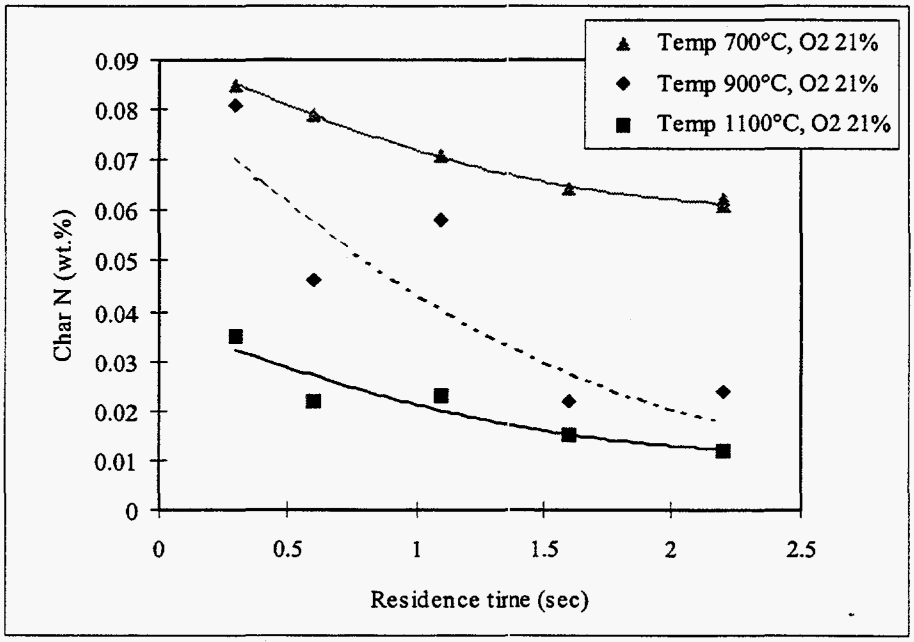

Figure 17. Char Nitrogen Content as a Function of Residence Time During Black Liquor Combustion in 21% Oxygen.

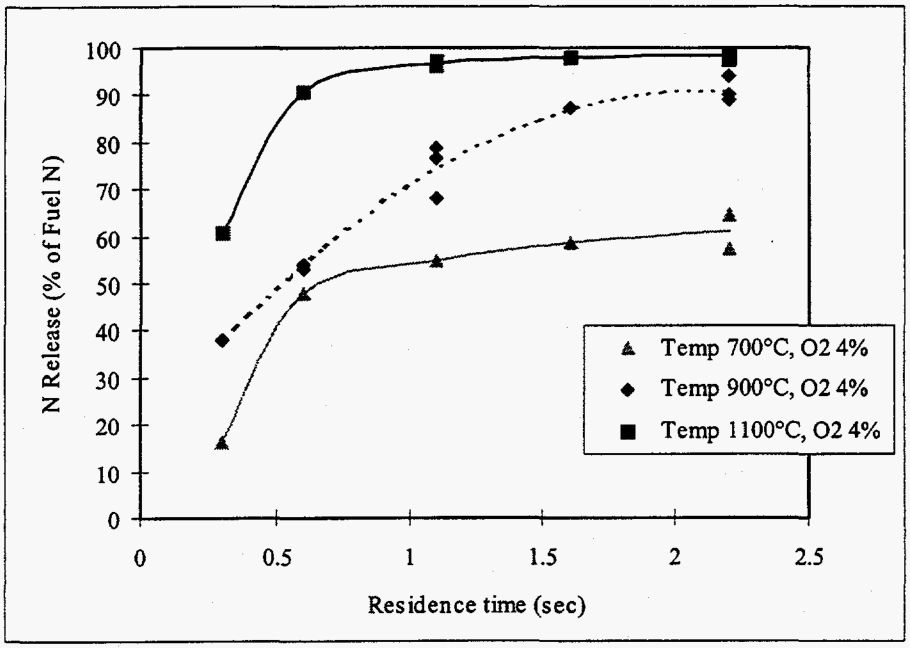

Figure 18. Nitrogen Release as a Function of Residence Time During Black Liquor Combustion in 4% Oxygen.

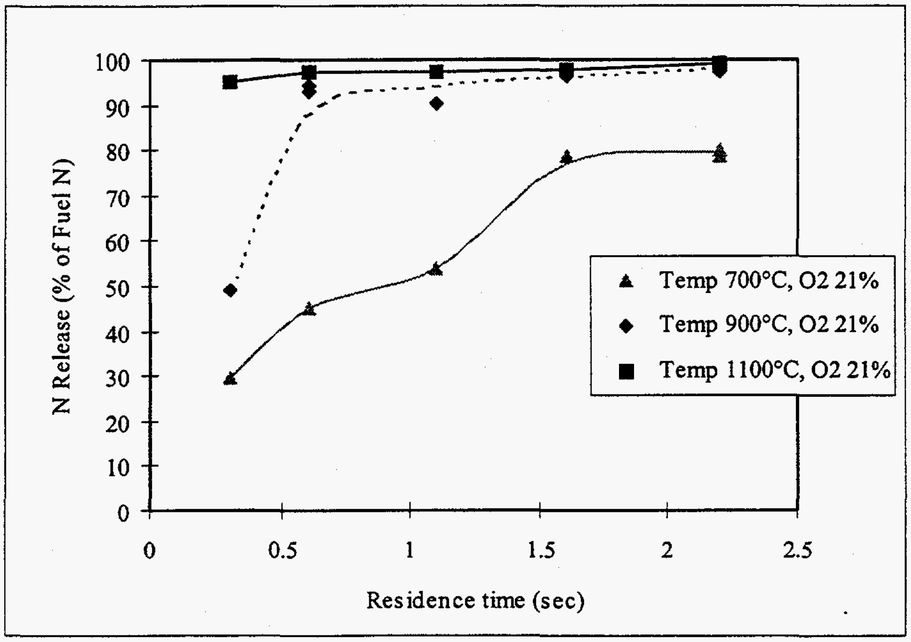

Figure 19. Nitrogen Release as a Function of Residence Time During Black Liquor Combustion in 21% Oxygen.

NO Formation

Figure 20, Figure 21, and Figure 22 show the NO formation as a function of residence time at temperatures 700, 900, and 1100°C respectively. Both pyrolysis and combustion data are included. At 700°C there was no combustion with 4 % O_2 at any residence time studied or with 21 % until 1.1 s or after 1.6 s, and the NO formation is consistent with this. For pyrolysis conditions, the typical behavior of a maximum in the amount of NO formed as a function of residence is seen. With 4 % O_2 the NO formation is equal to that during pyrolysis only. With 21 % O_2 the NO formation increases between 1.1 and 1.6 s when the combustion takes place to a value slightly higher than that for pyrolysis. At 2.2 s the NO remains at a value that is approximately as much higher than the pyrolysis value as the NO at 1.6 s.

At 900°C with 4 % O_2 the amount of NO increases as long as there is combustion, i.e. until 1.6 s. After that, the amount of NO slightly decreases. Based on the char yield all combustion occurred between 0.3 and 0.6 s at 900°C with 21 % O_2. The NO content increases rapidly in this time interval but it continues to increase until 1.6 s after which it decreases. At 1100°C with 4 % O_2 there was combustion between 0.3 and 1.6 s. The NO content increased in this temperature interval and decreased after that. With 21 % O_2 combustion was complete by 0.3 s, and the NO was formed by that time after which there was a gradual decrease in the NO content.

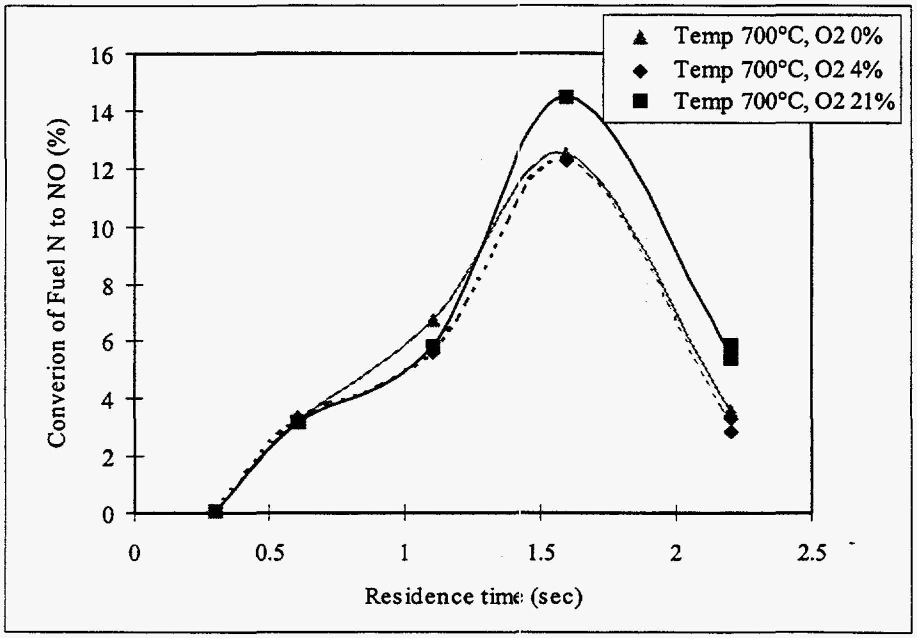

Figure 20. NO Formation as a Function of Residence Time During Pyrolysis and Combustion of Black Liquor at Reactor Temperature 700°C.

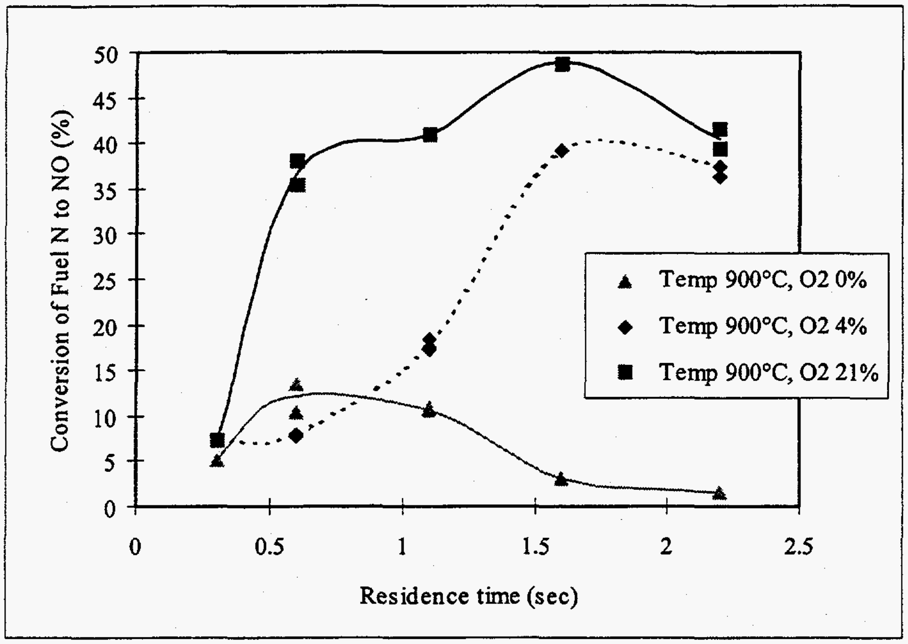

Figure 21. NO Formation as a Function of Residence Time During Pyrolysis and Combustion of Black Liquor at Reactor Temperature 900°C.

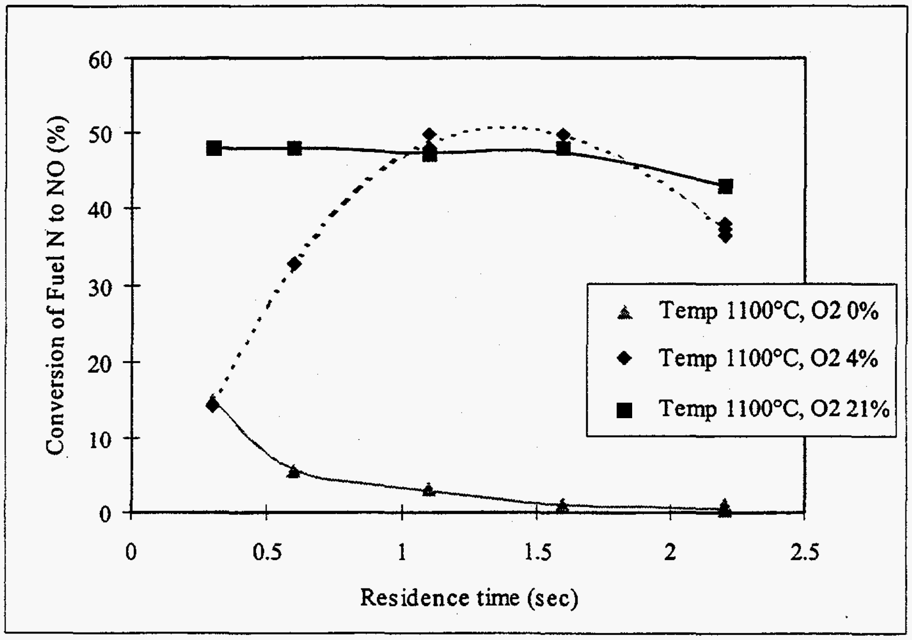

Figure 22. NO Formation as a Function of Residence Time During Pyrolysis and Combustion of Black Liquor at Reactor Temperature 1100°C.

Thus there was NO formation always when combustion took place, and in most cases after combustion was complete there was a decrease in the NO content of the gases. This means that the char N is oxidized in parallel with the carbon, and that reactions accounting for NO reduction are important. The only exception is the data at 900°C with 21 % O_2. It shows considerable NO formation after combustion was deemed to be complete. The data at these conditions had some other anomalies as well, e.g., the amount of N release showed a decrease between 0.6 and 1.1 s. There may have been a problem in these runs. Alternatively, under these conditions considerable amounts of N may be retained in the char at the end of combustion, and the N is then released as NO. Forssen et al. (1995a) showed that at low O_2 contents (1 %) and low temperatures (800°C) nitrogen is retained in the smelt residue and becomes oxidized after combustion is complete. The O_2 content in this run was high, however, and temperature relatively high so those conditions do not seem applicable to these results. At 700°C there was no NO formation after combustion was complete. Further, the amount of N released should not decrease as residence time increases. Therefore it seems justified to assume that the data at 900°C with 21 % O_2 is erroneous.

The NO contents are given as percentages of the nitrogen in the black liquor solids. The highest NO contents corresponded to approximately 50 % of the black liquor nitrogen being converted to NO. They occurred at 1.6 s with 21 % O_2 at 900°C, at 1.1-1.6 at 1100°C with 4 % O_2, and at 0.3 s at 1100°C with 21 % O_2.

NO Formation from Combustion Air

All of the pyrolysis and combustion experiments described in the previous sections were made in nitrogen or mixtures of nitrogen and oxygen, and there may have been some formation of NO from the combustion air. This includes thermal NO and prompt NO formation. The former takes place at high temperatures and the latter early during hydrocarbon combustion. The formation of NO from the combustion air was studied here. The results are given also in the thesis by Rompho (1997).

To test whether any NO was formed from the combustion air, combustion and pyrolysis experiments in which the nitrogen was replaced by an inert gas mixture were made. The composition of the inert gas was chosen so that the heating rates were the same as with nitrogen. A mixture of 99% argon and 1% helium gave very similar heating rates as nitrogen. Figure 23 shows the temperature of black liquor particles in nitrogen, helium and the mixture of argon and helium at 900°C.

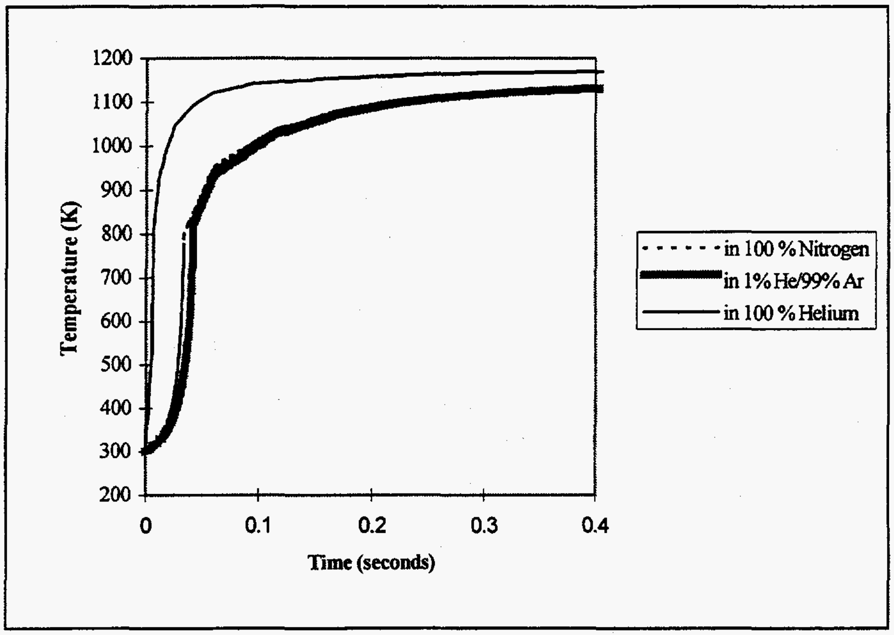

Figure 23. The temperature of 100 µm black liquor particles in nitrogen, helium, and a mixture of argon and helium in the proportion 1:99 at 900°C.

The experiments were conducted at three different temperatures, which were 700, 900, and 1100°C, and at two residence times: 0.6 and 1.6 seconds. Figure 24, Figure 25, and Figure 26 show the char yields both in nitrogen and the inert gas atmosphere.

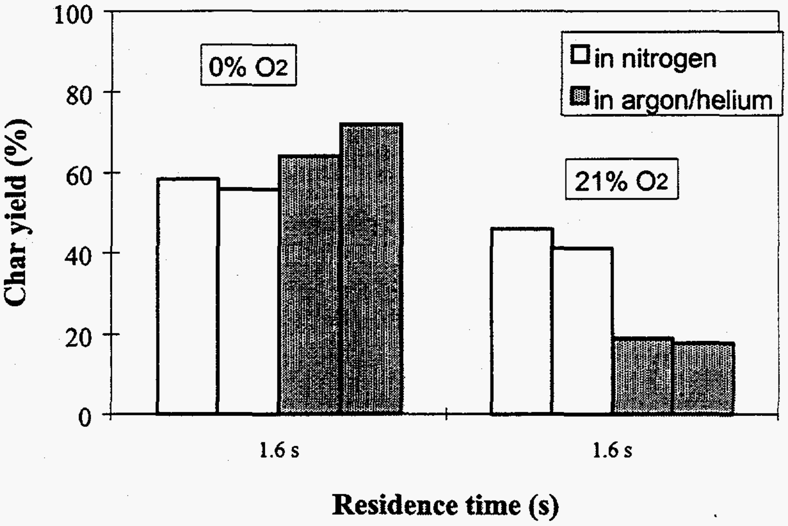

Figure 24. Char yields versus residence time at 700°C in nitrogen and the argon/helium atmosphere.

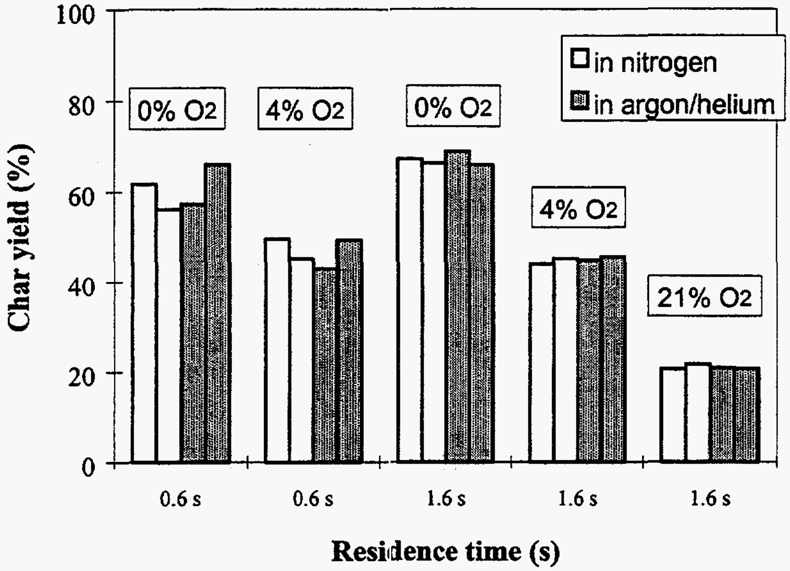

Figure 25. Char yields versus residence time at 900°C in nitrogen and the argon/helium atmosphere.

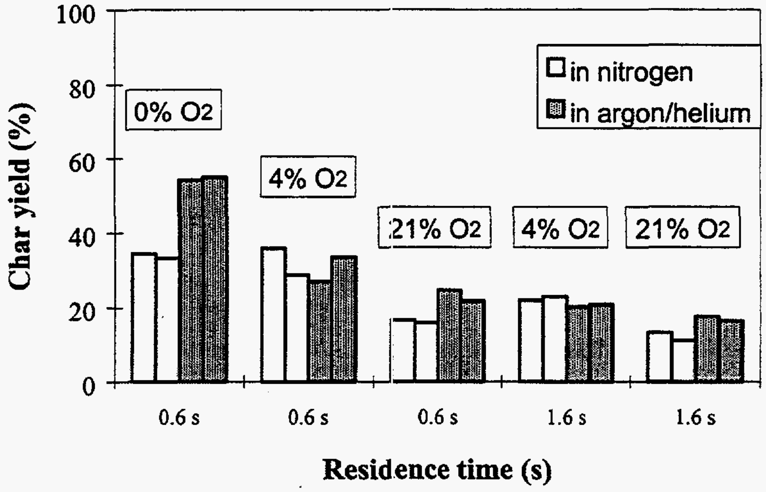

Figure 26. Char yields versus residence time at 1100°C in nitrogen and the argon/helium atmosphere.

In most cases (all data at 900° and most data at 1100°C) the char yields in N_2 and in the Ar/He mixture were the same within the uncertainty of the data. This indicates that the combustion was at the same stage at each data point, and a comparison between NO formation in the presence and absence of molecular nitrogen can be made.

The char yields during pyrolysis (0 % O_2) were slightly lower in N_2 indicating that pyrolysis may have proceeded somewhat further in N_2 than in the inert mixture. As seen in Figure 23, the heating rate was slightly higher in N_2 than in the inert mixture, which is consistent with the lower char yields. Based on the earlier data, the NO content in the pyrolysis gases either increases or decreases as a function of time depending on temperature and residence time. At 1.6 s at 900°C the NO content decreased as a function of residence time, as well as at 1100° at 0.6 s. Thus having more complete pyrolysis would yield in a lower NO content in these conditions. The pyrolysis was more complete in N_2. Consequently the observed formation of NO from nitrogen in the combustion air may be lower than if the heating rates had been exactly the same. At 700°C, the maximum in the NO content is approximately at 1.6 s, and at this condition a more complete pyrolysis might either increase or decrease the NO content. The same is true at 900°C at 0.6 s.

At 700°C with 21 % O_2 the char yield was considerably lower with the Ar/He mixture than with the N_2. This means that more combustion had taken place in the Ar/He mixture. This is expected to have a great impact on the NO formation at this condition, and this point can not be used to assess the formation of NO from combustion air. At 100°C with 21 % O_2 the char yields were also slightly lower in N_2. However, combustion is complete at both residence times, and this difference is not expected to have an impact on NO formation.

Figure 27, Figure 28, and Figure 29 show NO formation during black liquor pyrolysis and combustion with nitrogen and the argon/helium mixture. At all other conditions except at 700°C with 21 % O_2 the NO contents were higher in N_2 than in the Ar/He mixture. As discussed earlier, at 700°C with 21 % O_2 combustion had proceeded further in the Ar/He mixture, and this point can not be included in the comparison. Thus there was NO formation from the nitrogen in the combustion air at all conditions.

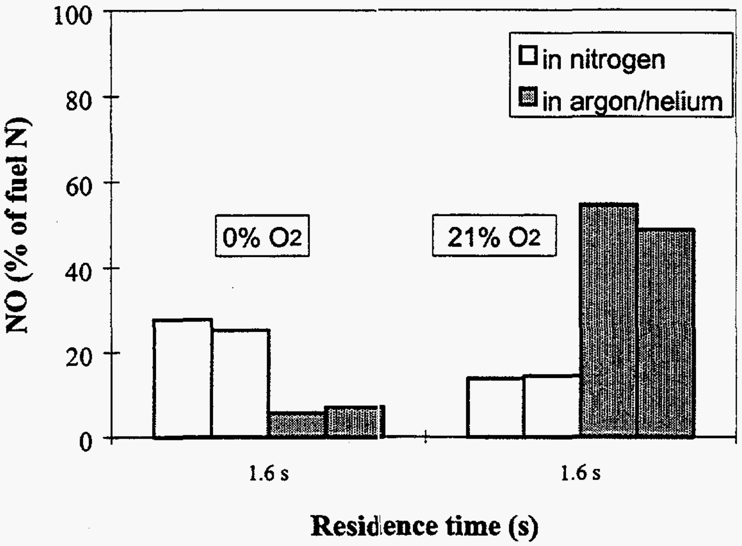

Figure 27. NO formation versus residence time at 700°C in nitrogen and the argon/helium atmosphere.

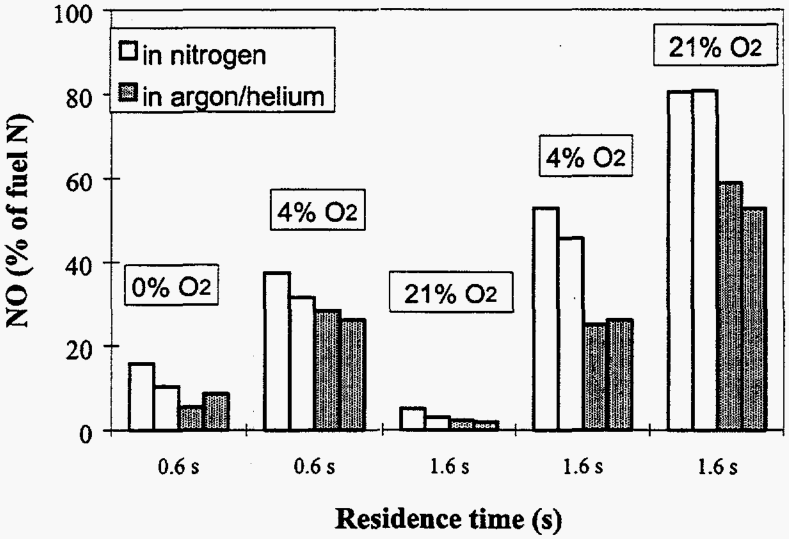

Figure 28. NO formation versus residence time at 900°C in nitrogen and the argon/helium atmosphere.

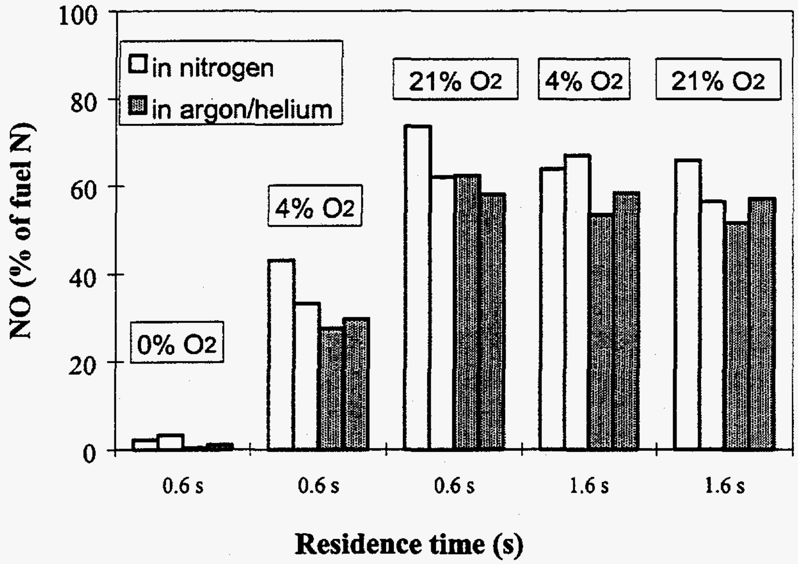

Figure 29. NO formation versus residence time at 1100°C in nitrogen and the argon/helium atmosphere.

During combustion, the difference in NO was highest at 900°C with 4 % O_2 at 1.6 s when the NO in the Ar/He mixture was only about half of that in the N_2 mixture. Combustion was still proceeding at that time. At the same temperature with 21 % O_2 at 1.6 s combustion was complete, and the NO in Ar/He was approximately two thirds of that in N_2. The differences between the N_2 and Ar/He atmospheres were smaller at 1100°C, when the NO in the Ar/He mixture was 10-15 % lower than in N_2. The difference was approximately the same whether combustion was complete or still proceeding.

Figure 30 shows the difference in NO formed in nitrogen and NO formed in the argon/helium atmosphere as a function of temperature at 1.6 seconds residence time. For all oxygen contents, the difference in NO formation decreased as temperature increased. This indicates that the NO formation from the combustion air is not thermal NO, because thermal NO formation increases rapidly with rising temperature. On the other hand, prompt NO takes place at low temperature and may decrease as temperature is increased as observed in our experiments. Therefore the results suggest that the NO formation from the combustion air in our experiments was prompt NO.

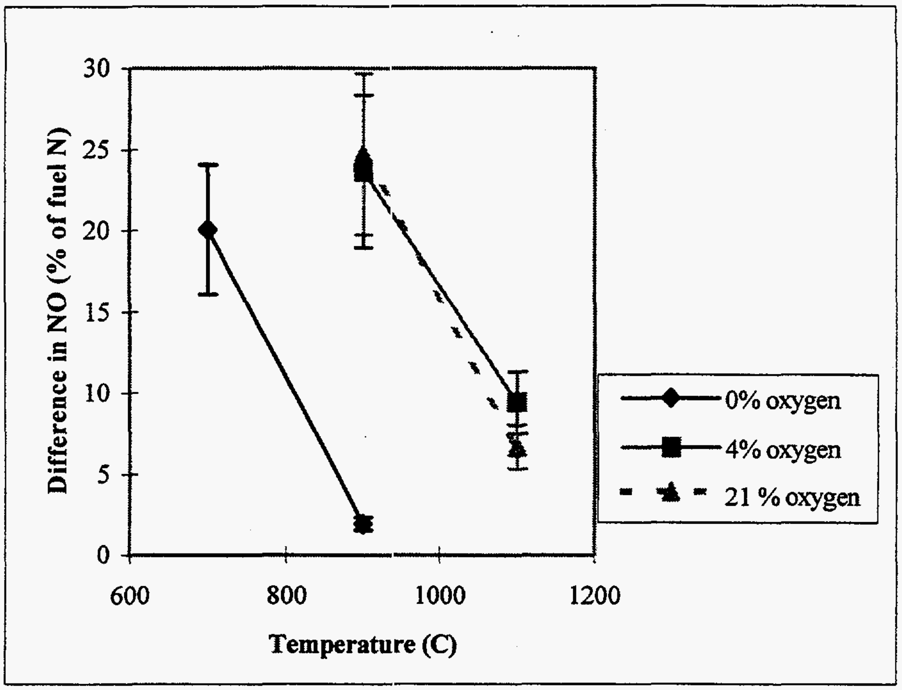

Figure 30. The difference in NO formation between N_2 and Ar/He atmosphere versus temperature at 1.6 s.

Figure 31 shows the difference in NO formed in nitrogen and NO formed in the argon/helium atmosphere as a function of residence time at 900 and 1100°C. At 900°C, and 0% oxygen, the NO formation from the combustion air or the prompt NO formation was the same at both residence times. At this condition, fast devolatilization was over by 0.6 seconds, the shorter residence time, and there was only extended pyrolysis after that. Prompt NO was thus formed during the fast initial devolatilization stage. The oxygen necessary for the NO formation comes from the volatiles released during this stage. The prompt NO corresponded to NO formation of about 5 % of fuel nitrogen.

At 900°C, in 4% oxygen, the difference in NO formation increased as the residence time increased. The char yield shows only a slight decrease and there is no change in the amount of NO in the Ar/He atmosphere. This indicated that the combustion may be just beginning. The NO from combustion air or the prompt NO corresponded to about 25 % of the fuel nitrogen. Thus the formation during early combustion was about 20 % of fuel nitrogen.

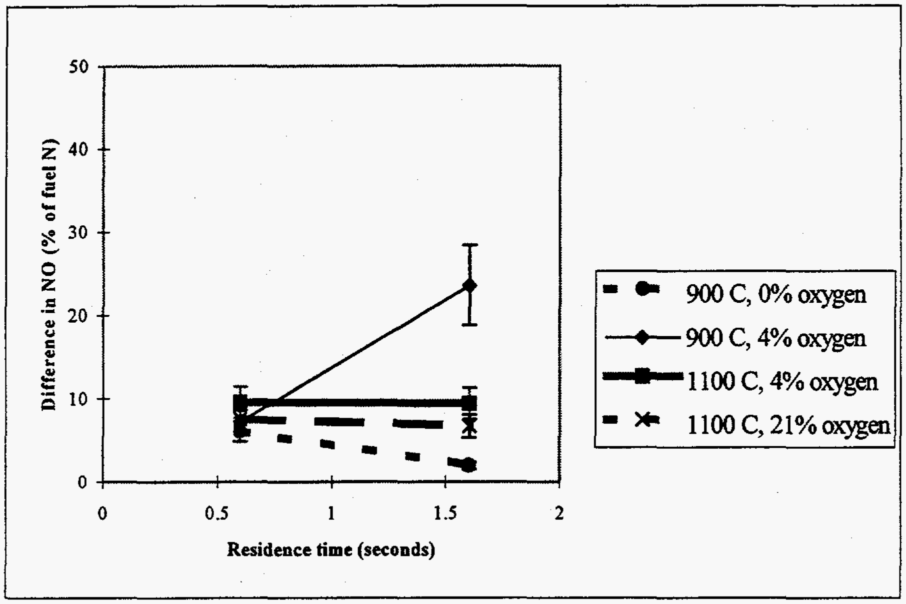

Figure 31. The difference in NO formation between N_2 and Ar/He atmosphere versus residence time.

At 1100°C, 4 and 21% oxygen, the NO formation from the combustion air was the same at a given oxygen level regardless of the residence time. With 21% oxygen, combustion was complete by 0.6 s; but with 4% oxygen, there was combustion in this time interval. There was no additional NO formation from combustion during this stage. Thus there is NO formation from the combustion air during devolatilization and early combustion. This is consistent with prompt NO formation.

Figure 32 further illustrates when during combustion prompt NO was formed. It shows the difference in NO formed in nitrogen and NO formed in the argon/helium mixture as a function of carbon release at 900°C with different oxygen contents and residence times. The amount of carbon released is an approximate measure of the completeness of combustion. At low temperatures and low oxygen contents, combustion was never complete, and the data presents what happens during pyrolysis and early combustion. On the other hand, at high temperatures and high oxygen contents, combustion was complete or nearly complete before the first data point, and the data show prompt NO formation during late combustion.

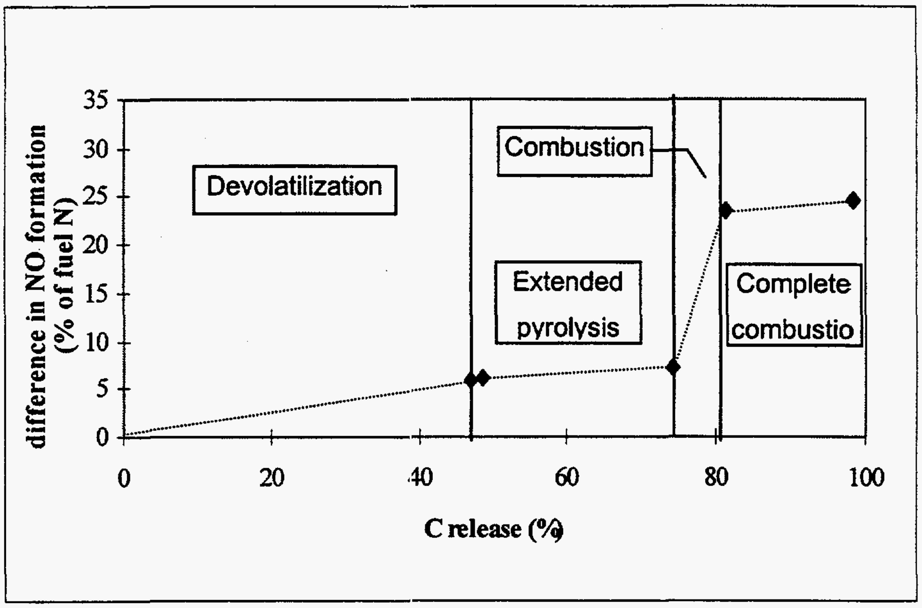

Figure 32. The difference in NO formation between N_2 and Ar/He atmosphere at 900°C versus carbon release.

The NO from the combustion air (prompt NO) was formed during devolatilization at a level corresponding to around 5% conversion of fuel nitrogen to NO as stated earlier. After devolatilization but before combustion occurred or in the extended pyrolysis stage, between 45 and 70% of carbon release, the amount of prompt NO was almost constant. Ignition then occurred between 75 and 80% of carbon release. At this stage, the amount of prompt NO formed increased rapidly to 25% of fuel nitrogen and remained constant after that. This indicates that prompt NO formation occurred at a level of 5% of fuel N during the devolatilization, and that additional 20% occurred at the beginning of the combustion stage. The amount of prompt NO remained constant after combustion was complete.

To assess if NO was formed from combustion air during the char burning stage separate experiments of black liquor char combustion were made. The char was prepared in N_2 at 1100°C at a residence time of 2.2 s. The char was then burned at 900°C for 2.2 s. One experiment was in a mixture of O_2 and N_2, the other in a mixture of O_2 and He. A high O_2 content was used. Due to an error in setting the mass flows the O_2 contents were different: 21 % in N_2 and 16 % in He. This is, however, not expected to affect the results since at both conditions the char combustion was complete. The amounts of NO formed were the same: 32.1 % in He (average of two runs) and 32.3 % in N_2. This indicates that during char combustion there is no NO formation from the combustion air. Thus the NO formation from combustion air that was observed during black liquor combustion stems from pyrolysis and volatiles burning. This further confirms that the NO is formed by the prompt NO mechanism.

Catalytic Effect of Recovery Boiler Fume Compounds on NH_3 Oxidation

NH_3 is the main fixed nitrogen compound that is evolved during black liquor pyrolysis. The impact of fume compounds on the reactions of NH_3 was studied. The results are reported in the thesis by Tangpanyapinit (1995) as well.

Objectives of the Study

The reactive intermediate NH_3, which is found during the pyrolysis of black liquor in recovery boilers as the volatile nitrogen compound, could be oxidized to NO or N_2 by many possible reactions. Fume compounds, which are produced during the process of black liquor combustion, are potential catalysts for reactions of NO_X formation and reduction. These catalytic reactions may take place in the region between the char bed surface and the upper part of the furnace.

The primary chemical components of fume are Na_2SO_4, Na_2CO_3. In addition, there are mainly potassium salts, and chlorides. The fume composition depends on combustion conditions and changes due to chemical reactions when fume is transported from the lower part of a recovery boiler (char bed) to the upper part (convective section).

The importance of catalytic NH_3 oxidation by fume compounds in recovery boilers was studied. Na_2CO_3 and Na_2SO_4, the two main constituents in fume, were used as catalysts in a fixed bed reactor.

The objectives of this work were:

1. To study the rate of NH_3 destruction and oxidation by Na_2CO_3 and Na_2SO_4
2. To investigate the effect of NO on NH_3 oxidation in the above reactions
3. To compare the catalytic activity of the two fume compounds
4. To obtain global kinetic expressions for the important reactions
5. To estimate the importance of the reactions in recovery boilers.

Experimental

Materials

Na_2CO_3 and Na_2SO_4 (fume species) were used as the catalysts in this study. Both chemicals were prepared from anhydrous granules from Mallinckrodt company. The purity of Na_2CO_3 was 99.62% and that of Na_2SO_4 99.49%.

Backman et al. (1985) had studied the kinetics of sulfation of Na_2CO_3 in artificial flue gases in the temperature range 300 °C to 700 °C. They found that the available surface area of Na_2CO_3 decreased due to sintering. To reduce the effect of sintering during the experiments, it was suggested that the compounds should be presintered before use. In this study, each sodium compound was sieved and the particle size of 90 to 125 μm in diameter was collected. This fraction was treated in a ceramic crucible in a muffle furnace at 780 °C, 1 atm for ½ hour. After cooling down, the presintered sodium compounds were sieved once again and the same particle size range (90 to 125 μm) was collected. Both untreated and presintered sodium Na_2CO_3 were analyzed for BET surface area. The BET surface area of the untreated Na_2CO_3 was 0.26 m^2/g and that of the presintered Na_2CO_3 was 0.18 m^2/g. The analysis gas was N_2.

NH_3, NO, and air were used as the reactant gases in the experiments with the following concentrations.
NH_3 : 476-514 ppm in He (differences in NH_3 concentrations due to different gas cylinders used)
NO: 2050 ppm in He (with other oxides of N <20 ppm)
Air: 21% O_2 in N_2
He: 99.999% (grade 5 high purity)

Helium was used as an inert gas to dilute the concentration of the other reactant gases and also as a purge gas to flush the experimental system.

Equipment

The fixed bed reactor used in the experiments was made of quartz glass. It had a 1.3 cm inside diameter and a length of 95 cm. A sintered quartz glass plate was used to support the fixed bed particles (Na_2CO_3 and Na_2SO_4) and it was located in the center of the reactor. Quartz wool was placed between the fixed bed particles and the sintered quartz glass to avoid direct contact of these two materials. This prevented the catalyst particles from depositing in the pores of the sintered glass, which might have caused errors in the subsequent experiments, in particular, in empty bed tests or in experiments with the other catalyst. Na salts may have also reacted with the sintered quartz.

In this study, a Fourier Transform Infrared Spectrometer was used for the quantitative analysis of nitrogen compounds (NH_3 and NO) in the reactants and the gaseous products. The spectrometer used in these experiments was a Bomem MB100 mid IR FT-IR with a 7 meter pathlength gas cell.

A calibration curve for each interesting gaseous species (NH_3 and NO) was prepared before doing all the quantitative analysis. The wavelengths used for the NH_3 analysis were 980-900 cm^{-1}, and the wavelengths used for NO were 1970-1780 cm^{-1}. An average reproducibility of the measurements was better than 3%.

A Teflon FEP gas sampling bag was used to collect the outlet gas from the reactor and to supply it to the FT-IR for gas analysis.

The experimental equipment was set up according to the schematic diagram shown in Figure 33. Reactant gases flowed through rotameters, and were mixed. The mixed gas was led to the three-way valve, which was used to select the path between by-pass and reactor. The by-pass was selected when the initial concentrations of the reactants in the mixed gas were to be analyzed. In the reactor path, the mixed gas flowed downward through the heated fixed bed reactor, which contained a known amount of the catalyst. The gas lines from the reactor and from the by-pass were joined and connected to the other three-way valve, which was used to select between exhaust line or sampling line. The sampling line was connected to the gas sampling bag, which was used to collect the outlet gas for analysis.

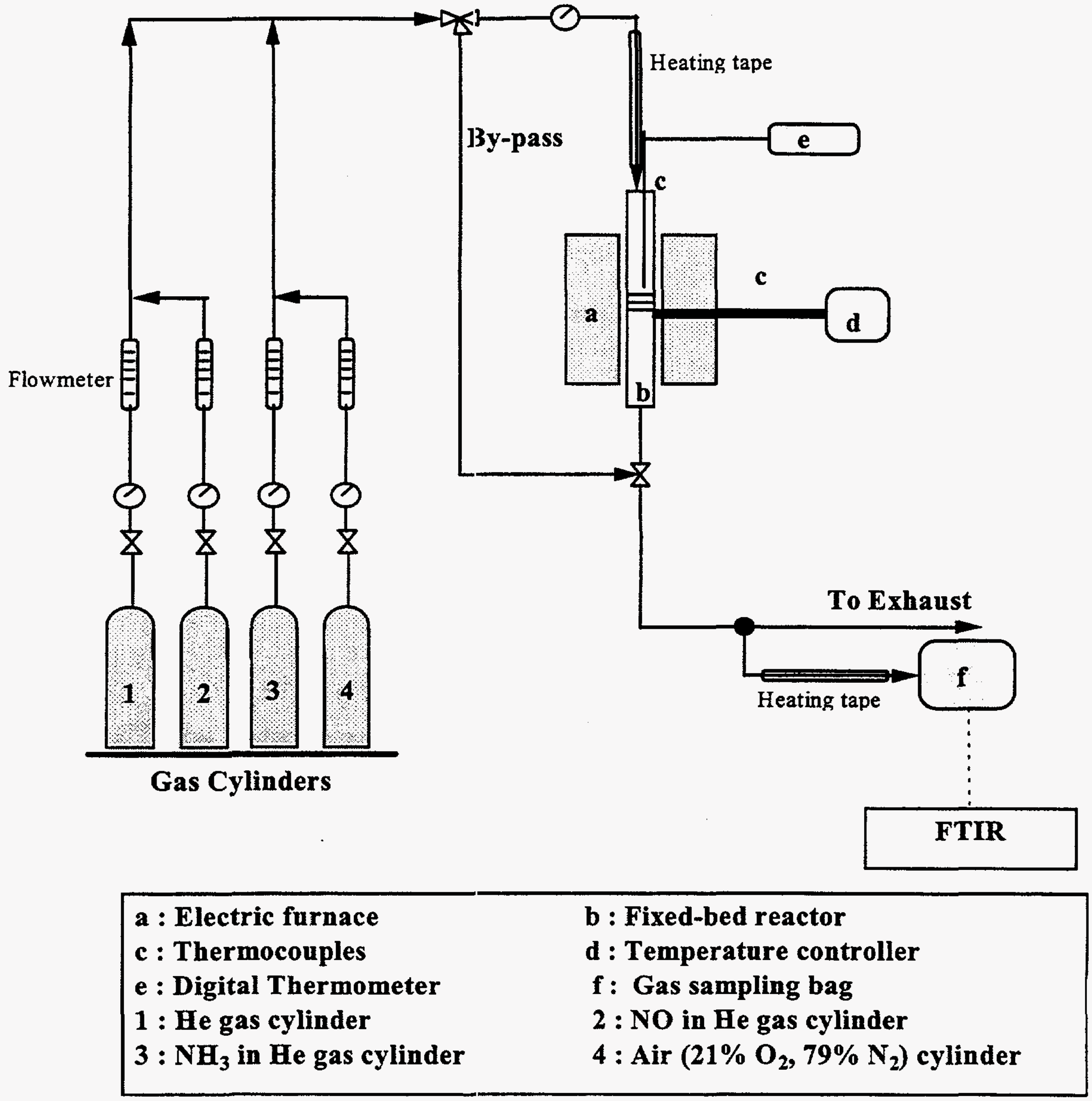

Figure 33. Schematic diagram of the experimental equipment setup.

Experimental Method

A predetermined amount of the presintered Na_2CO_3 or Na_2SO_4 was placed on quartz wool, which was held by a fritted quartz glass at the center of the reactor. Both ends of the reactor were connected to the gas lines. The fixed bed reactor was set to be at the center of a cylindrical furnace in both vertical and radial directions. The furnace was heated up to the lowest experiment temperature (550 °C) at the rate of about 10 °C/min. During the heating process, there was a He flow of 13.0 cm^3/sec (25 °C, 1 atm) through the reactor to purge the system.

Before the temperature reached the set point (at approximately 500 °C), the gas was switched to by-pass the reactor and the gas flows were set to those of the experiment. After the gas flows had stabilized in about 5 minutes, a sample was taken to analyze the concentration in the reactor inlet gas. The gases by-passed the reactor, and the outlet was taken through the sampling line, which was connected to the gas sampling bag. When the sampling bag was nearly filled up to its full capacity (4.7 liters), the increase of gas pressure in the sampling bag caused the gas flow rates to decrease. To reduce this problem, the sampling bag was filled with the outlet gas to less than its full capacity but enough for gas analysis each time. The sample was immediately taken to the Fourier Transform Infrared Spectrometer (FT-IR) for analysis. Two samplings were conducted for one gas analysis. The first sampling was used to flush the gas chamber of the FT-IR, and the second sampling was used for gas analysis by the FT-IR. At least two samples were made at each experiment, and the average value of the gas concentrations was calculated. After each sample collection, the sampling bag was evacuated to be ready for being used again.

After the samples of the reactor inlet gas were taken, the gas was switched back to flow through the reactor. The same reactant gas flow rates were used as when the samples of the by-pass gas were collected. After the reactant gases had flowed for about 10 minutes through the reactor, the outlet gas was collected and analyzed by the FT-IR. After at least two samples for the FT-IR were taken, the flows of the reactant gases were stopped. He was used to purge the system again, while the temperature in the reactor was increased to the next set point. The same steps of experiment were repeated.

When measuring the gas concentrations with the FT-IR, the FT-IR detector was first filled with liquid nitrogen. The gas sampling chamber was preheated by electrical heating to above 70 °C to prevent gas adsorption from the sample on the gas chamber walls. Before starting the sampling, He was used to flush the gas chamber for at least five minutes to purge all undesired gas residual from inside the chamber. Then the sampling chamber was evacuated and the inlet gas line was connected to the gas sampling bag. The gas chamber was flushed with the sample gas with almost its volume capacity (about 1.2 liters) and was evacuated. For the measurement, the inlet valve was left open to let the gas flow into the chamber until the pressure in the chamber was at atmospheric pressure. After finishing the scanning, the chamber was evacuated and was prepared by the same steps to be ready for the next analysis.

Experimental Conditions

The importance of external mass transfer (film diffusion) limitation was tested by experiments at the same residence time but with different gas flow rates and different catalyst weights at the highest temperature studied (750 °C). The rate data obtained were also used to estimate the effect of film mass transfer by comparing to the Mears' criterion (Fogler, 1992). The importance of internal mass transfer (pore diffusion) effect was tested by the Weisz-Prater criterion (Fogler, 1992).

In order to obtain the rate constants and the activation energy, each reaction was studied at five different temperatures: 550, 600, 650, 700, and 750 °C. Two initial concentrations of NH_3, 250 and 500 ppm, were used in these tests. In order to obtain the reaction order, the analysis method was determined first. For differential reactor, only the inlet concentration of NH_3 was varied in the experiments (Levenspiel, 1972). For integral reactor, the ratio between the weight of the catalyst and the volumetric gas flow rate was varied in the experiments (Levenspiel, 1972). A summary of all the experimental conditions is shown in Table 4.

Table 4. The experimental conditions studied.

Na_2CO_3 (particle size 90-125 μm)	0.38-3.0±0.1 g			
Inlet gases	Temp., °C	NO inlet, ppm	NH_3 inlet, ppm	Flow rate, cm^3/s
NH_3	550-750	--	115-500	13.0
NH_3+NO	550-750	250-1250	150-400	13.0
NH_3+O_2 (1% O_2)	550-750	--	250,500	6.3, 13.0
NH_3+O_2+NO (1% O_2)	550-750	250	250	13.0
Na_2SO_4 (particle size 90-125 μm)	3.0±0.1 g			
Inlet gases	Temp.,°C	NO inlet, ppm	NH_3 inlet, ppm	Flow rate, cm^3/s
NH_3	550-750	--	500	13.0
NH_3+NO	550-750	250	250	13.0
NH_3+O_2 (1% O_2)	550-750	--	500	13.0
NH_3+O_2+NO (1% O_2)	550-750	250	250	13.0

Results and Discussion

Four catalytic reactions were studied in the temperature range from 550 °C to 750 °C. They were decomposition of NH_3 in the absence of any oxidative gases (referred to as NH_3 reaction in the following), decomposition and oxidation of NH_3 in the presence of NO (referred to as NO + NH_3 in the following), destruction and oxidation of NH_3 in the presence of O_2 (referred to as NH_3 + O_2), and decomposition and oxidation of NH_3 in the presence of both O_2 and NO (referred to as NH_3 + O_2 + O_2). Two species of fume compounds (Na_2CO_3, and Na_2SO_4) were used in the experiments as the catalysts. All the experiments were conducted in a fixed bed reactor. The inlet and outlet concentrations of NH_3 and also those of NO, were measured in each experiment.

Reactions in an Empty Bed

The purpose of the experimental runs in the empty bed was to test whether there were gas phase reactions or catalytic effects of the reactor materials on the NH_3 reactions. If the effects were *significant, the empty bed reaction kinetics would be used to correct the kinetic data obtained for* the fume catalytic reactions.

In the empty bed tests, all reactor materials (quartz wool and fritted quartz glass), except fume compounds were the same as in the fume catalytic experiments. Reactions of NH_3 (with inlet NH_3 = 500 ppm), NH_3+NO (with inlet NH_3 = 250 ppm, NO = 250 ppm), NH_3+O_2 (with inlet NH_3 = 500 ppm, 1% O_2), and NH_3+O_2+NO (with inlet NH_3 = 250 ppm, NO = 250 ppm, 1% O_2) were tested at 550 °C, 650 °C, 700 °C and 750 °C at the same total gas flow rate of 13 cm^3/s. Figure 34 shows the NH_3 conversions of all the reactions in the empty bed in the temperature range studied. At the temperature of 650 °C and lower, there was no NH_3 conversion detected for any of the reactions studied but some at the highest temperature studied (750 °C) for all of them. At 750 °C, for the reactions NH_3, and NH_3+O_2 the conversions of NH_3 were 5%, and 8%, respectively, and no NO was detected. For the reactions NH_3+NO, and NH_3+O_2+NO at 750 °C, the conversions of NH_3 were 10%, and 15%, respectively. The outlet NO concentrations in both the reactions were unchanged from the inlet concentrations.

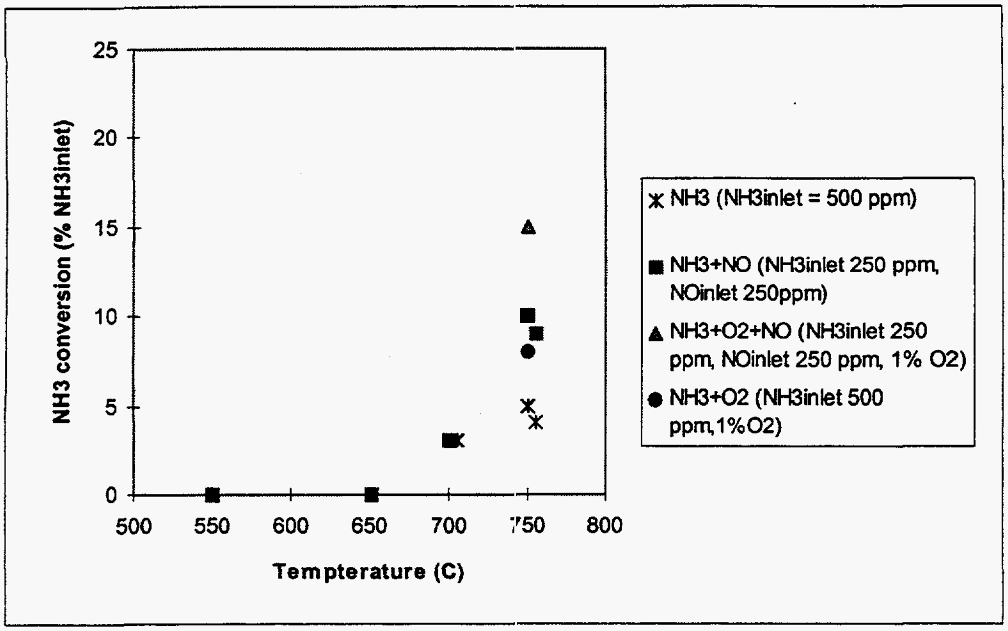

Figure 34. NH_3 conversions as a function of temperature in the empty bed experiments.

Conversion with Na_2CO_3 as a Catalyst

Reactions in the Absence of O_2

The conversions of NH_3 as a function of temperature are shown in Figure 35 for the reactions of NH_3, and NH_3+NO with Na_2CO_3 as the catalyst in the reactor bed. The inlet concentration of NH_3 was 500 ppm in the absence of NO. When both NO and NH_3 were present in the inlet gases, the concentrations of NH_3 and that of NO were equal (250 ppm). In each run, the total gas flow rate was 13 cm^3/s at 25 °C and the amount of Na_2CO_3 used was 3.0 g. For both reactions, the conversion of NH_3 increased with increasing temperature, and the conversion was slightly higher in the presence of NO. With and without NO, the conversions of NH_3 were less than 5% at 600 °C or below. At 750 °C, the conversions of NH_3 were 25-26% without NO and 25-30% with NO.

The NO conversion for the NO + NH_3 is shown in Figure 36. It increased with increasing temperature and was less than 5% at 600 °C or below and was approximately 17 % at 750 °C. The NO conversion was lower than the corresponding NH_3 conversion for this reaction (e.g., at 750 °C 17 vs. 28 %). However, the NO conversion was significantly higher than the difference between the NH_3 conversion in the presence and absence of NO (28 % vs. 25 % at 750 °C).

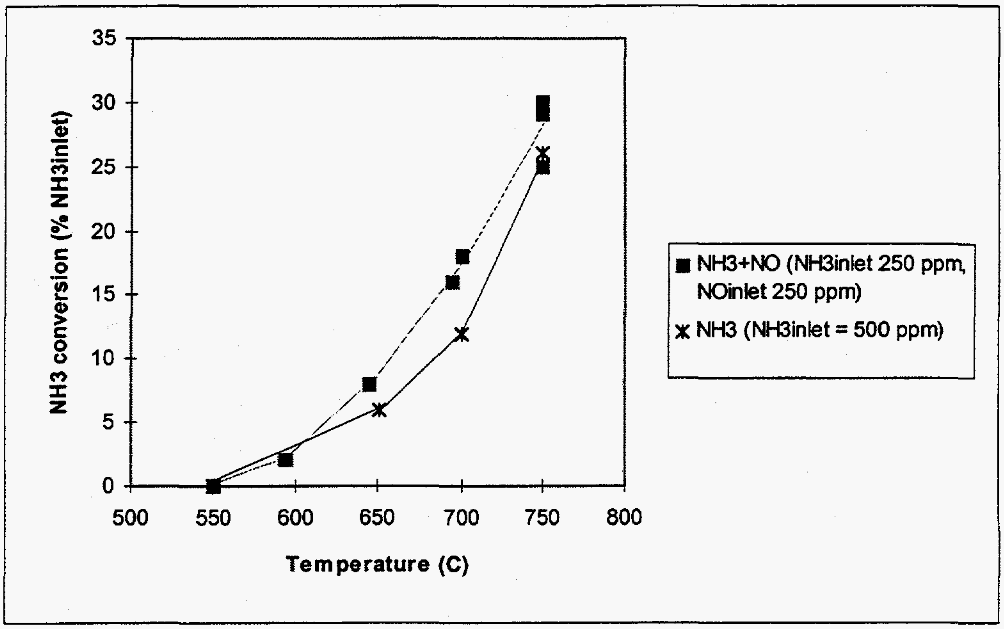

Figure 35. NH_3 conversions as a function of temperature of the catalytic reactions NH_3, and NH_3+NO with 3.0 g Na_2CO_3 and a total flow rate of 13 cm^3/s at 25 °C.

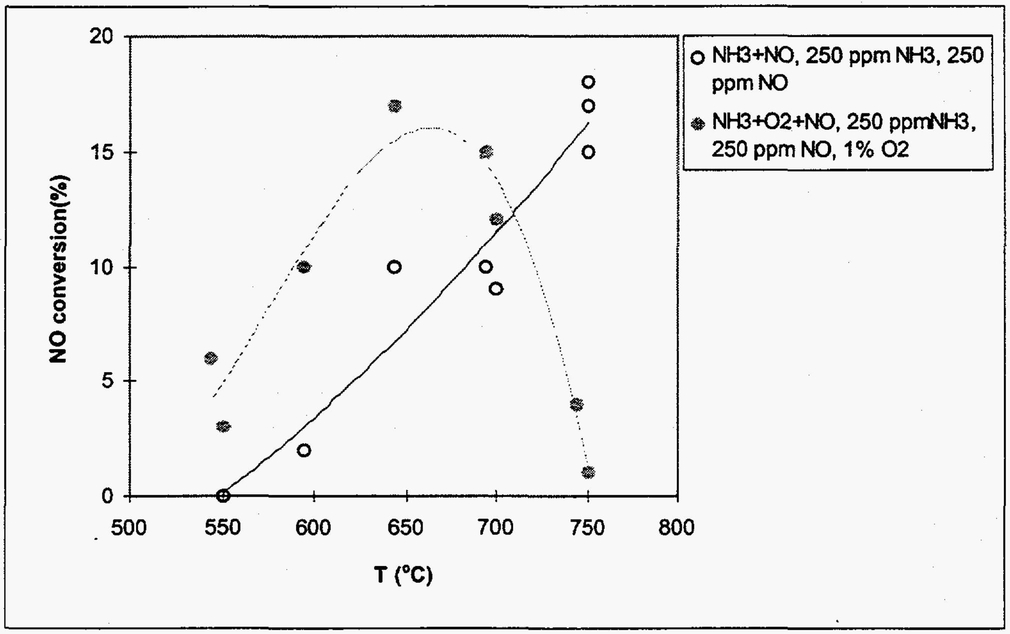

Figure 36. NO conversions as a function of temperature for the reactions NH_3+NO and NH_3+O_2+NO, 3.0 g Na_2CO_3 at a total flow rate of 13 cm3/s at 25 °C.

Reactions in the Presence of O_2

Figure 37 illustrates the conversion of NH_3 in the presence of O_2 both with and without NO (NH_3+O_2 and NH_3+O_2+NO) as a function of temperature. The total gas flow rate was 13 cm^3/s, mass of Na_2CO_3 3.0 g, and O_2 concentration 1 %. For the reaction of NH_3+O_2, two different inlet concentrations of NH_3 - 250 ppm and 500 ppm - were tested. The NH_3 conversions increased with temperature and were significant at temperatures higher than 550 °C and almost 100% at 750 °C.

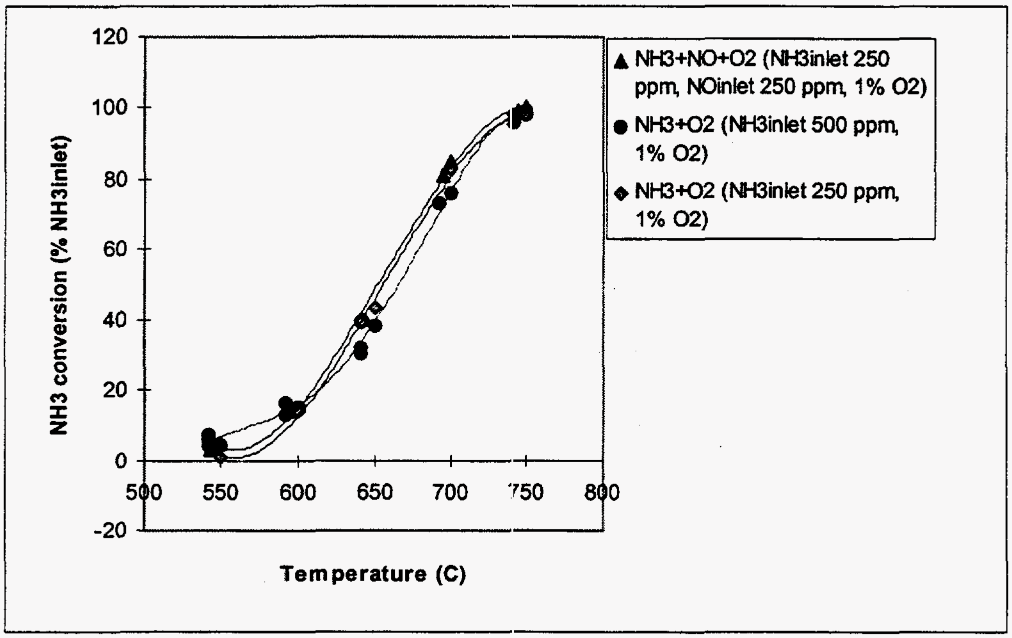

Figure 37. NH_3 conversions as a function of temperature of the catalytic reactions NH_3+O_2 and NH_3+O_2+NO, 3.0 g Na_2CO_3 at a total flow rate of 13 cm^3/s at 25 °C.

For the reaction NH_3+O_2, the conversions of NH_3 were close with the two NH_3 concentrations: The difference was less than 1 percentage point at 550-650 °C. At 650 °C and 750 °C, the conversion was slightly higher with the lower NH3 concentration. The presence or absence of NO did not make a significant difference in the NH_3 conversion.

When only NH_3 and O_2 (and inert gases) were present in the reaction gases, NO was found as one of the products. Figure 38 shows the NO production based on the inlet concentration of NH_3 as a function of temperature for the NH_3+O_2 reaction. The amount of NO formed increased as temperature was increased, was less than 5 % at 550-600 °C and 28-38 % at 750 °C. As the Figure shows, at each temperature, the fractions of NH_3 that formed were almost the same regardless of the NH_3 conversion.

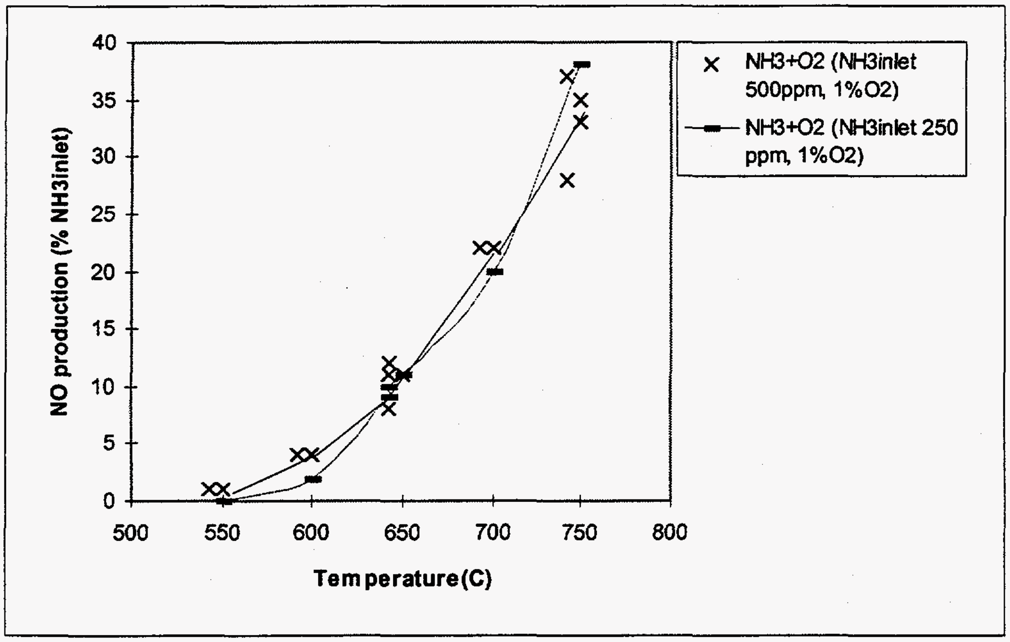

Figure 38. NO production as a function of temperature for the NH_3+O_2 reactions with two different NH_3 inlet concentrations (500 ppm and 250 ppm), 3.0 g Na_2CO_3 at a total flow rate of 13 cm^3/s at 25 °C.

The amounts of NO produced were not equal to the amounts of NH_3 converted. This is because NH_3 could decompose by itself, and NO could be reduced by NH_3 or the products of NH_3 destruction. Figure 39 shows the ratio of moles NO produced per mole of NH_3 reacted. The data in this Figure have more scatter than the data of NO production based on inlet NH_3. A possible explanation is that the effects of any errors in the amounts of NO produced are magnified by the smaller values of denominators (NH_3 reacted < NH_3 inlet). Any errors in the amount of NH_3 reacted also contribute to the scatter.

At most temperatures (550-700 °C), the fraction of NH_3 that exited as NO was higher with the higher NH_3 inlet concentration. It is not known if this a true effect or the result of errors in the measurements. At 650 °C, the fraction of inlet NH_3 that exited as NO seemed to be the same regardless of the NH_3 concentration but the overall conversion of NH_3 was lower for the higher NH_3 concentration. On the other hand, at 600 °C the overall NH_3 conversion seemed to be the same regardless of the NH_3 concentration but the fraction of the inlet NH_3 that exited as NO was higher with the higher NH_3 concentration.

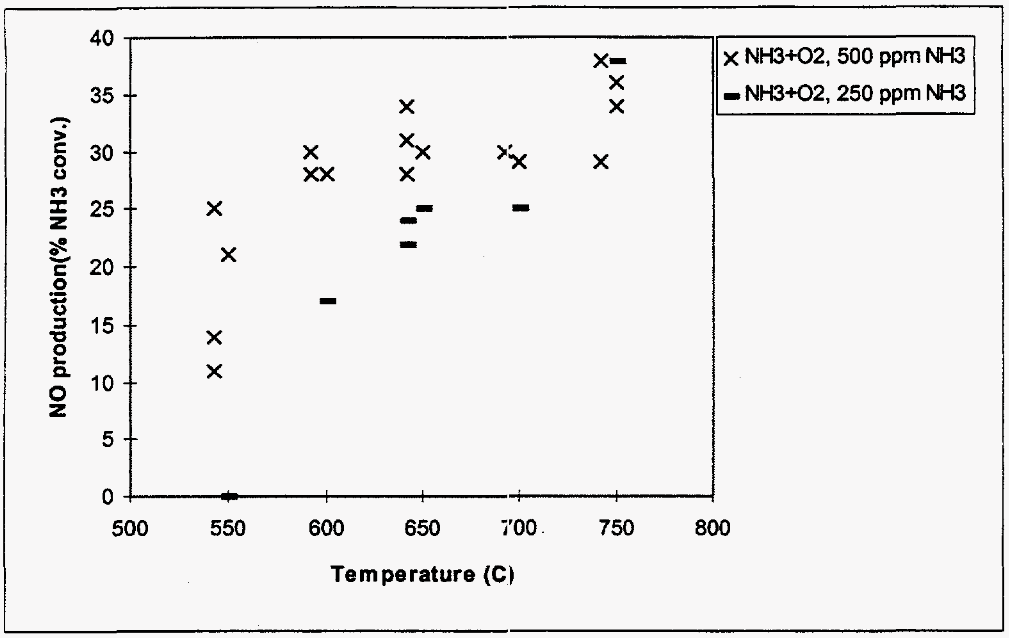

Figure 39. Moles of NO produced per mole of NH_3 reacted as a function of temperature for the NH_3+O_2 reaction with two different NH_3 inlet concentrations (500 ppm and 250 ppm), 3.0 g Na_2CO_3 at a total flow rate of 13 cm^3/s at 25 °C and 1 % O_2.

The data seems to suggest that the fraction of NH_3 reacted that exited as NO increased as temperature was increased. At 600-700 °C, the average fractions of NH_3 that reacted to NO were 26-28 % and at 750 °C it was 35 %.

In the presence of NH_3, NO and O_2, the outlet NO concentration was always lower than the inlet NO concentration. The NO conversions were shown in Figure 4. There was a maximum in the No conversion. The NO conversion was about 5 % at 550 °C, increased to 17 % as temperature was increased to 650 °C and was less than 5 % at 750 °C. An explanation for the decreasing conversion is that the rate of NH_3 oxidation increases more rapidly than the rate of NO reduction as temperature is increased from 650 °C to 750 °C.

Conversion with Na_2SO_4 as a Catalyst

The same amount of bed material (3.0 g±0.1g) was used in the tests with Na_2SO_4 as in the tests with Na_2CO_3. All other conditions were the same as well.

Reactions in the Absence of O_2

Figure 40 shows the NH_3 conversion as a function of temperature with only NH_3 in the inlet gases, and that with NH_3 and NO. The highest conversion of NH_3 without NO was less than 5%, while for the reaction of NH_3+NO, the highest conversion was 7% at 750 °C. The conversions in the empty bed experiments were 5% for NH_3 and 10% for NH_3+NO. For the NH_3+NO reaction, the outlet concentration of NO did not change from the inlet concentration at any temperatures studied, which is the same result as in the empty bed. The results thus indicated that the decomposition of NH_3 or the oxidation of NH_3 by NO in the absence of O_2 was not catalyzed by Na_2SO_4 at the conditions studied.

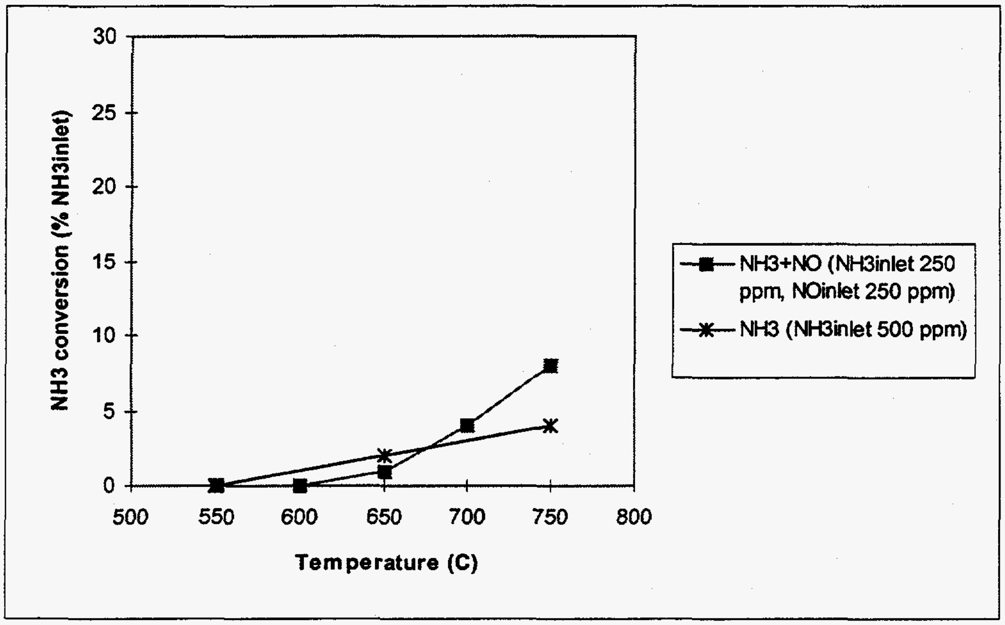

Figure 40. NH_3 conversions as a function of temperature for the catalytic reactions of NH_3 and NH_3+NO, 3.0 g Na_2SO_4, at a total flow rate of 13 cm^3/s at 25 °C.

Reactions in the Presence of O_2

The graphs between NH_3 conversion and temperature for the reactions with in the presence of O_2 are shown in Figure 41. Only one inlet NH_3 concentration, 500 ppm, was used in the experiments with Na_2SO_4 for the reaction of NH_3+O_2. For the NH_3+O_2 reaction, the NH_3 conversions were less than 10% and no NO was produced at 700 °C or below. The highest conversion of NH_3 was 17% and the highest NO outlet concentration was 6 ppm. These were higher than the values in the empty bed experiments (8% NH_3 conversion, and no NO produced) at 750 °C. For the reaction

NH_3+O_2+NO, 10% of NH_3 inlet or less was converted at 700 °C or below. At 750 °C, the NH_3 conversion was 22%, which was higher than the conversion in the empty bed experiment (15%). The outlet NO concentration was always within 3 % of the inlet NO concentration.

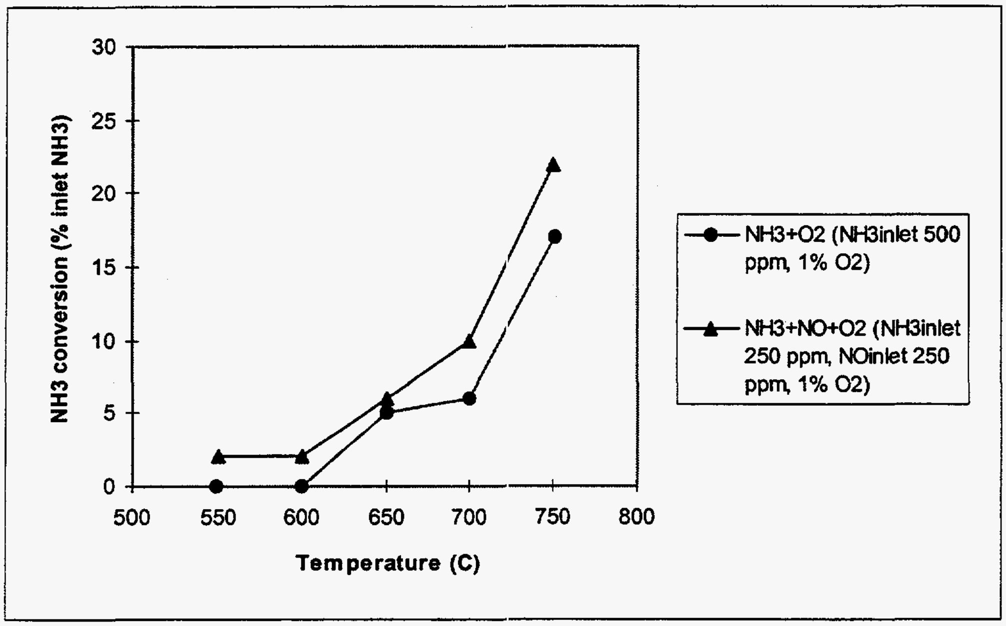

Figure 41. NH_3 conversions as a function of temperature for the catalytic reactions NH_3+O_2, and NH_3+O_2+NO, 3.0 g Na_2SO_4, at a total flow rate of 13 cm^3/s at 25 °C.

Summary of Initial Tests

The NH_3 conversion data in the empty bed indicated that there were no gas phase reactions or catalytic effect of the reactor materials at 650 °C or below. There was some reaction at 700-750 °C (5-15 % conversion). In the absence of O_2, the NH_3 conversions in the empty bed were about 25% to 30% of the conversions in the Na_2CO_3 bed at the highest temperature and were equal to the conversions in the Na_2SO_4 bed. In the presence of O_2, the NH_3 conversions in the empty bed were 8% to 15% of the conversions in the Na_2CO_3 bed and were 50% to 70% of the conversions in the Na_2SO_4 bed at 750 °C.

With both bed materials, the NH_3 consumption was considerably higher in the presence of O_2 than in the absence of O_2 above 550 °C. In the presence of O_2, the highest conversions over Na_2CO_3 were approximately 100% at 750 °C, while without O_2 they were 25-30%.

Over the Na_2SO_4 bed the highest conversions with O_2 were 17-22%, while without O_2 they were 4-7% at 750 °C. The comparison with the empty bed data showed that Na_2SO_4 had no catalytic effect of in the absence of O_2 at any temperature studied. The catalytic effect in the presence of O_2 initially showed at 750 °C but the effect was minor when compared that over the Na_2CO_3 bed.

In conclusion, the data indicated that Na_2CO_3 had a higher catalytic effect than Na_2SO_4 did on the reactions. Therefore, only the kinetics of the reactions in the Na_2CO_3 bed were to be studied further. The data of all the reactions in the Na_2CO_3 bed should be corrected with the empty bed data except at 550-600 °C.

Global Catalytic Reaction Rate for the Destruction and Oxidation of NH_3 over Na_2CO_3

Kinetic data for each reaction over Na_2CO_3 was obtained by either differential reactor or integral reactor analysis. The maximum conversion of NH_3 for each reaction was considered the main factor in selecting the interpretation method. Different experiments were used for differential reactor and integral reactor analysis to obtain data for the determination of the reaction orders and the rate constants.

In the absence of O_2, the highest percentage conversions of NH_3 at the studied experimental conditions were less than 45%, and differential reactor analysis was accepted. The following equation was used.

$$\text{Eq. 5:} \quad -r'_{NH3,ave} = \frac{F_{NH3,o} \cdot X_{NH3}}{W} = k' C^{n}_{NH3,ave}$$

The experiments were conducted by varying the inlet concentration of NH_3. A graph between $\ln(-r'_{NH3,ave})$ and $\ln(C_{NH3,ave})$ should give a straight line whose slope equals the reaction order (n). The interception with the Y-axis can be used to determine the rate constant k'.

In the presence of O_2, the highest percent conversions of NH_3 were almost 100% at the experimental conditions studied. Integral analysis of the integral reactor was used for these reactions. The following equations were used for this analysis method in the interpretation of the experimental data

$$\text{Eq. 6:} \quad (n=1): \; k'\frac{W}{F_{NH3,o}} = -\ln(1-X_{NH3})\frac{1}{C_{NH3,o}} \equiv Y_{1st}$$

$$\text{Eq. 7:}\quad (n \neq 1):\ k'\frac{W}{F_{NH3,o}} = \{\frac{1}{(1-n)} - \frac{1}{(1-n)}.(1 - X_{NH3})^{(1-n)}\}\frac{1}{C^{n}_{NH3,o}} \equiv Y_{nth}$$

These equations can be derived by integration of the nth order performance equation in a plug flow reactor ($-r' = V/W*dc/dt = k'c^n$ and the substitution $X = 1-c/c_o$).

The experiments were performed by varying W, while the other experimental variables were kept constant. If a straight line through the origin is obtained for a plot of $-\ln(1-X_{NH3})/c_{Nh3,o}$ versus $W/F_{NH3,o}$,, the reaction can be regarded to be of first order with respect to NH_3 concentration. The slope of the line is then equal to the reaction rate coefficient. For an nth order reaction a plot of Y_{nthh} versus W/F_{NH3} should similarly yield a straight line through the origin with the slope equal to k'. Y_{nth} depends on the reaction order (n), and therefore a trial and error method is used to select the line that gives the best linear fit. The value of n that gives the smallest sum of square of errors could be selected as the reaction order n.

Destruction of NH_3 in the Absence of NO and O_2

The experiments to find the reaction order were performed by varying the inlet concentration of NH_3 from 115 to 500 ppm at the same total flow rate (13.0 cm^3/s at 25 °C), amount of Na_2CO_3 (3.0 g) and temperature (750 °C). The NH_3 conversions at the different NH_3 inlet concentrations are shown in Table 5.

Table 5. NH_3 conversions at the different NH_3 inlet concentrations with 3.0 g Na_2CO_3, total flow of 13.0 cm^3/s (at 25 °C) at reactor temperature 750 °C.

NH_3 inlet concentration (ppm)	NH_3 conversion (%)
455	26
453	25
274	27
243	34
115	45

The NH_3 conversions depended on the inlet concentrations of NH_3. The lower the concentration of NH_3, the higher the conversion of NH_3 was. This implied that the reaction order was lower than first order. The plot of $\ln(-r'_{NH3,ave})$ and $\ln(C_{NH3,ave})$ according to the differential reactor analysis is shown in Figure 42. The reaction order value obtained is 0.53 with respect to NH_3 concentration.

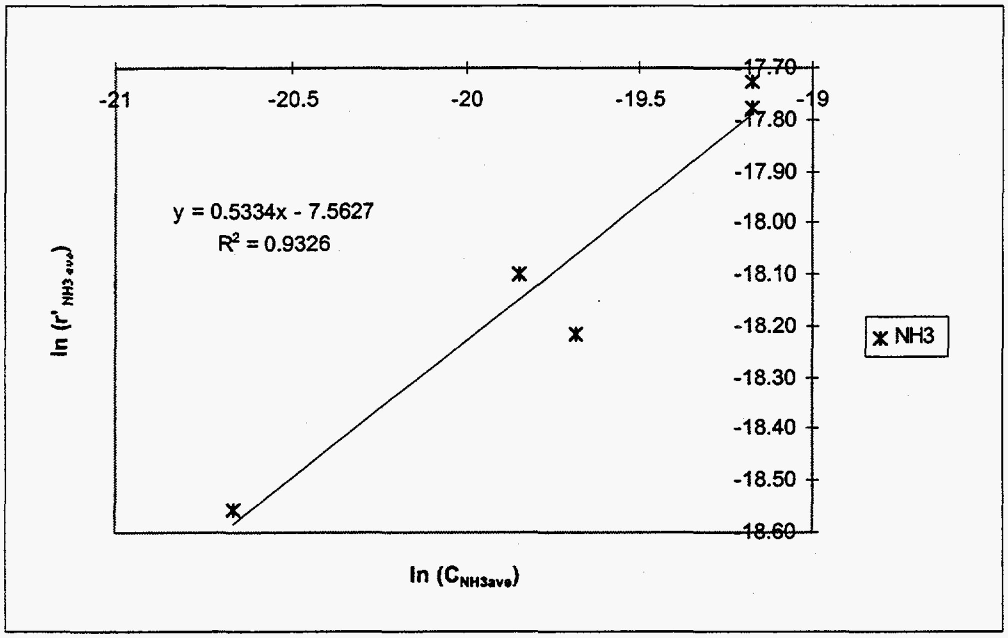

Figure 42. Differential reactor analysis of the NH3 reaction with NH3 = 115 to 500 ppm, and 3.0 g Na_2CO_3, total flow 13.0 cm^3/s 25 °C at 750 °C.

NH_3+NO

The effect of NO on NH_3 conversion was tested by varying the inlet concentration of NO from 0 to 1253 ppm while the inlet concentration of NH_3 was kept constant at 250 ppm. The total flow rate was 13 cm^3/s at 25 °C and the experimental temperature was 750 °C. The amount of Na_2CO_3 used was 3.0 g. Figure 43 shows the relationship between NH_3 and NO conversions and the inlet concentration of NO. There was little variation in the NH_3 conversion as the NO concentration was changed: Without NO, the NH_3 conversion was 34 %. It decreased to an average of 28% at 250 ppm NO. As the concentration was further increased from 250 to 1250 ppm, the NH_3 conversion again increased to 34%.

One possible explanation for this behavior is that, initially, when NO is added, the rate of NH_3 disappearance decreases because NO occupies catalytic sites and prevents NH_3 from adsorbing on them. As the NO concentration is further increased, the rate of the reaction between NH_3 and

NO increases and the overall effect is that the rate of NH_3 disappearance increases. For the purpose of this work, however, it seemed that the effect of NO on the NH_3 conversion was insignificant. Therefore the global rate of NH_3 destruction in the presence of NO but absence of O_2 was based on NH_3 concentration only.

The NO conversion is shown in the same figure. Even though the NO did not significantly impact the NH_3 conversion No was consumed. The moles of NO consumed per mole of NH_3 consumed varied from 0.58 to 0.93, and were highest at high NO concentrations. The effect of NO on NO conversion is discussed separately in the section on global rates for NO destruction.

Experiments in which the inlet concentration of NH_3 was varied, were conducted at the same conditions (3.0 g Na_2CO_3, 13 cm^3/s total flow, 750 °C). The inlet NH_3 concentration was varied from 150 to 400 ppm while the inlet concentration of NO was constant at 250 ppm. Figure 44 shows the relationship between NH_3 and NO conversions and the inlet concentration of NH_3.

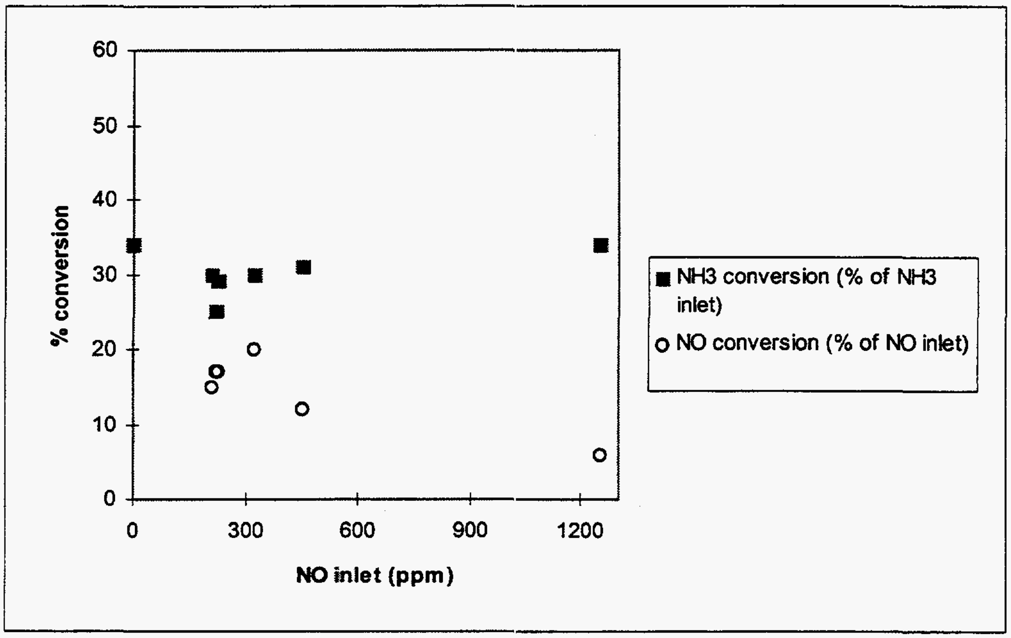

Figure 43. Effect of inlet NO concentration on NH_3 conversion and NO conversion with 0-1250 ppm NO and 250 ppm NH_3, and 3.0 g Na_2CO_3, 13 cm^3/s total gas flow and 750 °C.

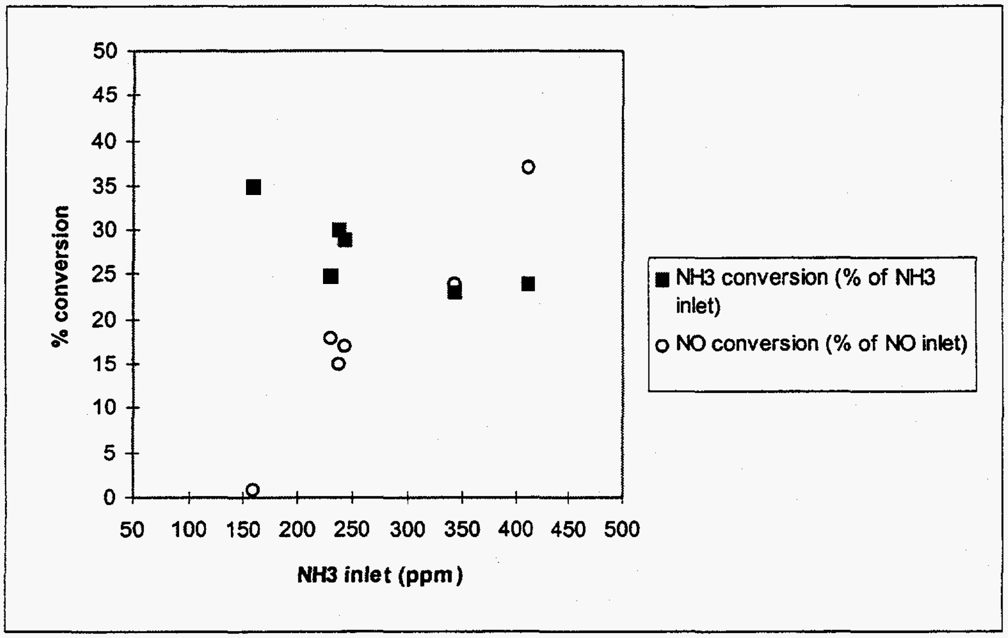

Figure 44. Effect of inlet NH_3 concentration on NH_3 conversion and NO conversion with 0-1250 ppm NO and 250 ppm NH_3, and 3.0 g Na_2CO_3, 13 cm^3/s total gas flow and 750 °C.

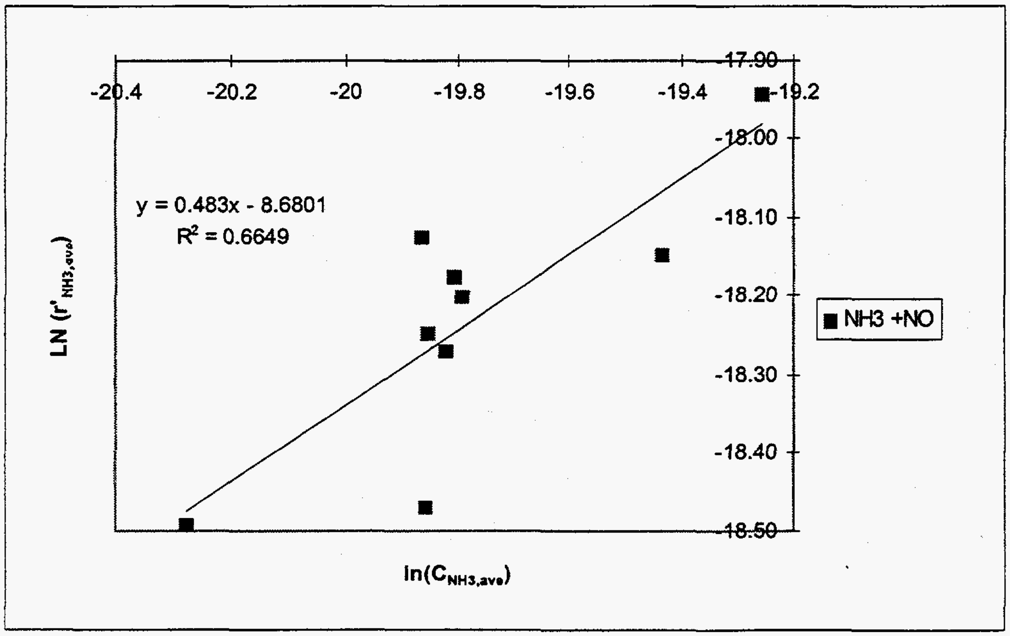

Figure 45. Differential reactor analysis of the NH_3+NO reaction with 115-400 ppm NH_3, 250-1250 ppm NO, and 3.0 g Na_2CO_3, 13 cm^3/s total flow rate at 25 °C, and at 750 °C

For this reaction as well the conversion of NH_3 depended on the inlet concentration of NH_3. The NH_3 conversion was lower when the inlet concentration of NH_3 was higher. This suggests a reaction order, which is lower than first order. The relationship between $-r'_{NH3,ave}$ and $C_{NH3,ave}$ is illustrated in Figure 45. The global reaction order from the plot in Figure 13 is 0.48 with respect to NH_3 concentration. There is a lot of scatter in the data. Therefore, the same reaction order as found in the absence of NO (0.53) was accepted for the purpose of reaction rate comparison.

NH_3+O_2

The kinetics of NH_3 destruction in the presence of O_2 was obtained according to integral analysis by experiments in which the amount of Na_2CO_3 (W) was varied. The weight ranged from 0.38 to 1.53 g. The inlet concentration of NH_3 was 500 ppm and the O_2 concentration 1%. A total flow rate of 13.0 cm^3/s at 25 °C was used in all runs. The temperature was 750 °C. The method of trial and error was used for the nth order reaction to find the order of reaction (n) that gave the highest value of R^2 for a straight line through origin for a plot between Y_{nth} and $W/F_{NH3,o}$. An order of 1.27 with respect to NH_3 was found ($R^2 = 0.85$). However, the R^2 value for a first order reaction plot was not much higher (shown in Figure 46). Within the uncertainty of the data, a first order reaction with respect to NH_3 seems to be acceptable.

NH_3+O_2+NO

The experiments were similarly performed by varying the amount of Na_2CO_3 from 0.38 to 1.53 g, while the inlet concentration of NH_3 and that of NO were equal to 250 ppm with 1% O_2 at a total flow rate of 13.0 cm^3/s at 25 °C. The temperature of the reactor was 750 °C. The reaction order of 1.2 with respect to NH_3 gave the best fit to the experimental data ($R^2 = 0.99$). However, the fit for the first order reaction expression (shown in Figure 47) could be accepted as well within the uncertainty of the data.

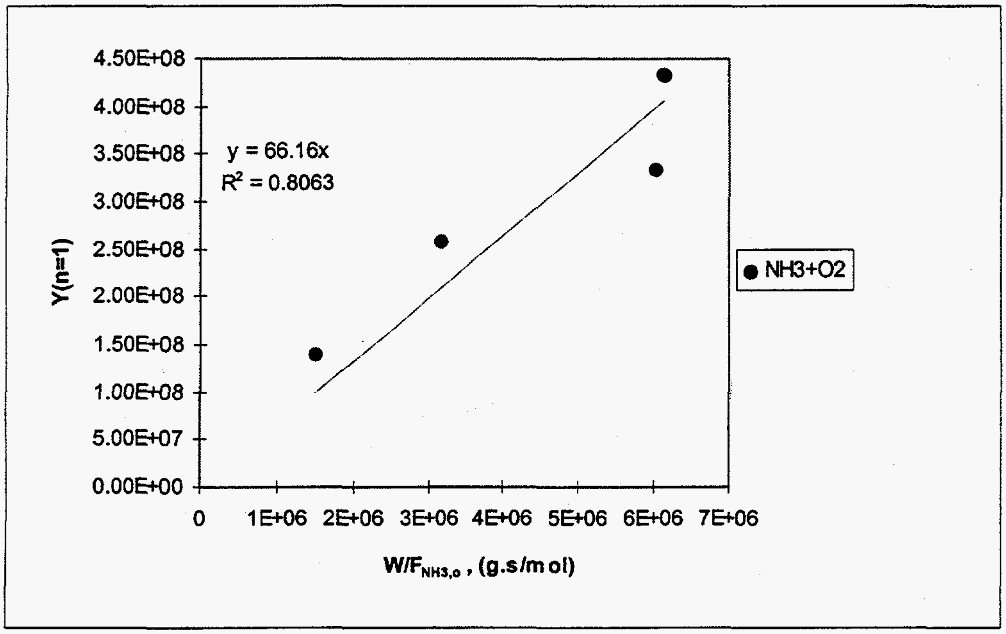

Figure 46. Integral analysis of the NH_3+O_2 reaction (n=1) with 500 ppm NH_3, 1% O_2, 0.38-1.53 g Na_2CO_3, 13 cm^3/s (25 °C), at 750 °C.

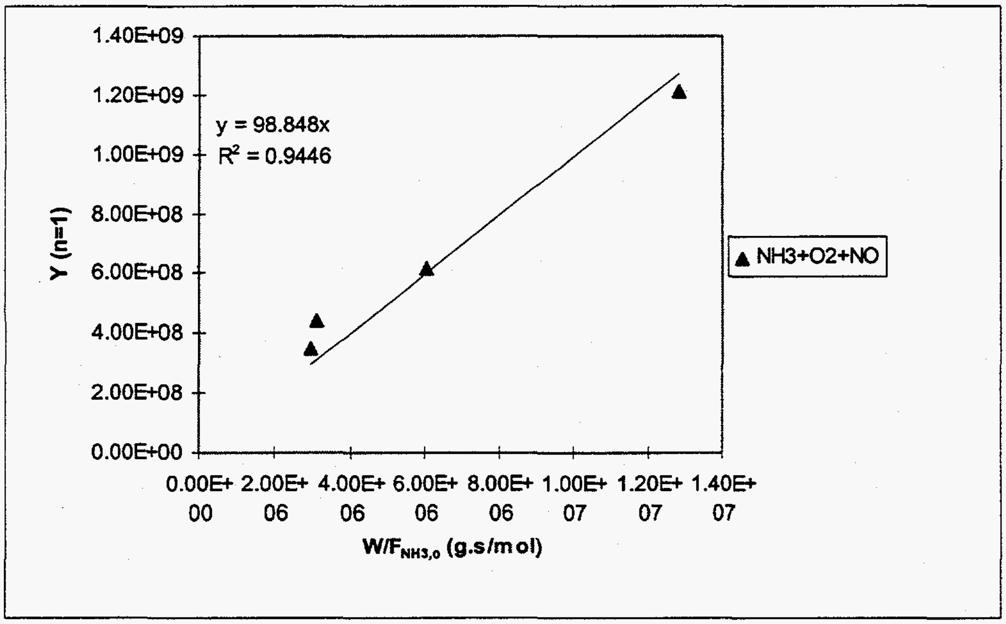

Figure 47. Integral analysis of the NH_3+O_2+NO reaction (n=1), with NH_3 = 250 ppm NO = 250 ppm, 1% O_2, 13 cm^3/s (25 °C), at 750 °C.

Examination of Mass Transfer Effects on the Global Reaction Rate

In this study, the effect of film mass transfer was investigated by both experiments and a theoretical criterion (Mears' criterion, Fogler, 1992). The tests were conducted at the temperature which yielded the highest rates of reaction (750 °C). The amount of catalyst and the total flow rate were reduced to half of the values used in the kinetic data experiment. This condition yielded the same residence time but a different gas velocity. The reaction NH_3+O_2 was chosen for the test of the film mass transfer effect. Other reactions studied were investigated by using the rate of reactions from the experimental data to evaluate the Mears' criterion. The effect of pore diffusion was examined by the Weisz-Prater criterion (Fogler, 1992). The experimental data of all the studied reactions were used to evaluate the satisfaction of the Weisz-Prater criterion.

The results of the test for the mass transfer effect and the calculations are shown in Table 6. For the film mass transfer resistance test of the NH_3+O_2 reaction, the higher gas velocity gave a slightly higher NH_3 conversion (2-4 percentage points higher). The difference in the NH_3 conversions was of the same order as the uncertainty in the measurement. The Mears' criterion was satisfied for all the reactions studied at 750 °C. Therefore, it was concluded that there were no external mass transfer limitations.

Table 6. Evaluation of mass transfer effects in the reactions at 750 °C.

Reaction	Na_2CO_3 mass, W, g	Total flow rate, V, cm^3/s	Inlet NH_3 conc., ppm	NH_3 conversion, X, %	Mears' criterion	Weisz-Prater criterion
NH_3+O_2	1.53	6.3	488	94	0.0042	0.039
	1.53	6.3	488	96	0.0042	0.039
	3.09	12.3	475	98	0.0028	0.037
NH_3+O_2+NO	3.05	13.2	241	99	0.0041	0.055
NH_3	3.07	12.7	451	25	0.0001	0.002
NH_3+NO	3.09	12.5	236	30	0.0001	0.002

the Mears' criterion < 0.15, no film mass transfer limitation

the Weisz-Prater criterion << 1, no pore diffusion limitation

For the investigation of pore diffusion control, the Weisz-Prater criterion was satisfied for all the reactions studied at 750 °C. In conclusion the mass transfer effects could be ignored at 750 °C. For the conditions at temperatures lower than 750 °C, the reaction rates are slower, which causes the mass transfer effects to be less important, too. So, it can be concluded that neither film transfer control nor pore diffusion control is important at the experimental conditions studied.

Kinetic Rate Constants for NH_3 Disappearance and Arrhenius plots

The experiments in the empty bed showed the possibility of gas phase reactions or catalysis by the reactor walls occurring at 750 °C. Thus the rate constants obtained from the performance equations are the total rate constants (k'_{total}) which include the impacts of both Na_2CO_3 and the empty bed. With the assumption that the reactions in the gas phase (or catalyzed by an empty bed) have the same reaction order as the catalytic reactions, the total rate constant is given as

Eq. 8: $$k'_{total} = k' + V_{zone}/W*k_{empty}$$

where

k'_{total} = observed kinetic rate constant, $(cm^3)^n/mol^{(n-1)}.g.s$
k' = kinetic rate constant of the catalytic reaction, $(cm^3)^n/mol^{(n-1)}\cdot g.s$
k_{empty} = kinetic rate constant of the gas phase reaction, $(cm^3/mol)^{(n-1)}/s$
where n = reaction order
Vzone = volume of the gas phase reaction zone, cm^3
$= \pi*(d_r/2)^2*h_r = 31\ cm^3$
d_r = diameter of reactor, 1.3 cm
h_r = the length of reactor which has uniform temperature, 23 cm
W = weight of catalyst used in the catalytic reaction, g

The values of k_{empty} for each reaction are calculated from the reaction rate equation of a homogeneous reaction with differential reactor analysis. The values of k_{empty} for the reactions at 750 °C are shown in Table 7. At other temperatures, the reaction in the empty bed was insignificant.

The value assigned to V_{zone} is arbitrary and the values of k_{empty} depend on the value chosen for V_{zone}. However, for the evaluation of k', the value used for V_{zone} is not important. Since the same value is used to evaluate k_{empty} in the absence of Na_2CO_3 and the overall reaction, the value of k' is independent of the value chosen for V_{zone}.

Table 7. k_{empty} of the reactions at 750 °C

Reaction	k_{empty}
NH_3 (n=0.53)	$1.00*10^{-5}$, $(mol/cm^3)^{(0.47)}/s$
NH_3+NO (n=0.53)	$1.30*10^{-5}$, $(mol/cm^3)^{(0.47)}/s$
NH_3+O_2 (n=1)	0.12, 1/s
NH_3+O_2+NO (n=1)	0.23, 1/s

Reactions in the Absence of O_2

The reaction order (n = 0.53) which was derived at 750 °C, is assumed to be valid at other temperatures studied (550-700 °C). At each temperature, the data from the experiments are directly inserted into the performance equation, and the rate constants (k') are calculated. Except at 750 °C, the value of the rate constant obtained is the total rate constant (k'total). Once k'_{total} is known, k' can be calculated from the correlation equation. Both the rates of reaction and the rate constants are based on the mass of catalyst in this study. Figure 48 shows the Arrhenius plots both in the absence and presence of O_2.

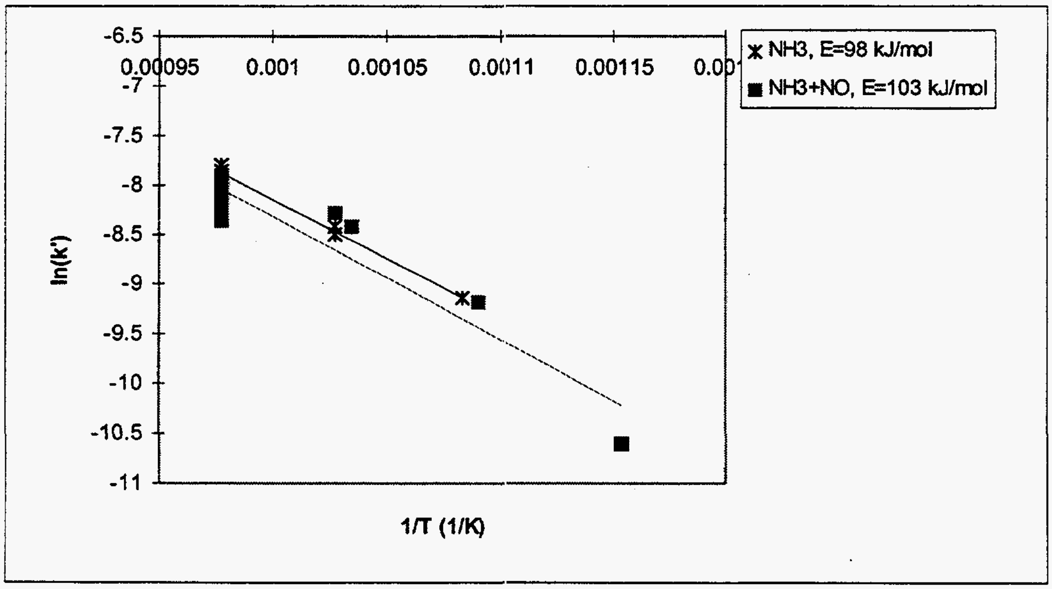

Figure 48. The temperature dependencies of the rate constants according to Arrhenius' law for the NH_3 reaction (n=0.53) at NH_3 = 500 ppm, and the NH_3+NO reaction (n=0.53), at NH_3 = 150-400 ppm, NO = 250- 1250 ppm.

The activation energy of the decomposition of NH_3 is 98±3 kJ/mol (95% confidence interval), while the activation energy of NH_3 oxidation by NO is 103±6 kJ/mol (95% confidence interval) in the temperature range studied. Thus the activation energies are not significantly different. The average reaction rate constants at each temperature studied are shown in Table 8. The rate of NH_3 decomposition is slightly faster than the rate of the reaction NH_3+NO at the temperatures studied.

Table 8. The average reaction rate constants for NH_3 destruction over Na_2CO_3 in the absence of O_2 at the temperatures studied.

Temperature, °C	Reaction of NH_3 k', ($mol^{0.47}$ $(cm^3)^{0.53}$/g.s)	Reaction of NH3+NO k', ($mol^{0.47}$ $(cm^3)^{0.53}$/g.s)
550	-*	-*
600	-*	$3.90*10^{-5}$
650	$1.08*10^{-4}$	$8.40*10^{-5}$
700	$2.09*10^{-4}$	$1.67*10^{-4}$
750	3.80*10-4	$3.11*10^{-4}$

Note: (*) no reaction observed at the temperature

The kinetic data of the reactions can be summarized as follows: the reaction orders with respect to NH_3 and the activation energy values very close (0.53th order with E = 98 kJ/mol). NO consumption in the reaction NH_3+NO was also present but the rate of NH_3 disappearance was independent of the NO concentration. The details of a rate of NO reduction in the NH_3+NO are illustrated and discussed later in the section on global rate for NO reduction.

Reactions in the Presence of O_2

The rate constants of the two reactions can be obtained by the equation for first order reaction in an integral reaction. The experimental data at each temperature are used to calculate the rate constants separately. At 750 °C, the total rate constant (k'_{total}) is used to calculate the catalytic rate constants (k') from the correlation equation. The temperature dependencies of the rate constants according to Arrhenius' law are shown in Figure 49. The rate constants of both reactions at different temperatures are exhibited in Table 9.

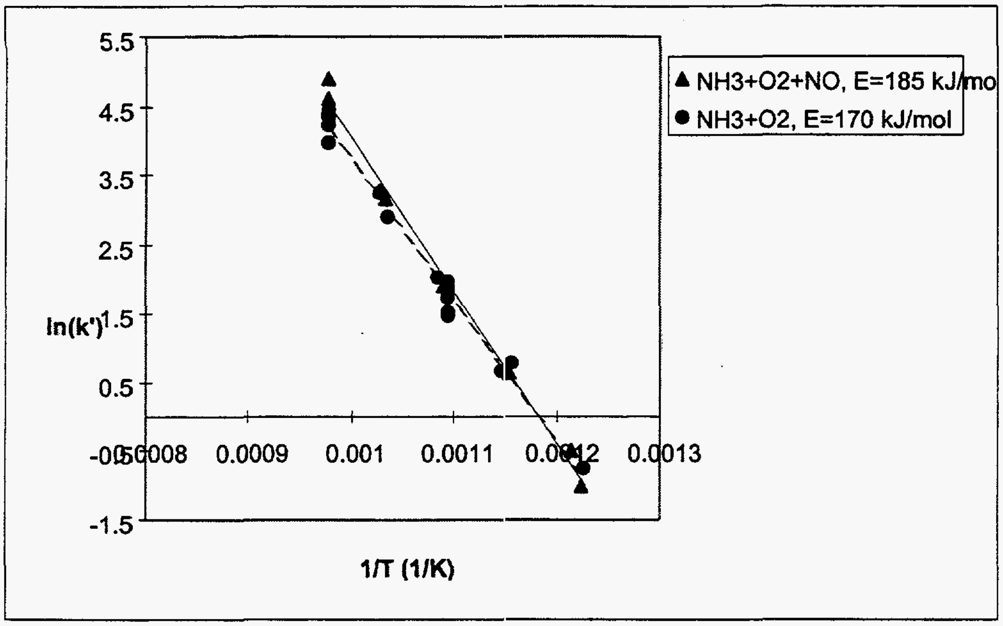

Figure 49. The reaction rate constants of the NH_3+O_2 reaction (n=1), at 500 ppm and 250 ppm NH_3 with 1% O2, and the NH_3+O_2 +NO reaction (n=1), at NH_3 250 ppm, NO 250 ppm and 1% O_2, with Na_2CO_3.

In the Arrhenius plot, the two reactions seem to be almost indistinguishable. The activation energy of the NH_3+O_2 reaction is 170±23 kJ/mol and that of the NH_3+O_2+NO reaction is 185±42 kJ/mol. The reaction rate constants indicate that the reaction rates are slightly higher when NO is present at temperatures above 600 °C.

Table 9. The reaction rate constants of the NH_3+O_2 reaction and the NH_3+O_2+NO reaction over $Na_2CO_3$with an inlet concentration of NO of 250 ppm.

Temperature, °C	NH_3 +O_2 k', (cm^3)/g.s	Reaction of NH_3+O_2+NO k', (cm^3)/g.s
550	0.498	0.483
600	2.06	2.27
650	7.30	9.02
700	22.7	31.1
750	63.3	95.0

Global Reaction Rate for NO Reduction

The NO conversion was increased by an increase in the inlet NH_3 concentration and was decreased by an increase in the inlet NO concentration at 750 °C. The only exception was the measurement at 322 ppm NO. With 250 ppm NH_3 and 250 ppm NO, the highest NO conversion was 18% at 750 °C.

The kinetics of the rate of NO consumption was found by differential analysis. First, the reaction order of NO reduction with respect to NH_3 concentration was studied by experiments in which the NH_3 was varied from 150 to 400 ppm. The NO concentration was kept constant at 250 ppm and the mass of Na_2CO_3 was 3.0 g. The temperature was 750 °C. The order with respect to NH_3 was 1.4 as seen in Figure 50. The reaction order of NO reduction with respect to NO was tested by experiments in which the NO concentration was varied from 250 to 1250 ppm. The NH_3 concentration was constant at 250 ppm. The mass of Na_2CO_3 was 3.0 g and the temperature 750 °C. The order with respect to NO was found to be 0.4 as shown in Figure 51.

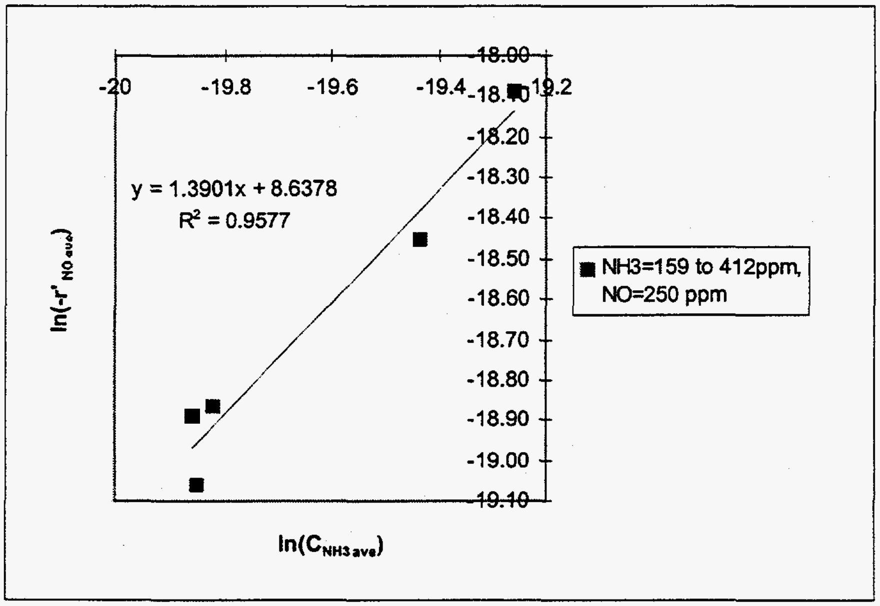

Figure 50. The plot to find the reaction order with respect to NH_3 concentration for the reaction NH_3+NO with 150-400 ppm NH_3, 250 ppm NO, and 3.0 g Na_2CO_3 at 750 °C.

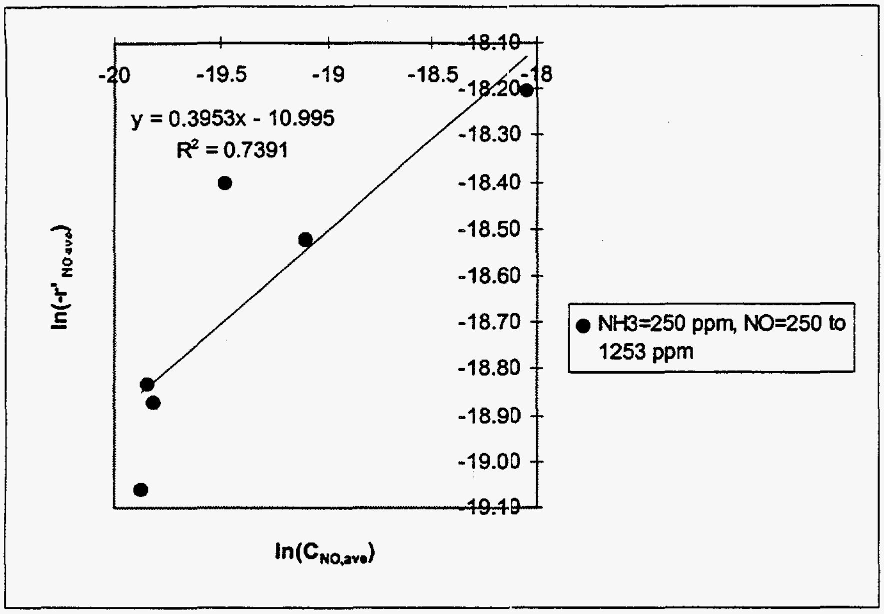

Figure 51. The plot to find the reaction order with respect to NO concentration for the reaction NH_3+NO with 250 ppm NH_3, 250-1250 ppm NO, and 3.0 g Na_2CO_3 at 750 °C.

The reaction rate constants at different temperatures were found from the reaction rate equation:

Eq. 9: $-r'_{NO,ave} = k' (C_{NH3,ave})^{1.4}(C_{NO,ave})^{0.4}$

where $-r'_{NO,ave}$ = average rate of reduction of NO, mol/g.s
k' = reaction rate constant of NO reduction, $(cm^3)^{1.8}/mol^{0.8}$.g.s
$C_{NH3,ave}$ = average concentration of NH_3, mol/cm^3
$C_{NO,ave}$ = average concentration of NO, mol/cm^3

The rate constant obtained at 750 °C did not need to be corrected for a reaction in the empty bed because no NO consumption occurred in the empty bed experiments. The temperature dependency according to Arrhenius' law is shown in Figure 52. The activation energy from the plot is 100±24 kJ/mol (95% confidence interval). This activation energy is close to that of the rate of NH_3 disappearance in the reaction NH_3+NO (103±6 kJ/mol). The average rate constants at different temperatures are shown in Table 10. The results indicate that the NO consumption rate depends more on the NH_3 than the NO concentration.

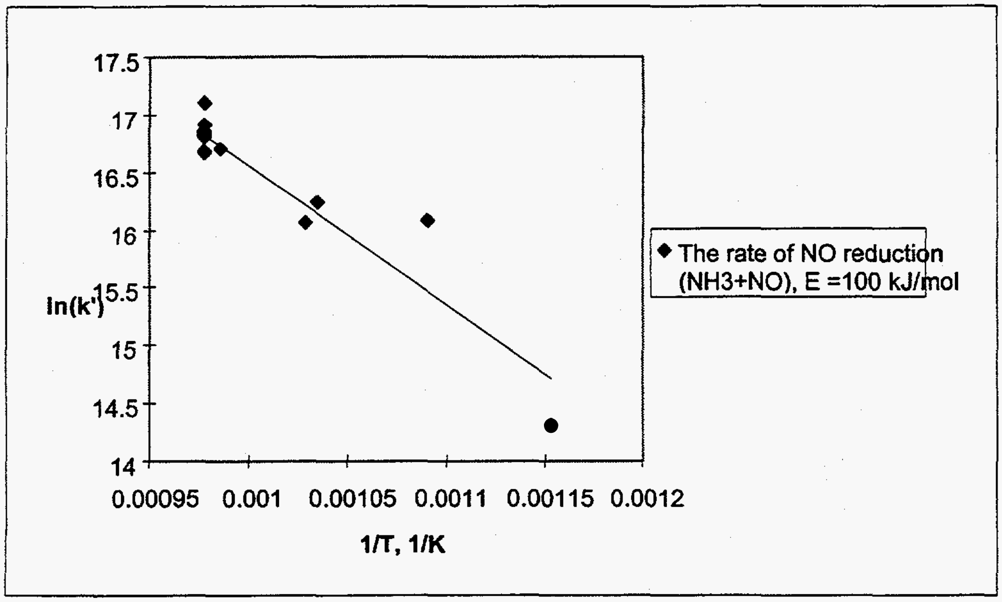

Figure 52. Temperature dependency of the rate of NO reduction according to Arrhenius' law for the reaction NH_3+NO at the temperatures studied.

Table 10. The NO reaction rate constants of the NH_3+NO reaction with 150 to 400 ppm NH_3, 250 to 1250 ppm NO and 3.0 g Na_2CO_3 at the temperatures studied

Temperature, °C	**Reaction of NH_3 +NO k', $(cm^3)^{1.8}/g.s.mol^{1.8}$**
550	-
600	$2.74*10^6$
650	$5.79*10^6$
700	$1.13*10^7$
750	$2.07*10^7$

Sources of Error in Experimental Measurements

For the calculation of the reaction rate coefficients for NH_3 disappearance, the following values were needed: mass of catalyst, gas flow rate, NH_3 conversion, and in some cases NH_3 inlet concentration. The mass of the catalyst was typically 3.0 g and was measured to an accuracy of 0.001 g. The gas flows were measured by rotameters whose accuracy was 5 % of the reading. For NH_3 conversion, both the inlet and outlet NH_3 concentrations were needed and measured. The NH_3 concentration was the major source of error in most experiments.

FTIR spectroscopy was used to determine the NH3 content in grab samples of both the inlet flow and outlet flow. One reason for inaccuracies in the NH_3 measurements is that NH_3 can easily be adsorbed on the surface of gas lines or sampling system. Heating tape was used to warm part of the lines to minimize the effect of this. Another source of error in the conversion is the use of a different path of gas flow when the inlet and outlet concentration of NH_3 were measured (flow through by-pass or reactor). Due to rotameter inaccuracies and the difficulty of maintaining a constant flow, the inlet concentration with gas flows through the by-pass and the reactor may not have been the same. The inlet gas concentrations that were measured were compared to those that were calculated from the gas flows. In most cases, the calculated and measured inlet concentrations were within 10% but in some cases the errors were larger than that. Using the values calculated from the rotameter settings gave considerably less scatter in the results. Because of this, the value calculated from rotameter settings was used as the inlet NH_3 concentration in the calculations of the conversions and reaction rate coefficients. - To minimize the impact of measurement inaccuracies two measurements of the NH_3 concentrations were made for each experiment and the average was taken. For each condition two tests were made.

The errors in the conversion were estimated based on the errors in NH_3 measurements and rotameter readings. The relative error in the NH_3 measurement was taken to be 5 %. The highest and lowest relative errors for each reaction are given in Table 11.

Table 11. Estimates for accuracy of the NH_3 conversions.

Reactants	Error, ± percentage points
NH_3	5-6
NH_3 + NO	6-9
NH_3 + O_2	9-10
NH_3 + NO + O_2	9-10

The absolute errors were to be 5-10 % points at all conditions. The reactions in which more rotameters were used have slightly larger errors in the conversion data. In the reaction with only NH_3, only one rotameter was used, in the NH_3+O_2 two rotameters, in the NH_3+NO three rotameters, and in the NH_3+O_2+NO four of them. At low conversions the relative errors in NH_3 conversion could be very high: in excess of 100 %.

Prediction of the Importance of NH_3 Oxidation Catalyzed by Fume Species in a Recovery Boiler

In this section, data presenting a typical recovery boiler (Adams and Frederick, 1988) were combined with laboratory data to roughly estimate the importance of NH_3 oxidation by fume species in a recovery boiler.

First, a potential reaction zone for NH_3 oxidation by fume compounds in a recovery boiler was defined. The catalytic activity of Na_2CO_3 was substantially higher than that of Na_2SO_4 in promoting NH_3 oxidation at the temperatures studied (600 to 750 °C), while the oxidation data were insignificant over both Na_2CO_3 and Na_2SO_4 at 550 °C. It is assumed that the reaction mechanisms are the same at higher temperatures (> 750 °C) than at 550-750 °C. Thus the reaction zone is the location in the boiler where fume particles are primarily composed of Na_2CO_3 and the temperature is higher than 550 °C.

The fraction of Na_2SO_4 in submicron fume particles increases from the bottom of the furnace to the top of the furnace. In a study by Rizhinshvili and Kaplun (1983), Na_2CO_3 was almost the only component in fume particles above the char bed surface, while Na_2SO_4 was the major fume component at the outlet of the boiler. The Na_2SO_4 content in fume particles was 64% at the tertiary air level while at the furnace outlet it was 96% Na_2SO_4. The gas phase above the char bed contains mostly N_2, CO_2, O_2, and H_2O with only a small amount of SO_2 (1 ppm) and thus very little Na_2SO_4 is formed. The concentration of SO_2 in the gas phase increases significantly near the tertiary air level and is enough to convert Na_2CO_3 to Na_2SO_4. Thus the possible reaction zone was defined to be from the char bed surface to the tertiary air level.

The NH_3 consumption was calculated by the rate equation for NH_3 disappearance in the presence of O_2. The rate of reaction based on the weight of Na_2CO_3 was changed to be based on Na_2CO_3 surface area by dividing it with the BET surface area (0.18 m^2/g). The rate obtained is shown below:

Eq. 10: $$-r''_{NH3} = 1.62*10^7 \text{ cm/s* } \exp(-20400 \text{ K/T}) *C_{NH3}$$

The reaction zone was treated as a plug flow reactor and the fume droplets and the flue gas were assumed to flow at the same velocity (i.e., that the terminal velocity of the fume particles was zero). The temperature was assumed to be uniform. It was further assumed that all fume and NH_3

were produced instantaneously at the base of the reaction zone, and that the structure and composition of the fume remained unchanged.

Integration of the rate equation yields NH_3 conversion (X_{NH3}) as a function of temperature (T), total surface area of Na_2CO_3 (S_{Na2CO3}, cm^2/s), total flue gas flow rate (V_F, cm^3/s), and average residence time (t_{avg}, s).

Eq. 11: $$1.62*10^7 \text{ cm/s}* \exp(-20400 \text{ K/T})\ S_{Na2CO3}\ t_{avg} / V_F = -\ln(1-X_{NH3})$$

The average furnace gas temperature is about 1100 °C in the lower furnace (for a black liquor loading of 0.18 $kg/s.m^2$, Adams and Frederick, 1988), and this is taken as the reaction temperature. The average residence time in this reaction zone is 1.3 s.

The amount of fume needs to be specified. The liquor Na content was taken to be 19.5 %. It was assumed that 9% of the Na became vaporized in the boiler and formed Na_2CO_3 (Borg et al., 1974). The fume was taken to consist entirely of Na_2CO_3 in the reaction zone. This gives 4.0 kg Na_2CO_3 fume per 100 kg black liquor solids fed into the boiler. The fume particles were assumed to be spherical droplets of a uniform size. Mikkanen et al. (1994) had studied particle size and chemical species distributions of aerosols generated during kraft black liquor combustion. In experiments conducted in a recovery boiler with two different black liquor sources (hardwood and softwood), the dominant fume particle size was 0.7 µm on an average, and was taken as the fume particle diameter. This gives the Na_2CO_3 surface area as $1.9*10^8$ cm^2/s per 100 kg black liquor solids.

Since the reaction is first order with respect to NH_3 the conversion is independent of the NH_3 concentration. The total amount of the flue gas generated is 664 kg/ 100 kg BLS with 15% excess air (Adams and Frederick, 1988) and the average flow rate corresponding to the amount of flue gas is 390 m^3/s.

With these assumptions, the reaction of NH_3 over Na_2CO_3 in the presence of O_2 was found consumed 40% of the NH_3 at the average residence time from char bed to the tertiary air port (1.3 s). The estimate suggests that NH_3 decomposition by fume may be important but that there could be other dominant reactions to efficiently consume NH_3 in a recovery boiler. Examples of competing reactions are gas phase reactions and char catalyzed reactions.

This is a rough estimate that is based on several oversimplified assumptions. A significant source of uncertainty in the model is the extrapolation of the kinetic data from 750 to 1100 °C. The mechanism of the reaction and thus the rate may be considerably different at 1100 °C. Fume is solid at 750 °C and molten at 1100 °C, which makes a change in the reaction mechanism likely. The conditions in the boiler were assumed to be constant with respect to temperature, gas flow, and fume amount and composition. All of these vary with the location in the boiler. For the reaction rate estimation, the use of an average temperature often leads to serious errors because of the exponential temperature depending of the reaction rates.. The validity of the assumption of the gas flow patterns in the boiler is also essential for the accuracy of the estimation.

Summary and Conclusions

The catalytic effects of recovery boiler fume compounds on NH_3 both in the presence and absence of NO and O_2 were studied in the temperature range 550-750 °C. The fume compounds were Na_2CO_3 and Na_2SO_4. The inlet gas concentrations were: 115-1250 ppm NH_3, 0-1250 ppm NO, 0 or 1 % O_2. The amounts of Na_2CO_3 ranged from 0.38 to 3.0 g and that of Na_2SO_4 were 3.0 g. The total gas flow rate was 6.3-13.0 cm^3/s, at 25 °C.

The conclusions from the study are stated as follows:

1. There was significant NH_3 consumption over Na_2CO_3 at 600-750 °C. In the presence of O_2, the highest NH_3 conversions were almost 100% at 750 °C, and the conversions were 30 without O_2.
2. The effect of Na_2SO_4 on the studied reactions was significantly less than that of Na_2SO_4 at the experimental conditions. Therefore only the effect of was studied in more detail.
3. The rate of NH_3 disappearance over Na_2CO_3 in the absence of O_2 was almost independent of the NO concentration.
4. The reaction order with respect to NH_3 concentration for NH_3 decomposition over without O_2 was 0.53 and the activation energy was 98±3 kJ/mol at 95% confidence interval in the temperature range studied.
5. Even though the NO concentration had little impact on NH_3 conversion, NO was consumed in the reaction, up to 18% at 750 °C. The NO conversion was increased by an increase in NH_3 concentration.
6. With O_2, the disappearance of NH_3 was first order with respect to NH_3 both in the absence and presence of NO in the temperature range studied. The activation energies were 170±23 kJ/mol and 185±42 kJ/mol (95% confidence interval) without and with NO, respectively.
7. For the reactions in the presence of O_2, the rate of NH_3 disappearance was slightly promoted by the presence of NO.
8. NO was produced when NH_3 reacted with O_2. The average fraction of NH_3 reacted that formed NO was 0.28 in the temperature range 600-700 °C and 0.35 at 750 °C.

9. NO disappearance with both O_2 and NO was highest at 650-700 °C. At 750 °C, the conversion decreased possibly due to an increase in NO production in the reaction.

10. A simple model for the estimation of the importance of the reactions gave an NH_3 conversion of 40%. This suggests that other reactions of NH_3 consumption may be significant.

Reduction of NO

In recovery boilers, reduction of NO after it has been formed may be significant. In a study by Nichols and Lien (1993) substantial NO reduction was observed in a laboratory reactor designed to simulate conditions in a recovery boiler. This reactor consists of a 4-meters-tall tube furnace placed on top of a char bed furnace. Black liquor droplets are introduced at the top of the tube furnace and they fall through the furnace onto the char bed in the bottom. Primary air is added at the char bed surface and secondary air at the lower sections of the tube furnace. The gases rise countercurrent to the droplets, and the droplets undergo drying and partial devolatilization in-flight. The highest NO concentrations were measured 2.8 m from the bottom of the furnace. The outlet concentrations were 60 % of the maximum; in other words 40 % of the NO had become reduced.

Reduction by char and homogeneous gas phase reactions are deemed the most important reduction mechanisms in fossil fuel combustion (Goel et al., 1996). Due to its high sodium content char black liquor char is more efficient in reducing NO than char from e.g. coal combustion. Another possible NO reducing mechanism in recovery boilers involves reactions with sodium salts. The kinetics of NO reduction by molten sodium compounds has been investigated by Thompson and Empie (1995) and Thompson (1995). NO reduction by char was studied in the first DOE project (report DOE/CE/40936-T3, also in Wu and Iisa, 1998).

Here, some additional experiments of NO reduction by char and fume compounds were made. The kinetics of NO reduction by char and sodium salts is reviewed and compared to the rates of NO reduction measured in laminar entrained experiments.

NO Reduction by Black Liquor Char

NO reduction by one char was studied at 450-650°C by Wu and Iisa (1998). The reason for the low temperature range is that a fixed bed reactor was used, and due to the melting of the sodium salts higher temperatures could not be used. The char that was used in this study had a total surface area of 14.6 m^2/g, and it contained 7.6 weight % fixed carbon.

The rate of NO reduction by black liquor char was approximately three orders of magnitude faster than by other carbonaceous material. The reduction rate was enhanced by the presence of a reducing gas such as CO. The rate was first order in NO both in the presence and absence of CO. The reaction rate expression for NO reduction by the char in the absence of CO was

Eq. 12: $-r_{No} = 0.204\ m^3/(m^2s)\ \exp[-67\ kJ/mol\ /(RT)]\ p_{NO}$ at 450-650°C

and in the presence of 4 % CO

Eq. 13: $-r_{No} = 1.46\ m^3/(m^2s)\ \exp[-73\ kJ/mol\ /(RT)]\ p_{NO}$ at 450-650°C.

The rates are based on the total surface area of the char.

The activation energies are consistent with those for NO reduction by other carbonaceous materials in this temperature range (Chan et al., 1983, Furusawa et, 1980 and 1985, Suuberg et al., 1991, Kaptejn et al., 1984). For the carbon other materials the activation energy increases at temperatures above 650°C and becomes approximately 240 kJ/mol (Furusawa et al., 1980, Suuberg et al., 1991).

The rate of NO reduction increased as CO was added to the gases. The pseudo first order rate coefficient in the presence of 4 % CO was approximately three times the first order reaction rate coefficient in the absence of CO. The change in NO reduction as the CO concentration was increased is shown in Figure 53.

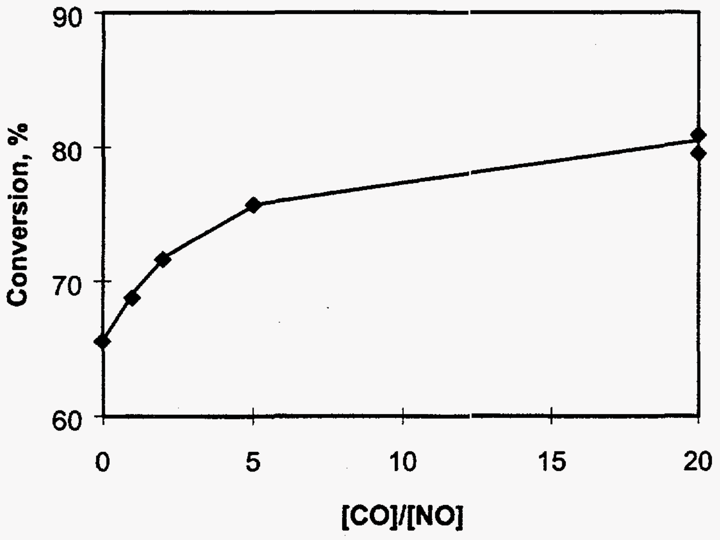

Figure 53. Effect of the ratio of CO to NO on NO reduction. 550°C, 500 ppm NO, 0.2 g of black liquor char with 14.6 m^2/g and 7.95 l/min total gas flow at 25 °C.

In the absence of CO the main global reaction was

Reaction 1: $2NO + C(s) \rightarrow CO_2 + N_2$

and in the presence of CO the reaction became catalytic

Reaction 2: $NO + CO \rightarrow \frac{1}{2} N_2 + CO_2$.

For other carbonaceous materials without CO there is a shift in the reaction mechanism as the temperature exceeds 650 °C (Chan et al., 1983, Furusawa et al., 1980, Suuberg et al., 1991) and more CO is produced according to the following global reaction

Reaction 3: $NO + C(s) \rightarrow CO + N_2$.

A model that would account for the effect of CO on NO reduction was developed based on these earlier results. The model needed to fulfill the following criteria:

1) The rate is first order in NO both in the presence and absence of CO.
2) The rate increases as CO concentration increases.

The simplest rate expression that would account for this behavior is of the form

Eq. 14: $-r_{NO} = (k_1 + k_2p_{CO})\ p_{NO}$.

In this model the rate constant k_1 is equal to the rate constant in the absence of CO. The rate constant k_2 can be determined from the pseudo first order reaction rate constant with 40320 ppm NO. The pseudo first order constant will be equal to $k_1 + k_2p_{CO}$. From this expression

Eq. 15: $k_1 = 0.204\ m^3/(m^2s)\ \exp[-67\ kJ/mol\ /(RT)]$ 450-650°C

and

Eq. 16: $k_2 = 3.78*10^{-5}\ m^3/(m^2s\ ppm)\ \exp[-76\ kJ/mol\ /(RT)]$ 450-650°C

Figure 54 shows the conversions of NO predicted by this equation versus the measured conversions at 550°C. The figure covers data taken at 500-1640 ppm NO, 500-40320 ppm CO, and CO to NO ratios of 1-100. The predicted reduction was always within 10 % of that measured.

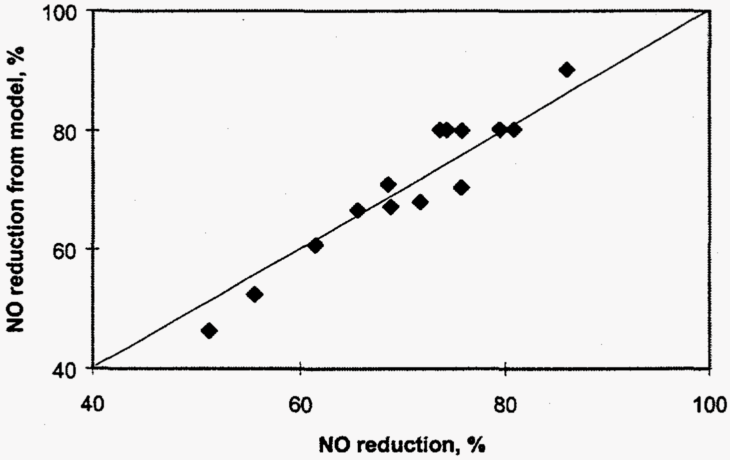

Figure 54. Correlation between NO reduction predicted by Eq. 14 and that measured in the experiments. 550°C, 500-1460 ppm NO, 500-40320 ppm CO, ratio of CO to NO 1-100.

The above equations are valid in the temperature interval 450-650°C. At temperatures above 650°C the activation energies of both reactions are assumed to become 240 kJ/mol. The reaction rate coefficients above this temperature are

Eq. 17: $k_1 = 1.26*10^9\ m^3/(m^2 s)\ \exp[-240\ kJ/mol\ /(RT)]$ $T>650°C$

and

Eq. 18: $k_2 = 7.12*10^4\ m^3/(m^2 s\ ppm)\ \exp[-240\ kJ/mol\ /(RT)]$ $T>650°C$

NO Reduction by Char at High Temperatures

Experiments were made in the laminar-entrained flow reactor to study the rate of NO reduction by black liquor char at high temperatures (800°C-1100°C). The black liquor char was prepared from a char that had been initially pyrolyzed for four hours in N_2 at 700 °C (Char 1 in appendix III of this report). To complete the pyrolysis and prevent any further carbon loss during the NO reduction experiments, the char was further pyrolyzed by heating it to 900 °C in N_2 and holding for four hours. No analysis of the char was made after the additional pyrolysis.

A limited set of experiments was made mainly to determine the activation energy at higher temperatures. The NO concentration was 250 ppm, and the temperatures 800-1100 °C. The total gas flow rate was 11.3 l/min (at 25 °C) and the solid feed rates 0.07-0.37 g/min.

In analyzing the data it was assumed that the gas and solid flow velocities were the same, and that there was perfect mixing in the radial direction and no mixing in the axial direction (i.e. plug flow of both solids and gas). The performance equation for a first order reaction with concurrent plug flows of both solids and gas is

Eq. 19: $-\ln(1-X) = kt\ w/V$

where k is the rate constant ($m^3/s{\cdot}g$), X is the fractional conversion, w is the solid feed rate (g/min), V is the gas flow rate (l/min), and t is the residence time (s).

An Arrhenius plot of the results is shown in Figure 55. The activation energy was 233 kJ/mol. This is close to the value 240 kJ/mol reported for other carbonaceous sources in this temperature range.

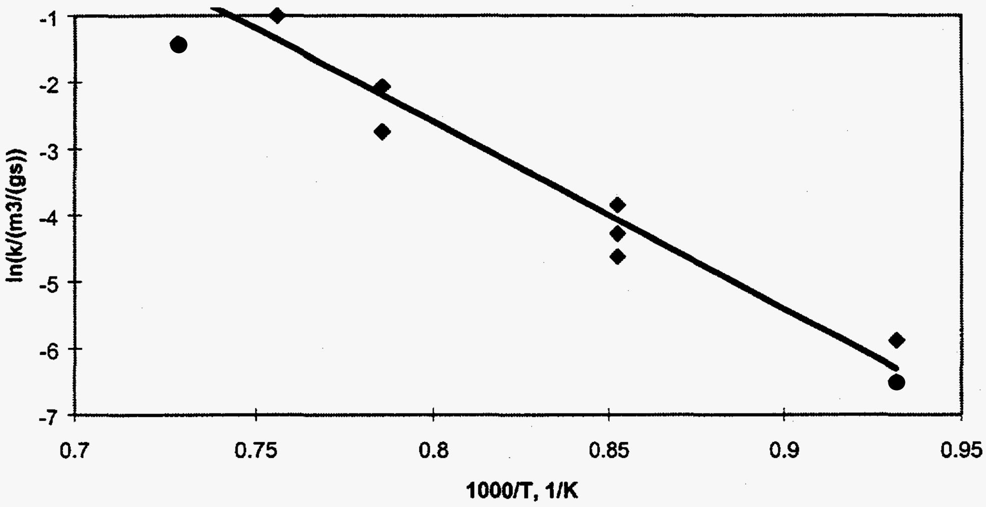

Figure 55. Arrhenius plot for NO reduction by black liquor char in the laminar entrained-flow reactor. NO concentration 250 ppm, gas flow rate 11.3 l/min (at 25 °C) and solid feed rate 0.07-0.38 g/min.

The internal surface area of the char used in the high temperature experiments was not measured. The char was prepared at a higher temperature and for longer times (four hours at 900 °C versus 40 minutes at 700 °C) than that used in the low temperature experiments. This may have resulted in a lower internal surface area. An internal surface area of 1 m^2/g for the char in the high temperature experiments would give the same reaction rate coefficients at 650 °C. This is the temperature for the shift in mechanism based on data from other carbonaceous materials. The comparison of the two sets of rate data is shown as an Arrhenius plot in Figure 56.

Additional experiments were conducted to analyze the effect of CO on NO reduction at high temperatures and to determine the activation energy of the reaction. The NO concentration in these experiments was 250 ppm, and the CO concentration 5000 ppm. The Arrhenius plot of the pseudo-first order reaction rate coefficient in the experiments is presented in Figure 57. The activation energy was 234 kJ/mol, which is the same as in the experiments without CO.

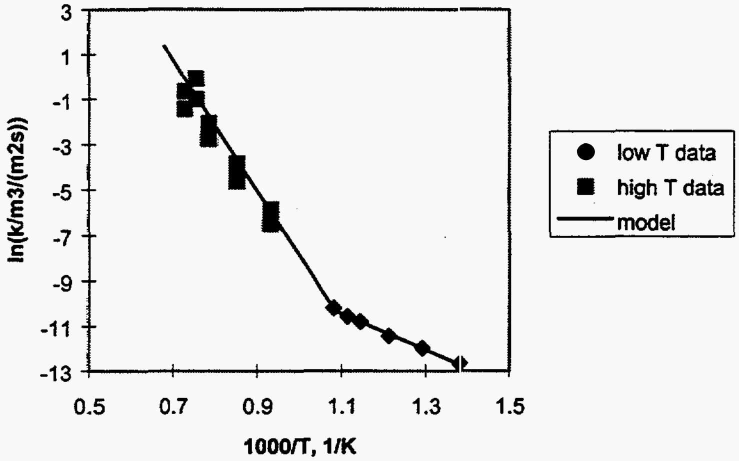

Figure 56. Comparison of low temperature and high temperature reaction rate coefficients. The internal surface area of the char in the low temperature experiments is 14 m^2/g and that in the high temperature experiments is taken to be 1 m^2/g.

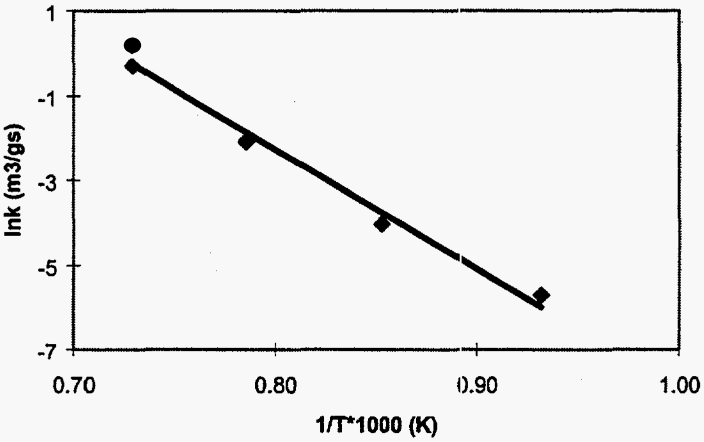

Figure 57. Arrhenius plot for pseudo-first order reaction rate coefficient for NO reduction by black liquor char in the presence of CO in the laminar entrained flow reactor. NO concentration 250 ppm, CO concentration 5000 ppm , gas flow rate 20.0 l/min (at 25 °C) and solid feed rate 0.045-0.45 g/min.

The reaction rate was slightly higher in the presence of CO than when no CO was present in the feed. The average pseudo-first order reaction rate coefficient at 700-1000 ° was 1.2 to 1.7 times that in the experiments without CO but at 1100 °C 2.5 times that. Based on the equations for the model

Eq. 20: $$-r_{NO} = (k_1 + k_2[CO])[NO]$$

the rate coefficient would be expected to be higher by a factor of 1.3. This shows good agreement between the experimental values and those predicted by the model except at 1100 °C. The data without CO at 1100 °C may be erroneous. Without CO, the rate was lower at 1100 °C than at 1050 °C.

NO Reduction by Fume

Fume particles are another possible source of NO reduction. At the temperatures of the recovery furnace the sodium salts are molten. Therefore, we will have a gas-liquid reaction. In general, rates for reactions between a gas component A and a liquid component B depend on the mass transfer from bulk gas to the gas-liquid interface, solubility of the gas component in the liquid, mass transfer in the liquid phase and the chemical reaction. The rate of disappearance of the gaseous component A can be presented as (e.g. Levenspiel, 1996)

Eq. 21: $$-r_A'''' = \frac{p_A}{\frac{1}{k_{A_g}a} + \frac{1}{H_A k_{A_l} a E} + \frac{1}{H_A k c_B f_l}} \text{*}$$

Here $-r_A''''$ = overall rate of reaction for A per unit volume of reactor, mol/(m^3 reactor s)
k_{Ag} = gas side mass transfer coefficient, mol/(m^{2}Pas)
k_{Al} = liquid side mass transfer coefficient, (m^3 liquid)/m^{2}s)
a = interfacial surface area, m^2/(m^3 reactor)
H_A = Henry's law coefficient, mol/(Pa m^3 liquid)
k = second order reaction rate constant, (m^3 liquid/(mols)
c_B = concentration of the liquid component B in the liquid phase, mol/(m^3 liquid)
f_l = fraction of liquid in the reactor, (m^3 liquid)/(m^3 reactor)

---

* Often, a phase distribution coefficient which is equal to the reciprocal of Henry's law coefficient is used for gas-liquid reactions. The use of Henry's law constant was adopted here because the equilibrium data is more frequently available as Henry's law coefficient.

E = enhancement factor

Here, the reaction rate in the liquid phase is assumed to be of second order, i.e. first order in the concentrations of A and B. If there is a reaction consuming the gaseous species A in the liquid film, the gradient of A in the liquid film becomes steeper. Therefore the rate of mass transfer through the film becomes faster. This increase in the mass transfer rate is taken into account by the liquid film mass transfer enhancement factor E. E is defined as the ratio of the rate of mass transfer of A from gas with reaction to the absorption rate without reaction.

The enhancement factor E has been shown to depend on two other dimensionless groups, E_i and M_H (Hatta number) (Levenspiel, 1996). E_i is the the enhancement for an infinitely fast reaction. It is the ratio of two hypothetical overall reaction rates: that of an infinitely fast reaction with the actual liquid side transfer rates for A and B and the highest possible rate of mass transfer of A without reaction. In the first case, all A consumed in the liquid film. In the latter case, the concentration of A is zero in the bulk liquid. E_i depends on the diffusivities of A and B in the liquid phase and the stoichiometric coefficient..

Eq. 22: $$E_i = 1 + \frac{D_B c_B}{D_A b}$$

where D_A = diffusion coefficient for A in the liquid, m^2/s

D_B = diffusion coefficient for B in the liquid, m^2/s

b = stoichiometric coefficient for reaction $A + bB \rightarrow$ products

The other dimensionless number, Hatta number, relates the maximum possible rate in the liquid film to the maximum rate of transfer of A through the film. The square of the Hatta number is equal to the ratio of the two rates. The maximum rate in the liquid film refers to that of the actual reaction in the film in the absence of liquid side mass transfer limitations (concentration of B in the film equal to the bulk liquid concentration and that of A equal to the gas/liquid interface concentration). The maximum transfer of A through the film refers to the rate by mass transfer alone without any reaction and with bulk liquid concentration equal to zero.

Eq. 23: $$M_H^2 = \frac{D_A k c_B}{k_{Al}^2}$$

The Hatta number characterizes whether the reaction takes place predominantly in the liquid film (fast reactions, $M_H > 2$) or the bulk liquid (slow reactions, $M_H < 0.02$), or to significant extents in both (intermediate reactions, $0.02 < M_H < 2$). Simplifications can be made in equations for both fast and slow reactions. For fast reactions, the third term in the denominator, which signifies the reaction in the bulk liquid, can be ignored. For slow reactions the enhancement factor E is equal to 1.

Expressions relating the enhancement factor E to M_H and E_i have been developed (Levenspiel, 1996). In special cases for fast reactions, the relationship is simple and E equals either E_i or M_H. This depends on the relative magnitudes of M_H and E_i. If E_i is much larger than M_H ($E_i > 5M_H$), E equals M_H. Conversely, if E_i is much larger than M_H ($M_H > 5Ei$), E is equal to M_H.

For the special case of fast reactions with $E = M_H$, the rate of reaction becomes

Eq. 24: $$-r_A'''' = \frac{ap_A}{\frac{1}{k_{Ag}} + \frac{1}{H_A\sqrt{D_A k c_B}}}$$ (fast reaction, $M_H > 2$, $E_i > M_H$)

If the concentration of the liquid reactant B is so high that it remains essentially constant, the second order reaction rate coefficient kc_B can be replaced by a pseudo first order reaction rate coefficient $k_1 = k\ c_B$.

Thompson and Empie (1994) had studied NO reduction by fume compounds by bubbling a gas containing NO through a molten pool of Na_2CO_3 at 863-930 °C. Substantial NO reduction was observed. The reaction was shown to be fast with the reaction taking place in the liquid film and Eq. 24 to be valid. The following pseudo first order rate constant was obtained

Eq. 25: $$k = 3.09 * 10^{22}\ s^{-1} \exp[-372\ kJ/mol/(RT)]$$

The overall reaction was determined to be decomposition of NO

Reaction 4: $NO \rightarrow \frac{1}{2} N_2 + \frac{1}{2} O_2$.

In this project, experiments of NO reduction by black liquor char were made in the laminar entrained-flow reactor. The experiments were made at two different temperatures: 800°C, which is lower than the melting point of sodium carbonate, and 900°C, which is higher than the melting point of sodium carbonate. The particle size of the inlet was 90-125 um. Table 12 shows the results from the experiments.

Table 12. NO reduction by 90-125 um Na_2CO_3 droplets in laminar entrained-flow reactor experiments.

Temperature, °C	800	800	900	900
Residence time, s	5.2	5.2	5.2	5.2
Gas flow rate, l/min	7.9	7.9	7.9	7.9
Na_2CO_3 feed rate, g/min	.073	.083	.206	.199
NO inlet concentration, ppm	100.82	100.82	102.05	100.64
NO outlet concentration, ppm	100.72	100.78	101.39	99.97
NO conversion, %	0.10	0.04	0.64	0.67

The conversions were low at both temperatures. At 900 °C, the pseudo-first order reaction rate coefficient was calculated from the rate equation by rearranging it. Since the change in the NO concentration was less than 1 %, differential analysis was used. The reactor was assumed to be a plug flow reactor, and the velocity of the particles was taken to be equal to that of the gas. Further, the volume of the Na_2CO_3 droplets was assumed to be negligible compared to the volume of the gas.

With these assumptions, the reaction rate $-r_{NO}''''$ was calculated by

Eq. 26:

$$-r_{NO}'''' = \frac{c_{NOin} - c_{NOoit}}{t}$$

where c_{NOin} = inlet NO concentration, mol/m^3
c_{NOout} = outlet NO concentration, mol/m^3
t = residence time, s

H_{NO} and $D_{NO/Na}$ depend on temperature and were taken from correlations found in the literature.

Eq. 27:

$$D_{NO/Na} = \frac{(117.3 \times 10^{-18}\,\mathrm{cm}^2/\mathrm{s})\sqrt{\varphi \frac{M_{Na2CO3}}{g/mol}}\,\frac{T}{K}}{\frac{\mu}{cP}\,\frac{\nu}{m^3/kmol}}$$

(Treybal, 1980).

where $N_{NO/NA}$ = diffusivity of NO in molten Na_2CO_3,
φ = association factor for solvent = 1

M_w = molecular weight of sodium carbonate, 106 g/mol

μ = viscosity of molten sodium carbonate (cP)

= 3.832×10^{-5} cP exp(13215K/T), T is temperature (Janz et al., 1968)

T = temperature (K)

ν = solute molal volume at boiling point of NO (m^3/kmol)

= 0.0236 m^3/kmol

The Henry's law constant H_{NO} can be calculated from the following correlation (Andersen, 1979)

Eq. 28: $$H_{NO} = (\text{mol/m}^3\text{-atm}) \exp\left(\frac{-4\pi N r^2 \gamma}{82.06T/K}\right)$$

where N = Avogadro's number = 6.022×10^{23}

r = molecular radius (m) = 1.26×10^{-10} m

γ = (254.8 - 0.0502t/°C)/1000 (N/m), t = temperature (°C) (Janz et al., 1969)

T = temperature (K)

k_{ag} is the gas side mass transfer coefficient expressed in the units of mol/(m^2 Pas). Its relationship to the more commonly used k_g is

Eq. 29: $$k_{ag} = \frac{k_g}{RT}$$

For forced convection around a solid sphere, k_g is given by (Cussler, 1984)

Eq. 30: $$\frac{k_g d}{D} = 2.0 + 0.6Re^{1/2}Sc^{1/3}$$

where Re = Reynolds number = $du\rho/\mu$

Sc = Schmidt number = $\mu/(\rho D)$

By assuming that the gas velocity is equal to the solid velocity, Re = 0 and Eq. 30 becomes

Eq. 31: $$k_g = \frac{2D}{d}$$

where D = diffusivity of NO in nitrogen (m^2/s)

d = diameter of the particle (m)

The diffusivity of NO in nitrogen can be calculated by using equation

Eq. 32: D

$$= \frac{1.86\times10^{-3}\,m^2/s\left(\frac{T_f}{K}\right)^{3/2}\left(\frac{g/mol}{M_{NO}}+\frac{g/mol}{M_{N_2}}\right)}{\frac{p}{atm}\left(\frac{\sigma_{NO-N_2}}{Å}\right)^2\Omega}$$

where T_f = film temperature (K)

Mi = molecular weight (mol/g)

P = atmospheric pressure (atm)

σ_{N2-O2} = Lennard-Jones parameter, collision diameter (Å)

Ω = collision integral (-)

The collision integral depends on the value of a second Lennard Jones parameter, k. Values for both parameters and how to evaluate for the collision integral can be found in e.g. Sherwood et al. (1975).

In estimating the interfacial surface area a it was assumed that the droplets were spherical and that there was no fume formation. a is given by

Eq. 33: a = particle surface area/ reactor volume

$$= \frac{\frac{m}{\rho}\frac{4\pi r_p^2}{4\pi r_p^3/3}}{V_r} = \frac{3m}{\rho r_p V_r}$$

where m = total mass of sodium carbonate input (g)

ρ = density of sodium carbonate (g/cm^3)

= $2.4797 - 0.4487 \times 10^{-3}$ T/K (27), T = temperature (K)

r_p = radius of sodium carbonate particle = 120×10^{-6} m

Vr = reactor volume, m^3

To verify that Eq. 24 is applicable, the Hatta number was also calculated. In this case, the Hatta number is much higher than 2, which indicates that the reaction takes place only in the liquid film (Levenspiel, 1996). The enhancement factor was also calculated to classify the reaction as fast or slow. It was found to be considerably higher than the Hatta number, thus it suggests that the reaction of NO in molten sodium carbonate is fast and it is appropriate to use Eq. 24 for calculations.

The rate constant was calculated and is compared to that obtained by Thompson and Empie (1995) in Table 13. There is good agreement between the rate constant despite the very different experimental systems and several assumptions used in the calculations.

Table 13. Comparison of NO reduction by Na_2CO_3 in the experiments of Thompson and Empie (1995) and the current study.

Reactor	Temperature (°C)	Conversion of NO (%)	Ea/R (K)	k_1 at 900°C (1/s)
Gas containing NO bubbled through molten Na_2CO_3	860 - 973	10 - 75	44,780	0.81×10^6
Droplets of Na_2CO_3 entrained in a gas containing NO	900	0.64-0.67		1.2×10^6

This is the rate of NO reduction by Na_2CO_3 in the absence of any reducing gas components. There is some evidence that the rate may be enhanced if gases such as CO are present. As part of the earlier DOE project the reduction of NO by fume had been studied in a fixed bed reactor at temperatures 550-750°C. Na_2CO_3 and Na_2SO_4 were used as the fume particles. Limited reduction of NO was detected with Na_2CO_3 in the absence of CO but an enhanced rate of NO reduction when CO was added. Without CO there was reduction only at the highest temperature (less than 3 %) but with 5000 ppm CO a reduction of 40 % was obtained with the conditions used.

Assuming pseudo-first order kinetics in NO the rate coefficient with 5000 ppm CO was

Eq. 34: $k = 59400\ m^3/(m^2s)\ \exp(-180\ kJ/mol/RT).$ (5000 ppm CO, 550-750°C)

No reduction of NO was detected over Na_2SO4_3 regardless of whether CO was present or not.

Some experiments were made in the laminar entrained-flow reactor to study the effect of CO on the reduction of NO by molten Na_2CO_3. In these experiments, the NO concentration was 250 ppm and the CO concentration 5000 ppm and the temperature 900-1100 °C. The feed rates of Na_2CO_3 varied from 0.016 to 0.83 g/min. The NO reduction with Na_2CO_3 and CO was 1.1-5.7 %. At 900 °C, the pseudo first order reaction rate coefficient with 5000 ppm was on average 50 times the rate coefficient without CO. Using the same form of reaction rate equation as for NO reduction by char

Eq. 35 $-r_{NO} = (k_1 + k_2[CO])[NO]$.

The rate coefficients at 900 °C are

Eq. 36 $k_1 = 0.8 \times 10^6$ 1/s

Eq. 37 $k_2 = 0.0078$ 1/(s ppm)

Comparison of NO Reduction in the LEFR to the Rates of NO Reduction by Black Liquor Char and Fume.

NO reduction had been observed in the laminar entrained-flow reactor experiments of black liquor combustion and pyrolysis. The reduction during pyrolysis experiments was very rapid, and up to 90 % of the NO formed during pyrolysis became reduced. The reduction during combustion was more limited.

The rates of black liquor reduction in the laminar entrained-flow reactor experiments were compared to the rates of NO reduction by black liquor char and fume. During combustion, NO reduction was detected only when there was no char left. Therefore only fume was included in the comparison during combustion.

In black liquor pyrolysis and combustion experiments, NO reduction was observed at the following conditions

at 700°C, 0,4 and 21 % O_2, 1.6 - 2.2 residence time
at 900°C, 0 % O_2, 0.6 - 2.2 residence time
at 900°C, 4 and 21 % O_2, 1.6 - 2.2 residence time
at 1100°C, 0 % O_2, 0.3 - 2.2 residence time
at 1100°C, 4 % O_2, 1.6 - 2.2 residence time

NO reduction by molten sodium carbonate was calculated for these conditions. The calculations were made at 900°C, which is in the temperature range studied by Thompson and Empie (1995). First, the amounts of fume at that condition must be found. The amounts of fume were calculated based on LEFR experiments by Reis (1995). Table 14 shows the percentages of sodium carbonate fume produced at each condition at 900°C.

Table 14. The percentages of sodium carbonate fume at 900 °C (Reis, 1995).

Oxygen content (%)	Fume production as a fraction of black liquor solid (wt.%)	Na_2CO_3 content in fume (wt%)	Na_2CO_3 in fume as a fraction of black liquor solid (wt%)
0	3	49.8	1.49
4	3	67.6	2.03
21	16	97.4	15.58

The conversion of NO was calculated by assuming that the gas velocity was the same as the black liquor solid velocity, and that there was complete mixing in radial direction but no mixing in axial direction. In other words the reactor was treated as a plug flow reactor with cocurrent flows of the gas and particles. This can be treated as a batch reactor.

The change in concentration can be solved from the following equation:

Eq. 38:
$$t = \frac{c_{NO,o} V}{V_r} \int_0^{X_{NO,f}} \frac{dX_{NO}}{-r_{NO}''''}$$

where t = residence time (s)
$C_{NO,o}$ = initial NO concentration (mol/m^3)
V_r = reactor volume (V_r)
X_{NO} = NO conversion (-)
$X_{NO,f}$ = NO conversion at time t (-)
V = void volume in the reactor (m^3)
$-r_{NO}''''$ = rate of reaction based on reactor volume (mol/m^3-s)

By assuming that the void volume of the reactor is approximately the same as the reactor volume, Eq. 38 becomes

Eq. 39:
$$t = C_{NO,o} \int_0^{X_{NO,f}} \frac{dX_{NO}}{-r_{NO}''''}$$

By inserting equation Eq. 24 into equation Eq. 39 and integrating, the concentration of NO is given by

Eq. 40: $C_{NO} = C_{NO,o} \exp(-KRTt)$

where C_{NO} = NO concentration at time t (mol/m^3)
$C_{NO,o}$ = initial NO concentration (mol/m3)
R = universal gas constant = 8.314 J/mol-K
T = temperature (K)
$K = \dfrac{a}{1/k_{ag} + 1/H_{NO}D_{NO/Na}k_1}$

The NO concentrations at each residence time were calculated by using the rate constant of Thompson and Empie(1995). Thus, these concentrations were calculated based on the effect of molten sodium carbonate only. The results are presented in Table 15. The table shows, for the periods when NO reduction was detected the concentrations that were actually measured in the LEFR and the concentration based on the effect of molten Na_2CO_3.

In the pyrolysis experiments (at 900 °C, 0% O_2), the NO reduction calculated based on the effect of molten sodium carbonate accounted for less than 2 % of the NO reduction that actually occurred. During combustion, the NO reduction by Na_2CO_3 accounted for 5 - 6 % of the total NO reduction.

Table 15. The comparison between the concentrations obtained from calculations and concentration obtained from experiments at different residence times at 900 °C.

Oxygen (%)	Residence Time Range (s)	Time Beginning (s)	Time Ending (s)	NO at time beginning (%)	NO at time ending from calculations (%)	NO at time ending from experiments (%)
0	0.6 - 2.2	0.6	1.1	12.04	12.02	10.68
			1.6		12.02	3.01
			2.2		12.02	1.45
4	1.6 - 2.2	1.6	2.2	39.07	38.99	37.73
21	1.6 - 2.2	1.6	2.2	48.78	48.23	40.38

During pyrolysis, the NO reduction has been attributed to NO reduction by char (Iisa et al., 1995). There was good agreement between the NO reduction observed and that by black liquor char. The reduction rates by black liquor char were of the same order of magnitude as the total NO reduction rates but The rates by fume particles were about five orders of magnitude slower than the total reduction rates. It was concluded that the reduction by fume was negligible during pyrolysis and that reduction by black liquor char was significant.

However, in the combustion experiments (at 900 °C, 4 and 21% O_2), there was not much char left, in particular in the experiments conducted in 21% O_2. Black liquor char, in this case, may not be a significant factor in NO reduction.

One reason for the estimated low effect during combustion is that molten sodium carbonate may not be the only substance that can reduce NO. Thompson (1995) also found that the depletion of NO was greatly enhanced by the presence of Na_2S. This may account for part of the NO reduction in our experiments.

Another possibility for the higher measured NO reductions is that the presence of CO might increase the NO reduction rate. For solid sodium carbonate, there was a huge difference between NO reduction depending on if CO was present or not. The same might be true for molten sodium carbonate. From these reasons, it can be concluded that the presence of Na_2S and/or CO may increase the reduction rate and it may account for the total NO reduction observed in the combustion experiments.

Model for NO Formation During Black Liquor Combustion

Model for NO Formation from Nitrogen in the Black Liquor

There are two sources of fuel nitrogen: volatile N and char N. For the release of volatile N from the black liquor the equations were developed in the experimental section for N release during pyrolysis. The N is to be released as 50 % N_2 and 50 % NH_3. This estimate is based on measurements of NH_3 release by during black liquor pyrolysis by Aho et al. (1994). For the oxidation of NH_3 two routes will be taken into account: homogeneous gas phase reactions and reactions catalyzed by fume compounds.

NO formation from black liquor char strongly depends on the gas atmosphere. Forssen et al. (1995) had studied the char nitrogen oxidation by single droplet experiments. At higher gas temperatures (>800 °C) and higher oxygen concentrations (>1%) the char nitrogen was oxidized at the same time as char carbon, and NO was formed. At low temperatures and low oxygen contents, however, the nitrogen was not released until all of char carbon was consumed. If oxidation was stopped, the N remained in the char. During gasification in 20% CO_2 there was little formation of NO, and approximately two thirds of the original char nitrogen was retained in the residue.

These results suggest that under oxidative conditions NO is formed but if the atmosphere is reducing, no NO is formed. A model taking this difference into account is suggested. Here, the difference between an oxidative or reducing atmosphere is made based on whether O_2 reaches the char surface or not. In the former case, char oxidation occurs by reactions with O_2, in the latter by gasification reactions with either H_2O or CO_2. The NO formation will be the following:

1) If O_2 reaches the char surface, all of the N remaining in the char forms NO. The release of N and formation of NO is taken to occur proportionally to the carbon conversion in the char.
2) If O_2 does not reach the char surface, there is only N release that is consistent with the N release during extended pyrolysis. This N is released as N_2.

This model does not take into account the finding by Forssen at al. (1995a) that at temperatures below 800 °C, when it is more likely that O_2 reaches the char surface, NO was not formed simultaneously with CO_2. However, the char temperatures are typically higher than 800 °C, and it is expected that the impact of this is negligible. A change could be made requiring that the char temperature exceeds a certain value before any NO is formed. Increases in both the gas temperature and the O_2 concentration increase the char surface temperature. Thus the introduction of a threshold char surface temperature would account for the observed impacts of both the gas temperature and bulk gas oxygen concentration.

Homogeneous NH_3 Oxidation (Volatile Fuel NOx)

During fossil fuel combustion, fuel nitrogen is mainly released as HCN. Therefore, most of the global reaction mechanisms for fuel NO formation apply to HCN intermediate, and not to NH_3. However, global reaction schemes have been developed for selective non-catalytic NO reduction in which NH_3 reacts with NO in the presence of excess O_2. One such mechanism was developed by Duo et al. (1992), and it has been selected here to present volatile fuel NOx formation.

The reaction scheme by Duo et al. consists of two reactions, one in which NO and NH_3 react to form N_2 and one in which NH_3 is oxidized to NO. The reaction rate coefficient of the first reaction is k_{ox} and of the second k_r. Globally the rates of NO disappearance or formation and NH_3 formation are presented as

Eq. 41: $r_{NO} = k_{ox}[NH_3] - k_r [NH_3] [NO]$

Eq. 42: $r_{NH3} = -k_{ox} [NH_3] - k_r [NH_3] [NO]$

The reaction rate coefficients are

Eq. 43: $k_{ox} = (2.21 \pm 0.33) *10^{14}\ s^{-1} \exp[-(38160 \pm 170)K/T]$

Eq. 44: $k_r = (2.45 \pm 0.49) *10^{14}\ s^{-1} \exp[-(29400 \pm 250)K/T]$

The expressions were developed from experiments with O_2 contents of 4 %, and are therefore strictly valid only under those conditions.

Prompt NOx

De Soete (1974) developed an expression for prompt NO formation during ethylene combustion:

Eq. 45: $d[NO]/dt=1.2*10^7(RT/p)^{1+b}[O_2]^b[N_2][Fuel]*\exp[-250\ (kJ/mol)/RT]$

where [i] = molar concentration of species i, mol/m^3
R = universal gas constant, 8.314 J/(mol*K)
T = temperature, K
p = pressure, Pa
b = reaction rate order with respect to O_2

The reaction order with respect to the O_2 concentration (b) depends on temperature and fuel/air ratio. No values for the reaction order were given in the paper. It was stated that at high temperatures typical of hydrocarbon flames it is close to one but approaches zero at low temperatures. A value for b was calculated based on the experimental data and the model in the paper. The values varied from 1.1 to 0.58 depending on temperature, and they are given in Table 16.

Table 16. Reaction rate order b for prompt NOx formation in experiments by de Soete.

Temperature	b
2200K	1.1
1950K	0.68
1800K	0.58

These temperatures are considerably higher than those encountered in recovery boilers. No data are available for lower temperatures. It could be assumed that b is between 0 and 0.58.

The model by de Soete was later modified by Dupont et al. (1993) for other fuels. Their model takes into account the impact of fuel air molar ratio.

Eq. 46: $d[NO]/dt=f*k'_{pr}*[O_2]^b[N_2][Fuel]^a*exp(-E_a'/RT)$

Eq. 47: $f=4.75+C_1n-C_2\theta+C_3\theta^2-C_4\theta^3$

where k'_{pr} = reaction rate constant, depends on fuel type

E_a' = activation energy, depends on fuel type and temperature, J/(mol*K)

b = reaction order with respect to O_2, depends on T and θ, -

a = reaction order with respect to fuel concentration, depends on T, -

C_1 through C_4= constants: $C_1=8.19*10^{-2}$, $C_2=23.2$, $C_3=32$, $C_4=12.2$

n = number of carbon atoms in fuel molecule

θ = equivalence fuel/air ratio

The values of C_i are given to be valid for aliphatic hydrocarbons and for equivalence ratios between 0.62 and 1.43. Here, the reaction rate coefficient and E_a depend on the fuel species. The activation energy is given as 178 kJ/mol for temperatures below 1650 °C for natural gas (mainly CH_4). The coefficient a for the fuel reaction order is one for low temperatures (less than 1500 K). Dupont et al. report that the reaction order with respect to O_2 is 0 at temperatures below 1000 K, and rises with temperature approaching 1 at high temperatures. No values for the reaction rate coefficient k' are given.

Since thermal NOx is not believed to contribute to NO emissions from recovery boilers, no equation describing thermal NOx formation is included. Equations for the rate of global thermal NOx formation can be found in e.g. Bartok and Sarofim (1991).

References

Adams, T.N., Frederick, W.J. (1988), Kraft Recovery Boiler Physical and Chemical Processes, American Paper Institute, New York, NY.

Aho, K., Hupa, M., Nikkanen, S. (1994), Fuel nitrogen release during black liquor pyrolysis, Part 2: Comparisons between different conditions, *TAPPI Jl.*, **77**, No7, 182-187.

Aho, K., Hupa, M., Vakkilainen, E. (1994), Fuel nitrogen release during black liquor pyrolysis, Part 1: Laboratory measurements at different conditions, *TAPPI Jl.*, **77**, No5, 121-127.

Andersen, R. E., J. (1979), *Transactions of Electrochemical Society*, 328-334.

Backman, R., Hupa, M., Uusikartano, T. (1985), Kinetics of Sulphation of Sodium Carbonate in Flue Gas, *1985 International Chemical Recovery Conference*, sponsored by CPPA and TAPPI, 445-450.

Barok, W., Sarofim, A. F., ed. (1991) Fossil Fuel Combustion: A Source Book, John Wiley & Sons, New York, NY.

Borg, A., Teder, A., Warnqvist, B. (1974), *Tappi J.*, **57**, No.1, p.126-129, 1974.

Cameron, J.H., Clay, D.T., Grace, T.M. (1985), Oxidative fuming-the phenomenon and possible interpretations, *Preprints, 1985 International Chemical Recovery Conference*, New Orleans, LA,1985, sponsored by Tappi/CPPA, 435-444.

Caranga, A. B. (1994), The release of NO during black liquor pyrolysis, MS Thesis, Oregon State University, Department of Chemical Engineering, Corvallis, OR.

Chan, L.K., Sarofim, A.F., Beer, J.M. (1983), *Combustion and Flame*, **52**, 37-45.

Cussler, E. L. (1984), Diffusion Mass Transfer in Fluid Systems, Cambridge University Press, Cambridge, England.

De Soete G., G. (1974), Overall reaction rates of NO and N_2 formation from fuel nitrogen, *15th Symp. (Int.) on Combustion*, 1093-1102.

Duo, W., Dam-Johansen, K., Østergaard, K. (1992), Kinetics of the Gas-Phase Reaction Between Nitric Oxide, Ammonia and Oxygen, *Can. Jl of Che. Eng.*, **70**, 1014-1020.

Dupont V., Pourkashanian, M., Williams, A. (1993), Modelling of process heaters fired by natural gas, *Journal of the Institute of Energy*, **66**, March 1993, 20-28.

Flaxman, R.J., Hallett, L.H. (1987), Flow and particle heating in an entrained flow reactor, *Fuel*, **66**, 607.

Fogler, H.S. (1992), Elements of Chemical Reaction Engineering, 2nd edition, Prentice Hall, NJ, p.625-635.

Forssen, M., Hupa, M., Hellstrom, P. (1995b), Liquor-to-liquor differences in combustion and gasification processes: nitrogen formation tendency, *1995 TAPPI Engineering Conference*, Preprints, Sponsored by TAPPI.

Forssen, M., Hupa, M., Pettersson, R., Martin, D. (1995a),Nitrogen oxide release during black liquor char combustion and gasification, *1995 International Chemical Recovery Conference*, sponsored by Technical Section, CPPA and TAPPI, B231-B239.

Furusawa, T., Kunii, D., Osuma, A., Yamada, N. (1980), *International Chemical Engineering*, **20**, 239-244.

Furusawa, T., Tsunoda, M., Tsujimura, M. and Adschiri, T. (1985), *Fuel*, **64**, 1306-1309.

Goel, S. K., Beer, J. M., and Sarofim, A. F. (1996), *Journal of the Institute of Energy,* **69**, 201-213.

Iisa, K., Carangal, A., Scott, A. (1995), Nitrogen oxide formation and destruction in recovery boilers, *1995 International Chemical Recovery Conference*, sponsored by Technical Section, CPPA and TAPPI, B241-B250.

Janz, G. I., Dampier, F. W., Lakshminarayanan, G. R., Lorenz, P. K., and Tomkins, R. P. T. (1968), Molten Salts: Volume 1, Electrical Conductance, Density, and Viscosity Data, National Standard Reference Data Series-National Bureau of Standards, October 15, 1968.

Janz, G. I., Lakshminarayanan, G. R., Tomkins, R. P. T., Wong, J. (1969), Molten Salts: Volume 2, Section 2: Surface Tension Data, National Standard Reference Data Series-National Bureu of Standards, August 28, 1969.

Kapteijn, F., Mierop, A.J.C., Moulijn, J.A (1984)., *J. Chem. Soc., Chem. Commun.*, 1085-1086.

Levenspiel, O. (1972), Chemical Reaction Engineering, 2nd edition, Wiley International Edition, p.483-485.

Levespiel, O. (1996), The Chemical Reactor Omnibook, OSU Book Stores, Corvallis, OR.

Mikkanen, E.I., Kauppinen, Jokiniemi, J.K., Singquefield, S.A., Frederick, W.J., Mäkinen, M. (1994), *AIChE Symposium Series*, **90**, No. 302.

Nichols, K. M., Lien, S. J., (1993), Formation of fuel NOx during black liquor combustion, *TAPPI J.*, **3**, 185-191.

Phimolmas, V. (1997), The effect of temperature and residence time on the distribution of carbon, sulfur and nitrogen between gaseous and condensed phase products from low temperature pyrolysis of kraft black liquor, MS Thesis, Oregon State University, Department of Chemical Engineering, Corvallis, OR.

Pianpucktr, R. (1995), Formation of NO during pyrolysis and combustion of kraft black liquor, MS Thesis, Oregon State University, Department of Chemical Engineering, Corvallis, OR.

Reis, V. V. (1994), Potassium and Chloride Release During Black Liquor Combustion, M.S. Thesis, Oregon State University, July 1994.

Rizhinshvili, G.V., Kaplun, L.V. (1985), *Bummazh. Prom.* (Moscow), **1**, p.26, Available Inst. Paper Chemical Translation No. T-2260 referenced by Cameron et al. (1985).

Rompho, N. (1997), Preliminary study of modeling of NO formation during black liquor combustion, MS Thesis, Oregon State University, Department of Chemical Engineering, Corvallis, OR.

Sherwood, T. K., Pigford, R. L., Wilke, C. R., Mass Transfer, McGraw-Hill, Inc., 1975.

Suuberg, E. M., Teng, H., Calo, J. M. (1991), *23rd Symposium (International) on Combustion*, The Combustion Institute, 1199-1205.

Tangpanyapinit, V. (1995) Catalytic effect of recovery boiler fume compounds on NH_3 oxidation, MS Thesis, Oregon State University, Department of Chemical Engineering, Corvallis, OR.

Thompson, L. M. (1995), The Depletion of Nitric Oxide by Reaction with Molten Sodium Carbonate and Sodium Carbonate/Sodium Sulfide Mixtures, PhD Thesis, Institute of Paper Science and Technology, Atlanta, Georgia.

Thompson, L. M., Empie, H. J. (1995), "Kinetics of NO Depletion by Reaction With Molten Sodium Carbonate", *AIChE Symposium Series*, **90**, No.302, 33-38.

Treybal, R. E. (1980), Mass-Transfer Operations, 3rd Edition, McGraw-Hill Book Company, New York, NY.

Wu, S. L., Iisa, K. (1998), Kinetics of NO reduction by black liquor char, *Energy & Fuels*, in press.

SINTERING AND DENSIFICATION OF RECOVERY BOILER DEPOSITS

LABORATORY DATA AND A RATE MODEL[1]

By:

U. Techakijkajorn, W.J. Frederick, and H.N. Tran

INSTITUTE OF PAPER SCIENCE AND TECHNOLOGY

---

[1] The results reported here were part of the M.S. Thesis of Udom Techakijkajorn (1995).

TABLE OF CONTENTS

LIST OF FIGURES

LIST OF TABLES

Abstract

The rate of sintering of dust particles from a kraft recovery boiler was measured experimentally by measuring the shrinkage of pellets made from the dust. The dust used was low in chloride content and high in potassium. The rate of sintering was measured constant temperature, from 300°C to 550°C, for times up to 8 hours. Microstructural changes of the sintered specimens were measured using scanning electron microscopy.

Sintering began at 350°C and increased rapidly with temperature over the temperature range investigated. At the higher temperatures, sintering was so rapid that deposits would densify to the point where they may not be removable by soot blowing in less than the normal soot blowing cycle. The three stages of sintering which have been reported for other materials were observed as well in this study.

The rate of sintering was modeled using rate models that had been used for sintering of other materials. The initial and intermediate stage sintering data fit well with models proposed by others for when volume diffusion is the controlling mechanism. A general, semi-empirical model for the sintering process of a well-packed dust is presented.

Introduction

Fouling of heat transfer surfaces and plugging of gas passages in kraft recovery boilers is a critical, production-limiting problem in many kraft pulp mills. The main method of removing these deposits is by soot blowing. A key issue for operators with boilers that foul and plug rapidly is how to optimize the frequency of soot blowing and the locations of the soot-blowers along the gas flow path of the boiler. The optimum frequency of soot blowing depends upon both how rapidly dust deposits on superheater, boiler bank, or economizer tubes, and how rapidly the deposit hardens to the point where soot blowing is ineffective in removing it. Earlier work by Tran et al.[1] showed that the strength of pellets made from recovery boiler dusts increase exponentially with pellet density. Their work showed that the time required for recovery boiler deposits to harden to the point where soot blowing would be ineffective could be as short as 15-20 minutes.

Sintering, the process of densification of the porous deposits, is responsible for hardening of recovery boiler deposits that form at temperatures below their lower melting point. In microscopic terms, sintering is a combining of small solid particles in contact into a single unit solid body[2]. There has been relatively little information available on the kinetics of the sintering of fume deposits, and there has been no way to predict the rate at which these deposits densify and harden.

The sintering process can be divided into three stages, labeled respectively the initial, intermediate, and final stages. Figure 1 shows the changes in microstructure during each stage of sintering process. The *initial stage* sintering, which is the least complex, involves inter-particle bridging, forming necks between the individual particles. Particles in contact will start forming necks while there still is a continuous open-pore channel within the particle assemblage. Neither grain growth nor a decrease in the number of voids occurs in this stage. However, as the necks become larger, the void space within the particle assemblage becomes smaller. At some point, smaller particles will combine with larger particles and disappear, resulting in a measurable increase in average grain-size. This is where the *intermediate stage* starts. The final stage occurs when all the pores are closed and only grain growth continues. Shrinkage or densification occurs mostly in the first two stages. In the final stage, the densification rate is extremely low. In real particle assemblages, there is no clear transition point between each stage because the compact material contains particles with a distribution of sizes and packing densities.

The basic mechanism of the sintering process is solid state mass transfer. Sintering is a diffusion-controlled process that involves the transport of atoms through different kinds of defects in the atomic structure. These defects may be vacant atom sites, interstitial atoms, or substitution of a foreign atom for a normal one. For a pure ionic or metallic compound, a sintering model can be from vacancy diffusion flux equations, with the equations specific to the diffusion mechanism(s). The motion of atoms from a normal position into an adjacent vacant site results in the movement of vacancies in the opposite direction. Mobility by means of this vacancy mechanism is the most common process, giving rise to the motion of atoms. For ionic species with more than one component, the diffusion process is controlled by the slower diffusing species[2].

Transport of the diffusing species can occur by a variety of mechanisms as illustrated in Figure 2. These include evaporation-condensation, surface diffusion, volume diffusion, and grain-boundary diffusion. Gas species which react with the solid phase can accelerate sintering[3,4]. More than one diffusion mechanism may occur simultaneously.

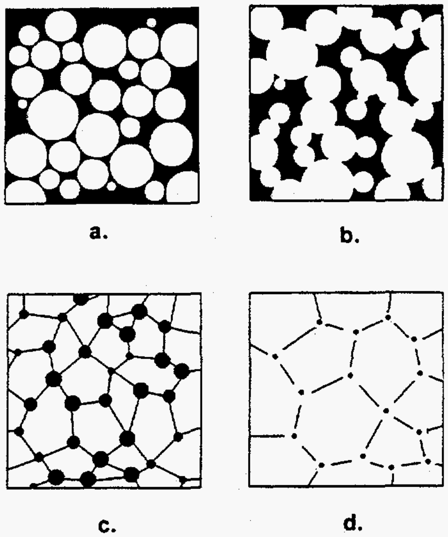

Figure 1. Microstructural development in each stage of sintering. (a) no sintering; (b) initial stage; (c) intermediate stage; (d) final stage.

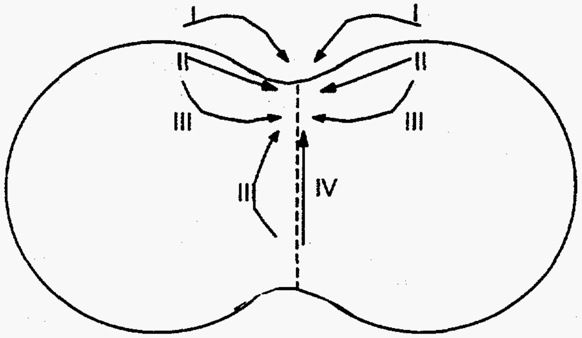

Figure 2. Diffusion mechanisms that occur during sintering. (i) Evaporation-condensation; (ii) surface diffusion; (iii) volume diffusion; (iv) grain boundary diffusion.

There has been very little work published on sintering of recovery boiler dusts or sodium salts in general. Tran et al.[5] investigated sintering of fume particles by heating pellets made from dusts collected in the electrostatic precipitator of a kraft recovery boiler. The pellets were heated for different times at temperatures from 300-600°C, and the changes in dimensions of the pellets were measured. They concluded that the minimum temperature for the sintering of fume dusts is about 300°C, and that the rate of sintering increases with temperature. Skrifvars et al.[6] evaluated the effect of dust chemical composition on the sintering of recovery boiler dusts and synthetic dusts. They sintered particle assemblages for fixed time periods (typically 4 hours) at constant temperature and measured the strength, rather than the dimensional changes of sintered specimens. Their work showed that both chloride and potassium content has significant effects on the degree of sintering of synthetic dusts, with chloride having the greater effect. Skrifvars and Hupa found no clear trend of the degree of sintering with composition of their boiler dusts. In neither of these studies were microstructural development or the kinetics of sintering evaluated.

Objectives

The objectives of the work reported here were to evaluate the mechanism of thermal sintering of dust deposits in kraft recovery boilers and to develop a model to predict the rate of sintering of these deposits in the convective heat transfer sections of kraft recovery boilers.

Experimental

In the work reported here, the rate of sintering was measured experimentally using pellets made from the precipitator catch (dust) from a kraft recovery boiler. Figure 3, a SEM photo of the dust used, shows that the grain size of the individual particles was 1 micron or less. The composition of dust is as follows: 26.0% Na, 9.9% K, 2.2 Cl, 58.6% SO_4^{2-}, 3.1% CO_3^{2-}. It was relatively low in chloride and high in potassium content in comparison with many recovery boiler dusts, but typical of the precipitator catch of recovery boilers operated hot in the lower furnace[7].

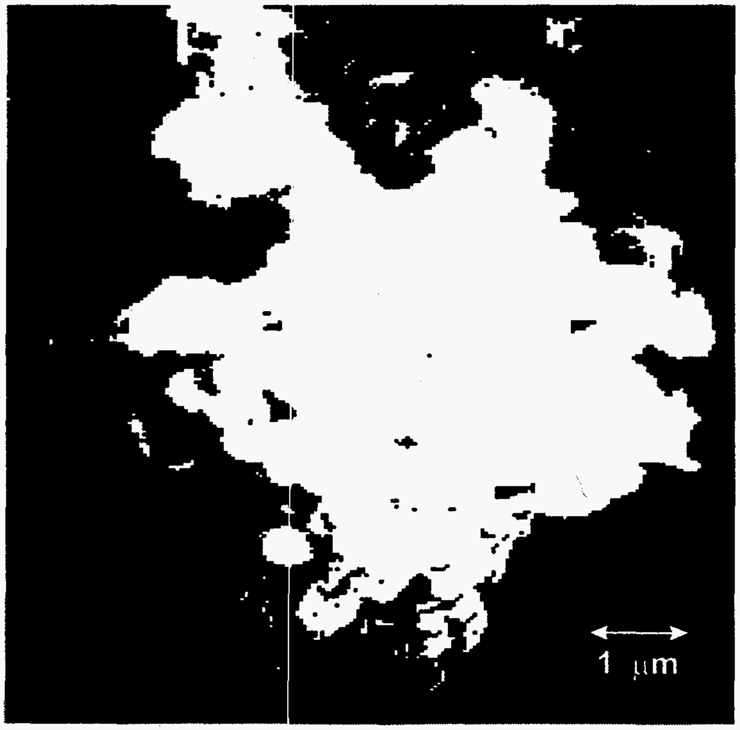

Figure 3. SEM photo of the dust (precipitator catch) used in this study.

The rate of sintering was measured by heating pretreated pellets at a constant temperature, ranging from 300°C to 550°C, for time intervals of 10 minutes to 8 hours and measuring the change in diameter and thickness of the pellets after heating. Pellets one inch (2.54 cm) in diameter were formed by by placing 3 g of dust into a cylindrical pellet mold and applying a pressure of 2500 psi (170 bar). Pellets that separated into layers upon removal from the press were rejected. Each pellet was then weighed to 0.1 mg and its thickness measured to 0.001 inch with a micrometer. The pellets produced had an average density of 1.43 g/cm^3. A few pellets were pressed at lower pressures to determine the effect of density on sintering rate.

The apparatus used to sinter the pellets is shown in Figure 4. For each sintering time and temperature, three pellets were placed on a ceramic plate and placed into the conditioning furnace at 200°C for 1 hour. This temperature was low enough so that no sintering occurred. The pellets and ceramic plate was then moved quickly to the sintering furnace that had been preheated to the desired sintering temperature. The ceramic plate was placed so that the thermocouple was in contact with the center pellet on the plate. The thermocouple measurements indicated that the pellets reached the temperature of the sintering furnace in 2-3 minutes.

When the pellets had been sintered for the desired time, the pellets and ceramic plate were removed from the sintering furnace and allowed to cool to room temperature. The thickness and diameter of each pellet were each measured three times at random positions on the pellet, and the average value of each was recorded as the pellet thickness and diameter. The pellets were again weighed. The sintering time and temperature were also recorded. Measurements were made with at least three pellets for each data point. Microstructural changes of many of the sintered specimens were measured using scanning electron microscopy.

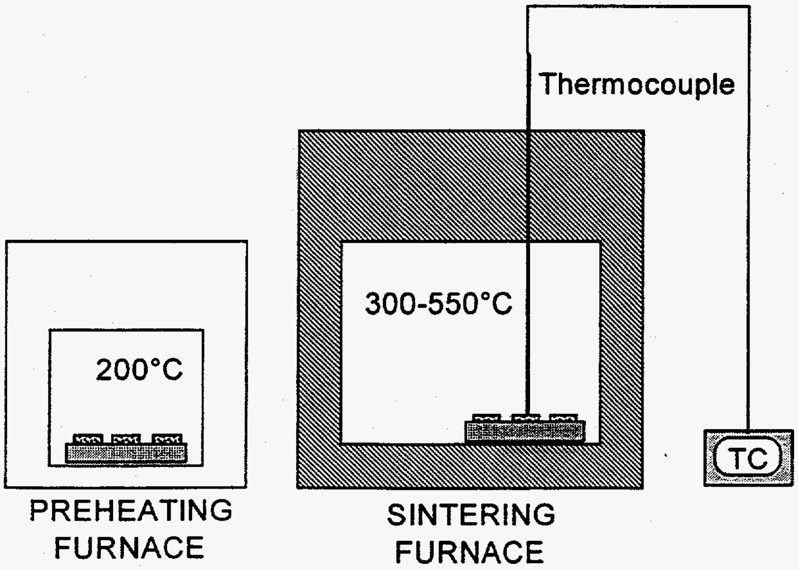

Figure 4. Experimental apparatus used for the sintering measurements.

Table 1 shows the sintering temperature and times and the initial density of the sintered pellets for the measurements made in this study.

Table 1. The sintering temperature and times and the initial density of the sintered pellets.

Temperature, °C	Initial density, g/cm^3	Sintering times, min
300	1.43	60, 120, 240, 480*
350	1.43	15, 20, 30, 45, 60, 90, 120, 180, 480*
400	1.43	5*, 7, 10*, 15, 20, 30*, 45, 60*, 120, 480*
450	1.43	3*, 4, 5, 7*, 10*, 15*, 20, 30*, 60*, 480*
450	1.36	5, 10, 15, 30, 60
450	1.19	5, 10, 15, 30, 60*
450	0.88	5, 10, 15, 30, 60
500	1.43	1, 2, 3*, 5*, 7, 10*, 15, 30, 60, 120, 240, 480*
550	1.43	30

*SEM analyses were made of pellets made at these conditions.

Results

Table 2 shows the degree of reproducibility obtained in the sintering measurements. The standard deviation of the pellet density was on average 1.1% and in the worst case 2.7% of the average density. In general the standard deviation decreased with increasing degree of sintering (density). The full set of experimental data are in Attachment A of this appendix.

Table 2. Reproducibility of sintering measurements.

Sintering temperature, °C	Sintering time, min	Number of pellets	Average density, g/cm^3	Standard deviation, g/cm^3
400	30	7	2.086	0.030
400	480	6	2.420	0.025
450	60	8	2.465	0.013
500	1	5	1.837	0.050
500	2	5	2.085	0.026
500	3	5	2.181	0.029
500	7	6	2.444	0.009
500	480	6	2.485	0.012

Figure 5 shows how the density of the dust pellets changed with time at different sintering temperatures. At 300°C, the pellets sintered very little in eight hours. At 350°C sintering occurred more rapidly. The pellets sintered at 450°C and 500°C reached the final stage of sintering, where the density no longer changes with time, in 60 minutes and 15 minutes respectively. As expected, the densification rate and the final density increased as the sintering temperature increased. This is in agreement with the sintering theory mentioned earlier that the process is thermally activated, and confirms the conclusion drawn by Tran et al.[5]

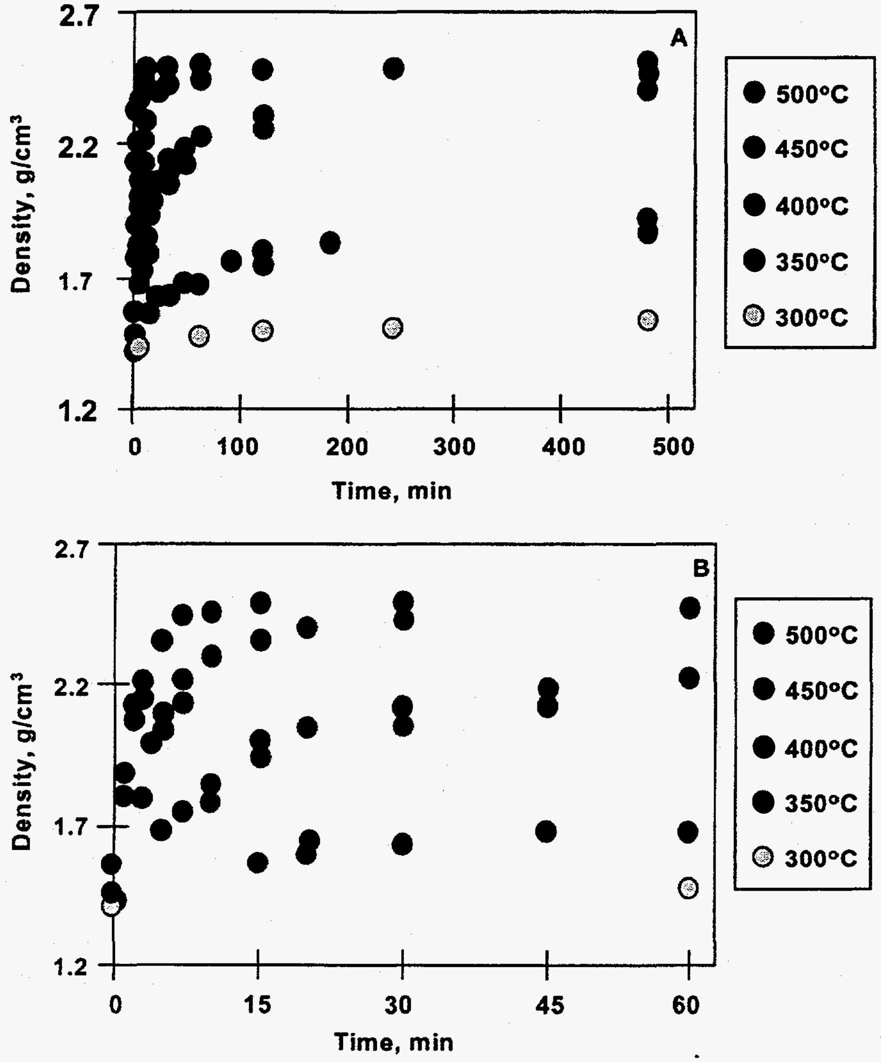

Figure 5. Pellet density versus time for fume pellets sintered at different temperatures. (A) all data; (B) expanded view of data to 60 minutes.

The densification rate was extremely low at 350°C and below, and the density increased very little during sintering. The lowest temperature at which sintering was observed was 300°C. Very little sintering occurred at temperatures below 400°C. The sintering rate was much faster at 400°C and above. The pellets reached their final density in less than 15 minutes when sintered at 500°C. At 450 and 500°C, the final density was independent of the sintering temperature. From 400°C to 500°C, some sintering had already taken place during heat-up in the sintering furnace before the pellet sample reached the desired temperature. The recorded density values at time zero for these temperatures are therefore higher than the density of an unsintered pellet. At lower temperatures, no sintering was detected during heat-up.

The upper limit for sintering temperature is defined by the fact that the material will begin to melt at a certain temperature. The existence of liquid phase at temperature above the first melting point results in a different densification mechanism. A detailed investigation of sintering above the onset of melting is beyond the scope of our study. However, in a few measurements of sintering made at 550°C, the final density of the pellets (2.20 g/cm^3) was less than that (2.49 g/cm^3) of pellets sintered at 500°C. SEM photos showed circular inclusions, indicative of entrapment of air bubbles during intermediate sintering[8].

Figure 6 shows how the final sintering increases with temperature. The SEM photos in this figure are all for pellets sintered for eight hours. At 300°C, only particle bridging occurred and. the average particle size did not increase. The pores are still open and connected. This photo shows that only initial stage sintering took place.

For the pellet sintered at 350°C, sintering occurred to the extent that some pores became closed and the average grain size increased slightly. This extent of sintering represents the transition between the end of the initial stage and the beginning of intermediate stage of sintering. The corresponding extent of linear shrinkage, which is about 10% for this pellet, was used as the criterion for the transition between the intermediate stages in the modeling work discussed later in this paper.

For the pellets sintered at 400-500°C for 8 hours, significant grain growth occurred. There were still some pores left in the 400°C pellet sample, but most of them are closed. The densification rate of this pellet had slowed very much by this point time (see Figure 5a). This indicates that sintering of dust pellets at 400°C reached the transition point between the intermediate stage and the final stage after 8 hours of sintering. At 450 and 500 °C, almost all of the pores were eliminated before 8 hours of sintering. There were still some tiny pores trapped at the grain corners, but the volume fraction of these pores is very small compared to the grain volume. The pellets sintered at these two temperatures reached the final stage in less than 30 minutes as can be seen in Figure 5b.

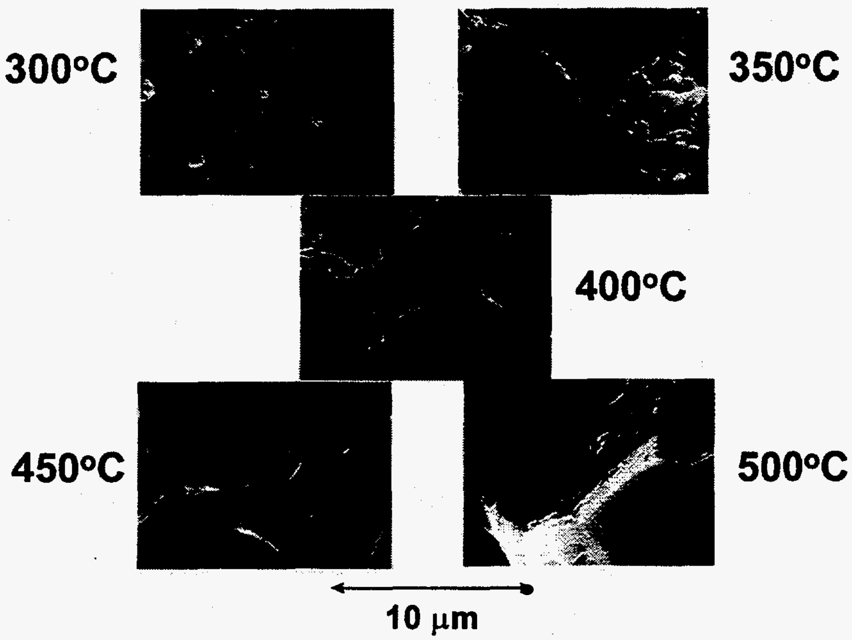

Figure 6. SEM photos of pellets sintered for eight hours at temperatures from 300-500°C.

The final grain size, determined by direct measurement from the SEM photos, is shown as a function of temperature in Figure 7. The final grain size increases sharply with sintering temperature.

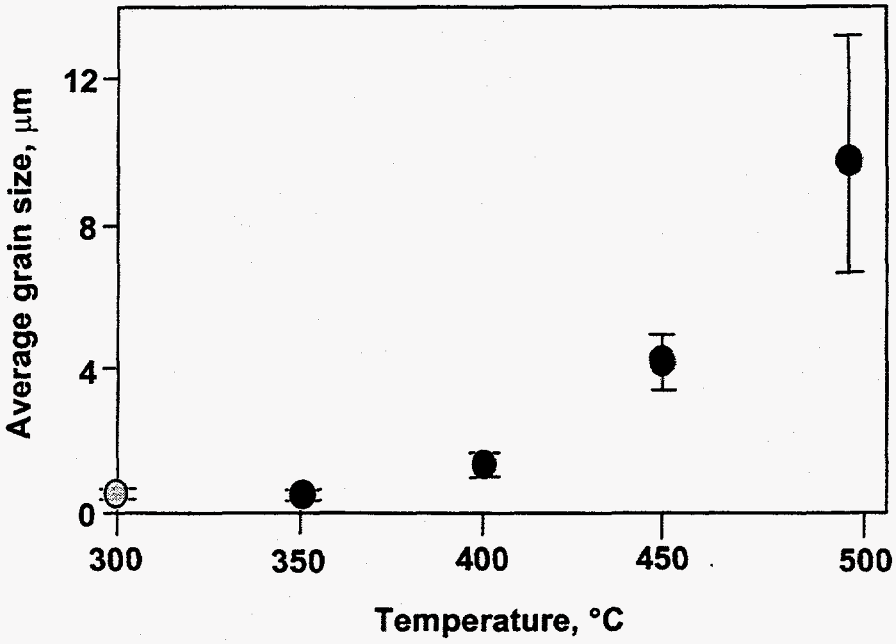

Figure 7. Final grain size at each sintering temperature. Error bars are standard deviations.

Figures 8-10 are SEM pictures of pellets sintered for different periods of time at 400, 450, and 500 °C respectively. At 400 °C, There was no grain growth for the pellets sintered for 5 and 10 minutes, but substantial grain growth after 30 minutes. Therefore, the intermediate stage sintering started somewhere between 10 and 30 minutes of sintering. At 450°C, there was no grain growth for the pellet sintered for 3 minutes, but substantial grain growth by 7 minutes. At 30 minutes, most of the pores were already eliminated and the sintering was in the final stage. This is in agreement with Figure 5 which shows that by 30 minutes the final density had been reached. At 500°C, the pellet sintered for 3 minutes experienced substantial grain growth and some degree of pore of closure. Hence, the sintering at this temperature reached the intermediate stage before 3 minutes. For the pellet sintered for 10 minutes, most of the pores were already eliminated and the sintering was already in the final stage. This agrees with Figure 5b which shows that at this time, the final density had been reached.

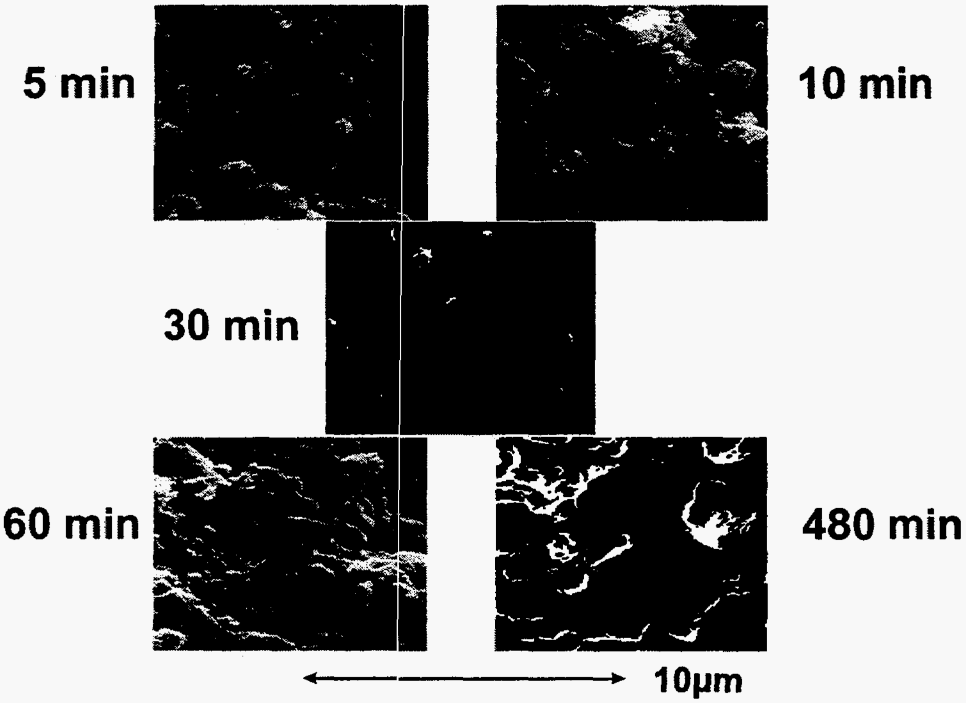

Figure 8. SEM photos of pellets sintered at 400°C for 5-480 minutes.

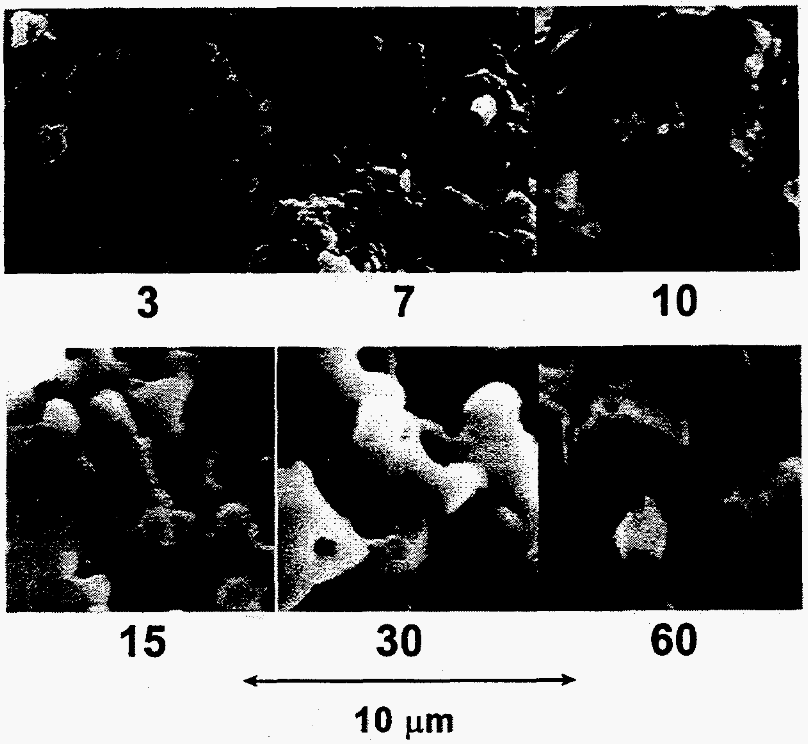

Figure 9. SEM photos of pellets sintered at 450°C for 5-480 minutes.

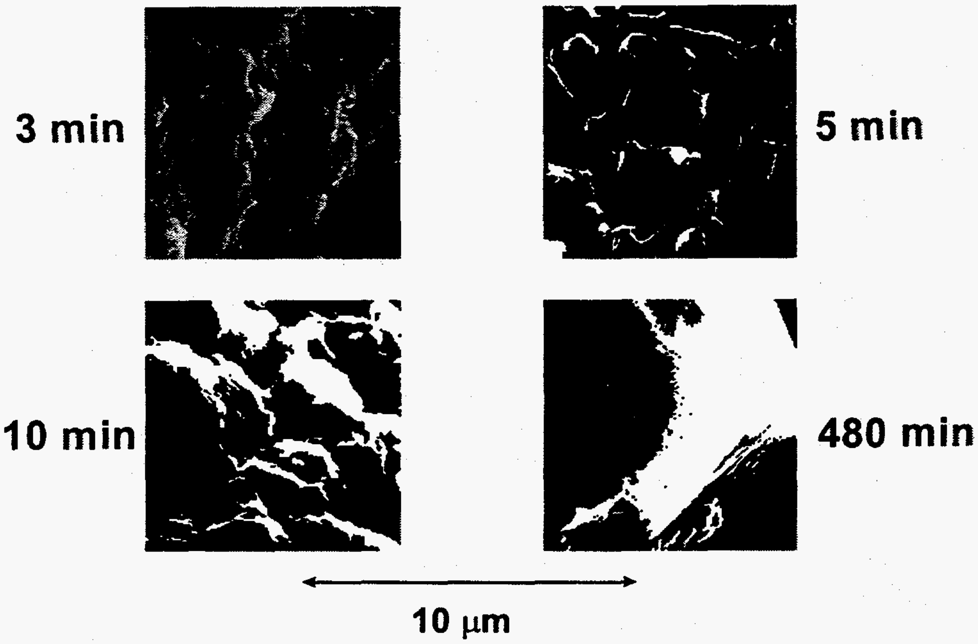

Figure 10. SEM photos of pellets sintered at 500°C for 3-60 minutes.

Grain size versus time data at each sintering temperature were obtained by direct measurement from the SEM photos. The isotherms of average grain size and its standard deviation versus time are shown in Figure 11.

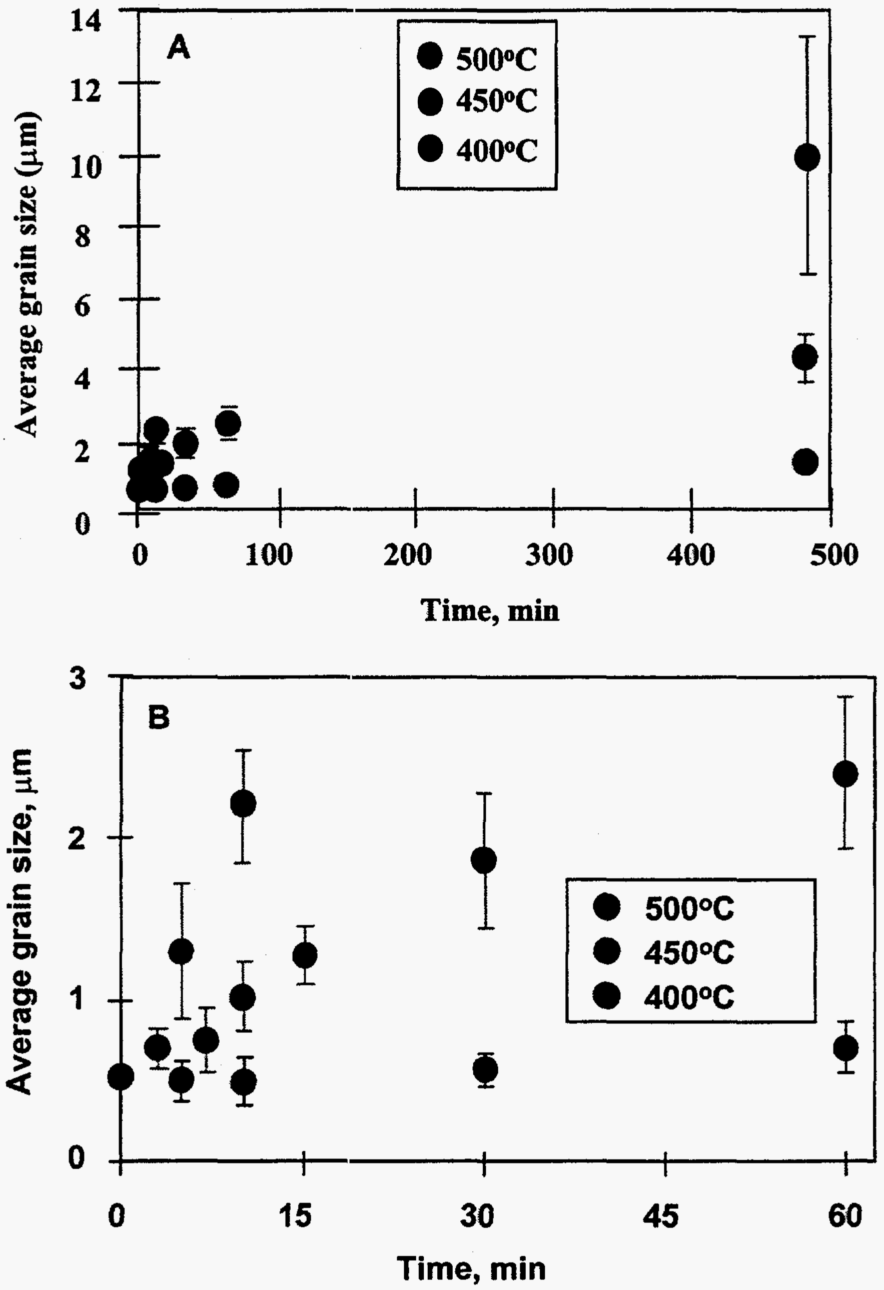

Figure 11.* *Grain size versus time at sintering temperatures from 400-500°C. Error bars are standard deviations.

The final grain sizes at each temperature were shown in Figure 7: The final grain size increases sharply with sintering temperature, from less than a micron to about 10 microns over the temperature range shown.

Effect of Initial Density on Sintering

A series of experiment were conducted to study the effect of the green density of pellets on the sintering kinetics. Pellets pressed to four different initial densities were sintered at 450°C for different period of time. The results are shown in Figure 12. The densification rate of these pellets was independent of the initial density of the pellet. All of the pellets reached their final density within about 60 minutes. The differences in final density were roughly the same as the differences in initial density.

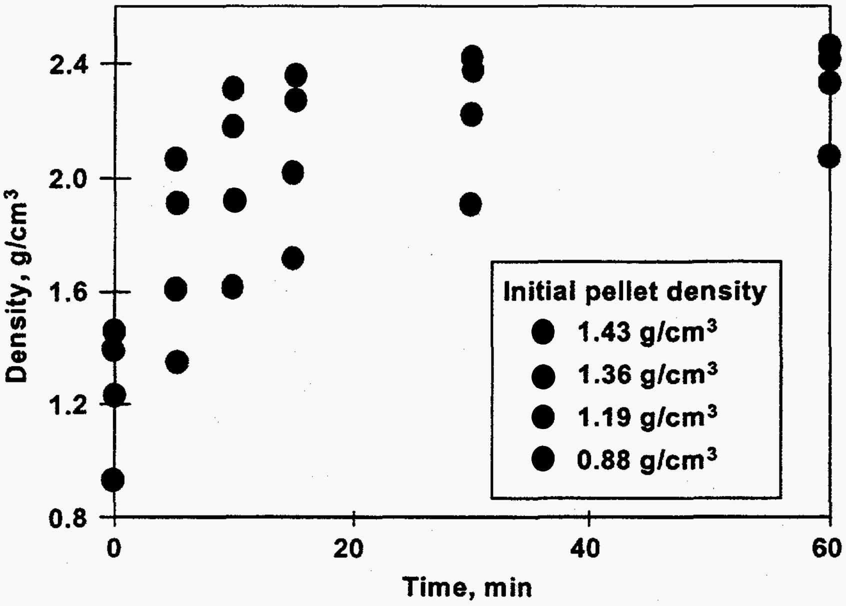

Figure 12. Sintering data for pellets with different initial densities at 450°C.

A Sintering Model

The basic mechanism of sintering is solid state mass transfer, i.e. a diffusion process which involves the transport of atoms through defects in the atomic lattice. These defects include vacant atom sites, interstitial atoms or substitution of a foreign atom for a normal one, and grain boundaries. For a pure ionic or metallic compound, a sintering model can be developed by using different vacancy diffusion flux equations depending on different diffusion mechanisms. The motion of atoms from a normal position into an adjacent vacant site results in the movement of vacancies in the opposite direction. Mobility by means of this vacancy mechanism is probably the most common process giving rise to atom motion. For multicomponent ionic species, the diffusion process is controlled by the slower diffusing species. Therefore, sintering is treated as a mass transfer due to chemical potential gradients of the constituents as recommended by Ready[2].

In this work, rate models that had been used for sintering of other materials were evaluated with the experimental data we obtained for recovery boiler dust. For the initial stage sintering, we used the model proposed by Kingery and Berg[9] when volume diffusion is the controlling mechanism, Eq. 2.

$$\frac{\Delta L}{L_0} = \left[\frac{k_1'\gamma\Omega D}{kTG_0^p}\right]^n t^n \qquad (2)$$

where $\Delta L/L_0$ = relative linear shrinkage

γ = surface energy

Ω = vacancy volume

D = self diffusion coefficient for either volume or grain-boundary diffusion

k = Boltzmann's constant

T = absolute temperature

G_0 = initial grain size

t = time

n,p,k_1' = numerical constants

Equation 2 applies when either volume or grain-boundary diffusion is the dominant mechanism in sintering. In earlier studies, the values of n and p have been found to be 0.4-0.5 and 3 respectively when volume diffusion dominates, and 0.3 and 4 respectively when grain-boundary diffusion dominates.

For intermediate stage sintering, we used the models developed by Coble[10] to predict the decrease in porosity of the particle assemblage with time. Eq. 3 applies for volume diffusion control and Eq. 4 for grain-boundary diffusion control.

$$\frac{dP}{dt} = \frac{-720D_v\gamma\Omega}{G^3kT} \qquad (3)$$

$$P = \left[\frac{2D_{GB}b\gamma\Omega}{G^4kT}\right]^{2/3} t^{2/3} \qquad (4)$$

where P = porosity

b = grain-boundary thickness

D_{GB} = grain-boundary diffusion coefficient

D_v = volume diffusion coefficient

Grain growth kinetics was described using a model developed by Yan et al.[11], Eq. 5.

$$G^N - G_0^N = m_0 e^{-\left(E_G/RT\right)}(t - t_0) \tag{5}$$

where N = grain growth kinetic exponent

m_0 = numerical constant

E_G = apparent activation energy for the grain growth process

R = ideal gas constant

The experimental sintering data obtained in this study was used to evaluate the parameters n, p, k_1', N, m_0, and t_0 in Eqs. 2 and 5. The time at which the transition from initial stage to intermediate stage sintering occurred (t_0) was taken as the time at which grain growth began to be observed. The grain size at the transition ($G_0(t_0)$) was also determined from these measurements.

Table 3. Experimentally determined values of t_0 and G_0 used in developing the sintering model.

Temperature, °C	Time at transition to intermediate stage (t_0), min	$G_0(t_0)$, micron
300	>480	0.50[1]
350	>480	0.50
400	30	0.57
450	7	0.75
500	3	0.70

[1] The average initial grain size of the dust.

The rate-controlling mechanism during initial stage sintering was determined by plotting the data from Figure 5 as relative linear shrinkage versus time on a log-log scale (Figure 13). At 400°C, the shrinkage at time zero was subtracted from the data points. Data above 400°C were omitted because there were too few points before the onset of intermediate stage sintering. The slopes of the three data sets are approximately 0.4, indicating that volume diffusion is the dominant sintering mechanism for this stage.

To develop the model for initial stage sintering, a value of 3, corresponding to the volume sintering mechanism, was assigned to the exponent p in Eq. 2. The constant k_1' and the terms γ, Ω, D, and k in Eq. 2 were combined as a single term (k_1) and evaluated at each temperature from the intercepts of the three data sets in Fig. 14. An initial grain size (G_0) of 0.5 microns was used to evaluate k_1. Logarithms of the three k_1 values were plotted versus 1/T to obtain a pre-exponential factor (8.71×10^3)

and an apparent activation energy (-227,900 kJ/mol) for volume diffusion. The resulting expression for k_l was inserted into Eq. 2 to yield the model for linear shrinkage during initial stage sintering, Eq. 6.

$$\frac{\Delta L}{L_0} = \left[\frac{8.71x10^3 e^{\left(-27,400/T\right)}}{TG_0^3} \right]^{0.4} t^{0.4} \tag{6}$$

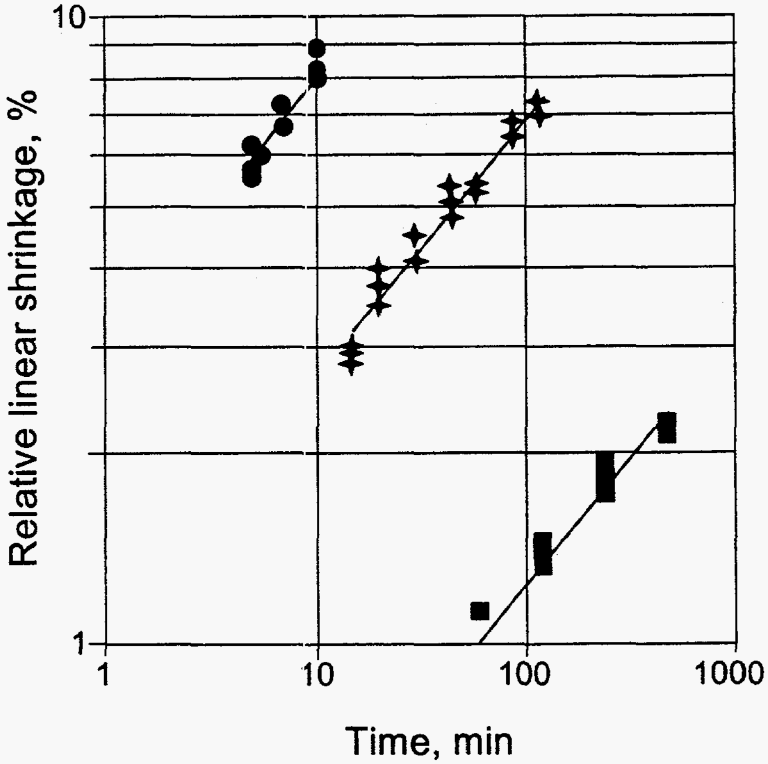

Figure 13. Relative linear shrinkage versus time for the initial stage sintering data.

To obtain the parameters m_0 and E_G for the grain growth model (Eq. 5), The grain size data in Figure 11 was plotted as G^N - G_0^N versus t-t_0. The values of G_0 and t_0 used at each temperature are those shown in Table 3. The slopes of these linear plots were then plotted as Arrhenius plots to obtain E_G, the apparent activation energy for grain growth (263.6 kJ/mol) and the constant m_0 ($1.42x10^{18}$ μm^3/min). The model for grain growth is then

$$G^3 - G_0^3 = 1.42x10^{18} e^{-\left(31,700/T\right)}(t - t_0) \tag{7}$$

To model shrinkage during intermediate stage sintering, we first assumed that the sintering mechanism was volume diffusion. Since grain size changes during intermediate sintering, an expression for G^3 from Eq. 5 was substituted into Eq. 3, and Eq. 3 was integrated to yield the Eq. 8 for the porosity of pellets during intermediate stage sintering. The ratio of terms $720D_v\gamma\Omega/k$ was combined into the constant k_2 in Eq. 7. The term m_0 in Eq 8 equals 1.42x10^{18} μm^3/min as in Eq. 7.

$$P = \frac{-k_2}{m_0 T}\ln\left[\frac{m_0\left(t - t_0\right) + G_0^3}{G_0^3}\right] + P_0 \qquad (8)$$

The constant k_2 was evaluated at each temperature by plotting the porosity of the pellets versus the term $\ln\left[\frac{m\left(t - t_0\right) + G_0^3}{G_0^3}\right]$. The slopes of the linear plots obtained were used in an Arrhenius plot to obtain $k_2 = 3.99\text{x}10^{17}\ e^{(-234{,}500/RT)}$. Substituting the values for k_2 and m_0 into Eq. 8 yielded the model for decrease in porosity during intermediate stage shrinking, Eq. 9.

$$P = \frac{-0.281}{T}e^{3500/T}\ln\left[1.42x10^{18}e^{-31{,}700/T}\frac{\left(t - t_{0e}\right) + G_0^3}{G_0^3}\right] + P_0 \qquad (9)$$

The apparent activation energies obtained for initial stage and intermediate stage sintering have very similar values, 228 kJ/mol and 235 kJ/mol. This supports our assumption that the sintering mechanism, volume diffusion, is the same for these two stages of sintering.

The sintering model represented by Eqs. 6, 7, and 9 was compared with data obtained in this study. To evaluate the sintering rate, the transition point from the initial stage to intermediate stage is set at 10% relative linear shrinkage. Grains start growing as soon as the intermediate stage begins. For the initial stage sintering, the porosity of cylindrical pellets can be calculated from the linear shrinkage using Eq. 10

$$P = 1 - \left(1 - P_{unsintered}\right)\left(1 - \frac{\Delta L}{L_0}\right)^{-3} \qquad (10)$$

where $P_{unsintered}$ is the porosity of an unsintered pellet. For the pellets pressed to a density of 1.43 g/cm^3 in this study, $P_{unsintered}$ is 0.43. The porosity of a sintered pellet at the start of intermediate stage sintering (P_0 in Eq. 8) is about 0.218. The average grain prior to the onset of intermediate stage sintering and grain growth (G_o) is about 0.5 mm The time intermediate stage sintering and grain growth begin can be calculated from Eq. 5 when $\Delta L/L_0 = 0.1$. Intermediate stage sintering is assumed to continue until the pore volume within the pellets is zero.

A comparison of the sintering model with experimental results is shown in Figure 14. The data are for pellets pressed to an initial density of 1.43 g/cm^3. The model agrees quite well with the experimental results. The largest disagreement between calculated and measured values occurs at 450 and 500°C. The model predicts a more rapid densification rate than was measured.. The model predicts that the initial stage ends within 1 minute at 450°C, while the experimental result indicate that the initial stage continued for 3 minutes. This implies that during the sintering test, the bulk of a pellet was significantly cooler than the surface of the pellet and slower to reach the sintering temperature. Therefore, these pellets did not shrink as much as predicted during the first few minutes of sintering. The effect of a temperature gradient in the pellet is more important at higher sintering temperatures. This effect also results in slower grain growth than predicted early in sintering at the higher temperatures. This limitation to the model could be overcome by including a heat transfer model to predict the temperature locally within the pellet until it reaches the furnace temperature.

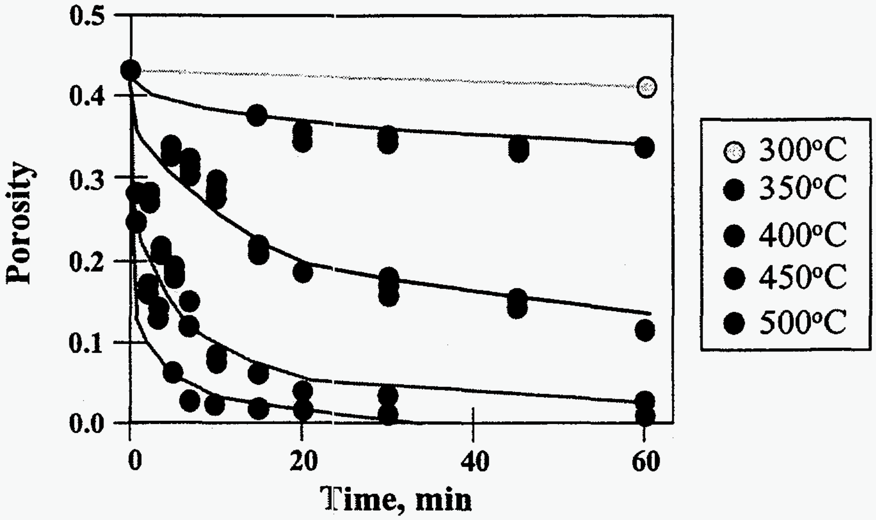

Figure 14. Porosity change with time for dust pellets with the same initial densities, sintered at different temperatures. Data are shown on an expanded time scale, 0-60 min. Solid lines were calculated with the sintering model.

The other deviation between the calculated and measured porosities was the higher final density predicted by the model at 400°C (not shown in Figure 14). This may be because intermediate stage sintering was assumed to occur until the porosity reached zero. It is likely that final stage sintering begins at the lower temperatures when there is still a significant pore volume within the pellets.

The model was also tested against the experimental result at 450°C for pellets of different initial density as shown in Figure 15. The model predicts a slower rate of densification than is actually observed for pellets of low initial density. This may be an effect of poorer heat transfer within the less dense pellets. The effect of heat transfer and other factors related to initial density clearly need to be accounted for in the model before it is applied to dust deposits on heat transfer surfaces in kraft recovery boilers.

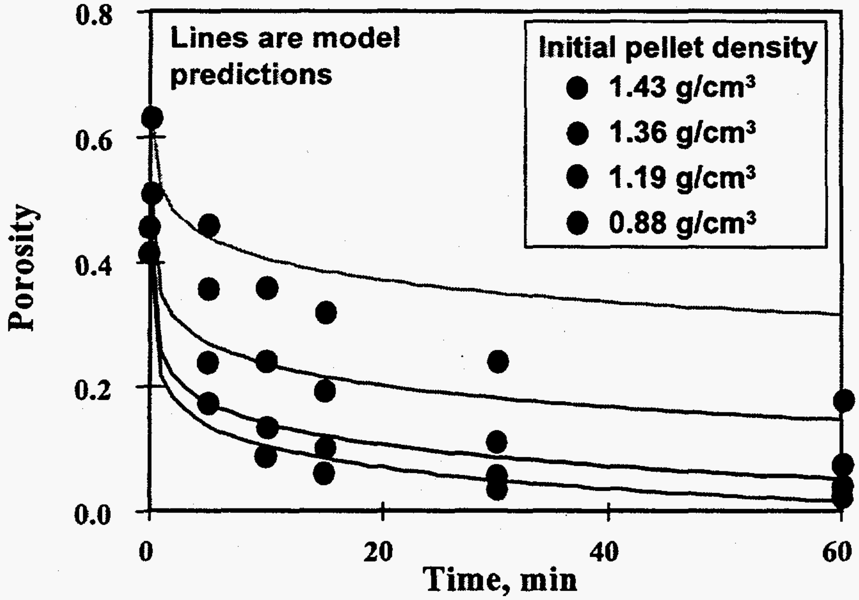

Figure 15. Porosity change with time for dust pellets with different initial densities, sintered at 450°C. Data are shown on an expanded time scale, 0-60 min. Solid lines were calculated with the sintering model.

Conclusions and Implications

The sintering behavior of the kraft recovery boiler dust evaluated below the onset of melting is similar to that of ceramic materials. Sintering occurs in three distinct stages, with densification but no grain growth in the initial stage, and both grain growth and densification rate in the intermediate stage. Sintering occurred via a volume diffusion mechanism.

The sintering rate data obtained in this study show that recovery boiler dusts can sinter and harden rapidly. In kraft recovery boilers, soot-blowers are normally activated on cycles ranging from two to eight hours. At temperatures between 400°C and the onset of melting, sintering was so rapid that deposits would densify to the point where they may not be removable by soot blowing at normal frequencies.

The model that has been presented here provides a basis for evaluating soot blowing strategies. The constants in the model probably depend on dust composition, so those presented here should not be considered universally applicable. Evaluations of sintering with dusts that encompass the range of variation in kraft recovery boilers need to be made to determine the influence of dust composition on sintering rate.

The data and model presented here do not account for the impact of reactive gases such as SO_2 on sintering rate. A parallel investigation of the impact of reactive gases on sintering of kraft recovery boiler dusts needs to be performed.

References

1. Kaliazine, A., Piroozmand, F., Cormack, D.E., and Tran, H.N., "Soot-blower Optimization - Part 2: Deposit-Soot-blower Interaction", Proceedings of 1996 Tappi Engineering Conference, Book 2, p.427-433, Tappi Press (1996).

2. Pask, J.A., "Grain boundaries in sintering", in *Science of Sintering*, p.381-393, Plenum Press, 1989.

3. Readey, D,W., "Mass transport and sintering in impure ionic solids"', *J. Am. Ceramic Society*, 49(17): 366-369 (1966).

4. Skrifvars, B.-J., W.J. Frederick, and M. Hupa, "Chemical Reaction Sintering as a Cause for Lime Kiln Rings," *Proc. 1992 TAPPI-CPPA Intl. Chemical Recovery Conf.*, TAPPI Press, Atlanta, June 7-11, pp. 161-167.

5. Lindblom, J., Hanson, C., Theliander, H., "Sintering of calcined lime mud - the influence of carbon dioxide." Proc. 1995 Intl. Chem. Recovery Conf., p. B141-B147, TAPPI Press, Atlanta (1995).

6. Tran, H.N., Barham, D., and Reeve, D.W., "Sintering of fireside deposits and its impact on plugging in kraft recovery boiler", *Tappi J.*, 70(4): 109-113 (1988).

7. Skrifvars, B., Hupa, M., and Hyoty, P., "Composition of recovery boiler dust and its effect on sintering", *Tappi J.*, 74(6):185-189.

8. Vakkilainen, E.K., W.J. Frederick, V.V. Reis, and K.J. Wåg, "Potassium and Chloride Enrichment During Black Liquor Combustion. Laboratory Data and Mechanistic Model," *Proc. 1995 TAPPI-CPPA International Chemical Recovery Conference*, Toronto, April 23-27, pp. B63-B76.

9. Techakijkajorn, U., "Sintering of Fume Deposits in Kraft Recovery Boilers." M.S. Thesis, Oregon State University, October, 1995.

10. Kingery, W.D. and Berg, M., "Study of the initial stages of sintering solids by viscous flow, evaporation-condensation, and self-diffusion", *Journal of Applied Physics*, 26(10): 1205-1212 (1955).

11. Coble, R.L., "Initial sintering of alumina and hematite", *Journal of American Ceramic Society*, 41(2): 55-62 (1958).

12. Yan, M.F., Cannon, R.M., and Bowen, H.K., "Grain boundary migration in ceramics", *Ceramics Microstructure*, p.276-307, Westview Press, 1976.

---

[1] Adams, T.N., Frederick, W.J., Grace, T.M., Hupa, M., Iisa, K., Jones, A., and Tran, H.N., *Kraft Recovery Boilers*, TAPPI Press, Atlanta (in press).

[2] Readey, D,W., "Mass transport and sintering in impure ionic solids"', *J. Am. Ceramic Society*, 49(17): 366-369 (1966).

[3] Skrifvars, B.-J., W.J. Frederick, and M. Hupa, "Chemical Reaction Sintering as a Cause for Lime Kiln Rings," *Proc. 1992 TAPPI-CPPA Intl. Chemical Recovery Conf.*, TAPPI Press, Atlanta, June 7-11, pp. 161-167.

[4] Lindblom, J., Hanson, C., Theliander, H., "Sintering of calcined lime mud - the influence of carbon dioxide." Proc. 1995 Intl. Chem. Recovery Conf., p. B141-B147, TAPPI Press, Atlanta (1995).

[5] Tran, H.N., Barham, D., and Reeve, D.W., "Sintering of fireside deposits and its impact on plugging in kraft recovery boiler", *Tappi J.*, 70(4): 109-113 (1988).

[6] Skrifvars, B., Hupa, M., and Hyoty, P., "Composition of recovery boiler dust and its effect on sintering", *Tappi J.*, 74(6):185-189.

[7] Vakkilainen, E.K., W.J. Frederick, V.V. Reis, and K.J. Wåg, "Potassium and Chloride Enrichment During Black Liquor Combustion. Laboratory Data and Mechanistic Model," *Proc. 1995 TAPPI-CPPA International Chemical Recovery Conference*, Toronto, April 23-27, pp. B63-B76.

[8] Techakijkajorn, U., "Sintering of Fume Deposits in Kraft Recovery Boilers." M.S. Thesis, Oregon State University, October, 1995.

[9] Kingery, W.D. and Berg, M., "Study of the initial stages of sintering solids by viscous flow, evaporation-condensation, and self-diffusion", *Journal of Applied Physics*, 26(10): 1205-1212 (1955).

[10] Coble, R.L., "Initial sintering of alumina and hematite", *Journal of American Ceramic Society*, 41(2): 55-62 (1958).

[11] Yan, M.F., Cannon, R.M., and Bowen, H.K., "Grain boundary migration in ceramics", *Ceramic Microstructure*, p.276-307, Westview Press, 1976.

Sintering Data, 300C													
	Sample Measurements												
	Before Heating			After Heating			Pellet Density			Shrinkage			
Time Heated	Weight	Height	Diameter	Weight	Height	Diameter	Before	After	Difference	Height	Diameter	Wt. Loss	ρ/ρ_{th}	P
min	g	mm	mm	g	mm	mm	g/cm3	g/cm3	%	%	%	%		
60.000	2.962	4.090	25.400	2.959	4.053	25.044	1.429	1.482	3.685	0.896	1.400	-0.101	0.591	0.409
60.000	2.960	4.110	25.400	2.956	4.087	25.112	1.421	1.460	2.751	0.568	1.133	-0.135	0.582	0.418
60.000	2.981	4.100	25.400	2.979	4.077	25.112	1.435	1.475	2.822	0.569	1.133	-0.067	0.588	0.412
Average	2.968	4.100	25.400	2.965	4.072	25.090	1.428	1.473	3.086	0.678	1.222	-0.101	0.587	0.413
120.000	2.958	4.070	25.400	2.956	4.030	25.053	1.434	1.488	3.740	0.983	1.367	-0.068	0.593	0.407
120.000	2.969	4.060	25.400	2.965	4.027	25.044	1.443	1.495	3.572	0.821	1.400	-0.135	0.596	0.404
120.000	2.957	4.060	25.400	2.954	4.013	25.027	1.437	1.496	4.091	1.149	1.467	-0.101	0.597	0.403
Average	2.961	4.063	25.400	2.958	4.023	25.042	1.438	1.493	3.801	0.984	1.411	-0.101	0.595	0.405
240.000	2.958	4.080	25.400	2.953	4.023	24.900	1.431	1.507	5.340	1.389	1.967	-0.169	0.601	0.399
240.000	2.961	4.060	25.400	2.958	4.003	24.934	1.439	1.513	5.132	1.396	1.833	-0.101	0.603	0.397
240.000	2.962	4.070	25.400	2.958	4.020	24.960	1.436	1.504	4.705	1.229	1.733	-0.135	0.600	0.400
Average	2.960	4.070	25.400	2.956	4.016	24.932	1.435	1.508	5.059	1.338	1.844	-0.135	0.601	0.399
480.000	2.963	4.050	25.400	2.959	3.977	24.824	1.444	1.537	6.479	1.811	2.267	-0.135	0.613	0.387
480.000	2.959	4.030	25.400	2.955	3.947	24.833	1.449	1.546	6.686	2.068	2.233	-0.135	0.616	0.384
480.000	2.960	4.100	25.400	2.957	4.020	24.850	1.425	1.517	6.450	1.951	2.167	-0.101	0.605	0.395
Average	2.961	4.060	25.400	2.957	3.981	24.836	1.439	1.533	6.538	1.943	2.222	-0.124	0.611	0.389

Sintering Data, 350C														
	Sample Measurements													
	Before Heating			After Heating			Pellet Density			Shrinkage				
Time Heated	Weight	Height	Diameter	Weight	Height	Diameter	Before	After	Difference	Height	Diameter	Wt. Loss	ρ/ρ_{th}	P
min	g	mm	mm	g	mm	mm	g/cm3	g/cm3	%	%	%	%		
15.000	2.964	4.070	25.400	2.960	3.980	24.638	1.437	1.560	8.538	2.211	3.000	-0.135	0.622	0.378
15.000	2.962	4.050	25.400	2.958	3.967	24.663	1.443	1.561	8.144	2.058	2.900	-0.135	0.622	0.378
15.000	2.960	4.040	25.400	2.962	3.960	24.680	1.446	1.564	8.130	1.980	2.833	0.068	0.623	0.377
Average	2.962	4.053	25.400	2.960	3.969	24.661	1.442	1.561	8.271	2.083	2.911	-0.067	0.623	0.377
20.000	2.961	3.960	25.400	2.958	3.843	24.384	1.476	1.648	11.687	2.946	4.000	-0.101	0.657	0.343
20.000	2.966	4.070	25.400	2.962	3.937	24.443	1.438	1.603	11.488	3.276	3.767	-0.135	0.639	0.361
20.000	2.965	4.040	25.400	2.962	3.923	24.511	1.448	1.600	10.467	2.888	3.500	-0.101	0.638	0.362
Average	2.964	4.023	25.400	2.961	3.901	24.446	1.454	1.617	11.214	3.037	3.756	-0.112	0.645	0.355
30.000	2.963	4.030	25.400	2.960	3.883	24.249	1.451	1.651	13.751	3.639	4.533	-0.101	0.658	0.342
30.000	2.964	4.050	25.400	2.961	3.910	24.249	1.444	1.640	13.536	3.457	4.533	-0.101	0.654	0.346
30.000	2.961	4.070	25.400	2.957	3.930	24.359	1.436	1.615	12.455	3.440	4.100	-0.135	0.644	0.356
Average	2.963	4.050	25.400	2.959	3.908	24.285	1.444	1.635	13.247	3.512	4.389	-0.113	0.652	0.348
45.000	2.964	4.040	25.400	2.959	3.870	24.028	1.448	1.686	16.454	4.208	5.400	-0.169	0.672	0.328
45.000	2.966	4.090	25.400	2.962	3.920	24.105	1.431	1.656	15.696	4.156	5.100	-0.135	0.660	0.340
45.000	2.964	4.020	25.400	2.960	3.883	24.172	1.455	1.661	14.147	3.400	4.833	-0.135	0.662	0.338
Average	2.965	4.050	25.400	2.960	3.891	24.102	1.445	1.668	15.432	3.921	5.111	-0.146	0.665	0.335
60.000	2.960	4.040	25.400	2.955	3.880	24.028	1.446	1.680	16.154	3.960	5.400	-0.169	0.670	0.330
60.000	2.959	4.080	25.400	2.955	3.897	24.011	1.431	1.675	17.006	4.493	5.467	-0.135	0.668	0.332
60.000	2.962	4.080	25.400	2.957	3.917	24.062	1.433	1.660	15.879	4.003	5.267	-0.169	0.662	0.338
Average	2.960	4.067	25.400	2.956	3.898	24.034	1.437	1.671	16.346	4.152	5.378	-0.158	0.666	0.334
90.000	2.966	4.020	25.400	2.961	3.807	23.647	1.456	1.771	21.632	5.307	6.900	-0.169	0.706	0.294
90.000	2.963	4.030	25.400	2.958	3.807	23.690	1.451	1.763	21.499	5.542	6.733	-0.169	0.703	0.297
90.000	2.964	4.020	25.400	2.960	3.820	23.757	1.455	1.748	20.128	4.975	6.467	-0.135	0.697	0.303
Average	2.964	4.023	25.400	2.960	3.811	23.698	1.454	1.761	21.086	5.275	6.700	-0.157	0.702	0.298

Sintering Data (Cont'd.), 350C														
	Sample Measurements													
	Before Heating			After Heating			Pellet Density			Shrinkage				
Time Heated	Weight	Height	Diameter	Weight	Height	Diameter	Before	After	Difference	Height	Diameter	Wt. Loss	ρ/ρ_{th}	P
min	g	mm	mm	g	mm	mm	g/cm3	g/cm3	%	%	%	%		
120.000	2.962	4.010	25.400	2.958	3.777	23.546	1.458	1.799	23.393	5.819	7.300	-0.135	0.717	0.283
120.000	2.965	4.100	25.400	2.960	3.877	23.630	1.427	1.741	21.987	5.447	6.967	-0.169	0.694	0.306
Average	2.963	4.067	25.400	2.958	3.832	23.563	1.438	1.771	23.136	5.766	7.233	-0.146	0.706	0.294
180.000	2.964	4.030	25.400	2.959	3.760	23.360	1.451	1.836	26.509	6.700	8.033	-0.169	0.732	0.268
180.000	2.955	4.000	25.400	2.950	3.753	23.495	1.458	1.813	24.344	6.167	7.500	-0.169	0.723	0.277
180.000	2.967	4.070	25.400	2.962	3.807	23.376	1.439	1.813	26.016	6.470	7.967	-0.169	0.723	0.277
Average	2.962	4.033	25.400	2.957	3.773	23.410	1.449	1.821	25.623	6.446	7.833	-0.169	0.726	0.274
480.000	2.967	4.120	25.400	2.961	3.773	22.818	1.421	1.919	35.026	8.414	10.167	-0.202	0.765	0.235
480.000	2.970	4.190	25.400	2.964	3.850	22.860	1.399	1.876	34.088	8.115	10.000	-0.202	0.748	0.252
480.000	2.967	4.140	25.400	2.962	3.820	23.012	1.414	1.864	31.810	7.729	9.400	-0.169	0.743	0.257
Avarage	2.968	4.150	25.400	2.962	3.814	22.897	1.411	1.886	33.641	8.086	9.856	-0.191	0.752	0.248

Sintering Data, 400C														
	Sample Measurements													
	Before Heating			After Heating			Pellet Density			Shrinkage				
Time Heated	Weight	Height	Diameter	Weight	Height	Diameter	Before	After	Difference	Height	Diameter	Wt. Loss	ρ/ρ_{th}	P
min	g	mm	mm	g	mm	mm	g/cm3	g/cm3	%	%	%	%		
0.000	2.950	4.080	25.400	2.946	4.080	25.358	1.427	1.430	0.198	0.000	0.167	-0.136	0.570	0.430
0.000	2.968	4.140	25.400	2.954	4.137	25.349	1.415	1.415	0.008	0.081	0.200	-0.472	0.564	0.436
0.000	2.970	4.130	25.400	2.957	4.130	25.341	1.419	1.420	0.029	0.000	0.233	-0.438	0.566	0.434
Average	2.963	4.117	25.400	2.952	4.116	25.349	1.420	1.421	0.078	0.027	0.200	-0.348	0.567	0.433
5.000	2.962	4.110	25.400	2.958	3.933	23.791	1.422	1.692	18.939	4.298	6.333	-0.135	0.675	0.325
5.000	2.960	4.100	25.400	2.956	3.937	23.961	1.425	1.665	16.879	3.984	5.667	-0.135	0.664	0.336
5.000	2.957	4.070	25.400	2.953	3.917	23.927	1.434	1.677	16.947	3.767	5.800	-0.135	0.669	0.331
Average	2.960	4.093	25.400	2.956	3.929	23.893	1.427	1.678	17.588	4.017	5.933	-0.135	0.669	0.331
7.000	2.959	4.050	25.400	2.954	3.833	23.546	1.442	1.770	22.740	5.350	7.300	-0.169	0.706	0.294
7.000	2.958	4.090	25.400	2.952	3.883	23.673	1.427	1.727	21.005	5.053	6.800	-0.203	0.689	0.311
7.000	2.963	4.080	25.400	2.957	3.900	23.707	1.433	1.718	19.851	4.412	6.667	-0.202	0.685	0.315
Average	2.960	4.073	25.400	2.954	3.872	23.642	1.434	1.738	21.199	4.938	6.922	-0.191	0.693	0.307
10.000	2.959	4.090	25.400	2.952	3.807	23.114	1.428	1.848	29.440	6.927	9.000	-0.237	0.737	0.263
10.000	2.956	4.060	25.400	2.951	3.793	23.292	1.437	1.826	27.067	6.568	8.300	-0.169	0.728	0.272
10.000	2.957	4.120	25.400	2.951	3.870	23.334	1.416	1.783	25.889	6.068	8.133	-0.203	0.711	0.289
Average	2.957	4.090	25.400	2.951	3.823	23.247	1.427	1.819	27.465	6.521	8.478	-0.203	0.725	0.275
15.000	2.957	4.040	25.400	2.952	3.663	22.598	1.444	2.009	39.096	9.323	11.033	-0.169	0.801	0.199
15.000	2.964	4.060	25.400	2.959	3.707	22.750	1.441	1.964	36.306	8.703	10.433	-0.169	0.783	0.217
15.000	2.954	4.050	25.400	2.950	3.720	22.809	1.439	1.941	34.825	8.148	10.200	-0.135	0.774	0.226
Average	2.958	4.050	25.400	2.954	3.697	22.719	1.442	1.971	36.743	8.725	10.556	-0.158	0.786	0.214
20.000	2.959	4.090	25.400	2.955	3.673	22.335	1.428	2.053	43.803	10.187	12.067	-0.135	0.819	0.181
20.000	2.969	4.080	25.400	2.964	3.687	22.394	1.436	2.041	42.130	9.641	11.833	-0.168	0.814	0.186
20.000	2.965	4.070	25.400	2.961	3.680	22.437	1.438	2.035	41.550	9.582	11.667	-0.135	0.811	0.189
Average	2.964	4.080	25.400	2.960	3.680	22.389	1.434	2.043	42.494	9.803	11.856	-0.146	0.815	0.185

Sintering Data (Cont'd.), 400C														
	Sample Measurements													
	Before Heating			After Heating			Pellet Density			Shrinkage				
Time Heated	Weight	Height	Diameter	Weight	Height	Diameter	Before	After	Difference	Height	Diameter	Wt. Loss	ρ/ρ_{th}	P
min	g	mm	mm	g	mm	mm	g/cm3	g/cm3	%	%	%	%		
30.000	2.959	4.090	25.400	2.954	3.667	22.208	1.428	2.080	45.668	10.350	12.567	-0.169	0.829	0.171
30.000	2.959	4.100	25.400	2.953	3.667	22.149	1.424	2.090	46.757	10.569	12.800	-0.203	0.833	0.167
30.000	2.961	4.100	25.400	2.956	3.637	22.039	1.425	2.131	49.500	11.301	13.233	-0.169	0.850	0.150
30.000	2.964	4.120	25.400	2.960	3.673	22.022	1.420	2.116	49.009	10.841	13.300	-0.135	0.844	0.156
30.000	2.957	4.080	25.400	2.952	3.653	22.208	1.430	2.086	45.842	10.458	12.567	-0.169	0.832	0.168
30.000	2.963	4.100	25.400	2.957	3.677	22.310	1.426	2.057	44.255	10.325	12.167	-0.202	0.820	0.180
30.000	2.957	4.070	25.400	2.953	3.673	22.377	1.434	2.044	42.559	9.746	11.900	-0.135	0.815	0.185
Average	2.960	4.094	25.400	2.955	3.664	22.188	1.427	2.086	46.227	10.513	12.648	-0.169	0.832	0.168
45.000	2.958	4.090	25.400	2.953	3.607	21.861	1.427	2.181	52.831	11.817	13.933	-0.169	0.870	0.130
45.000	2.966	4.090	25.400	2.961	3.650	21.971	1.431	2.140	49.508	10.758	13.500	-0.169	0.853	0.147
45.000	2.965	4.120	25.400	2.960	3.653	22.047	1.420	2.122	49.429	11.327	13.200	-0.169	0.846	0.154
Average	2.963	4.100	25.400	2.958	3.637	21.960	1.426	2.148	50.590	11.301	13.544	-0.169	0.856	0.144
60.000	2.963	4.100	25.400	2.958	3.587	21.717	1.426	2.226	56.109	12.520	14.500	-0.169	0.888	0.112
60.000	2.962	4.090	25.400	2.957	3.580	21.768	1.429	2.219	55.291	12.469	14.300	-0.169	0.885	0.115
60.000	2.967	4.080	25.400	2.958	3.580	21.683	1.435	2.238	55.913	12.255	14.633	-0.303	0.892	0.108
Average	2.964	4.090	25.400	2.958	3.582	21.723	1.430	2.228	55.771	12.415	14.478	-0.214	0.888	0.112
120.000	2.965	4.090	25.400	2.957	3.533	21.480	1.431	2.309	61.424	13.610	15.433	-0.270	0.921	0.079
120.000	2.961	4.040	25.400	2.955	3.520	21.573	1.446	2.297	58.782	12.871	15.067	-0.203	0.916	0.084
120.000	2.967	4.110	25.400	2.962	3.577	21.590	1.425	2.262	58.779	12.976	15.000	-0.169	0.902	0.098
Average	2.964	4.080	25.400	2.958	3.543	21.548	1.434	2.289	59.662	13.153	15.167	-0.214	0.913	0.087
480.000	2.969	4.170	25.400	2.963	3.553	21.040	1.405	2.398	70.691	14.788	17.167	-0.202	0.956	0.044
480.000	2.964	4.130	25.400	2.957	3.530	21.074	1.416	2.402	69.567	14.528	17.033	-0.236	0.958	0.042
480.000	2.972	4.120	25.400	2.965	3.537	21.116	1.424	2.394	68.162	14.159	16.867	-0.236	0.955	0.045
480.000	2.965	4.150	25.400	2.959	3.510	20.980	1.410	2.438	72.942	15.422	17.400	-0.202	0.972	0.028
480.000	2.967	4.150	25.400	2.960	3.500	20.955	1.411	2.452	73.799	15.663	17.500	-0.236	0.978	0.022
480.000	2.964	4.120	25.400	2.967	3.520	20.989	1.420	2.436	71.587	14.563	17.367	0.101	0.971	0.029
Average	2.967	4.140	25.400	2.962	3.525	21.026	1.414	2.420	71.125	14.854	17.222	-0.168	0.965	0.035

Sintering Data, 450C														
	Sample Measurements													
	Before Heating			After Heating			Pellet Density			Shrinkage				
Time Heated	Weight	Height	Diameter	Weight	Height	Diameter	Before	After	Difference	Height	Diameter	Wt. Loss	ρ/ρ_{th}	P
min	g	mm	mm	g	mm	mm	g/cm3	g/cm3	%	%	%	%		
0.000	2.964	4.160	25.400	2.950	4.120	24.934	1.406	1.466	4.283	0.962	1.833	-0.472	0.585	0.415
0.000	2.962	4.130	25.400	2.959	4.107	25.044	1.415	1.463	3.340	0.565	1.400	-0.101	0.583	0.417
0.000	2.966	4.110	25.400	2.952	4.093	25.070	1.424	1.461	2.583	0.406	1.300	-0.472	0.583	0.417
Average	2.964	4.133	25.400	2.954	4.107	25.016	1.415	1.463	3.402	0.644	1.511	-0.349	0.583	0.417
3.000	2.960	4.100	25.400	2.956	3.880	23.131	1.425	1.813	27.247	5.366	8.933	-0.135	0.723	0.277
3.000	2.962	4.110	25.400	2.957	3.890	23.326	1.422	1.779	25.071	5.353	8.167	-0.169	0.709	0.291
3.000	2.961	4.070	25.400	2.951	3.873	23.165	1.436	1.808	25.907	4.832	8.800	-0.338	0.721	0.279
Average	2.961	4.093	25.400	2.955	3.881	23.207	1.428	1.800	26.075	5.184	8.633	-0.214	0.718	0.282
4.000	2.962	4.110	25.400	2.954	3.740	22.377	1.422	2.008	41.203	9.002	11.900	-0.270	0.801	0.199
4.000	2.959	4.060	25.400	2.953	3.723	22.606	1.438	1.976	37.383	8.292	11.000	-0.203	0.788	0.212
4.000	2.966	4.040	25.400	2.961	3.717	22.555	1.449	1.994	37.616	8.003	11.200	-0.169	0.795	0.205
Average	2.962	4.070	25.400	2.956	3.727	22.513	1.437	1.993	38.734	8.433	11.367	-0.214	0.795	0.205
5.000	2.960	4.080	25.400	2.955	3.667	22.098	1.432	2.101	46.763	10.131	13.000	-0.169	0.838	0.162
5.000	2.964	4.120	25.400	2.959	3.723	22.301	1.420	2.035	43.299	9.628	12.200	-0.169	0.811	0.189
5.000	2.965	4.070	25.400	2.960	3.653	22.310	1.438	2.073	44.163	10.238	12.167	-0.169	0.826	0.174
Average	2.963	4.090	25.400	2.958	3.681	22.236	1.430	2.070	44.742	9.999	12.456	-0.169	0.825	0.175
7.000	2.965	4.010	25.400	2.960	3.543	21.937	1.459	2.210	51.463	11.638	13.633	-0.169	0.881	0.119
7.000	2.966	4.060	25.400	2.957	3.607	22.098	1.442	2.138	48.273	11.166	13.000	-0.303	0.852	0.148
7.000	2.963	4.060	25.400	2.958	3.613	22.090	1.440	2.136	48.313	11.002	13.033	-0.169	0.852	0.148
Average	2.965	4.043	25.400	2.958	3.588	22.042	1.447	2.161	49.350	11.268	13.222	-0.214	0.862	0.138
10.000	2.965	4.060	25.400	2.960	3.537	21.480	1.441	2.310	60.251	12.890	15.433	-0.169	0.921	0.079
10.000	2.963	4.020	25.400	2.957	3.507	21.590	1.455	2.303	58.348	12.769	15.000	-0.202	0.918	0.082
10.000	2.969	4.060	25.400	2.963	3.537	21.590	1.443	2.288	58.568	12.890	15.000	-0.202	0.912	0.088
Average	2.966	4.047	25.400	2.960	3.527	21.553	1.446	2.300	59.056	12.850	15.144	-0.191	0.917	0.083

Sintering Data (Cont'd.), 450C														
	Sample Measurements													
	Before Heating			After Heating			Pellet Density			Shrinkage				
Time Heated	Weight	Height	Diameter	Weight	Height	Diameter	Before	After	Difference	Height	Diameter	Wt. Loss	ρ/ρ_{th}	P
min	g	mm	mm	g	mm	mm	g/cm3	g/cm3	%	%	%	%		
15.000	2.964	4.050	25.400	2.956	3.497	21.328	1.444	2.366	63.837	13.663	16.033	-0.270	0.944	0.056
15.000	2.962	4.060	25.400	2.956	3.520	21.344	1.440	2.347	63.004	13.300	15.967	-0.203	0.936	0.064
15.000	2.967	4.060	25.400	2.963	3.527	21.344	1.442	2.348	62.807	13.136	15.967	-0.135	0.936	0.064
Average	2.964	4.057	25.400	2.958	3.514	21.339	1.442	2.354	63.216	13.366	15.989	-0.202	0.939	0.061
20.000	2.956	4.090	25.400	2.952	3.467	21.141	1.426	2.426	70.070	15.240	16.767	-0.135	0.967	0.033
20.000	2.964	4.040	25.400	2.959	3.453	21.260	1.448	2.414	66.709	14.521	16.300	-0.169	0.962	0.038
20.000	2.967	4.090	25.400	2.962	3.510	21.234	1.432	2.383	66.445	14.181	16.400	-0.169	0.950	0.050
Average	2.962	4.073	25.400	2.958	3.477	21.212	1.435	2.407	67.741	14.648	16.489	-0.158	0.960	0.040
30.000	2.969	4.050	25.400	2.964	3.453	21.184	1.447	2.435	68.326	14.733	16.600	-0.168	0.971	0.029
30.000	2.964	4.100	25.400	2.959	3.487	21.082	1.427	2.431	70.406	14.959	17.000	-0.169	0.969	0.031
30.000	2.963	4.060	25.400	2.956	3.473	21.158	1.440	2.421	68.059	14.450	16.700	-0.236	0.965	0.035
Average	2.965	4.070	25.400	2.960	3.471	21.141	1.438	2.429	68.930	14.714	16.767	-0.191	0.969	0.031
60.000	2.964	4.090	25.400	2.959	3.467	20.997	1.430	2.465	72.352	15.240	17.333	-0.169	0.983	0.017
60.000	2.968	4.030	25.400	2.963	3.413	21.082	1.453	2.487	71.095	15.302	17.000	-0.168	0.992	0.008
60.000	2.965	4.040	25.400	2.960	3.437	21.057	1.448	2.473	70.766	14.934	17.100	-0.169	0.986	0.014
60.000	2.966	4.030	25.400	2.960	3.447	21.057	1.452	2.466	69.792	14.475	17.100	-0.202	0.983	0.017
60.000	2.963	4.020	25.400	2.958	3.427	21.082	1.455	2.473	70.006	14.760	17.000	-0.169	0.986	0.014
60.000	2.967	4.150	25.400	2.961	3.517	20.887	1.411	2.457	74.157	15.261	17.767	-0.202	0.980	0.020
60.000	2.971	4.160	25.400	2.965	3.533	20.879	1.409	2.451	73.895	15.064	17.800	-0.202	0.977	0.023
60.000	2.963	4.130	25.400	2.957	3.487	20.997	1.416	2.449	72.981	15.577	17.333	-0.202	0.977	0.023
Average	2.966	4.081	25.400	2.960	3.466	21.005	1.434	2.465	71.881	15.077	17.304	-0.185	0.983	0.017
480.000	2.967	4.130	25.400	2.961	3.470	20.820	1.418	2.507	76.794	15.981	18.033	-0.202	0.999	0.001
480.000	2.963	4.210	25.400	2.957	3.527	20.684	1.389	2.495	79.652	16.231	18.567	-0.202	0.995	0.005
Average	2.965	4.170	25.400	2.959	3.498	20.752	1.403	2.501	78.223	16.106	18.300	-0.202	0.997	0.003

Sintering Data (Cont'd.), 450C														
	Sample Measurements													
	Before Heating			After Heating			Pellet Density			Shrinkage				
Time Heated	Weight	Height	Diameter	Weight	Height	Diameter	Before	After	Difference	Height	Diameter	Wt. Loss	ρ/ρ_{th}	P
min	g	mm	mm	g	mm	mm	g/cm3	g/cm3	%	%	%	%		
5.000	2.968	4.280	25.400	2.964	3.880	22.352	1.369	1.947	42.253	9.346	12.000	-0.135	0.776	0.224
5.000	2.970	4.290	25.400	2.965	3.923	22.657	1.366	1.874	37.196	8.547	10.800	-0.168	0.747	0.253
5.000	2.969	4.260	25.400	2.963	3.903	22.521	1.375	1.906	38.540	8.372	11.333	-0.202	0.760	0.240
Average	2.969	4.277	25.400	2.964	3.902	22.510	1.370	1.909	39.329	8.755	11.378	-0.168	0.761	0.239
10.000	2.970	4.280	25.400	2.964	3.723	21.463	1.369	2.200	60.665	13.006	15.500	-0.202	0.877	0.123
10.000	2.969	4.290	25.400	2.964	3.733	21.565	1.366	2.174	59.152	12.976	15.100	-0.168	0.867	0.133
10.000	2.970	4.290	25.400	2.964	3.737	21.590	1.366	2.167	58.583	12.898	15.000	-0.202	0.864	0.136
Average	2.970	4.287	25.400	2.964	3.731	21.539	1.367	2.180	59.467	12.960	15.200	-0.191	0.869	0.131
15.000	2.971	4.310	25.400	2.964	3.660	21.192	1.360	2.296	68.769	15.081	16.567	-0.236	0.915	0.085
15.000	2.968	4.240	25.400	2.963	3.637	21.311	1.381	2.284	65.351	14.230	16.100	-0.168	0.911	0.089
15.000	2.969	4.300	25.400	2.963	3.717	21.319	1.363	2.233	63.896	13.566	16.067	-0.202	0.890	0.110
Average	2.969	4.283	25.400	2.963	3.671	21.274	1.368	2.271	66.005	14.292	16.244	-0.202	0.906	0.094
30.000	2.969	4.310	25.400	2.964	3.620	20.836	1.359	2.401	76.627	16.009	17.967	-0.168	0.957	0.043
30.000	2.967	4.290	25.400	2.962	3.620	20.879	1.365	2.390	75.095	15.618	17.800	-0.169	0.953	0.047
30.000	2.967	4.290	25.400	2.962	3.647	20.980	1.365	2.349	72.135	14.996	17.400	-0.169	0.937	0.063
Average	2.968	4.297	25.400	2.963	3.629	20.899	1.363	2.380	74.619	15.541	17.722	-0.168	0.949	0.051
0.000	2.972	4.380	25.400	2.965	4.363	25.011	1.339	1.383	3.289	0.381	1.533	-0.236	0.551	0.449
0.000	2.970	4.340	25.400	2.967	4.317	25.129	1.351	1.386	2.616	0.538	1.067	-0.101	0.553	0.447
0.000	2.969	4.300	25.400	2.966	4.280	25.138	1.363	1.396	2.473	0.465	1.033	-0.101	0.557	0.443
Average	2.970	4.340	25.400	2.966	4.320	25.092	1.351	1.388	2.793	0.461	1.211	-0.146	0.554	0.446
60.000	2.973	4.320	25.400	2.964	3.593	20.735	1.358	2.443	79.860	16.821	18.367	-0.303	0.974	0.026
60.000	2.969	4.300	25.400	2.963	3.613	20.786	1.363	2.417	77.346	15.969	18.167	-0.202	0.964	0.036
60.000	2.973	4.340	25.400	2.967	3.633	20.803	1.352	2.403	77.721	16.283	18.100	-0.202	0.958	0.042
Average	2.972	4.320	25.400	2.965	3.613	20.774	1.358	2.421	78.309	16.358	18.211	-0.236	0.965	0.035

Sintering Data (Cont'd.), 450C														
	Sample Measurements													
	Before Heating			After Heating			Pellet Density			Shrinkage				
Time Heated	Weight	Height	Diameter	Weight	Height	Diameter	Before	After	Difference	Height	Diameter	Wt. Loss	ρ/ρ_{th}	P
min	g	mm	mm	g	mm	mm	g/cm3	g/cm3	%	%	%	%		
5.000	2.985	6.600	25.400	2.980	5.730	21.666	0.893	1.411	58.039	13.182	14.700	-0.168	0.562	0.438
5.000	2.983	6.740	25.400	2.979	6.030	22.106	0.873	1.287	47.363	10.534	12.967	-0.134	0.513	0.487
5.000	2.984	6.650	25.400	2.980	5.903	21.903	0.886	1.340	51.283	11.228	13.767	-0.134	0.534	0.466
Average	2.984	6.663	25.400	2.980	5.888	21.892	0.884	1.346	52.228	11.648	13.811	-0.145	0.537	0.463
10.000	2.985	6.810	25.400	2.979	5.590	20.320	0.865	1.643	89.968	17.915	20.000	-0.201	0.655	0.345
10.000	2.983	6.800	25.400	2.978	5.627	20.582	0.866	1.591	83.739	17.255	18.967	-0.168	0.634	0.366
10.000	2.986	6.750	25.400	2.981	5.617	20.532	0.873	1.603	83.618	16.790	19.167	-0.167	0.639	0.361
Average	2.985	6.787	25.400	2.979	5.611	20.478	0.868	1.612	85.775	17.320	19.378	-0.179	0.643	0.357
15.000	2.984	6.810	25.400	2.978	5.463	19.956	0.865	1.743	101.530	19.775	21.433	-0.201	0.695	0.305
15.000	2.985	6.790	25.400	2.979	5.537	20.091	0.868	1.697	95.612	18.459	20.900	-0.201	0.677	0.323
15.000	2.983	6.750	25.400	2.979	5.503	20.176	0.872	1.693	94.129	18.469	20.567	-0.134	0.675	0.325
Average	2.984	6.783	25.400	2.979	5.501	20.074	0.868	1.711	97.090	18.901	20.967	-0.179	0.682	0.318
30.000	2.983	6.660	25.400	2.966	5.223	19.304	0.884	1.940	119.491	21.572	24.000	-0.570	0.774	0.226
30.000	2.983	6.800	25.400	2.977	5.297	19.329	0.866	1.915	121.239	22.108	23.900	-0.201	0.764	0.236
30.000	2.985	6.780	25.400	2.980	5.337	19.499	0.869	1.870	115.222	21.288	23.233	-0.168	0.746	0.254
Average	2.984	6.747	25.400	2.974	5.286	19.377	0.873	1.909	118.651	21.656	23.711	-0.313	0.761	0.239
0.000	2.986	6.550	25.400	2.982	6.483	24.943	0.900	0.941	4.626	1.018	1.800	-0.134	0.375	0.625
0.000	2.987	6.600	25.400	2.985	6.547	25.044	0.893	0.926	3.628	0.808	1.400	-0.067	0.369	0.631
0.000	2.989	6.650	25.400	2.986	6.600	24.900	0.887	0.929	4.736	0.752	1.967	-0.100	0.370	0.630
Average	2.987	6.600	25.400	2.984	6.543	24.963	0.893	0.932	4.330	0.859	1.722	-0.100	0.372	0.628
60.000	2.986	6.430	25.400	2.981	4.957	19.050	0.916	2.110	130.235	22.913	25.000	-0.167	0.841	0.159
60.000	2.987	6.480	25.400	2.982	4.973	19.050	0.910	2.104	131.248	23.251	25.000	-0.167	0.839	0.161
60.000	2.988	6.690	25.400	2.985	5.233	19.075	0.881	1.996	126.429	21.774	24.900	-0.100	0.796	0.204
Average	2.987	6.533	25.400	2.983	5.054	19.058	0.903	2.070	129.304	22.646	24.967	-0.145	0.825	0.175

Sintering Data (Cont'd.), 450C														
	Sample Measurements													
	Before Heating			After Heating			Pellet Density			Shrinkage				
Time Heated	Weight	Height	Diameter	Weight	Height	Diameter	Before	After	Difference	Height	Diameter	Wt. Loss	ρ/ρ_{th}	P
min	g	mm	mm	g	mm	mm	g/cm3	g/cm3	%	%	%	%		
5.000	2.980	5.050	25.400	2.975	4.587	22.445	1.165	1.639	40.763	9.175	11.633	-0.168	0.654	0.346
5.000	2.979	5.000	25.400	2.973	4.597	22.860	1.176	1.576	34.019	8.067	10.000	-0.201	0.628	0.372
5.000	2.980	5.010	25.400	2.975	4.597	22.691	1.174	1.601	36.345	8.250	10.667	-0.168	0.638	0.362
Average	2.980	5.020	25.400	2.974	4.593	22.665	1.171	1.605	37.042	8.497	10.767	-0.179	0.640	0.360
10.000	2.979	4.950	25.400	2.974	4.293	21.251	1.188	1.953	64.428	13.266	16.333	-0.168	0.779	0.221
10.000	2.981	4.930	25.400	2.975	4.297	21.514	1.193	1.905	59.615	12.847	15.300	-0.201	0.759	0.241
10.000	2.978	4.980	25.400	2.973	4.320	21.539	1.180	1.889	60.038	13.253	15.200	-0.168	0.753	0.247
Average	2.979	4.953	25.400	2.974	4.303	21.435	1.187	1.915	61.360	13.122	15.611	-0.179	0.764	0.236
15.000	2.984	5.040	25.400	2.979	4.243	20.794	1.168	2.067	76.922	15.807	18.133	-0.168	0.824	0.176
15.000	2.980	4.970	25.400	2.976	4.203	21.014	1.183	2.041	72.512	15.426	17.267	-0.134	0.814	0.186
15.000	2.982	4.940	25.400	2.977	4.207	21.539	1.191	1.942	63.030	14.845	15.200	-0.168	0.774	0.226
Average	2.982	4.983	25.400	2.977	4.218	21.116	1.181	2.017	70.821	15.359	16.867	-0.156	0.804	0.196
30.000	2.979	4.900	25.400	2.974	4.033	20.422	1.200	2.251	87.625	17.687	19.600	-0.168	0.898	0.102
30.000	2.979	4.880	25.400	2.974	4.063	20.498	1.205	2.218	84.103	16.735	19.300	-0.168	0.884	0.116
30.000	2.980	4.840	25.400	2.974	4.043	20.574	1.215	2.212	82.079	16.460	19.000	-0.201	0.882	0.118
Average	2.979	4.873	25.400	2.974	4.047	20.498	1.207	2.227	84.602	16.961	19.300	-0.179	0.888	0.112
0.000	2.980	4.860	25.400	2.977	4.830	25.078	1.210	1.248	3.116	0.617	1.267	-0.101	0.498	0.502
0.000	2.979	4.900	25.400	2.976	4.863	25.112	1.200	1.235	2.973	0.748	1.133	-0.101	0.493	0.507
0.000	2.978	4.960	25.400	2.975	4.933	25.070	1.185	1.222	3.102	0.538	1.300	-0.101	0.487	0.513
Average	2.979	4.907	25.400	2.976	4.876	25.087	1.198	1.235	3.064	0.634	1.233	-0.101	0.492	0.508
60.000	2.979	4.960	25.400	2.973	4.010	20.074	1.185	2.342	97.625	19.153	20.967	-0.201	0.934	0.066
60.000	2.982	4.950	25.400	2.976	4.013	20.125	1.189	2.331	96.069	18.923	20.767	-0.201	0.929	0.071
60.000	2.977	4.900	25.400	2.971	3.990	20.210	1.199	2.321	93.591	18.571	20.433	-0.202	0.926	0.074
Average	2.979	4.937	25.400	2.973	4.004	20.137	1.191	2.332	95.762	18.882	20.722	-0.201	0.930	0.070

Sintering Data, 500C													
	Sample Measurements												
	Before Heating			After Heating			Pellet Density			Shrinkage			
Time Heate	Weight	Height	Diameter	Weight	Height	Diameter	Before	After	Differenc	Height	Diameter	Wt. Loss	ρ/ρth	P
min	g	mm	mm	g	mm	mm	g/cm3	g/cm3	%	%	%	%		
0.000	2.965	4.090	25.400	2.958	4.020	24.392	1.431	1.575	10.059	1.711	3.967	-0.236	0.628	0.372
0.000	2.963	4.100	25.400	2.958	4.040	24.587	1.426	1.542	8.123	1.463	3.200	-0.169	0.615	0.385
0.000	2.968	4.110	25.400	2.964	4.057	24.452	1.425	1.556	9.178	1.298	3.733	-0.135	0.620	0.380
Average	2.965	4.100	25.400	2.960	4.039	24.477	1.427	1.558	9.120	1.491	3.633	-0.180	0.621	[illegible]
1.000	2.963	4.100	25.400	2.958	3.837	22.775	1.426	1.892	32.689	6.423	10.333	-0.169	0.755	[illegible]
1.000	2.966	4.100	25.400	2.961	3.890	23.233	1.428	1.796	25.770	5.122	8.533	-0.169	0.716	[illegible]
1.000	2.965	4.120	25.400	2.961	3.900	23.241	1.420	1.790	26.010	5.340	8.500	-0.135	0.714	[illegible]
1.000	2.965	4.110	25.400	2.960	3.843	22.784	1.424	1.889	32.683	6.488	10.300	-0.169	0.753	[illegible]
1.000	2.965	4.120	25.400	2.961	3.897	23.063	1.420	1.819	28.070	5.421	9.200	-0.135	0.725	[illegible]
Average	2.965	4.110	25.400	2.960	3.873	23.019	1.424	1.837	29.044	5.759	9.373	-0.155	0.733	[illegible]
2.000	2.955	4.070	25.400	2.950	3.633	22.047	1.433	2.127	48.427	10.729	13.200	-0.169	0.848	[illegible]
2.000	2.975	4.150	25.400	2.970	3.743	22.115	1.415	2.066	46.001	9.799	12.933	-0.168	0.824	[illegible]
2.000	2.970	4.140	25.400	2.964	3.727	22.005	1.416	2.091	47.717	9.984	13.367	-0.202	0.834	[illegible]
2.000	2.951	4.070	25.400	2.945	3.683	22.157	1.431	2.074	44.912	9.500	12.767	-0.203	0.827	0.173
2.000	2.961	4.100	25.400	2.952	3.720	22.115	1.425	2.066	44.949	9.268	12.933	-0.304	0.824	0.176
Average	2.962	4.106	25.400	2.956	3.701	22.088	1.424	2.085	46.401	9.856	13.040	-0.209	0.831	0.169
3.000	2.961	4.080	25.400	2.956	3.607	21.776	1.432	2.201	53.646	11.601	14.267	-0.169	0.877	0.123
3.000	2.963	4.120	25.400	2.958	3.653	21.912	1.419	2.147	51.282	11.327	13.733	-0.169	0.856	0.144
3.000	2.960	4.070	25.400	2.954	3.590	21.751	1.435	2.214	54.288	11.794	14.367	-0.203	0.883	0.117
3.000	2.962	4.100	25.400	2.956	3.647	21.878	1.426	2.156	51.239	11.057	13.867	-0.203	0.860	0.140
3.000	2.958	4.070	25.400	2.950	3.600	21.836	1.434	2.188	52.565	11.548	14.033	-0.270	0.873	0.127
Average	2.961	4.088	25.400	2.955	3.619	21.830	1.429	2.181	52.604	11.465	14.053	-0.203	0.870	0.130
5.000	2.958	4.100	25.400	2.952	3.523	21.344	1.424	2.342	64.454	14.065	15.967	-0.203	0.934	0.066
5.000	2.954	4.100	25.400	2.948	3.493	21.302	1.422	2.368	66.526	14.797	16.133	-0.203	0.944	0.056
5.000	2.960	4.110	25.400	2.954	3.513	21.268	1.421	2.367	66.512	14.517	16.267	-0.203	0.944	0.056
Average	2.957	4.103	25.400	2.951	3.510	21.305	1.422	2.359	65.831	14.460	16.122	-0.203	0.940	0.060

Attachment 4

Sintering Data (cont'd.), 500C														
	Sample Measurements													
	Before Heating			After Heating			Pellet Density			Shrinkage				
Time Heate	Weight	Height	Diameter	Weight	Height	Diameter	Before	After	Differenc	Height	Diameter	eight Los	ρ/ρth	P
min	g	mm	mm	g	mm	mm	g/cm3	g/cm3	%	%	%	%		
7.000	2.963	4.050	25.400	2.958	3.450	21.090	1.444	2.454	69.980	14.815	16.967	-0.169	0.979	0.021
7.000	2.960	3.960	25.400	2.954	3.400	21.285	1.475	2.442	65.519	14.141	16.200	-0.203	0.974	0.026
7.000	2.961	4.020	25.400	2.955	3.437	21.167	1.454	2.444	68.101	14.511	16.667	-0.203	0.974	0.026
7.000	2.958	4.100	25.400	2.952	3.490	21.048	1.424	2.431	70.733	14.878	17.133	-0.203	0.969	0.031
7.000	2.968	4.090	25.400	2.962	3.483	21.065	1.432	2.440	70.369	14.833	17.067	-0.202	0.973	0.027
7.000	2.965	4.060	25.400	2.958	3.450	21.099	1.441	2.452	70.148	15.025	16.933	-0.236	0.978	0.022
Average	2.963	4.047	25.400	2.957	3.452	21.126	1.445	2.444	69.142	14.700	16.828	-0.203	0.974	0.026
10.000	2.964	4.040	25.400	2.958	3.443	21.099	1.448	2.457	69.695	14.769	16.933	-0.202	0.980	0.020
10.000	2.966	4.120	25.400	2.960	3.473	21.040	1.421	2.451	72.529	15.696	17.167	-0.202	0.977	0.023
10.000	2.962	4.140	25.400	2.953	3.497	20.955	1.412	2.449	73.427	15.539	17.500	-0.304	0.976	0.024
Average	2.964	4.100	25.400	2.957	3.471	21.031	1.427	2.452	71.883	15.335	17.200	-0.236	0.978	0.022
15.000	2.962	4.080	25.400	2.956	3.470	20.896	1.433	2.484	73.381	14.951	17.733	-0.203	0.990	0.010
15.000	2.965	4.070	25.400	2.959	3.433	20.972	1.438	2.495	73.536	15.643	17.433	-0.202	0.995	0.005
15.000	3.021	4.160	25.400	3.016	3.520	21.040	1.433	2.464	71.957	15.385	17.167	-0.166	0.983	0.017
Average	2.983	4.103	25.400	2.977	3.474	20.969	1.435	2.481	72.958	15.326	17.444	-0.190	0.989	0.011
30.000	2.961	4.160	25.400	2.955	3.487	20.811	1.405	2.492	77.370	16.186	18.067	-0.203	0.993	0.007
30.000	2.962	4.070	25.400	2.955	3.437	20.921	1.436	2.501	74.151	15.561	17.633	-0.236	0.997	0.003
30.000	2.966	4.120	25.400	2.951	3.450	20.989	1.421	2.472	74.007	16.262	17.367	-0.506	0.986	0.014
Average	2.963	4.117	25.400	2.954	3.458	20.907	1.421	2.488	75.176	16.003	17.689	-0.315	0.992	0.008
60.000	2.963	4.170	25.400	2.950	3.510	20.803	1.402	2.473	76.340	15.827	18.100	-0.439	0.986	0.014
60.000	2.959	4.200	25.400	2.951	3.520	20.769	1.390	2.475	77.983	16.190	18.233	-0.270	0.987	0.013
60.000	2.970	4.190	25.400	2.962	3.503	20.794	1.399	2.490	77.970	16.388	18.133	-0.269	0.993	0.007
Average	2.964	4.187	25.400	2.954	3.511	20.788	1.397	2.479	77.431	16.135	18.156	-0.326	0.988	0.012
120.000	2.968	4.110	25.400	2.962	3.477	20.879	1.425	2.488	74.605	15.410	17.800	-0.202	0.992	0.008
120.000	2.962	4.110	25.400	2.956	3.487	20.904	1.422	2.470	73.681	15.166	17.700	-0.203	0.985	0.015
120.000	2.956	4.120	25.400	2.950	3.480	20.904	1.416	2.470	74.436	15.534	17.700	-0.203	0.985	0.015
Average	2.962	4.113	25.400	2.956	3.481	20.896	1.421	2.476	74.240	15.370	17.733	-0.203	0.987	0.013

Sintering Data (cont'd.), 500C														
	Sample Measurements													
	Before Heating			After Heating			Pellet Density			Shrinkage				
Time Heated	Weight	Height	Diameter	Weight	Height	Diameter	Before	After	Difference	Height	Diameter	Weight Los	ρ/ρth	P
min	g	mm	mm	g	mm	mm	g/cm3	g/cm3	%	%	%	%		
240.000	2.966	4.130	25.400	2.961	3.487	20.836	1.417	2.491	75.722	15.577	17.967	-0.169	0.993	0.007
240.000	2.966	4.080	25.400	2.960	3.463	20.938	1.435	2.482	73.014	15.114	17.567	-0.202	0.990	0.010
240.000	2.965	4.180	25.400	2.955	3.500	20.786	1.400	2.488	77.738	16.268	18.167	-0.337	0.992	0.008
Average	2.966	4.130	25.400	2.959	3.483	20.853	1.417	2.487	75.491	15.653	17.900	-0.236	0.992	0.008
480.000	2.965	4.110	25.400	2.956	3.483	20.921	1.424	2.469	73.390	15.247	17.633	-0.304	0.984	0.016
480.000	2.967	4.140	25.400	2.960	3.470	20.836	1.414	2.502	76.874	16.184	17.967	-0.236	0.997	0.003
480.000	2.969	4.120	25.400	2.958	3.470	20.896	1.422	2.486	74.787	15.777	17.733	-0.370	0.991	0.009
480.000	2.962	4.040	25.400	2.956	3.423	21.057	1.447	2.480	71.373	15.264	17.100	-0.203	0.989	0.011
480.000	2.961	4.130	25.400	2.949	3.473	20.879	1.415	2.480	75.265	15.900	17.800	-0.405	0.989	0.011
480.000	2.965	4.080	25.400	2.958	3.453	20.913	1.434	2.494	73.878	15.359	17.667	-0.236	0.994	0.006
Average	2.965	4.103	25.400	2.956	3.462	20.917	1.426	2.485	74.261	15.622	17.650	-0.292	0.991	0.009

Table of Contents
Volume 3

APPENDIX III

University of Toronto Report

APPENDIX IV

Radiation Heat Transfer

APPENDIX V

Model Validation

APPENDIX III

University of Toronto Report

Experimental Data on Rates of
Particulate Formation During Char Bed Buring 54 pages

Experimental Data on Rates of Particulate Formation During Char Bed Burning

by

Saied H. Kochesfahani

(University of Toronto)

Thomas M. Grace
Steven Lien
Wolfgang Schmidl

(IPST)

Contents

Chapter 1: Summary

Experimental data have been obtained on the rates of formation of particulate matter during char bed burning under controlled conditions, using a laboratory char bed reactor. This is the first data of this type ever obtained. A major effort was made to obtain closure of sodium balances during the experiments, and this objective was successfully met.

The experiments were carried out with chars prepared separately using black liquor obtained from a kraft pulp mill. The main independent variables in the experiments were the composition of the gas stream passing over the bed and the chemical composition of the char. The oxygen content of the gas stream was the primary variable used to control the bed surface temperature, which was varied over a range from 800 to 1200°C. The CO_2 and H_2O content of the reacting gas stream was also varied. Most of the experiments were carried out with a char produced from as-fired black liquor obtained from the mill. Some experiments were also carried out with chars produced from liquor enriched with sodium sulfate and from liquor enriched with sodium carbonate.

The experimental system was designed to collect the sub-micron sized fume particles produced during bed burning and this worked effectively. Quantitative data on the quantity and chemical composition of the fume as a function of bed temperature and burning rate as well as gas and char composition were obtained.

During the initial test runs it became apparent that two different types of particulate were being produced. In addition to the fume particles, significant quantities of larger-sized particulate (generally in the 1 - 100 μm range) were also found to be released. We refer to these larger particles as ejecta, following the terminology of Verrill [1]. The amount of these larger ejecta particles was surprising. These data are the first quantitative data on the rates of formation of ejecta during char burning, and the first data of any type on ejecta under conditions where closed sodium balances were obtained.

Char composition was found to affect char burning rates. The sulfate-rich char burned faster than the base-case char and the carbonate-rich char. The faster burning rate was not accompanied by higher bed surface temperatures (they were slightly lower). These data show that sulfate in the char provides an additional path for burning char carbon through the reduction of sulfate to sulfide [2].

Fume production during bed burning behaved, in general, in accordance with expectations based on existing concepts of fume forming processes. The amount of sodium released as fume varied from about 0.5 % to 12% of the sodium present and was a very strong function (exponential-like) of bed surface temperature. In the range of typical bed temperatures from 950°C to 1050°C, the amount of fume ranged from about 1% to 6% of the sodium in the char. The fuming rate was much more strongly correlated with bed temperature than with bed burning rates per se. The fume produced is a composite of sodium vaporized as chloride and as sodium vapor. Chloride vaporization is predominate at low bed temperatures, but becomes overwhelmed by sodium vaporization at high bed temperatures. There was some indication that CO_2 in the reacting gases acted to suppress the rate of fume formation. This was most evident with the base case char and the carbonate-enriched char. The fume composition in these experiments generally contained more Na_2CO_3 than is typical of a recovery furnace. The main reason for this was that a substantial part of the sulfur in the black liquor was released during pyrolysis and was not available to participate in fume sulfation reactions in the laboratory furnace. Sulfate/sulfide sulfur was generally not volatile under these char burning conditions.

The ejecta particles were generally light brown in color and 1-100 µm in diameter. They were clearly produced by mechanical removal processes as distinct from vaporization processes. The mechanisms by which this material is formed are still basically unknown at this time, although it was clear from char burning video tapes that it was not simply a sweeping of loose char particles off the bed, but occasionally groups of fine particles were blown out of the bed at very high velocities. What is known is the amount of ejecta formed and the functional dependence on the experimental variables. The amount of sodium released as ejecta varied from 0 to 11% of the sodium originally in the char. For most experiments, the ejecta amount lay between 3 to 7% of the char sodium content. The amount of sodium released seemed to increase with temperature up to about 1000°C, but then decrease. The amount seems to correlate better with bed temperature than with char bed burning rate. There were limited indications that the amount of ejecta decreased when the gas velocity over the bed was decreased. However, decreasing gas velocity also decreased bed temperature which also affects the amount of ejecta, and most experiments were conducted at the same gas velocity, so the relation between gas velocity and ejecta formation remains unknown.

Chapter 2: Introduction

Recovery furnaces are subject to fouling and plugging from sodium and potassium salts that are carried into the heat recovery sections of the upper furnace. Prior to this work, two types of plugging material were generally recognized, so-called carryover (partially burned liquor or smelt drops swept out of the furnace by the gas) and fume. Carryover is primarily a function of liquor spray size, burning characteristics, and gas flow patterns in the furnace, and can be quantitatively understood through the use of CFD-based computer models of the furnace. Fume originates through the vaporization of alkali compounds. The basic chemistry of fume formation is generally understood and it is recognized that the high temperature reducing conditions that exist in the char bed are especially conducive to fume formation. It is widely held in the industry that higher bed temperatures mean increased fume formation, however, there are no quantitative data available relating fume production to bed burning conditions. This study was initiated to meet this need.

2 - 1 Background

Black liquor contains water, alkali (sodium and potassium) salts of wood organics dissolved during pulping, and inorganic salts. When black liquor is burned in a recovery boiler, the water in the black liquor evaporates and the dried liquor solids heat up and undergo thermal decomposition (pyrolysis). Pyrolysis of the black liquor solids produces combustible volatiles which burn in the gas phase and a solid carbonaceous char which tends to fall to the furnace hearth and burn in a so-called char bed. As the carbon in the char is burned away, the residual inorganic chemicals form molten smelt, which is drained from the furnace.

Although there are some conflicting data in the literature, the current consensus is that there is minimal vaporization of sodium and potassium during pyrolysis and volatiles burning, and that the great bulk of the vaporization that leads to fume formation occurs during char burning.

Char is the residual solids material produced when black liquor is pyrolyzed. It is an intimate mixture of carbon and sodium and potassium salts. The two main processes considered to be responsible for the formation of sodium fume are vaporization of sodium chloride and vaporization of metallic sodium formed by reduction of sodium carbonate. The carbonate reduction reaction can be written as;

$$Na_2CO_3 + C \rightarrow 2\,Na + CO + CO_2$$

Similar processes occur for potassium fume formation. KCl is more volatile than NaCl, so the presence of K enhances Cl volatility and vice versa.

Equilibrium models [3,4] have been developed for predicting the volatility of sodium and potassium from char beds. While these models do show the importance of a reducing environment and the role of increasing temperature in increasing fume production, their applicability to the recovery furnace has been questioned. Cameron [5] has shown that reactions of the volatile alkali with furnace gases can lead to increased fume production by minimizing the gas-side mass transfer resistance. No quantitative data have been available for testing these equilibrium models, or any other fume formation models.

It is extremely difficult to acquire data for testing fume formation models on operating recovery boilers. The recovery boiler geometry and fireside environment makes it nearly impossible to make quantitative measurements of the amount of fume leaving the furnace. There have been attempts to use the recirculating dust load from the electrostatic precipitator as a measurement of fume production, but this has limitations. The char bed itself is quite heterogeneous in surface temperature and the accuracy of measuring these temperatures is itself questionable. In addition, pronounced temperature gradient can exist underneath the bed surface and fume can also be formed from char burning in droplets while in flight.

Because of these difficulties, it was considered necessary to acquire data on fume formation during bed burning under carefully controlled conditions. The old char bed reactor in the DOE combustion system at IPST [6] provided a means for doing so. The reactor was modified to permit the necessary measurements of fume production and bed temperature. The main variables that had to be controlled to provide the necessary data were the char composition, the composition and velocity of the gas flow across the bed surface, and the bed surface temperature. The modified char bed reactor was generally capable of providing this. However, the bed temperature could not be controlled independently of the other variables, because of temperature limitations on the heaters. The bed temperature was varied by varying the oxygen content of the gas stream in different experiments.

The importance of ejecta was unsuspected at the start of this work, and the original intention was to obtain data on fume formation. Once experimental data began to be obtained, it became evident that a substantial part of the particulate being collected was not fume. Attention then focussed on devising a means for separating the fume from the ejecta, so that data on the production rates of each of these types of particulate could be obtained for analysis. Fortunately, it was found that the ejecta were caught in the initial parts of the collection system only, and this could be used in conjunction with material balances to separately determine the amounts and composition of fume and ejecta.

2 - 2 Objectives

The basic objective of this study was to obtain data on the rates of production of particulate matter during char bed burning as a function of chemical and operational conditions. These data were to be acquired under conditions where sodium material balances could be closed, so that the amounts of particulate were measured directly and not determined by difference. In addition, bed burning rate data could also be obtained as a function of operating conditions for use in testing char bed burning models.

Specific objectives for the study were as follows.

1. Develop a methodology for quantitative collection of the particulate produced during char bed burning experiments.
2. Obtain data on particulate production with closure of the key elemental balances for the particulate constituents.
3. Develop means for quantitatively distinguishing fume particulate from ejecta.
4. Develop a system and carry out a test plan to determine the effects of char composition, reacting gas composition and velocity, and bed temperature on fume formation.
5. Obtain sufficient data on the rate of fume formation during char bed burning to test models predicting fume formation rates.
6. Obtain sufficient data to characterize the effects of key chemical and operating variables on ejecta formation.

Chapter 3: Description of Experimental System

3 - 1 Overview

A schematic diagram of the experimental char bed burning system is shown in Figure 1. The system consists of two main sections; the char bed reactor where the black liquor char is combusted, and the particulate collection system where fume and ejecta particles generated in the combustion process are collected. The apparatus has several additional components including a gas delivery system (gas cylinders, air supply, gas manifold, flow meters, a steam generator, and a gas preheater), gas analyzers, an online data acquisition system, and an exhaust gas vacuum pump.

3 - 2 Char Bed Reactor

The char bed reactor used in this work was originally one component of a Black Liquor Flow Reactor constructed and operated in the 1980s in a DOE sponsored project on Fundamental Studies of Black Liquor Combustion. This system was previously used to obtain the only published data on bed burning rates [6, 7]. The old char bed reactor was substantially modified for the present work. Details of the modified char bed reactor are shown in Figures 1 and 2.

The simulated char bed is contained within an electrically heated furnace capable of reaching temperatures of about 800°C at the interior furnace walls. The stainless steel char bed retainer assembly, shown in Figure 2, is inserted into the bottom of the furnace. The char bed is supported on a 10 cm x 10 cm platform inside the retainer and can be driven upwards at a controlled rate. An additional clam shell type heater was mounted around the walls of the char bed retainer to reduce the heat up time and lessen the load on the main furnace heaters. At the top of the retainer, the emerging char is exposed to gas flowing from a four-sided slot jet arrangement.

The char to be burned is placed on a stainless steel platform (char tray) within the retainer. This char tray is connected to a manually-controlled, variable-speed, motor-driven piston. The simulated char bed can be raised at speeds from 0 to 3 in./min to gradually and continually expose fresh char to the combustion gas stream. The tray supporting the char has three fixed thermocouples attached which are initially located at different elevations within the bed. As the tray is gradually raised during the course of a burning run, each thermocouple gradually approaches and then goes through the bed surface. This thermocouple arrangement gives a measurement of the temperature profile within the bed, since the position of each thermocouple relative to the bed surface is known.

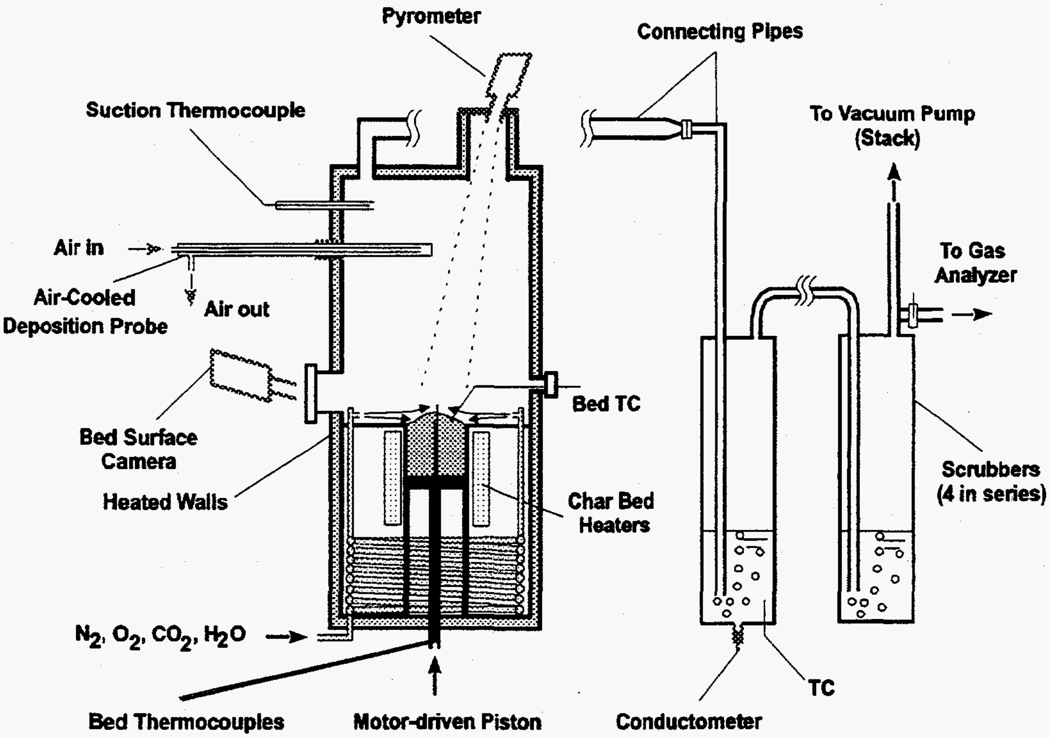

Figure 1. Overall Schematic of the Experimental Apparatus

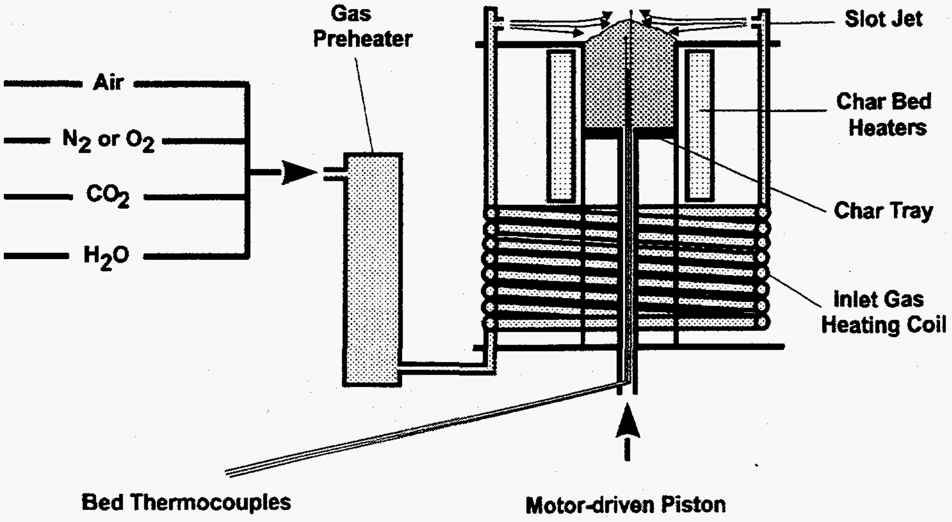

Figure 2. Schematic Diagram of the Char Bed Retainer Assembly and the Inlet Gas Mixing and Preheating

The reacting gas stream consists of mixtures of nitrogen, oxygen, carbon dioxide, and water vapor. The inlet gas flow rates are measured with mass flowmeters. The gas mixture passes through a gas preheater that increases its temperature to about 280°C. The gas stream then enters the bottom of the reactor and passes through tubing coiled around the char retainer in order to further increase its temperature. The gas stream is then split and sent to four headers surrounding the square retainer opening where it blows onto the char bed surface through four symmetrically oriented slot jets.

3 - 3 Particulate Collection System

The particulate collection system consists of two principle components: (1) a set of four clear plastic water-filled scrubber columns connected in series, and (2) the internal surfaces of the pipes connecting the reactor exit to the first scrubber column. In addition, an air-cooled particulate deposition probe is inserted into the reactor chamber above the char bed and in the gas flow path to the reactor exit.

Particulate deposition occurs on all surfaces exposed to the combustion gases, particularly on those surfaces which are cooler than the gas stream. A significant portion of the particles deposit on an uninsulated horizontal stainless steel pipe and a vertical quartz tube that connect the reactor exit to the first scrubber. The remainder of the particulate is absorbed in four scrubbers connected in series, which provide intense mixing between the flue gas bubbles and the scrubbing water. The first scrubber column, which is exposed to hot flue gases and experiences the highest scrubbing solution temperatures, is made of Lexan polycarbonate and measures 4" od x 3.75" id x 54" tall. The other three scrubbers are made of acrylic plastic and measure 4.5" od x 4" id x 60" tall. A static height of about 9-12 inches of water is used in each scrubber. The water column rises to a level 1.5 to 2 times its initial height after gas bubbling starts. The remaining height in each scrubber is used for mist recovery to prevent solution from being carried by gas flow on to the next scrubber. A vacuum pump draws the flue gas through the scrubbers and provides a slightly negative pressure to prevent flue gas leakage into the surrounding atmosphere through the reactor openings.

The air-cooled deposition probe is composed of two concentric tubes. Cool air enters to the inner tube, turns around the far end of this tube, passes through the annulus, and exits from the outer tube. The collecting surface of the probe is 1" in diameter and placed at about 2' above the char bed surface and 6"-8" inside the active furnace chamber. The primary purpose of the deposition probe was to obtain samples for microscopic analysis and size determination.

3 - 4 Auxiliary Subsystems

The important reactor subsystems are the gas delivery system, the gas sampling and analysis system, the online data acquisition system, and the vacuum pump exhaust gas system.

The gas delivery system includes gas cylinders, a compressed air supply, a gas manifold, flowmeters, a steam generator, and a gas preheater. The gas manifold was designed so that three separate gases could be metered simultaneously to produce the desired gas composition. This was adequate for producing mixtures of N_2, O_2, and CO_2. For those experiments in which water vapor was added to the reactant gases, a steam generator was used. The steam generator is a 2kW tube furnace (Lab Line Instruments, Inc. model 4304) with a 2" schedule 10 stainless steel pipe running through it to serve as an evaporation chamber. Deionized water is metered into the steam generator at 0 to 30 ml/min using a manually-controlled flowmeter. The resultant steam is added to the reactant gas stream in the gas preheater.

The gas sampling and analysis system and the data acquisition system are described in detail in Section 3-6-1. The gas exhaust system employs a rotary-type vacuum pump to draw the combustion gases through the scrubber train and exhaust them to the atmosphere

3 - 5 Operating Procedures

The amount of char to be used in the test is dried at 105°C, weighed (usually about 400 g was used), and then gently poured into the cavity in the retainer assembly and the surface leveled. This corresponds to a bed depth of 9-12 cm, with the three bed thermocouples buried at different depths. The char bed retainer assembly is then inserted into the reactor, bolted into place, sealed, and the necessary gas line and thermocouple connections made. The air-cooled particulate probe is also inserted into the reactor.

A nitrogen purge gas flow is turned on to prevent gradual oxidation of the char during reactor heatup. The nitrogen purge rate is 40-50 standard liters/min (slpm) to the char bed and 35 slpm to the pyrometer window. The main reactor heaters and the internal char bed heater are then turned on and the reactor brought up to temperature. Cooling air to the pyrometer and the particulate probe are also turned on at this time. The reactor requires about 45-60 minutes to reach the starting temperature for a run. During the heatup phase, the gas analyzers are calibrated, the VHS video camera is mounted into place, and the VCR and TV monitor are connected. If steam is needed in the reactor gas, the steam generator tube furnace is turned on and set to 800°C. When it has reached this temperature, the deionized water is turned on, set to 30 ml/min, and allowed to stabilize.

The heatup phase is completed when the char bed has reached the desired temperature. At this point, the nitrogen purge flow is increased to about 200 slpm and the vacuum pump is turned on. The amount of vacuum is adjusted by means of a bypass valve so that a slightly positive pressure is maintained inside the reactor. A nitrogen purge flow of about 15 slpm to the pyrometer sight tube is turned on at this time. When the slot gas temperature stabilizes, the char tray is raised to the starting position. The experimental run is then initiated by simultaneously switching the inlet gas flow to the reactant gas (some combination of O_2, N_2, CO_2, and H_2O), starting the char tray motor drive, and the timer on the video camera. The gas mass flow rates are quickly adjusted to the desired level, the vacuum is immediately increased to ensure a slightly negative pressure in the reactor, and the rise rate of the char tray adjusted manually to maintain a constant amount of exposed bed surface.

Experimental runs lasted approximately 5 to 20 minutes, depending on conditions. Runs were stopped while there was still enough char on the tray to avoid unsteady burning and excessive smelt oxidation. Usually this was just after the last of the three embedded thermocouples had emerged above the bed surface. The run was stopped by switching the gas flows back to the nitrogen purge. All of the heaters were then turned off. The vacuum pump remained on until the measured gas concentrations for O_2, CO, and CO_2 returned to zero. The nitrogen purge flows were maintained throughout the cooldown.

Reactor cooldown required about four hours. During this period, the components of the particulate collection system were washed with deionized water, the amounts of the washings were measured, and samples were taken for chemical analysis. After disassembling the char bed retainer assembly, the char residue was collected and weighed. The char bed retainer was then cleaned by immersion in deionized water. The reactor windows and the exit tube were also washed with deionized water. The amounts of all of these solutions were measured and samples taken for chemical analysis.

3 - 6 Experimental Measurements

3 - 6 - 1 Online Data Acquired During a Run

The types of online data acquired during a run are summarized in Table 1. This data consists of gas flow rates for three reactant gas components (N_2, air and CO_2, or O_2, air and CO_2), outlet gas composition (CO, CO_2, and O_2), electric conductivity of the first two scrubber solutions, various process temperatures, and a video of the burning process during the run. The char bed surface temperature is measured both by type K thermocouples and by a two-color infrared pyrometer. Three of the thermocouples are imbedded in the char bed and pass through the surface as the run proceeds. Another thermocouple is fixed in space at a location approximately at the bed surface. The pyrometer is positioned so that it "sees" a 3" diameter circle centered on the bed surface. A purged sight tube mounted inside the reactor is used to keep fume particles and IR absorbing gases out of the pyrometer view path. This was necessary to eliminate interference with the IR pyrometer temperature measurement and was installed just prior to run #12.

Table 1. Summary of Online Data Acquired During a Run

Type of Data	Measurement Ranges	Instrument & Method
Inlet Gas Flow Rates (3)	0-50 slpm 0-100 slpm 0-200 slpm	Hastings Instruments Mass Flowmeter model HFM201
Outlet Gas O_2 Concentration	0-20 or 0-100 mole%	Illinois Instruments, Inc. model 2556 Oxygen Analyzer; electrochemical sensor (fuel cell)
Outlet Gas CO Concentration **Outlet Gas CO_2 Concentration**	0-0.6 / 0-6 mole % 0-2 or 0-20 mole %	Infrared Industries, Inc. model IR702 dual channel nondispersive infrared gas analyzer
Scrubber 1 and 2 Solution Conductivity	0-4,000 µS/cm	Myron L Co., model 758 digital conductivity monitor/controller
Slot Jet Temperature	0-1,250°C	Type K thermocouples
Char Bed Internal Temp. (3)		
Char Bed Surface Temperature		
Char Bed Retainer Wall Temp. (2)		
Fume Deposition Probe Temp. (3)		
Scrubber 1 and 2 Temperatures		
Upper Furnace Flue Gas Temp.	0-1,250°C	Suction thermocouple probe containing a type K thermocouple
Char Bed Surface Temperature	700-1,400°C	Mikron Instruments model M77 two color infrared pyrometer
Bed Burning Images		Video camera and recorder

The instrumentation for analyzing the outlet gas composition is housed in a self-contained cabinet which also contains the necessary sampling and switching valves, flowmeters, a vacuum pump for gas sampling, a chilled water tank for drying the gas, and calibration gases. The sampling point for outlet gas composition was located between the second and third scrubbers.

The signals from the various sensors were fed to data acquisition hardware obtained from Keithley Instruments, Inc. interfaced with a Pentium-133 MHz equipped computer from HiQ Technologies. The data processing software was Labtech Notebook Pro running on a Windows 95 operating system.

3 - 6 - 2 Analysis of Collected Material

Eight solution samples were taken in each experimental run, seven from the particulate collection system and one from the smelt recovered from the char bed retainer. These samples were analyzed for the major cations and anions using standard analytical techniques as follows:

- Total sodium, potassium, and sulfur by Inductively Coupled Plasma - Atomic Emission Spectroscopy (ICP-AES) on acidified samples.
- Total sulfate and chloride by Capillary Ion Electrophoresis (CIE)
- Total carbonate, bicarbonate, and hydroxide by potentiometric titration.

The presence of bicarbonate interfered with the use of the CIE method for measuring carbonate concentration and a potentiometric titration had to be used instead. The potentiometric titration using hydrochloric acid is able to measure separately concentrations of carbonate, bicarbonate, and hydroxide.

Reduced sulfur species such as sulfide interfered with both the ICP and CIE analyses. Consequently hydrogen peroxide was added to the samples to convert all reduced sulfur species to sulfate prior to analysis by these methods.

3 - 6 - 3 Photomicrographs of Particles

Scanning electron microscopy (SEM) was used to examine the particles collected on the air-cooled deposition probe in order to see their morphology and measure the particle size distribution. Numerous photomicrographs were obtained.

Chapter 4 : Char Production

4 - 1 Purpose

Since the objective of the experiments was to obtain data on fume formation (and release of other aerosols) during char bed burning under well-defined conditions, it was necessary to produce a supply of stable, well-characterized char to serve as a starting material in the laboratory furnace beds.

In the original char bed burning work [6] the char was produced by introducing liquor drops into the in-flight section of the DOE black liquor combustion reactor and allowing the pyrolyzed drops to accumulate in the char bed reactor section directly beneath until a sufficient amount was produced for a run. This made it difficult to characterize the char produced, because the residence time at elevated temperatures varied widely and access for sampling was difficult. In addition, a separate batch of char needed to be produced for each run, increasing the likelihood that the char composition varied between runs. For these reasons, it was decided to prepare char in batches external to the reactor system for use in the experiments. With this in mind, the DOE combustion reactor was modified so that the in-flight portion was decoupled from the char bed reactor. This was necessary to allow an effective fume collection system to be added to the char bed reactor, as discussed in Chapter 3.

The mechanics of operation of the char bed reactor required that the char be inserted into the reactor some period of time before the experiment started. In order to do this, the char used had to be chemically stable and easy to handle. This meant that the char could not be produced under high temperature reducing conditions which could form elemental sodium, which would subsequently react when exposed to air, or large quantities of Na_2S, which would make the char hydroscopic. After some preliminary experimentation, a batch pyrolysis procedure was selected for producing the char. The objective of this char production process was to generate large quantities of char with known characteristics, for the bed burning experiments.

4 - 2 Char Preparation Procedure

4 - 2 - 1 System

Black liquor char was prepared by batch pyrolysis in the furnace pictured in Figure 3. This is an electrically heated 9.8 kW tubular furnace (Applied Test Systems, Inc. model 3110) capable of reaching a maximum temperature of 1100°C. A cylindrical metal retort containing an alumina crucible sat inside the furnace and acted as the pyrolysis chamber. In addition to the regular temperature control thermocouples of the furnace, a type K thermocouple was used to monitor the external wall temperature of the crucible. The furnace was purged with a small flow of an inert gas throughout the initial warmup, pyrolysis, and cooldown process. This purge gas stream maintained an oxygen free atmosphere and served to exhaust the pyrolysis gases from the chamber. The exhaust gases were vented through a water scrubber system where they were cleaned and then discharged to the atmosphere by means of an induced draft fan.

4 - 2 - 2 Procedure

The char production procedure is as follows. The desired amount of black liquor was put into the crucible. and the crucible placed inside the retort, The retort was then sealed and placed inside the furnace. The nitrogen purge gas flow was turned on and set to 10-15 slpm, the draft fan was turned on, and the heaters were turned on and set to 700°C. The heaters reached their setpoint temperature in approximately 40-60 minutes. The furnace was maintained at this temperature until the crucible containing black liquor had been exposed to the desired temperature for one hour. The heaters were then turned off, and the purge gas flow maintained during cooldown. When the crucible had cooled to under

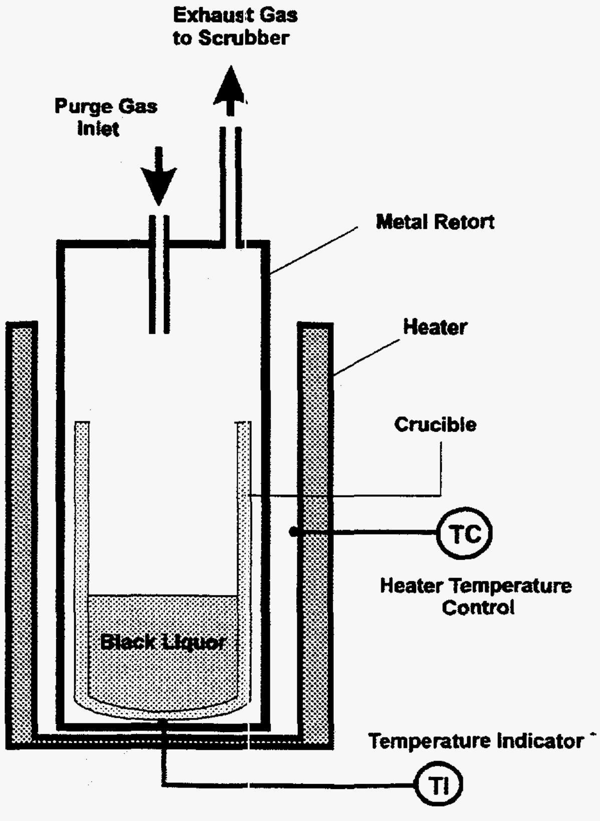

Figure 3. Schematic Diagram of the Black Liquor Pyrolysis Furnace

about 200°C, the retort was opened, and the char removed and cooled further in the ambient air. The batch of char was then stored inside sealed bags, to minimize moisture absorption. The individual batches of char that were produced under identical conditions were then mixed together, crushed, and screened to the proper size range (approximately 1.5-9 mm). Representative samples of the mixture were taken and sent for detailed chemical analysis (Table 2).

4 - 3 Types of Chars and Characterization

Three types of char were produced using the above procedure. All used a single source of black liquor, a sample of as-fired liquor taken from the mill used as the Case 1 validation study during the time that the validation field testing was in progress. The three chars were as follows:

Char 1: The **Base Case Char** produced by pyrolyzing the black liquor directly without any additives. Because of sulfur loss during pyrolysis, it had a S/Na_2 molar ratio of approximately 0.2.

Char 2: The **High Sulfate Char** produced by pyrolyzing black liquor to which sufficient sodium sulfate (about 14 wt% based on dried liquor solids) was added to yield a char with a S/Na_2 molar ratio of approximately 0.35.

Char 3: The **High Carbonate Char** produced by pyrolyzing black liquor loaded with additional sodium carbonate in the amount of 10 wt% based on dried liquor solids.

The compositional analysis for the three starting black liquors, their resultant chars, and data on the three pyrolysis processes are presented in Table 2.

4 - 4 Pyrolysis Characteristics

The pyrolysis process used to generate char, can be characterized in terms of carbon (C), sodium (Na), sulfur (S), potassium (K) and chloride (Cl) losses. Table 2 shows the average amount of C, Na, S, K, and Cl losses calculated using the ratio of char / black liquor dry solids, and the chemical composition of char and liquor.

The data show that, as expected for low temperature pyrolysis, a significant portion of the initial sulfur present in liquor is released to the gas phase during pyrolysis. Since the char production was carried out completely separate from the char burning experiments, the sulfur released during pyrolysis is not available to react with the gaseous sodium and potassium compounds released during char burning. The S/Na_2 ratio of 0.2 for Char 1 is significantly less than the value of about 0.35 in the smelt at the Case 1 mill. This would be expected to affect the chemistry of fume formed during char bed burning.

In order to produce a char with a S/Na_2 ratio comparable to that actually present on the bed of the Case 1 mill, a high sulfate char (Char 2) was produced by adding sodium sulfate to the as-fired black liquor. Since sulfate is known to be stable under pyrolysis conditions, the additional sulfur added will remain as such in the char.

The data presented in Table 2 show that the addition of both sulfate and carbonate to the black liquor before pyrolysis caused a slight decrease in the amount of sulfur released from the original as-fired black liquor, (38.0% and 43.4% vs. 57.3% for the original liquor). The negative values for the sodium released during pyrolysis for the two inorganic enriched cases, is merely reflective of inaccuracies in sodium determinations. The data indicate that, as expected, there is minimal volatilization of sodium during pyrolysis. The indicated release of potassium may be real, as it is likely to vaporize as KCl. There is a significant vaporization of Cl in all of the chars. This would be expected for the temperatures and times used for the pyrolysis experiments.

The object of these pyrolyses was simply the production of char for bed burning experiments and not to acquire quantitative data on black liquor pyrolysis. There are some minor discrepancies in the pyrolysis information presented in Table II, such as negative values for the sodium released from char 2 and char 3. One source of error is the unrecoverable portion of char, which is stuck to the wall of crucible. Another is the accuracy of chemical analysis methods used for char and liquor, which are not better than ±10 percent.

Table 2. **The Composition of Black Liquors Used for Pyrolysis and the Resultant Chars, Pyrolysis Characteristics**

Black Liquor / Char Analysis	**Pyrolyzing BL 1 As-Fired Black Liquor**		**Pyrolyzing BL 2 BL 1 + Na_2SO_4**		**Pyrolyzing BL 3 BL 1 + Na_2CO_3**	
	BL 1	**Char 1**	**BL 2**	**Char 2**	**BL 3**	**Char 3**
Dry Solids (DS), wt. %	71.4	100	73.9	100	73.3	100
Total Carbon (C), wt. %	35.7	30.1	31.4	24.2	33.5	26.7
Organic Carbon (OC), wt. %	35.3	23.4	31.1	18.3	32.1	19.3
Inorganic Carbon (IC), wt. %	0.4	6.7	0.3	5.9	1.4	7.4
Hydrogen (H), wt. %	4.2	0.5	3.7	0.4	3.8	0.3
Oxygen (O), wt. %	34.6	34.8	35.9	35.6	35.6	35.8
Sulfur (S), wt. %	4.9	3.3	7.0	7.3	4.5	3.5
Chloride (Cl), wt. %	0.6	1.0	0.5	0.9	0.5	0.9
Sodium (Na), wt. %	17.7	26.3	19.5	28.3	20.3	30.3
Potassium (K), wt. %	3.3	4.9	2.9	3.8	3.0	4.0
Relative Compositions						
S / Na_2, mole %	39.8	18.0	51.8	37.0	31.6	16.4
S / (Na_2 + K_2), mole %	35.9	16.2	47.7	34.3	29.1	15.2
K / (Na + K), mole %	9.9	9.8	8.1	7.2	8.0	7.3
Cl / (Na + K), mole %	2.0	2.2	1.6	1.9	1.6	1.8
Pyrolysis Characteristics						
Char / Liquor DS Ratio, %	63.6		73.9		72.9	
C Loss (wt. % of C in BL)	46.3		43.2		41.8	
Na Loss, wt. % of Na in BL	5.6		-7.5		-8.8	
K Loss, wt. % of K in BL	6.5		4.5		1.7	
Cl Loss, wt. % of Cl in BL	41.1		47.0		47.0	
S Loss, wt. % of S originally Present in BL 1	57.3		38.0		43.4	

Chapter 5 : Test Plan

5 - 1 Purpose

The objective of the experimental program was to obtain data on char burning rates and the rates of formation of particulates (fume and ejecta) during bed burning as a function of the key dependent variables. Because of the nature of the experimental system, the variables that could be controlled were gas velocity, gas composition, and char composition. It was recognized that bed temperature (especially surface temperature) was a critical variable, but this could not be controlled independently of the other variables in this system. Another restriction was imposed by the amount of time needed to set up and carry out a run. It was difficult to do more than two runs per week, with three per week being the upper limit. This limitation on the amount of runs that could be carried out put a premium on getting the maximum amount of useful information out of each run.

For these reasons, a test plan was developed to ensure that the effects of all of the key variables were examined. This plan allowed obtaining data over a sufficiently wide range of bed temperatures and also provided information on which chemical factors were most important. Variable sets were chosen in such a way as to try to permit direct comparison of the effects of certain composition variables. A limited number of experiments were repeated in order to determine the reproducibility of the results.

5 - 2 Variables Tested

A total of 37 different runs were carried out in this experimental program. The test conditions are summarized in Table 3 below. Runs 2-8 were carried out before the pyrometric bed temperature measurement was reliable. The remaining runs (9-38) were carried out with reliable average bed temperature measurements.

The fundamental factor underlying the test plan is the use of the oxygen content of the gas stream as the primary independent variable determining bed temperature. The heaters in the reactor do not have the capability to bring the char bed up to the full range of bed temperatures desired in the experimental program. Some additional heat release from exothermic combustion reactions is needed to achieve reasonable bed surface temperatures. Thus all of the experiments which were carried out had some oxygen in the reactant gas. The greater the amount of oxygen used, the higher the bed temperatures obtained. All available information indicated that bed temperature was a critical variable in fume formation, and since it was not possible to make bed temperature an independent variable, oxygen content became a very useful surrogate variable.

The specific variables that are incorporated in the test plan are the type of char, inlet gas composition, and inlet gas flow rate. However, except for two runs at ~170 slpm, the gas flow rate was fixed at ~250 slpm. This produced sufficiently high average bed temperatures and eliminated one variable from the test matrix. This was deemed necessary to obtain the maximum amount of useful information from a limited number of experiments.

Three different types of char, (as described in section 4-3), are used in this study: the base case char (Char 1), the high sulfate char (Char 2), and the high carbonate char (Char 3). Of the 37 total runs, Char 1 was used in 20 runs, Char 2 in 9 runs, and Char 3 in 8 runs (see Table 3).

The inlet gas composition consists of a combination of O_2, N_2, CO_2, and H_2O vapor. O_2 and N_2 were used in all of the runs, with O_2 used as the primary variable for changing bed temperature. The range of O_2 concentrations was from 4% to 30.5%. CO_2 was added to the gas mixture to examine the effects of simultaneous gasification and bed burning. CO_2 concentrations of 0 and 10% were used. Water vapor was added both to examine the effects of another gasifying agent that would be present in the recovery furnace and to expand the chemical reactions that could occur to include hydrogenous species. H_2O concentrations of 0 and 15% were used.

Table 3. Summary of Experimental Conditions

Run No.	Run Conditions					
	Char Type	Gas Composition, mole %				Gas Flow Rate, slpm
		O_2	CO_2	H_2O	N_2	
2	1	20.5	0	0	79.5	~250
3	1	20.5	0	0	79.5	~250
4	1	20.5	0	0	79.5	~250
5	1	20.5	0	0	79.5	~170
6	1	20.5	0	0	79.5	~250
7	1	20.5	0	0	79.5	~250
8	2	20.5	0	0	79.5	~250
9	2	8.0	0	0	92.0	~250
10	1	8.0	0	0	92.0	~250
11	3	8.0	0	0	92.0	~250
12	1	8.0	10.0	0	82.0	~250
13	1	4.0	10.0	0	86.0	~250
14	1	13.0	0	0	87.0	~250
15	3	13.0	0	0	87.0	~250
16	2	13.0	0	0	87.0	~250
17	2	13.0	10.0	0	77.0	~250
18	3	13.0	10.0	0	77.0	~250
19	1	13.0	10.0	0	77.0	~250
20	1	13.0	10.0	15.0	62.0	~250
21	1	18.5	0	0	81.5	~250
22	1	18.5	10.0	0	71.5	~250
23	3	13.0	10.0	15.0	62.0	~250
24	2	13.0	10.0	15.0	62.0	~250
25	2	18.5	10.0	15.0	56.5	~250
26	3	18.5	10.0	0	71.5	~250
27	2	18.5	10.0	0	71.5	~250
28	2	18.5	0	0	81.5	~250
29	1	18.5	10.0	15.0	56.5	~250
30	3	18.5	10.0	15.0	56.5	~250
31	3	18.5	0	0	81.5	~250
32	1	20.5	0	0	79.5	~250
33	1	18.5	0	15.0	66.5	~250
34	1	20.5	0	0	79.5	~170
35	1	18.5	10.0	0	71.5	~250
36	1	30.5	0	0	69.5	~250
37	3	30.5	0	0	69.5	~250
38	2	30.5	0	0	69.5	~250

Chapter 6 : Experimental Data Reduction

The experimental data obtained in a given char bed burning experiment included the measurements of the independent variables (reacting gas flow rate and composition, and the quantity and type of char used) and the dependent output variables. These output data can be divided in three general categories: char bed temperature, char burning rate, and particulate quantity and composition.

6 - 1 Char Bed Temperature Data

Char bed temperature was measured both by using a pyrometer and with thermocouples. Three of these bed thermocouples were fixed in position on the moving char tray. At the start of a run they were all submerged within the char bed. During an experiment, the char was burned away at the surface and the char tray was moved upward to provide fresh char. As a result, each submerged thermocouple would penetrate the surface of the bed sometime during the run. In effect, the temperature-time trace for each thermocouple corresponded to the vertical temperature profile within the bed at the thermocouple location. The peak temperature measured by these thermocouples provides a rough estimation of the bed surface temperature at that one location and time. One complication is that sometimes the gas temperature at the vicinity of the bed surface was higher than the bed surface temperature. A fourth thermocouple was fixed in position within the reactor close to the surface of the bed. This thermocouple showed the bed surface temperature

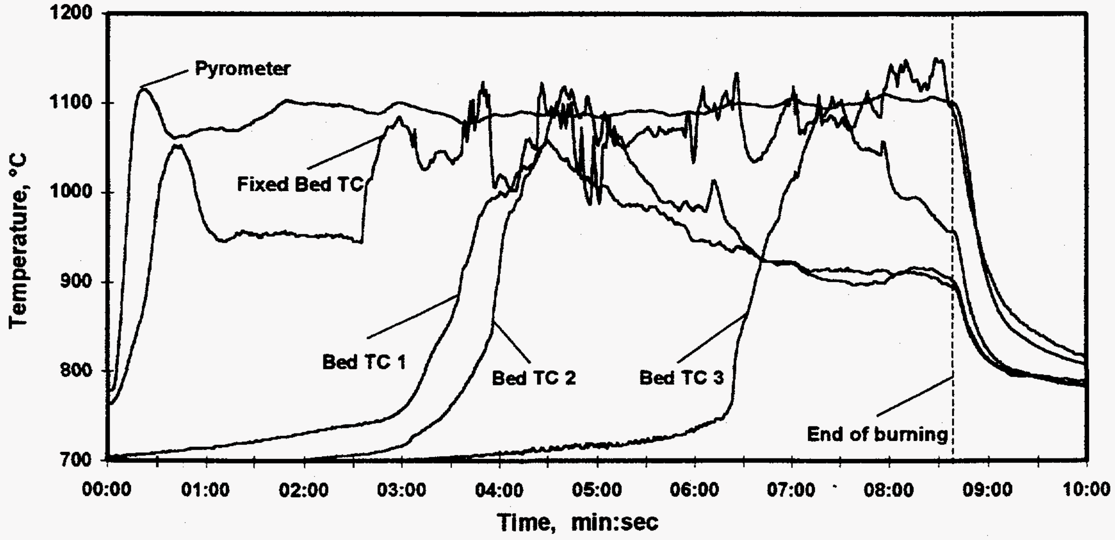

Figure 4. **Temperature vs. time profiles for the four thermocouples and the average bed surface temperature measured by the pyrometer for a typical char bed burning run (run 37).**

several times during the run (whenever it touches the bed surface). Typical temperature-time curves measured by these thermocouples are shown in Figure 4. The data show considerable variation among the local bed surface temperatures measured by the thermocouples. This is caused by non-uniformity in bed burning and in the combustion gas distribution over the bed surface, and variability in char tray upward movement and bed height (which varied the amount of exposed surface).

A measurement of the average bed surface temperature was provided by the bed pyrometer, which was focused on a 3" diameter circle in the 4" x 4" bed. A reasonable correlation was observed between the average of the local temperatures measured by the thermocouples and the pyrometer temperature. An example of this is evident in Figure 4. The average pyrometer temperature was used as a representative bed surface temperature value for analyzing the particulate data in this report.

6 - 2 Char Bed Burning Rate and the Amount of Char Burned

In order to avoid complications due to running out of burnable material near the end of a run, the char bed burning experiments were terminated before all of the char put into the reactor had been burned. Thus it was necessary to measure both the char burning rates and the total amount of char burned in each of the experiments. Char burning rate was considered a potential correlating variable for fume or ejecta production. The total amount of char burned was needed in order to put the amount of particulate found on a consistent basis for comparison between experiments.

The char bed burning rate and total char consumption for each run were calculated using two different methods. The first method used flue gas analysis and the inlet gas flow rate and composition to calculate the char bed burning rate. Since direct measurement of the output flue gas flow rate at high temperature and in the presence of entrained particles was not feasible, the char burning rate was obtained by using the measured inlet gas flow and a nitrogen (the inert gas) balance. The procedure is as follows:

Nitrogen Out = Nitrogen In = Inlet Nitrogen Flow Rate + 0.79 x Inlet Air Flow Rate

Nitrogen Composition in the Flue Gas = $X_{N2} = 1 - X_{O2} - X_{CO2} - X_{CO}$

Flue Gas Flow Rate = Nitrogen Out / X_{N2}

Carbon Released as CO_2 = X_{CO2} x Flue Gas Flow Rate - Inlet CO_2 flow rate

Carbon Released as CO = X_{CO} x Flue Gas Flow Rate

Char burning rate (mole C / sec) = Carbon Released as CO_2 + Carbon Released as CO

where all the flow rates and compositions are expressed on a dry molar basis. The total carbon released during char burning could then be determined by adding the carbon found in the collected particles to the carbon measured as CO or CO_2. The percent char consumption could also be calculated using the amount and carbon composition of the initial char.

Char burning rates calculated by the above method were very sensitive to the accuracy of the flue gas composition. Since bed burning runs were performed under slightly negative pressure and the apparatus was not completely sealed, ambient air could penetrate into the system and decrease the CO and CO_2 concentrations. As a result, this method tended to underestimate the burning rate and char consumption. However, it did give semi-quantitative information about burning rate variations with time and operating conditions. Figure 5 shows a typical char burning curve generated using the above method.

The second method is based on direct measurement of the char input and residue (on a dry basis) for each run. The char consumption is then determined by difference. By knowing the char carbon content and the burning time, the average char burning rate can also calculated as mole of carbon/second. This method provides a consistent and accurate measure of char consumption and average burning rate. The main sources of error are incomplete recovery of char residue after the experiment and the potential for contamination of the char residue with smelt that remains on the surface layer. These errors can be minimized by careful collection of the char residue.

The accuracy of the values for char consumption and burning rate calculated by this method was cross-checked against a volumetric estimation of char consumption based on the difference between the bed height before and after the run as detected on the char burning video tapes. There was close agreement. Furthermore, the second method of estimating char consumption results in a reasonable material balance closure (section 6-3-2), while the first method results in closures greater than 100%. Therefore, the second method was used as the best estimate of the char burning rate and quantity of char burned.

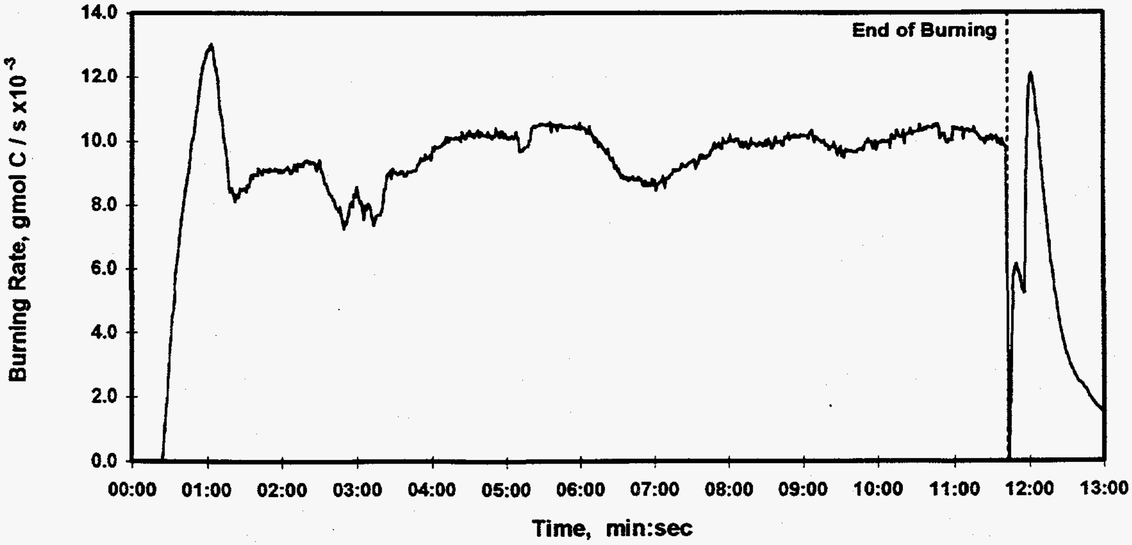

Figure 5. **Measured char burning rates vs. time for a typical run (run 29) based on the inlet gas flow and the flue gas (CO, CO2, and O2) analysis**

6 - 3 Particulate Quantity and Composition

Since the primary objective of this study was to characterize and quantify particulate formation during char bed burning by direct measurement, it was essential to collect all of the fume and ejecta particles produced during an experiment. Two key steps taken to ensure this were as follows.

1. A slightly negative pressure was maintained inside the char bed reactor to prevent the flue gas and the entrained particles from leaking to the atmosphere.

2. The reactor wall temperature was kept at about 800 °C to prevent thermophoretic deposition or direct condensation of fume particles on the reactor wall. Measurements of gas temperature at the exit of the reactor showed that the gas temperature was always lower than the reactor wall temperature. This should have eliminated any thermal driving forces for deposition on the reactor walls.

As will be shown in the following sections, the particulate collection system did work effectively and the vast majority of the input material was recovered as either collected particles or residual char and smelt in the bed after a burning run. Thus, the data on particulate quantity are considered accurate and reliable.

The measured amounts of sodium (and other elements) in the collected particulate were normalized by dividing by the amount of that element in the original char that actually participated in char burning. The amount of sodium (or other element) corresponding to the remaining unburned char in the reactor was not included in the normalization. For this reason, accurate measurement of the total amount of char burned (as discussed in section 6 - 2) were an essential part of obtaining good data on the amount of particulate produced.

6 - 3 - 1 Effectiveness of the Particulate Collection System

The particulate collection system was effective in collecting the small fume particles as well as the bigger ejecta particles. This can be seen in Table 4, which shows the distribution of sodium collected at different locations in the collection system for three char burning runs with significantly different levels of particulate quantity. These results are typical of other experiments. The seven locations shown in the Table are referred to as "Piping", Scrubbers 1, 2, 3, and 4, "Probe", and "Other". "Piping" refers to the material collected on the horizontal stainless-steel tube and vertical quartz tube connecting the reactor to the four scrubbers. The scrubbers are numbered in order in the direction of gas flow. "Probe" refers to the material collected on the air-cooled deposition probe inserted into the reactor, and "Other" refers to the material collected on the reactor exit port and side windows. It is evident that the majority of the particles are collected in the connecting piping and the first scrubber. The quantity of material collected in the third and fourth scrubbers is only a small portion of the total. The cumulative amount of particulate collected in proceeding downstream from the reactor through the scrubbers for these three runs is shown in Figure 6. The data show that the collected particulate tends to reach a plateau over the scrubbers. A similar trend was observed for all of the other char burning runs. All of this information indicates that the particulate collection system is effective in collecting the great majority of the particulate formed, including the sub-micron sized fume particles. Sodium material balances confirm that there was no significant amount of fume lost by passing through the scrubbers.

Table 4. Distribution of Sodium Collected at Different Locations in the Particulate Collection System for Three Typical Char Burning Runs

Location	Local Na Collected, % of Total Na Collected		
	Run 25	Run 31	Run 36
Piping	48.7	40.1	40.3
Scrubber 1	24.2	37.8	22.1
Scrubber 2	5.4	3.6	18.1
Scrubber 3	3.5	2.5	6.0
Scrubber 4	1.6	1.1	1.9
Probe	0.6	1.0	1.5
Others	16.0	13.9	10.2
	Total Na Collected / Initial Na in Char Burned, %		
Sum of All Locations	8.3	11.3	17.0

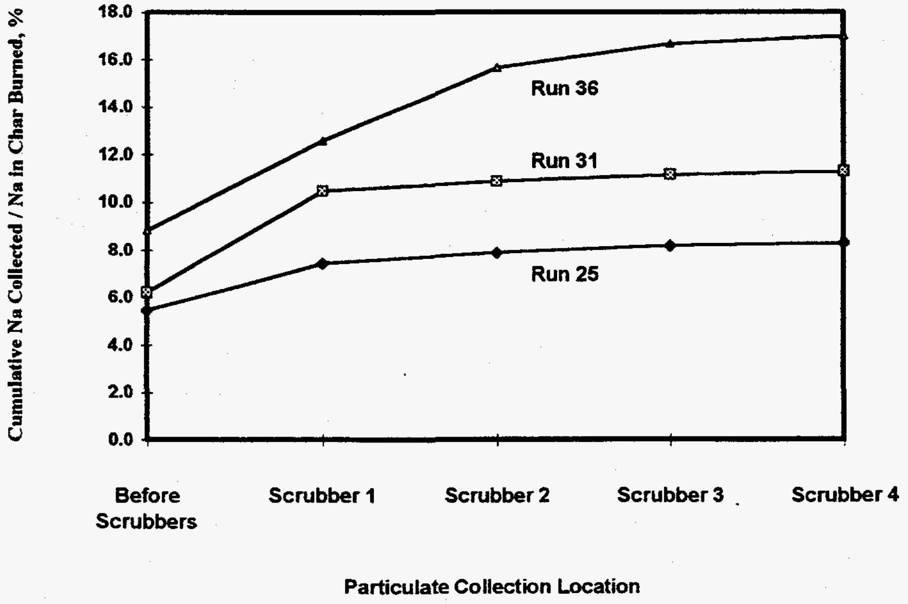

Figure 6. Cumulative Amount of Sodium Collected Along the Collection Scrubber Train for Three Typical Char Burning Runs.

6 - 3 - 2 Closure of Material Balance

In order to confirm the effectiveness of the fume collection system, elemental material balances were carried out for some of the experiments. Since the amounts of particulate alkali were typically only 5 to 15% of the alkali in the char that burned, successful closure of material balances required thorough recovery of the unburned char and smelt from within the reactor. In order to recover smelt, the bottom portion of the char bed reactor, which supported the char bed, was disassembled. After removing and measuring the char residue, the removed assembly was completely submerged in deionized water for a period of 5-10 hours. The aqueous solutions produced were quantified and analyzed for total anion and cations.

Elemental material balance calculations were performed for sodium (Na), sulfur (S), potassium (K), and chlorine (Cl). The elemental inputs were determined using total char consumption (section 6-2) and char chemical analysis information. The output streams included smelt and collected particulate. Losses of these elements in the flue gas were not measured. The results of the elemental balances are summarized in Table 5 as the percentage of the element found relative to the amount of that element initially present in char that burned.

The material balance closure was very sensitive to the efficiency of the smelt collection. Taking steps to improve smelt collection results in a higher degree of closure. The reason that the recovery values are low for runs 9, 10, and 11 is because the char bed assembly was submerged in water for only 1-1.5 hours. Increasing the dissolution time to 10-12 hours for run 12 and 13 resulted in a considerable improvement in the recovery values.

Table 5. **Material Balance Closure and Smelt Composition for Several Char Bed Burning Experiments.**

Run No.	Total Recovery, % of the Initial Element in Char Burned				Smelt Composition, mole %		
	Sodium	Potassium	Sulfur	Chloride	$S/(Na_2+K_2)$	Cl/(Na+K)	K/(Na+K)
8	96	94	67	73	23.7	1.4	7.0
9	67	67	46	64	23.0	1.7	7.2
10	85	73	65	88	12.1	2.2	9.5
11*	79 (70)	83 (73)	74 (54)	99 (86)	13.8 (11.1)	2.2 (2.1)	7.7 (7.6)
12**	88 (86)	84 (82)	65 (59)	92 (90)	10.8	2.2	9.3
13**	97 (94)	94 (92)	60 (52)	99 (97)	8.8	2.2	9.5

* The bed assembly was washed twice to achieve a better smelt recovery. The first numbers show total recovery values and the smelt compositions after the second wash, while the bracketed numbers indicate the same values after the first wash.

** The smelt solution was filtered and the material in the solid residue are included in recovery values. The first numbers show final recovery values, while the bracketed numbers indicate recovery values before adding the material in the solid residue.

Using a second water wash with another 10 hours submergence time for run 11 also resulted in a considerable increase in the recovery values. The highest smelt collection efficiency corresponds to run 12 and 13, where the smelt solution was filtered, the solid residue was acid digested and analyzed for Na, K, and S. As seen in Table 5, these two runs had some of the highest recovery values.

In general, the material balance closure data in Table 5 show reasonably good closure for Na, K, and Cl in these char bed burning experiments. Incomplete closure is affected by analytical inaccuracies and inaccuracies in estimating the amount of char burned as well as the effectiveness of smelt collection. On balance, the data indicate that the particulate collection system worked efficiently and that the particulate formed is quantitatively collected. Sulfur recovery was significantly lower than the other elements. It is believed that the most of the unrecovered sulfur was due to insoluble corrosion products, which remain in the bed assembly after the water wash. Sulfur compounds can be reactive with some of the heavy metal components in the stainless steel bed assembly. Improvement of sulfur recovery values was more significant than those for Na, K, and Cl after a second water wash (run 11) or filtering the smelt solution (run 12 and 13). It is also possible that some sulfur escaped as SO_2 with the flue gas from the particulate collection system.

6 - 3 - 3 Separation of Ejecta from Fume

The collected particulate is a mixture of fume and ejecta. Since these two types of particles are formed by entirely different processes, it is highly desirable to separate the particulate information into two different sets of data, one for fume and and the other for ejecta. A method for doing this was found and is described below.

Because of their larger particle size, the ejecta are caught early in the collection train. As will be seen, the data indicate that essentially all of the ejecta are caught in the "piping" and first scrubber, while fume is caught, in diminishing amounts, throughout the entire collection train. Thus the chemical composition of the fume is well-defined by the composition of the material recovered in scrubbers 2 through 4. If the composition of the ejecta were also known, material balances could be used to determine the proportions of fume and ejecta caught in the "piping" and scrubber 1. Although there is no definitive way to determine the exact composition of the ejecta, it is possible to make assumptions about the ejecta composition that then allow calculations that bracket the amounts of ejecta (and fume) produced. This method was used, and the results are considered to provide a reasonable separation of the particulate into fume and ejecta.

6 - 3 - 3 - 1 Particulate Composition

The composition of the collected particulate at seven different locations in the collecting system is shown in Table 6 for two different char burning runs. These two runs were carried out using significantly different conditions and the results are typical of all of the other runs. The data clearly indicate that the composition of collected particulate is essentially constant for scrubbers 2, 3, and 4. This composition can be taken to be the fume composition. Minor variations in the composition of solutions collected from scrubbers 2, 3, and 4 could be due to the accuracy of chemical analysis, slight differences in composition in different fume size fractions, or differences in dissolution of furnace gases.

Since fume and ejecta are formed by entirely different processes, significant differences in composition can be expected. The ratio of ejecta to fume in the particulate changes between sampling positions because of the size difference between these types of particles. The main reason for differences in the composition of particulate collected at different locations is caused by the ratio of ejecta to fume in the entrained particles.

The composition data in Table 6 indicate that ejecta are either deposited upstream of the scrubbers or dissolved in the first scrubber. In practice, the first scrubber acts as the final screen for the ejecta in the particulate collection system. Therefore, the samples from the last three scrubbers are almost purely fume samples. The average composition of samples collected from scrubber 2, 3, and 4 is assumed to be the fume composition.

Table 6. **Particulate Composition at Seven Sampling Locations in particulate Collection System for Two Typical Char Burning Runs.**

Location	Cl, wt%	SO_4, wt%	CO_3, wt%	Na, wt%	K, wt%	S, wt%
RUN NUMBER 8						
Piping	1.5	25	35	34	5.0	7.7
Scrubber 1	1.4	24	34	36	4.7	7.9
Scrubber 2	4.1	32	22	34	7.0	10.4
Scrubber 3	4.0	32	22	34	7.0	10.4
Scrubber 4	3.9	32	22	35	7.3	10.4
Probe	1.2	23	36	35	4.9	13.1
Other	2.6	24	33	36	5.0	7.6
RUN NUMBER 10						
Piping	2.8	14	42	35	6.9	4.0
Scrubber 1	2.5	13	43	35	6.5	3.9
Scrubber 2	9.5	23	28	30	9.6	6.5
Scrubber 3	10.1	25	25	29	10.0	7.0
Scrubber 4	11.0	25	24	29	10.7	7.3
Probe	3.3	14	41	35	7.0	3.9
Other	3.7	17	35	37	7.1	4.8

6 - 3 - 3 - 2 Separation Calculations

Elemental material balance calculations can be used to separate fume from ejecta. One total mass balance equation and a component balance equation can be written for each particulate sample as follows:

$$P = F + E$$

$$P\, x_P = F\, x_F + E\, x_E$$

where P, F, and E are the amounts of particulate, fume and ejecta respectively, and x_P, x_F, and x_E are the concentration of a particular component in particulate, fume, and ejecta respectively. P and x_P, are known from the measured particulate quantity and composition data. Fume composition (x_F) is also assumed to be equivalent to the average composition of the samples collected from the last three scrubbers That leaves three unknowns (F, E, and x_E) and two equations. One additional piece of information is needed to solve this system. It should be noted that although additional equations can be written using different components, the number of unknowns continues to increase on a one-to-one basis, and the system of equations remains indeterminate. An assumption about one of the unknowns is needed to obtain a solution. The most reasonable approach is to make an assumption about the concentration of one of the components in the ejecta.

6 - 3 - 3 - 3 Separation Calculation Assumptions

Ejecta are formed by mechanical processes such as ejection or fragmentation of char and smelt as opposed to the chemical processes of fume formation. In the char bed reactor, the zone of activity is limited to the vicinity of char bed surface. Thus the composition of the ejecta as they form should be similar to the char and smelt on the bed surface. Since the gas phase temperature above the char bed quickly drops down to about 750 °C and the gas residence time in the reactor is short, little variation in the inorganic composition of the ejecta while entrained by the flue gas is expected. Thus, the composition of the collected ejecta should be close to the composition of the material on the char bed surface. Furthermore, ejecta formation occurs at the bed surface where intensive burning generates very high temperatures. Under these conditions, the volatile char components such as chloride and potassium are more likely to be vaporized and thus present in lesser concentrations than in the original char.

The two extremes, which bound the ejecta composition are: 1) the ejecta are completely stripped of the limiting volatile (chloride), and 2) the ejecta have the same inorganic ratios as the original char. This can be stated mathematically as follows:

$$0 \leq \mathrm{Cl/(Na+K)}_{\mathrm{Ejecta}} \leq \mathrm{Cl/(Na+K)}_{\mathrm{Char}}.$$

$$0 \leq \mathrm{K/(Na+K)}_{\mathrm{Ejecta}} \leq \mathrm{K/(Na+K)}_{\mathrm{Char}}$$

The approach that was taken in this study was to calculate the amounts of fume (and ejecta) for each of these bounding cases, since the true value would have to lie somewhere in between. It turns out that the two calculated values are not that far apart, so the approach provides a very reasonable estimate of the amounts of fume and ejecta.

The upper bound on the amount of fume (and lower bound for ejecta) was determined by assuming that the chloride content of the ejecta was zero. The lower bound for fume (and upper bound for ejecta) was found by assuming either $K/(Na+K)_{Ejecta} = K/(Na+K)_{Char}$ or $Cl/(Na+K)_{Ejecta} = Cl/(Na+K)_{Char}$. Since potassium is less volatile than chloride, the assumption $K/(Na+K)_{Ejecta} = K/(Na+K)_{Char}$ is closer to reality than the chloride assumption and was used for most of the char burning runs. However, in some cases this assumption resulted in unacceptable results due to the relatively low concentrations of potassium and inaccuracies in chemical analyses. For these runs, the assumption $Cl/(Na+K)_{Ejecta} = Cl/(Na+K)_{Char}$ was used for calculating the lower bound for fume. In order to minimize clutter on graphs, the average of the upper and lower bound was used when the data were plotted.

The results of using the above procedure to calculate the amounts of fume and ejecta are shown in Table 7 for two typical char bed burning runs. The data are presented as the sodium fraction in the fume or ejecta normalized by the sodium content of the char that was burned. Although the separation calculation was performed for each particulate collection location, only the total values (the sum of fume or ejecta collected at all locations) are presented in Table 7.

Table 7. Results of Fume - Ejecta Separation Calculations for Two Typical Runs

Assumptions	Na Collected / Initial Na in Char Burned, %	
	Fume	Ejecta
RUN NUMBER 8		
$Cl_{Ejecta} = 0$	3.4	4.1
$K_{Ejecta} = 0$	5.4	2.1
$Cl/(Na+K)_{Ejecta} = Cl/(Na+K)_{Char}$	1.6	5.9
$K/(Na+K)_{Ejecta} = K/(Na+K)_{Char}$	1.5	6.0
Total Particulate	7.5	
RUN NUMBER 10		
$Cl_{Ejecta} = 0$	1.6	3.6
$K_{Ejecta} = 0$	3.2	2.0
$Cl/(Na+K)_{Ejecta} = Cl/(Na+K)_{Char}$	1.1	4.1
$K/(Na+K)_{Ejecta} = K/(Na+K)_{Char}$	0.8	4.4
Total Particulate	5.2	

Chapter 7: Experimental Results

The key experimental data acquired in the char bed burning experiments are presented in this chapter. These data include the measured char burning rates, average bed temperatures, the amounts of the elements sodium, sulfur, potassium and chlorine released as fume and ejecta, and the cation and anion composition of the fume and ejecta. The data presented are for runs 9 through 38, which are all of the runs for which a reliable pyrometric average bed temperature measurement was available. The purge tube for the pyrometer was installed after run 11, and runs 9-11 were all carried out at low bed temperatures, where the interference from fume scattering was minor.

In addition, some photomicrographs of the collected particulate are provided. These clearly show the morphological differences between fume and ejecta particles.

7 - 1 Char Bed Burning Rate and Bed Temperature

The average char burning rate and average bed temperature for each of the runs 9-38 are presented in Table 8. The key run conditions are also included. In this Table, char type 1 is the base case char without additives, char type 2 is the sulfate enriched char, and char type 3 is the carbonate enriched char.

There is a clear trend toward increasing char burning rates with increasing O_2 concentration in the reacting gas, as shown in Figure 7. This relationship exists for each of the different types of char separately. The data indicate that the highest burning rate belongs to the high sulfate char (char 2), while the burning rate variation with combustion gas oxygen concentration is very similar for the other two chars. The presence or absence of CO_2 and/or H_2O in the combustion gas does not appear to have an appreciable effect on char burning rate.

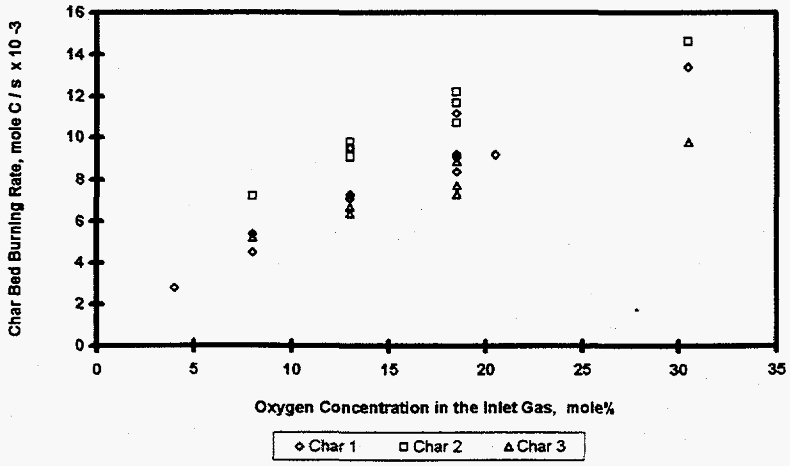

Figure 7. Effect of O_2 Concentration on Char Burning Rate

Table 8. Test Conditions, Average Char Burning Rates, and Average Bed Surface Temperature for the Char Bed Burning Experiments

Run No.	Run Conditions						Char Bed Burning Rate	Char Bed Surface Temperature (Pyrometric Average)
	Gas Component Concentration, Mole%				Gas Flow Rate	Char Type		
	O_2	CO_2	H_2O	N_2	SLPM		gmol C / s x 10^{-3}	°C
9	8.0	0.0	0.0	92.0	~ 250	2	7.2	923
10	8.0	0.0	0.0	92.0	~ 250	1	4.5	914
11	8.0	0.0	0.0	92.0	~ 250	3	5.2	923
12	8.0	10.0	0.0	82.0	~ 250	1	5.4	889
13	4.0	10.0	0.0	86.0	~ 250	1	2.8	828
14	13.0	0.0	0.0	87.0	~ 250	1	7.3	979
15	13.0	0.0	0.0	87.0	~ 250	3	6.4	972
16	13.0	0.0	0.0	87.0	~ 250	2	9.5	962
17	13.0	10.0	0.0	77.0	~ 250	2	9.1	933
18	13.0	10.0	0.0	77.0	~ 250	3	6.7	954
19	13.0	10.0	0.0	77.0	~ 250	1	7.1	953
20	13.0	10.0	15.0	62.0	~ 250	1	9.5	940
21	18.5	0.0	0.0	81.5	~ 250	1	11.2	1023
22	18.5	10.0	0.0	71.5	~ 250	1	8.4	995
23	13.0	10.0	15.0	62.0	~ 250	3	6.7	933
24	13.0	10.0	15.0	62.0	~ 250	2	9.8	913
25	18.5	10.0	15.0	56.5	~ 250	2	12.2	976
26	18.5	10.0	0.0	71.5	~ 250	3	7.3	982
27	18.5	10.0	0.0	71.5	~ 250	2	11.7	965
28	18.5	0.0	0.0	81.5	~ 250	2	10.7	980
29	18.5	10.0	15.0	56.5	~ 250	1	9.1	973
30	18.5	10.0	15.0	56.5	~ 250	3	8.9	982
31	18.5	0.0	0.0	81.5	~ 250	3	7.7	1007
32	20.5	0.0	0.0	79.5	~ 250	1	9.2	1005
33	18.5	0.0	15.0	66.5	~ 250	1	9.2	1009
34	20.5	0.0	0.0	79.5	~ 170	1	5.6	975
35	18.5	10.0	0.0	71.5	~ 250	1	8.4	1007
36	30.5	0.0	0.0	69.5	~ 250	1	13.4	1163
37	30.5	0.0	0.0	69.5	~ 250	3	9.8	1094
38	30.5	0.0	0.0	69.5	~ 250	2	14.6	1094

Average char bed surface temperature were measured with a pyrometer as discussed in section 6-1. The bed surface temperature data are plotted vs. char burning rate and combustion gas oxygen concentration in Figures 8 and 9 respectively. Surprisingly, there appears to be a better correlation with oxygen concentration than with bed burning rate. However, the best correlation is found when bed temperature is plotted vs. char bed burning rate separately for each type of char. At similar char burning rates, the high sulfate char (char 2) generates a lower bed temperature compared to the other two types of char. This is apparently due to the net endothermic heat of reduction associated with the conversion of sulfate to sulfide in the char.

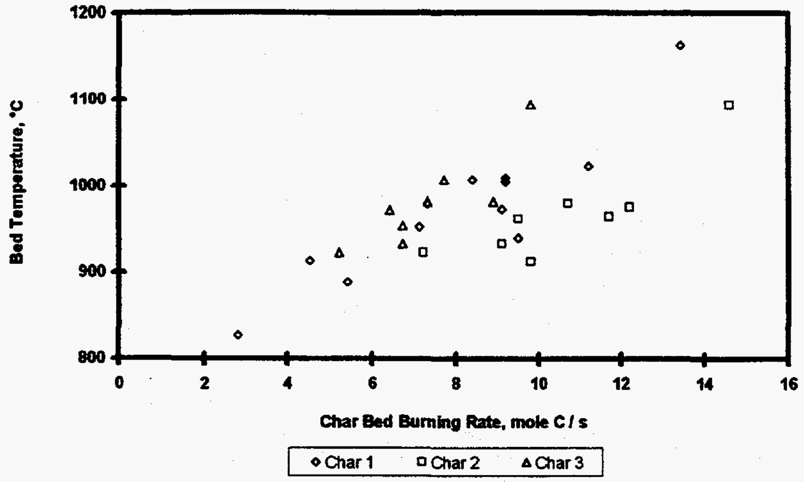

Figure 8. Average Char Bed Surface Temperature vs. Char Burning Rate

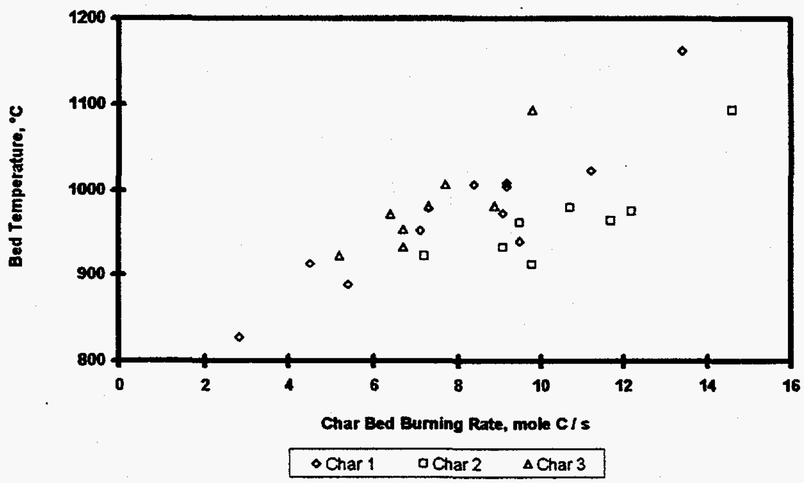

Figure 9. Average Char Bed Surface Temperature vs. O_2 Concentration

7 - 2 Particulate Formation

Two types of particles were observed in the deposits collected on the air-cooled deposition probe: fine white particles (fume), and coarser particles with a light brown color (ejecta). A scanning electron micrograph (SEM) of the particles collected on the probe is shown in Figure 10. There is a group of particles 1-100 μm in diameter and another group of particles < 1μm in diameter. Some of these smaller particles are even deposited on top of the larger particles (the first group). In addition, the micro-structure of the fume and ejecta looks quite different (Figures 11 and 12) which clearly indicates differences in formation mechanism between the two groups of particles. These two types of particles were also observed on the deposits found on components of the particulate collection system. Brown 1-100 micron particles tend to agglomerate and form strong deposits on the bends of tubes, while fine white particles deposited uniformly all over the tubes.

A distinct brown color was observed in the first scrubber solution after each char burning experiment, while the other three scrubber solution never showed any color. Some suspended dark particles could be observed in the first scrubber solution especially after

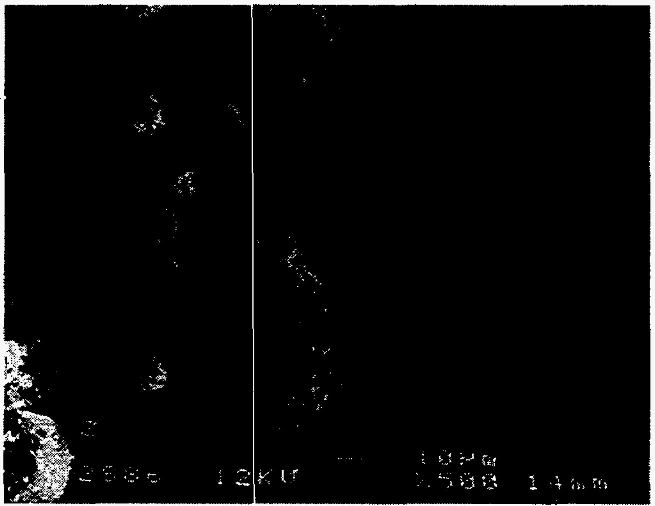

Figure 10. **Scanning Electron Micrograph (SEM) of Particles Collected on *the* Air-cooled Deposition Probe**

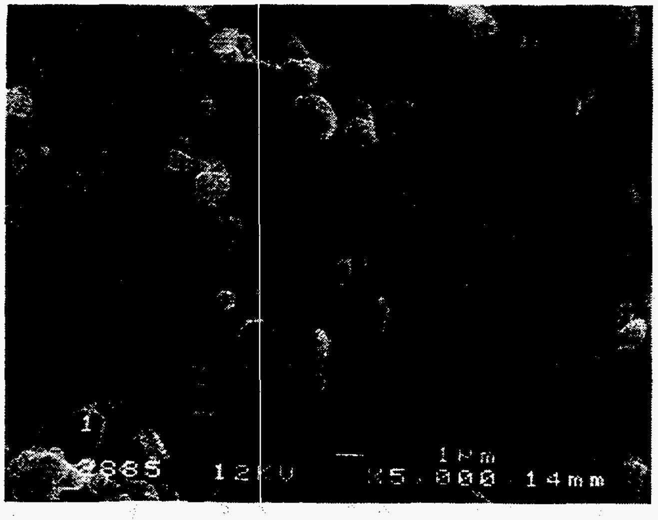

Figure 11. **Magnified SEM Photograph Showing Fume Particles**

high temperature char burning experiments. The brown color of the first scrubber solution indicates particles which probably contain some organic material and carbon.

Video tapes taken from char burning experiments show occasional ejection of fine particles from the bed at very high velocities. Figure 13 shows this in an image prepared using one of the video tapes. However, the bulk of the ejecta particles are too small to be seen as individual burning fragments, so the observation of occasional release of large fragments is likely to be misleading.

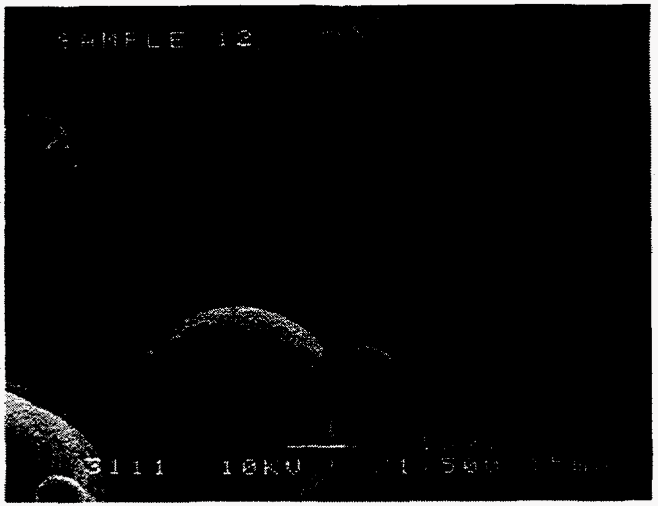

Figure 12. **Magnified SEM Photograph Showing Ejecta Particles**

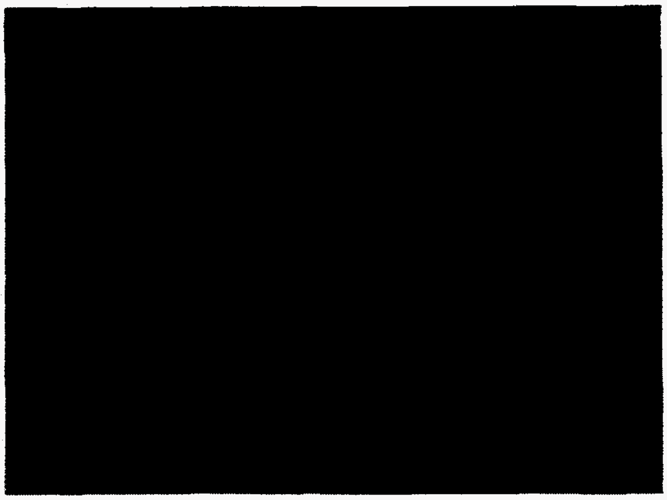

Figure 13. **Char Fragments Ejected from the Bed During Char Burning (the white trail shows the movement of the particle)**

7 - 2 - 1 Fume Characterization

Fume is formed by condensation of gaseous alkali metal compounds either homogeneously in the gas phase or directly on cool surfaces. As a result of formation from the gas phase, the particle size of fume is quite small, normally less than one micron. Fume particles are white because they are mainly composed of carbonate, sulfate, and chloride salts of sodium and potassium. The submicron-sized, amorphous, white particles shown in Figure 10 and 11 represent typical fume particles collected during char bed burning experiments. As seen in Figure 11, the fume particles in the deposit collected on the air-cooled probe are fused and sintered to a considerable extent. The small-sized fume particles are more difficult to collect, and a series of four scrubber was used in the particulate collection system in order to minimize the loss of fume.

7 - 2 - 2 Ejecta Characterization

Ejecta are formed by fragmentation of the char bed material into small burning particles which are then carried off by the gas phase. The chemical composition of ejecta particles is initially equivalent to the bed material they were fragmented from. Depending on the residence time of particles in the high temperature zone of the furnace, the particles will continue to burn and the chemical composition of these particles will change. In these char bed burning experiments, no special provisions were made for completing the burnout of suspended particles. Thus, it is expected that ejecta particles contain some carbon or organic compounds and even reduced sulfur at the time they are collected. These components could be responsible for the light brown color observed for ejecta in the char burning experiments.

Microphotographs of entrained particles, collected on the air-cooled deposition probe, show a particle size of 1-100 microns for ejecta. This particle size is big enough to cause inertial deposition of particles at locations where the flow direction changes, such as tube bends. Small ejecta particles could also deposit by thermophoresis. Visual inspection of the material collected on the deposition probe indicates ejecta particles on both leeward and windward side of the probe are significantly fused and sintered,

7 - 3 Fume and Ejecta Quantity and Chemistry Data

The amount and composition of the fume and ejecta for experiments 9 through 38 were calculated using the method described in section 6-3-3. Tables 9 and 10 give the release fractions for sodium, potassium, sulfur and chlorine relative to the amounts in the initial char that was burned. Tables 11 and 12 give the cation and anion composition for both types of particulates. The data on amounts are presented in the form of upper and lower bounds which should bracket the true values. Since the amounts of fume and ejecta are essentially determined by difference, the upper bound for one is the lower bound for the other and vice-versa.

Table 9. Amount of Sodium and Potassium in Initial Char Burned Converted to Fume and Ejecta

Run	Na Collected / Initial Na in Char Burned, %					K Collected / Initial K in Char Burned, %				
		Fume		Ejecta			Fume		Ejecta	
No.	Total	Upper	Lower	Upper	Lower	Total	Upper	Lower	Upper	Lower
9	3.7	0.7	0.4	3.3	3.0	4.4	2.0	1.1	3.3	2.5
10	5.3	1.6	0.8	4.4	3.6	6.0	3.0	1.5	4.4	2.9
11	4.7	1.1	0.8	3.9	3.6	5.6	2.4	1.7	3.9	3.3
12	3.4	1.1	0.6	2.8	2.3	4.2	2.6	1.4	2.8	1.6
13	1.3	0.9	0.5	0.8	0.4	1.9	1.9	1.1	0.8	0.1
14	10.7	5.9	3.4	7.3	4.7	12.3	7.4	4.2	8.0	4.8
15	7.1	2.3	1.6	5.5	4.8	8.3	4.0	2.8	5.5	4.2
16	4.8	1.3	0.8	4.0	3.5	5.8	2.8	1.8	4.0	2.9
17	5.5	1.3	0.6	4.9	4.2	6.2	2.9	1.4	4.9	3.3
18	7.2	1.2	0.5	6.7	6.0	8.1	3.2	1.4	6.7	4.9
19	7.9	1.8	0.7	7.2	6.1	8.5	4.0	1.6	6.9	4.5
20	6.0	2.2	0.8	5.2	3.9	6.8	4.1	1.5	5.2	2.6
21	12.1	6.6	3.5	8.5	5.5	13.4	8.5	4.5	8.9	4.9
22	16.1	4.1	2.1	14.0	12.0	17.5	7.9	4.0	13.5	9.6
23	4.8	1.4	0.6	4.2	3.5	6.2	3.0	1.3	4.9	3.2
24	4.3	1.5	0.8	3.5	2.8	5.5	3.6	2.0	3.5	1.9
25	8.3	3.0	1.4	6.9	5.3	9.6	5.7	2.6	6.9	3.9
26	7.5	1.8	1.0	6.5	5.7	8.7	4.0	2.3	6.5	4.7
27	8.5	2.3	1.3	7.2	6.2	10.1	5.2	2.9	7.2	4.9
28	8.4	2.3	1.7	6.8	6.2	10.0	4.4	3.2	6.8	5.6
29	10.3	3.6	1.9	8.4	6.7	12.0	6.9	3.6	8.4	5.1
30	7.2	3.1	1.9	5.2	4.1	8.8	5.7	3.5	5.2	3.1
31	11.3	3.2	2.1	9.2	8.2	12.8	5.4	3.6	9.2	7.4
32	14.4	4.9	2.1	12.3	9.5	15.4	7.3	3.1	12.3	8.1
33	10.7	5.8	3.0	7.7	4.9	12.3	8.6	4.4	8.0	3.7
34	11.6	2.8	0.7	10.9	8.8	11.7	4.8	1.2	10.5	7.0
35	13.3	3.1	1.2	12.1	10.2	14.5	6.3	2.4	12.1	8.2
36	17.0	12.2	8.4	8.7	4.8	18.9	14.0	9.6	9.3	4.9
37	11.7	7.2	4.2	7.5	4.6	12.5	8.0	4.6	7.8	4.5
38	14.4	10.4	5.8	8.6	4.0	16.0	11.2	6.1	9.9	4.8

Table 10. **Amount of Sulfur and Chlorine in Initial Char Burned Converted to Fume and Ejecta**

Run	S Collected / Initial S in Char Burned, %					Cl Collected / Initial Cl in Char Burned, %				
		Fume		Ejecta			Fume		Ejecta	
No.	Total	Upper	Lower	Upper	Lower	Total	Upper	Lower	Upper	Lower
9	3.9	1.8	1.0	2.9	2.0	9.0	9.0	5.0	4.0	0.0
10	6.2	3.6	1.8	4.3	2.5	14.4	14.4	7.2	7.1	0.0
11	5.8	3.3	2.4	3.3	2.4	12.2	12.2	9.0	3.2	0.0
12	4.2	3.8	2.1	2.1	0.4	11.2	11.2	6.1	5.1	0.0
13	2.0	1.9	1.2	0.8	0.1	7.7	7.7	4.1	3.6	0.0
14	9.1	3.7	2.1	6.9	5.3	18.7	18.7	10.5	8.2	0.0
15	7.5	4.4	3.0	4.5	3.1	11.5	11.5	7.9	3.6	0.0
16	4.6	2.4	1.5	3.1	2.2	8.4	8.4	5.3	3.1	0.0
17	5.6	3.1	1.5	4.1	2.4	8.5	8.5	3.9	4.6	0.0
18	8.8	6.0	2.7	6.1	2.8	9.2	9.2	4.1	5.1	0.0
19	9.6	7.0	2.8	6.8	2.5	12.7	12.7	5.1	7.7	0.0
20	8.3	7.5	2.8	5.5	0.7	11.8	11.8	4.4	7.4	0.0
21	10.5	6.2	3.3	7.2	4.3	20.2	20.2	10.7	9.5	0.0
22	16.8	13.1	6.7	10.1	3.7	20.2	20.2	10.3	9.9	0.0
23	7.6	5.9	2.6	4.9	1.7	8.2	8.2	3.6	4.5	0.0
24	5.0	4.1	2.3	2.7	0.9	6.4	6.4	3.6	2.8	0.0
25	8.8	6.3	2.9	5.9	2.5	10.3	10.3	4.7	5.6	0.0
26	9.8	7.4	4.2	5.6	2.4	9.9	9.9	5.6	4.3	0.0
27	8.8	5.5	3.1	5.7	3.3	13.9	13.9	7.9	6.0	0.0
28	8.5	4.0	2.9	5.5	4.5	13.6	13.6	9.9	3.7	0.0
29	14.0	11.9	6.2	7.9	2.1	14.2	14.2	7.3	6.9	0.0
30	10.8	10.5	6.5	4.3	0.4	11.2	11.2	7.0	4.3	0.0
31	12.4	6.3	4.2	8.2	6.1	14.9	14.9	10.0	4.9	0.0
32	14.1	7.5	3.2	10.9	6.6	19.9	19.9	8.5	11.4	0.0
33	12.8	10.3	5.2	7.5	2.5	17.1	17.1	8.6	8.5	0.0
34	12.0	6.7	1.7	10.3	5.3	15.2	15.2	3.9	11.4	0.0
35	14.7	11.2	4.3	10.5	3.6	16.9	16.9	6.4	10.4	0.0
36	13.9	5.0	3.4	10.4	8.9	31.6	31.6	21.5	10.1	0.0
37	11.1	5.2	3.0	8.1	5.9	19.4	19.4	11.2	8.2	0.0
38	10.6	4.6	2.5	8.1	6.1	20.4	20.4	11.1	9.3	0.0

Table 11. Fume Composition Data

Run	SO_4 / (Na_2 + K_2)	CO_3 / (Na_2 + K_2)	Cl_2 / (Na_2 + K_2)	K_2 / (Na_2 + K_2)
No.	mole%	mole%	mole%	mole%
9	79.2	0.0	22.3	18.3
10	33.1	55.2	18.6	16.8
11	40.8	50.4	18.2	14.0
12	50.3	30.0	21.1	20.4
13	32.6	51.0	18.0	15.7
14	10.2	84.3	7.2	12.0
15	27.6	61.6	8.7	12.1
16	58.2	29.4	11.7	14.4
17	77.7	11.0	12.1	15.4
18	70.2	13.5	12.9	17.8
19	56.0	29.5	14.5	19.0
20	51.3	36.0	11.0	17.0
21	14.9	82.1	6.9	12.4
22	47.4	42.6	10.5	17.2
23	61.1	26.4	10.1	14.8
24	85.2	2.9	7.6	15.9
25	68.1	22.6	6.4	13.0
26	57.4	34.6	9.2	15.1
27	76.3	20.5	11.0	15.2
28	56.5	38.2	11.1	13.1
29	49.0	48.1	8.4	17.1
30	48.8	47.5	6.3	12.7
31	28.7	64.0	8.2	11.7
32	23.8	67.5	9.0	13.9
33	27.3	69.1	6.6	13.9
34	36.5	52.1	11.8	15.6
35	53.5	35.6	11.5	18.2
36	6.5	91.1	6.0	11.1
37	10.9	85.5	5.0	8.1
38	15.0	88.2	3.9	7.9

Table 12. Calculated Ejecta Composition Data

Run	SO_4 / (Na_2 + K_2), mole%		CO_3 / (Na_2 + K_2), mole%		Cl_2 / (Na_2 + K_2), mole%		K_2 / (Na_2 + K_2), mole%	
No.	assum.1	assum.2	assum.1	assum.2	assum.1	assum.2	assum.1	assum.2
9	23.5	29.4	79.2	71.7	0.0	2.4	6.0	7.3
10	11.5	15.8	90.0	85.2	0.0	3.7	8.1	9.8
11	10.5	13.0	87.9	84.8	0.0	1.5	6.7	7.3
12	2.8	12.4	96.1	82.8	0.0	4.2	7.2	9.8
13	7.1	15.5	73.2	65.8	0.0	10.4	4.0	9.9
14	18.2	15.3	76.3	79.2	0.0	2.6	9.9	10.7
15	10.1	12.5	90.6	86.6	0.0	1.2	6.5	7.3
16	21.7	26.5	81.1	74.3	0.0	1.5	6.2	7.3
17	20.2	29.0	81.1	70.3	0.0	1.9	5.8	7.3
18	7.1	14.0	94.9	86.1	0.0	1.4	6.0	7.3
19	7.0	15.4	95.3	84.0	0.0	2.5	7.5	9.5
20	3.2	16.9	90.0	74.6	0.0	3.3	7.0	9.8
21	12.9	13.6	88.3	86.0	0.0	2.6	8.9	10.2
22	5.1	13.3	96.2	85.8	0.0	2.0	8.0	9.8
23	7.3	17.7	88.8	76.8	0.0	1.9	6.8	8.3
24	10.7	26.3	85.2	67.9	0.0	1.6	5.0	7.3
25	16.3	29.0	83.0	68.2	0.0	1.6	5.4	7.3
26	6.5	13.2	97.7	89.4	0.0	1.2	6.1	7.3
27	18.5	27.2	91.4	80.8	0.0	1.7	5.9	7.3
28	25.0	28.0	82.0	77.8	0.0	1.1	6.6	7.3
29	5.3	15.2	98.3	86.9	0.0	1.9	7.7	9.8
30	1.3	12.5	105.5	91.9	0.0	1.5	5.6	7.3
31	11.5	13.6	92.1	88.7	0.0	1.0	6.7	7.3
32	11.5	14.4	89.9	84.6	0.0	2.1	8.5	9.8
33	8.5	15.7	92.6	83.5	0.0	2.5	7.7	10.1
34	9.9	15.4	90.0	82.2	0.0	2.4	7.9	9.5
35	5.8	14.0	96.2	85.7	0.0	2.0	8.1	9.8
36	29.9	19.4	75.0	82.6	0.0	2.7	10.0	10.5
37	19.9	16.3	75.5	79.5	0.0	2.0	7.2	7.6
38	51.3	31.9	48.2	69.6	0.0	2.1	6.6	8.2

The composition of the fume is based on an average of the composition of the material collected in the last three scrubbers. The composition of the ejecta is then calculated by the same material balance procedures used for determining the amounts of fume and ejecta, and is thus dependent on the assumption used to make that calculation. Assumption 1, that the chloride content of the ejecta is zero is the assumption used to determine the upper bound for the amount of fume. Assumption 2, is the assumption used for determining the lower bound for the amount of fume as discussed in section 6-3-3.

In many cases, the sum of the anions (sulfate, carbonate and chloride) lies between 100% and 110% of the sum of cations. This is partly a reflection of inaccuracies in the analytical measurements. Part of it is also believed to be due to some absorption of CO_2 produced by burning char carbon in the scrubbers. Thus the carbonate content of both fume and ejecta may be slightly overestimated.

Since it was only possible to bracket the amounts of fume and ejecta produced in a given experiment, graphical presentations of the data should indicate the range of individual values. However, when this is done with a large number of data points, the resulting clutter makes it difficult to interpret the graphs. In order to prevent such confusion, the average of the calculated upper and lower bound is used in graphical presentations.

Sodium is the major cation in both the fume and ejecta, and the data on the release of sodium during char bed burning are the most important data obtained in this study. The potassium and chloride content of the fume and the amounts of these two elements released to form fume are also important information, since they can provide information on the relative importance of KCl vaporization in the total fume forming process. The amounts of sulfur in fume and ejecta are of relatively minor importance, since the sulfate content of the fume is primarily a function of sulfur balances in the overall combustion process and only the sulfur which is released during char bed burning. The carbonate data are of the least importance, since the amount of carbonate formed is essentially determined by difference (availability of sulfur and chlorine) and thus a matter of material balances only.

7 - 4 Fume Production During Char Bed Burning

7 - 4 - 1 - Sodium Released

The primary variable governing the release of sodium as fume is bed temperature. This is evident in Figure 14, which shows that sodium released increases strongly with increasing bed temperature. The relationship between sodium released and bed temperature appears to be relatively independent of char type and combustion gas composition. There is some evidence that CO_2 in the combustion gas has a small suppressing effect on sodium released as fume for the base case char and the high carbonate char. No CO_2 suppression was observed for the high sulfate char.

The amount of sodium released as fume shows much more scatter when plotted vs. char bed burning rate as seen in Figure 15. Some dependence on char type is also evident in Figure 15, where the lowest sodium released corresponds to the high sulfate char (char 2). This seems to be a consequence of the previously discussed fact that bed temperatures were lower for the same burning rate for char 2 and reinforces the importance of bed temperature in determining the amount of sodium released as fume.

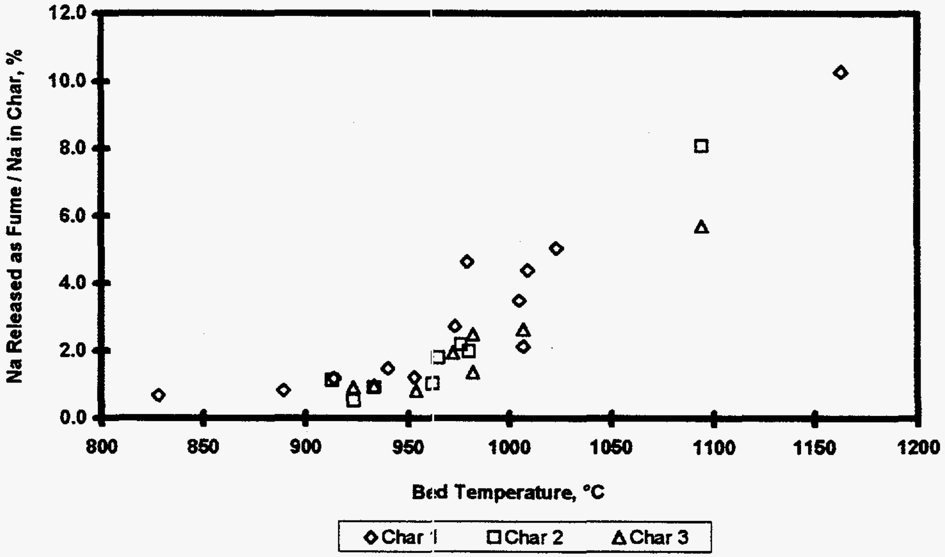

Figure 14. Effect of Bed Temperature on Sodium Released as Fume

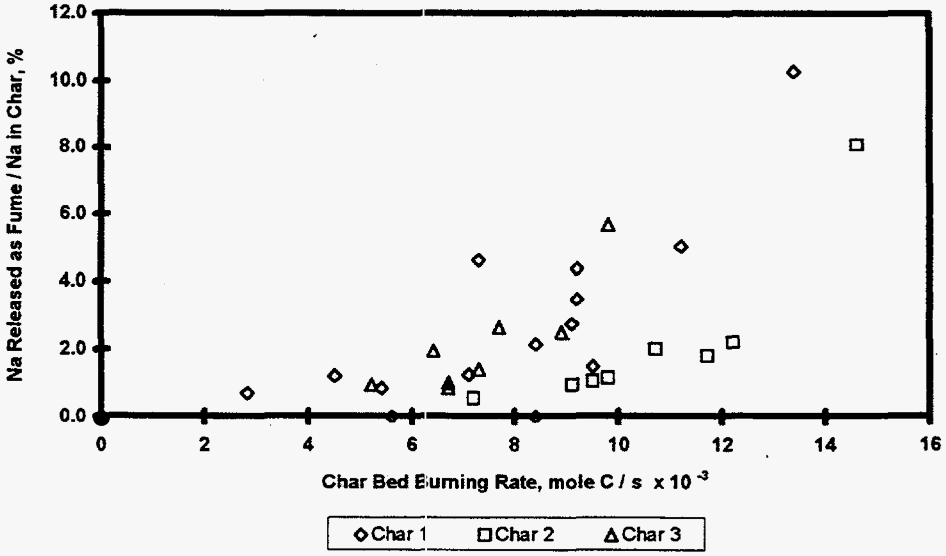

Figure 15. Effect of Char Burning Rate on Sodium Released as Fume

7 - 4 - 2 Potassium Released

In general, the potassium released as fume is higher than the amount of sodium released under similar burning conditions. Potassium release also increases strongly with increasing bed temperature as seen in Figure 16. No dependence on char type and combustion gas composition is evident. As with sodium, the amount of potassium released as fume shows much more scatter when plotted vs. char burning rate and the high sulfate char shows the lowest potassium release (Figure 17). The reasons for this are the same as for sodium release.

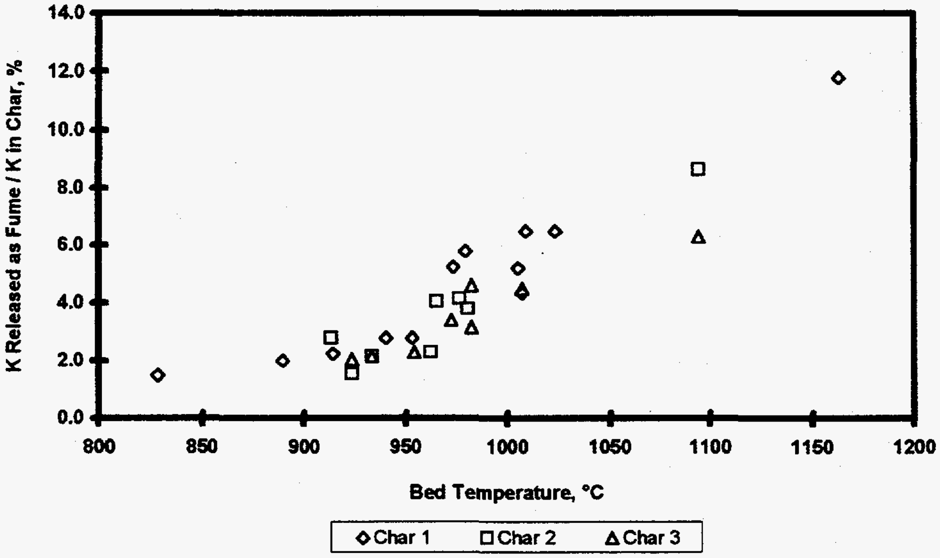

Figure 16. Effect of Bed Temperature on Potassium Released as Fume

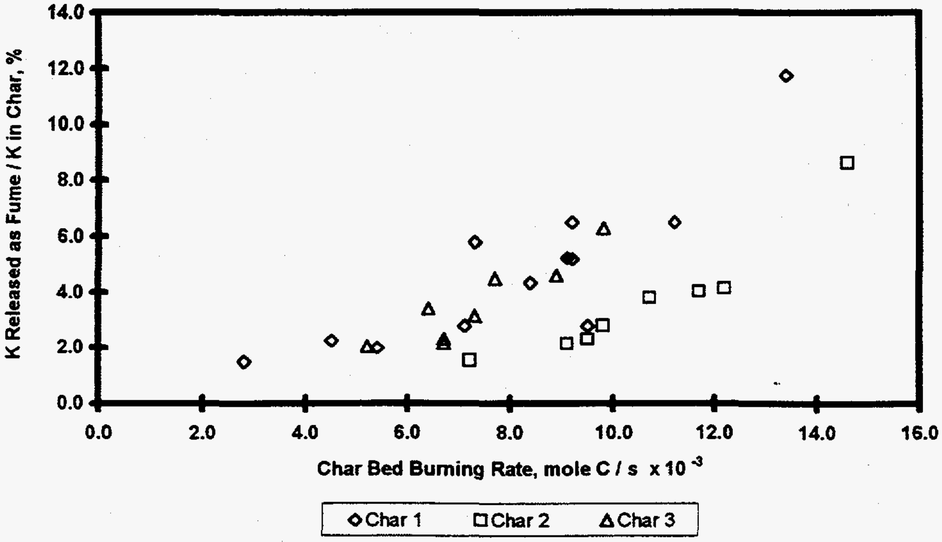

Figure 17. Effect of Char Burning Rate on Potassium Released as Fume

7 - 4 - 3 Chloride Released

There is much more scatter when all of the chloride release data are plotted against bed temperature. Both char type and combustion gas composition appear to affect chloride release as well as temperature. A reasonable correlation is found if chloride release is plotted vs. bed temperature separately for each type of char. This is seen in Figure 18 for the base-case char. The temperature dependence of chloride release is less sensitive than that of sodium and potassium release at high temperatures. These results are consistent with simple KCl and NaCl vaporization being the main mechanism for chlorine release as fume.

7 - 4 - 4 Sulfur Released

There is much more scatter when sulfur released as fume is plotted vs. either bed temperature or char burning rate. Figure 19 shows some tendency for sulfur release to increase with increasing temperature up to about 1000°C, but the sulfur then appears to decrease at higher temperatures.

The data indicate that sulfur release increases when the combustion gas contains CO_2 and/or H_2O. This may be due to the following reactions:

$$2\,CO_2 + Na_2S = COS + Na_2CO_3$$

$$H_2O + CO_2 + Na_2S = H_2S + Na_2CO_3.$$

The sulfur released by these reactions would be available to react with released alkali to form sulfate fumes in the oxidizing zone of the reactor system.

Interestingly, the data indicate that under similar conditions, the lowest sulfur release was obtained with char 2, the sulfate enriched char with the highest total sulfur content. This confirms that sodium sulfate fume is not produced directly from sodium sulfate in the char and that the sulfur present in the char as Na_2SO_4 and Na_2S is not volatile.

7 - 4 - 5 Fume Chemistry

Fume composition was measured directly as the average composition of the last three scrubber solutions. These data are summarized in Table 11.

Carbonate and sulfate are the major anions in the fume, but chloride can range up to over 20% and is clearly enriched in the fume relative to the chloride content of the char being burned. In general, the fume CO_3 content increases and SO_4 content decreases with increasing bed temperature (as seen in Figures 20 and 21). This is likely to be a dilution effect, since the release of both sodium and potassium increase strongly with temperature and will react to form carbonate fumes if sulfur is not available. This behavior is consistent with the concept that alkali release occurs by chloride vaporization and metallic sodium (and potassium) formation and vaporization with subsequent formation of sulfate and carbonate fumes in the gas phase. With a limited amount of sulfur in the gas phase, increasing alkali vaporization will tie up all available sulfur as sulfate and the remainder will form carbonate.

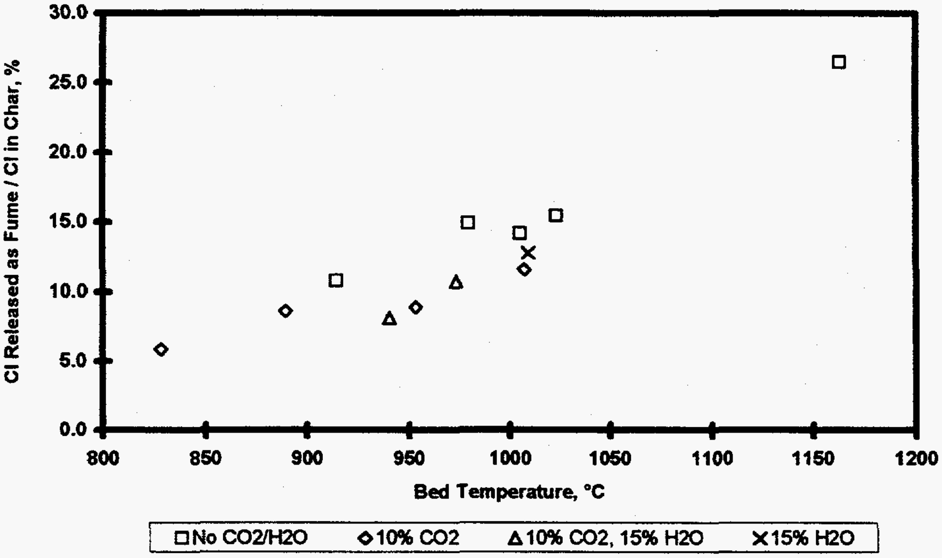

Figure 18 **Effect of Bed Temperature on Chloride Released as Fume for Char 1**

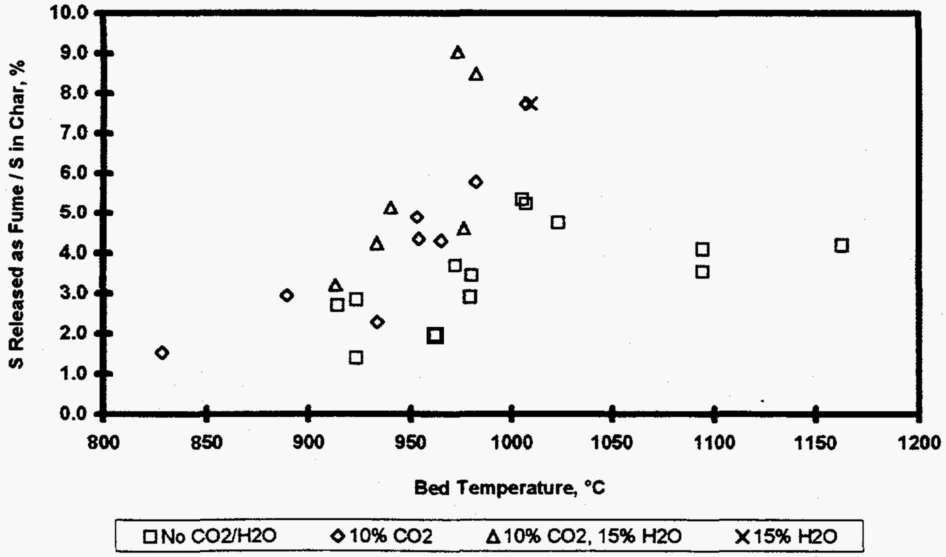

Figure 19 **Effect of Bed Temperature on Sulfur Released as Fume**

The presence of CO_2 and/or H_2O in the combustion gas tends to increase the sulfate content and decrease the carbonate content of the fume by providing additional reaction paths for sulfur release. This is evident in Figure 22. In the absence of CO_2 and H_2O, the high sulfate char (char 2) gave fume with the highest sulfate content (see Figure 21) and the lowest carbonate content.

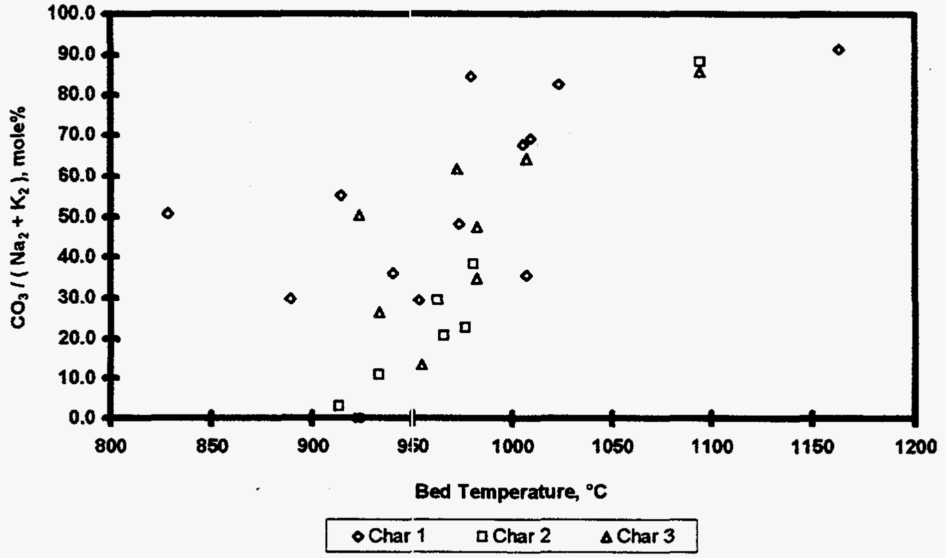

Figure 20. Effect of Bed Temperature on Carbonate Content of Fume

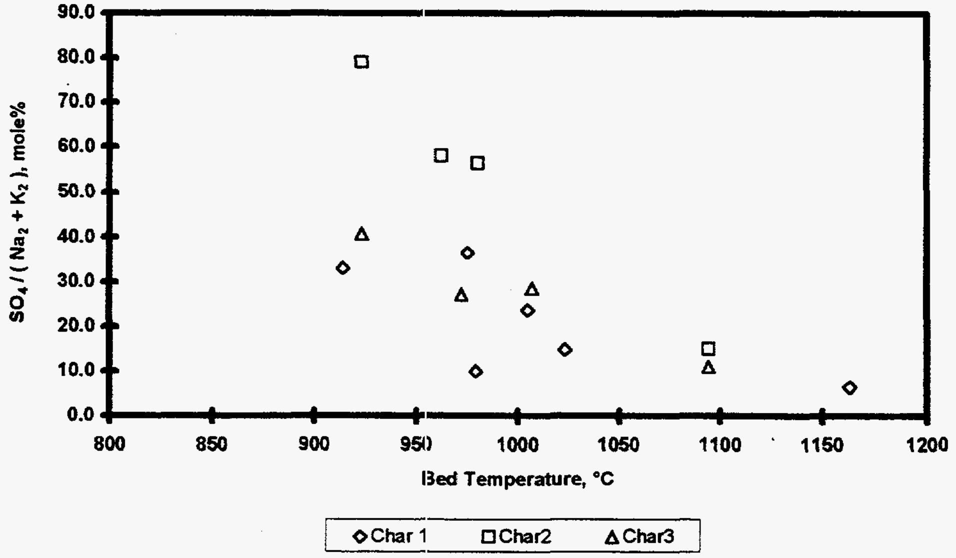

Figure 21. Effect of Bed Temperature on Sulfate Content of Fume When CO_2 and H_2O Are Absent

Figures 23 and 24 show the effect of bed temperature on the potassium and chloride content of the fume respectively. Both the potassium and chloride concentration in the fume decrease with increasing bed temperature. The temperature effect is stronger for chloride. This behavior is completely consistent with current concepts of fume formation.

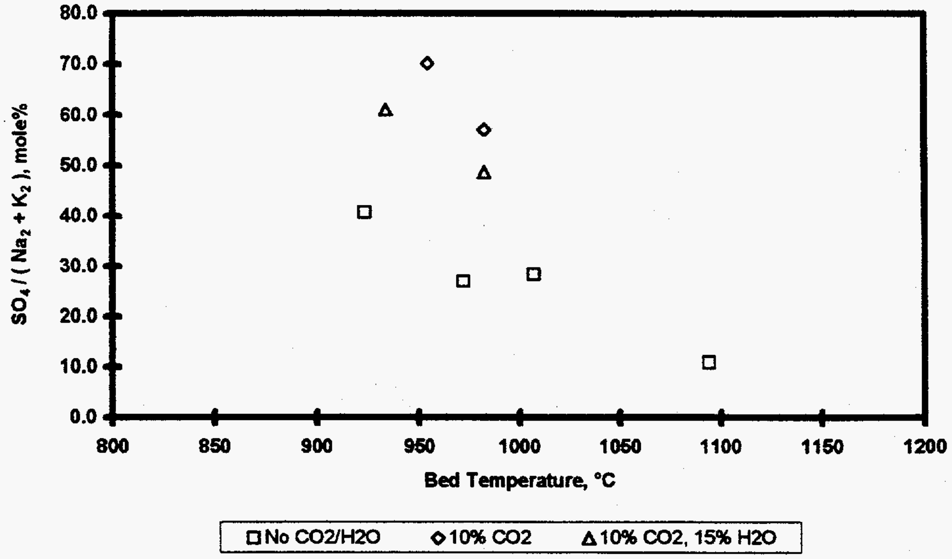

Figure 22. **Effect of Reactant Gas Composition on Sulfate Content of Fume for Char 3**

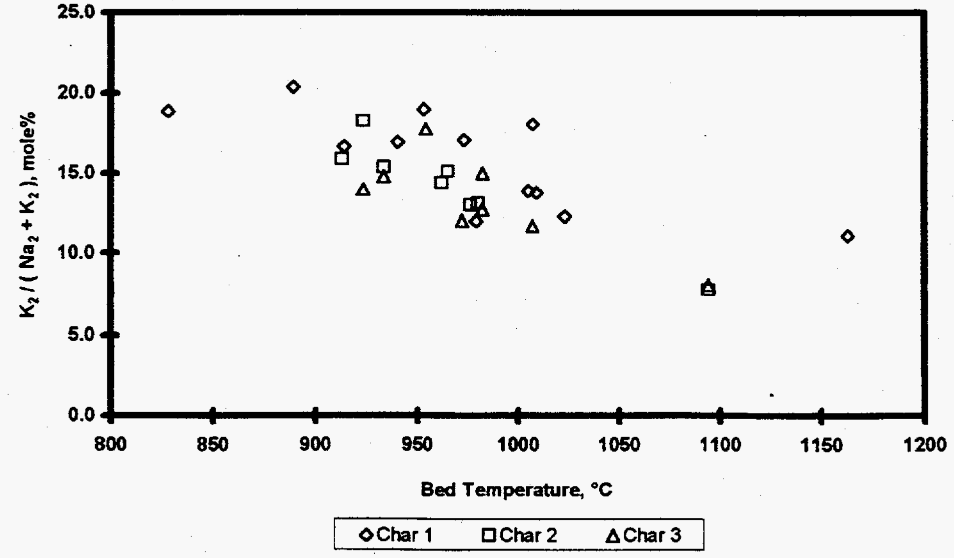

Figure 23. **Effect of Bed Temperature on Potassium Content of Fume**

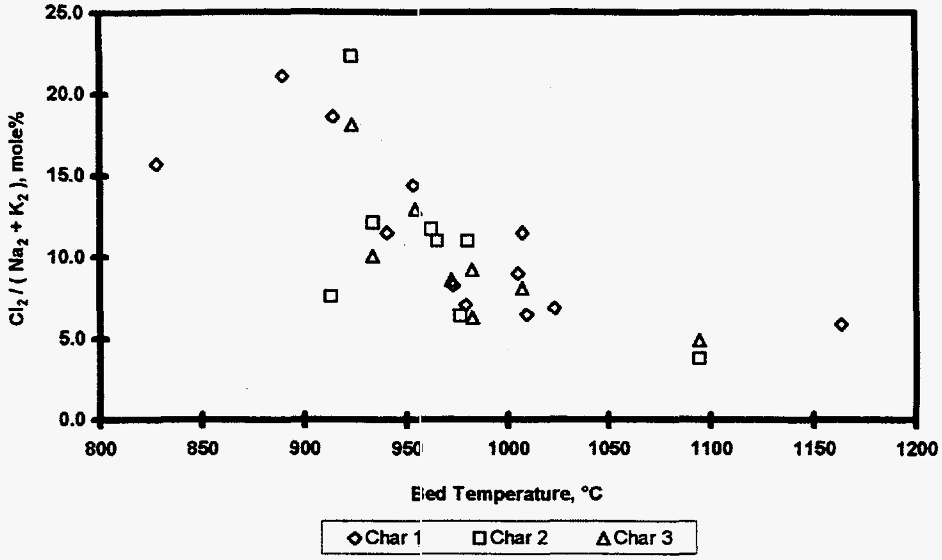

Figure 24. Effect of Bed Temperature on Chloride Content of Fume

7 - 5 - Ejecta Formation During Char Bed Burning

7 - 5 - 1 Alkali Released as Ejecta

The amounts of sodium and potassium released from the burning bed as ejecta particles are plotted vs. bed temperature in Figures 25 and 26 respectively. There is considerably more scatter than there is in the plots of fume formation vs. bed temperature. However, ejecta alkali release still appears to correlate better with bed temperature than with bed burning rate. The sodium and potassium release as ejecta appear to be substantially identical, both with respect to the temperature dependence and with respect to the fractions of each element released. This is consistent with a formation mechanism that is essentially mechanical and not chemical. The alkali release appears to increase strongly with increasing bed temperature up to about 1000°C, but then appears to drop off at higher bed temperatures. Because of the limited amount of data at very high bed temperatures, the apparent decrease with temperature above 1000°C is considered tentative. It is clear, however, that release of alkali as ejecta does not continue to increase with temperature in the same manner as does fume.

7 - 5 - 2 Ejecta Chemistry

The composition of the ejecta particles is also consistent with a mechanical formation mechanism. There is a strong relationship between the composition of the ejecta and the composition of the char being burned. The ejecta are very rich in carbonate, with relatively low concentrations of sulfate and very little chloride. The sulfate content of the ejecta is plotted vs bed temperature in Figure 27. There is considerable scatter, with some suggestion of an increase in sulfate content with increasing bed temperature. The highest sulfate concentrations in ejecta are found with the high sulfate char (char 2) as would be expected.

The potassium content of the ejecta does appear to increase slowly with increasing bed temperature as can be seen in Figure 28. As shown in the preceding section, the fume was enriched in potassium relative to sodium. Fume enrichment in potassium decreases

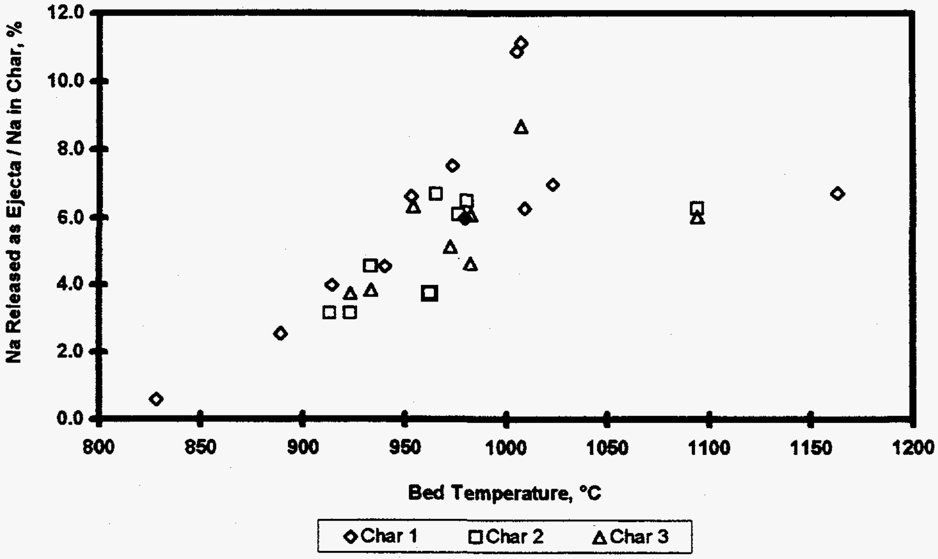

Figure 25 Effect of Bed Temperature on Sodium Released as Ejecta

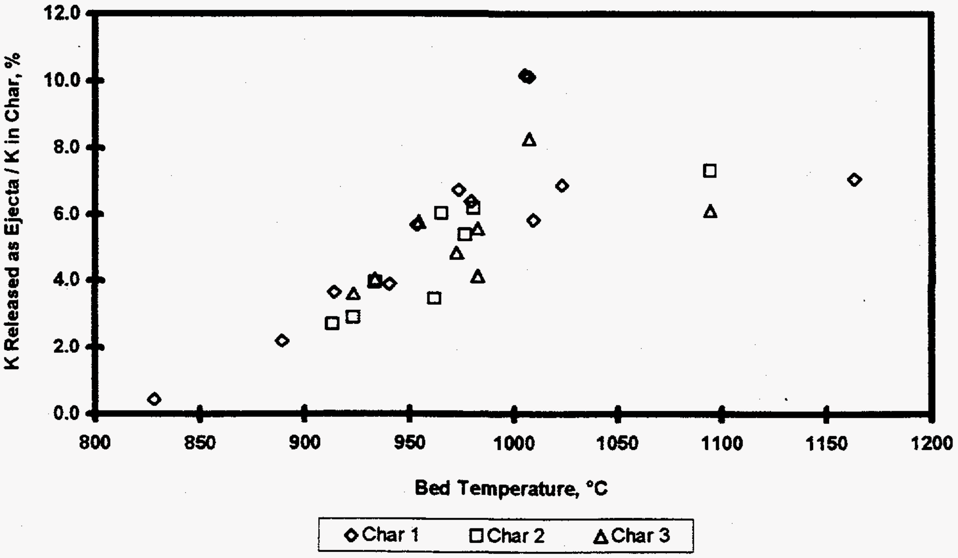

Figure 26 Effect of Bed Temperature on Potassium Released as Ejecta

with increasing bed temperature. Thus, the opposite behavior is expected for the ejecta which consists of the material that remains in the bed. As expected, the base-case char (char 1) gives the highest potassium content in ejecta, since there is no dilution with the sodium sulfate and sodium carbonate added in forming chars 2 and 3.

The chloride content of the ejecta is generally very low. No conclusions can be drawn with respect to the chloride in the ejecta because the amounts are very small and small differences are likely to be quite inaccurate.

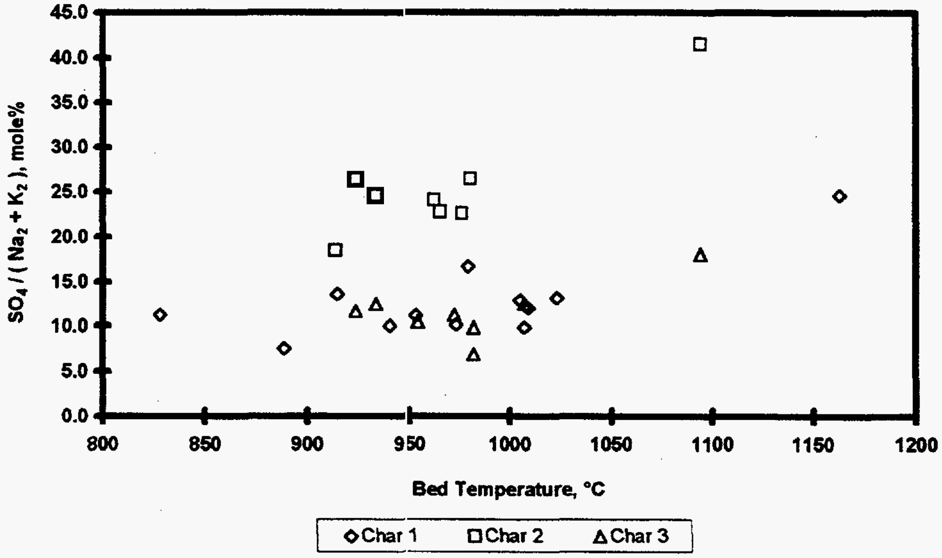

Figure 27. Effect of Bed Temperature on Sulfate Content of Ejecta Particles

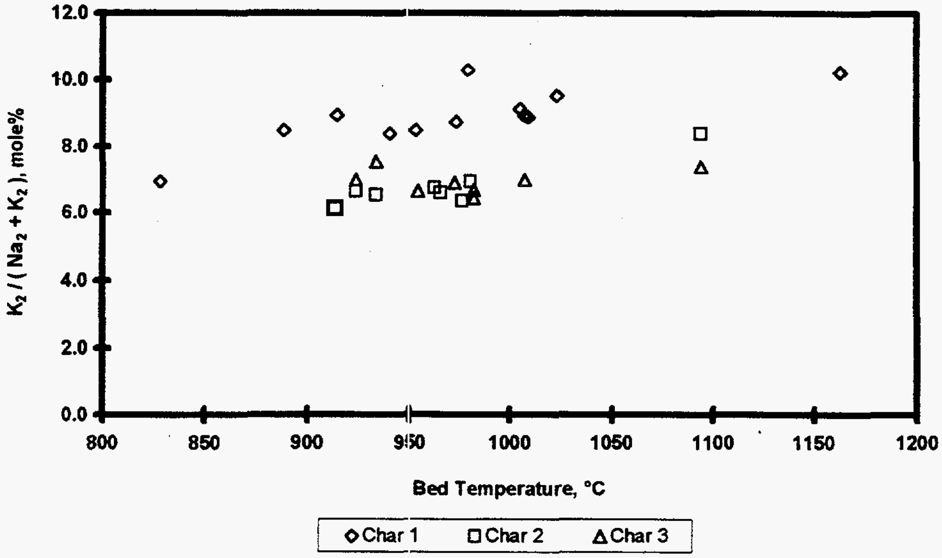

Figure 28. Effect of Bed Temperature on Potassium Content of Ejecta Particles

Chapter 8: Interpretation and Conclusions

The purpose of this chapter is to summarize the experimental results obtained and to draw some conclusions based on a preliminary interpretation of the data. Detailed theoretical explanation of the experimental data is left for the future.

Experimental data on the rates of formation of particulate matter during char bed burning were obtained under controlled conditions, using a laboratory char bed reactor. This is the first data of this type ever obtained. A very significant feature of these experiments was that the sodium release as particulate was measured under conditions where closed sodium balances were obtained.

8 - 1 Particulate Characterization

Two distinctly different types of particulate were produced in the bed burning experiments. The first type was sub-micron fume, which was expected. In addition, significant quantities of larger-sized particulate (in the 1 - 100 μm range) was also formed. This second type is referred to as ejecta, following the terminology of Verrill [1]. The amount of these larger ejecta particles was of the same magnitude as the amount of fume. These are the first quantitative data on the rates of formation of ejecta during char burning, and the first data of any type on ejecta formation under conditions where closed sodium balances were obtained.

Fume is formed by condensation of volatilized sodium and potassium compounds. The fume particles tend to be round submicron-sized particles. The SEM photomicrographs of fume collected on the particulate deposition probe inserted within the reactor, show sintered submicron-sized particles.

The second type of particulate, the ejecta, is formed by mechanical processes of fragmentation and entrainment. The ejecta particles were generally light brown in color, spherical and from 1-100 μm in diameter. The ejecta deposited on both the windward and leeward sides of the deposition probe, in the first scrubber as well as in the connecting piping, especially where the flow direction suddenly changed. This suggests that both inertial deposition and thermophoresis were involved.

8 - 2 Char Burning Rate and Bed Temperature

Increases in oxygen concentration in the reactant gas led to increased bed surface temperatures. This is apparently due to increased rates of exothermic char combustion, although there was a closer relation between increased bed temperature and increased oxygen concentration than there was between bed temperature and char burning rates.

Char composition was found to affect char burning rates. The sulfate-rich char burned faster than the base-case char and the carbonate-rich char. The faster burning rate was not accompanied by higher bed surface temperatures (they were slightly lower). These data show that sulfate in the char provides an additional path for burning char carbon through the reduction of sulfate to sulfide.

Under similar operating conditions, the presence of CO_2 and/or H_2O in the reactant gas does not show an obvious effect on char burning rate or bed temperature. However, at constant char burning rate, the addition of CO_2 and/or H_2O to the combustion gas slightly decreases the bed temperature.

8 - 3 Sodium and Potassium Released as Fume

The experimental system was designed to collect the sub-micron sized fume particles produced during bed burning and this worked effectively. Quantitative data on the quantity and chemical composition of the fume as a function of bed temperature and burning rate as well as gas and char composition were obtained.

Fume production during bed burning generally behaved in accordance with existing concepts of fume forming processes. The amount of sodium released as fume varied from about 0.5 % to 12% of the sodium present and was a very strong function (exponential-like) of bed surface temperature. In the range of typical bed temperatures from 950°C to 1050°C, the amount of fume ranged from about 1% to 6% of the sodium in the char. The fuming rate was much more strongly correlated with bed temperature than with bed burning rates per se.

The sodium fume produced was a composite of sodium vaporized as chloride and as sodium vapor. Chloride vaporization was predominate at low bed temperatures, but was overwhelmed by sodium vaporization at high bed temperatures. There was some indication that CO_2 in the reacting gases acted to suppress the rate of fume formation. This was most evident with the base case char and the carbonate-enriched char.

Potassium behaved in a similar manner to sodium. The potassium release as fume was also strongly dependent on bed temperature, with an exponential-like temperature dependence. The potassium was slightly more volatile (on the order of 20 to 30%) than the sodium. This was expected based on current concepts of fume formation.

8 - 4 Fume Chemistry

The fume produced in these experiments generally contained more Na_2CO_3 than is typical of a recovery furnace. The main reason for this was that a substantial part of the sulfur in the black liquor was released during pyrolysis and was not available to participate in fume sulfation reactions in the laboratory furnace. Sulfate and sulfide sulfur was generally not volatile under these char burning conditions.

The fume was enriched in both chloride and potassium, as indicated by the $Cl_2/(Na_2+K_2)$ and $K_2/(Na_2+K_2)$ ratio in the fume relative to those in the starting char. This is in accordance with the known fact that KCl is the most volatile single substance in the char. Enrichment of both potassium and chloride in fume decreases with increasing bed temperature. This indicates that the significance of alkali chloride vaporization relative to the other sources of Na and K release decreases with increasing temperature.

The carbonate content of the fume increases and the sulfate content decreases with increasing bed temperature. This is consistent with the concept that alkali release occurs by both vaporization of alkali chlorides and by formation and subsequent vaporization of sodium and potassium metal. Sulfate and carbonate fumes are subsequently formed in the gas phase. With a limited amount of sulfur in the gas phase, increasing alkali vaporization must lead to more carbonate in the fume, since there is always an excess of CO_2 available to form carbonate.

In general, the addition of CO_2 and/or H_2O to the combustion gas increases the amount of sulfur released and thus increases the sulfate content (and decreases the carbonate content) of the fume. The sulfate content of the fume is also increased as a result of the suppressing effect of CO_2 on sodium and potassium released. Water vapor and CO_2 in the combustion gas seem to suppress the chloride released. The reason for this is unknown, but may be connected to reactions of sulfur gases with alkali chlorides to produce HCl gas, which is all absorbed in the first scrubber and thus may appear as part of the ejecta.

8 - 5 Quantity and Composition of Ejecta

Depending on burning conditions, about 30 to 80 percent of total sodium collected as particulate was ejecta. The fraction of ejecta is greater at lower bed temperatures, because fume production increases strongly with temperature, while ejecta formation appears to peak at a bed temperature of about 1000°C. The amount of sodium released as ejecta particles varied from about 0 to 11% of the sodium originally in the char. For most experiments, the ejecta amount lay between 3 to 7% of the char sodium content. The amount of sodium released as ejecta seems to correlate better with bed temperature than with char bed burning rate. The type of char used did not appear to affect the amount of ejecta produced. There were limited indications that the amount of ejecta decreased when the gas velocity over the bed was decreased. However, decreasing gas velocity also decreased bed temperature which also affects the amount of ejecta, and most experiments were conducted at the same gas velocity, so the relation between gas velocity and ejecta formation remains unknown.

The composition of the ejecta are clearly consistent with the concept that ejecta formation is due to mechanical processes as opposed to chemical processes. The relative proportions of sodium and potassium in the ejecta are very similar to the proportions that exist in the original char. The potassium content of the ejecta does appear to increase slowly with increasing bed temperature. This is predictable because the reverse effect is observed for fume. The presence of CO_2 and/or H_2O in the reactant gas, which allow additional sulfur gas formation, decreases sulfur concentration in the bed and results in ejecta with a lower sulfate content. On the other hand, the ejecta produced from the burning of the sulfate enriched char, are highest in sulfate content.

REFERENCES:

1. Verrill, C.L., Grace, T.M. and Nichols, K.M., JPPS 20(12):J354-J360 (1994)

2. Grace, T.M., Cameron, J.H. and Clay, D.T., Tappi J. 69(10): 108-113 (October 1986)

3. Pejryd, L. and Hupa, M., Proceedings of TAPPI Pulping Conference, San Francisco, November 1984

4. H-Kochesfahani, S., Tran, H.N., Tavares, A., Mao, S. and Barham, D., 82nd Annual Meeting Technical Section CPPA. Montreal (January 1996)

5. Cameron, J.H., Clay, D.T. and Grace, T.M., Proceedings of TAPPI/CPPA 1985 Intl. Chemical Recovery Conf. pp. 435-444, New Orleans (April 1985)

6. Brown, C.A., Grace, T.M., Lien, S. and Clay, D.T., Tappi J. 72(10): 175-181 (October 1989)

7. Grace, T.M., Lien, S.J. and Brown, C.A., “Char Bed Burning - Laboratory Studies” Proceedings of TAPPI/CPPA 1992 International Chemical Recovery Conference, pp 539-550, Seattle (June 1992)